



# Deracemisation of chiral amines via a cyclic oxidation and reduction sequence

Reuben Carr

University of Edinburgh

2005

A thesis submitted for the degree of Doctor of Philosophy



---

## Declaration

I declare that this thesis is based on results obtained from investigations which I have personally carried out, and that the entire thesis is my own composition. Any work other than my own is clearly stated and acknowledged with reference to any relevant investigators or contributors. This thesis has never been published previously, in whole or in part, for the award of any higher degree.

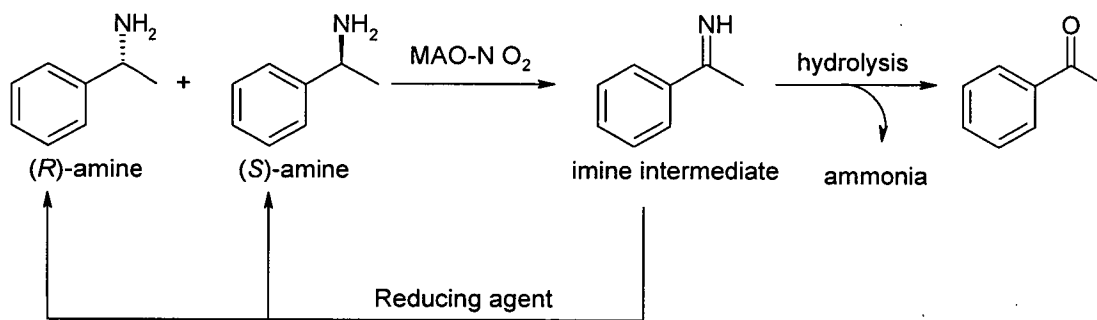
---

This thesis is dedicated to the memory of Leanne Green.

## Abstract

Enantiomerically pure chiral amines are important intermediates in the fine chemical, pharmaceutical and agrochemical industries. The aim of this work was to investigate novel methods to deracemise a wide range of chiral amines. An important aspect of this work consisted of identifying variant enzymes, with activity towards novel amine substrates, which could be developed as suitable biocatalysts for deracemisation.

The deracemisation process relies on the combination of iterative cycles of enantioselective oxidation of a racemic amine (to an achiral imine intermediate) using an amine oxidase and non-specific chemical reduction. Previous work had led to the identification of a monoamine oxidase MAO-N variant from *Aspergillus niger* (Asn336Ser) which exhibited a ca. 47 fold improvement of  $k_{cat}$  towards (*S*)- $\alpha$ -methylbenzylamine compared with the wild type. The MAO-N variant had been used in the deracemisation of *rac*  $\alpha$ -methylbenzylamine to give (*R*)- $\alpha$ -methylbenzylamine in 77% yield and 93% e.e.



In this work the MAO-N N336S variant was initially screened for activity towards a panel of amine substrates and was shown to have a broad substrate specificity and high enantioselectivity towards the (*S*)-enantiomer. Further directed evolution of MAO-N N336S enzyme towards a secondary amine identified a new variant (I246M N336S). This variant had a 6.6 fold improvement in  $k_{cat}$  towards the target substrate with maintenance of the (*S*)-enantioselectivity. This variant was used for the

preparative deracemisation of secondary cyclic amines in either whole cell (expressed in recombinant *E. coli*) or immobilised formulation.

The MAO-N I246M N336S variant underwent further directed evolution by randomising amino acid residues identified as potentially important by a homology model. The homology model was based on an alignment of the MAO-N sequence with MAO-B, the human form of the enzyme. Directed evolution identified a I246M N336S M348K T384N D385S variant with a 19.3 fold improvement in  $k_{\text{cat}}$  compared with the parent and 1354 fold improvement compared to wild type for the (*S*)-enantiomer of the target substrate. The *E*-factor remained high (110) which is expected to translate to an excellent e.e. for the deracemisation of this substrate.

Reducing agents were examined to identify those that showed the fastest rate of imine reduction. The fastest reducing agents were used in deracemisation reactions. The evolved MAO-N I246M N336S M348K enzyme was used in the preparative deracemisation of secondary amines in high yield and enantiomeric excess. Preparative deracemisations were performed with purified enzyme immobilised on resin and whole cells expressing MAO-N.

## Acknowledgements

There are plenty of people I need to thank for their help with my project. Firstly I would like to thank Nicholas Turner for his supervision and encouragement during my studies. I would also like to thank Mike Dawson for his supervision through my course and for giving me the opportunity for working with the rest of the Novacta team (Brian, Jesus, Chris, Steve, Fiona, and Martin).

I would like to thank all current and previous members of the Turner-Flitsch group for making my work enjoyable and providing a colourful experience. I owe a big thanks to Marina Alexeeva for her knowledge and practical training on my project. Thanks to Vicente Gotor-Fernandez for his help on many of the chemistry aspects of the project, developing analytical methods and keeping the Leigh group goal hangers at bay! I would like to thank Toni Fleming for her helpful and thoughtful discussions on monoamine oxidase. I would like to thank Gideon Grogan for preparing the monoamine oxidase homology model. I would also like to thank Cara Humphrey, Geoff Roff and Colin Dunsmore for their contributions to amine deracemisation and exploiting the deracemisation potentials of monoamine oxidases. I would like to thank Tom Eve for his help on examining enantioselectivity of MAO oxidations. Thanks to John White for providing his fermentation expertise for producing the enzymes used during my project. Thanks to Franck Escatales for useful advice with directed evolution. Thanks are also due to David Clarke for his help with mass spectrometry of the MAO enzyme. Finally I would like to thank the people who kindly proofread early drafts of this thesis; in particular Rob Speight, Toni Fleming, Alison Arnold, Annette Turner and Ian Archer.

Abbreviations

abs	absorbance
acetyl CoA	acetyl coenzyme A
AGAO	<i>Arthrobacter globiformis</i> amine oxidase
BASPHOS	2,5- <i>bis</i> (oxymethyl)-substituted <i>bis</i> (phospholanes)
BINAP	2,2'- <i>bis</i> (diphenylphosphino)-1,1'-binaphthyl
BLAST	basic local alignment search tool
BSA	bovine serum albumin
CAL-B	<i>Candida antarctica</i> lipase B
CD	circular dichroism
cDNA	complementary deoxyribonucleic acid
CE	capillary electrophoresis
CFE	Cell free extract
CHARMM	Chemistry at HARvard Molecular Mechanics
CHESS	Chemische Entwicklungs und Synthese Service
CTH	catalytic transfer hydrogenation
CuAO	copper containing amine oxidase
DAB	3,3'-diaminobenzidine
DCM	dichloromethane
d.e.	diastereomeric excess
DKR	dynamic kinetic resolution
DMSO	dimethyl sulfoxide
DNA	deoxyribonucleic acid
dNTP	any deoxyribonucleoside triphosphate
d.r.	diastereomeric ratio
DTT	dithiothreitol

## Abbreviations

---

DuPHOS	1,2- <i>bis</i> ((2 <i>R</i> ,5 <i>R</i> )-2,5-diethylphospholano) benzene
<i>E</i>	enantiomeric ratio
EDTA	ethylenediaminetetraacetic acid
e.e.	enantiomeric excess
epPCR	error prone polymerase chain reaction
EPSPS	enolpyruvylshikimate-3-phosphate synthase
ES	enzyme-substrate complex
ES <sup>‡</sup>	enzyme-substrate transition state
exp	exponential
FACS	fluorescence activated cell sorting
FAD	flavin adenine dinucleotide (oxidised state)
FADH <sub>2</sub>	flavin adenine dinucleotide (reduced state)
FDA	Food and Drug Administration
FPLC	fast protein liquid chromatography
FT	fourier transform
GAT	glyphosate <i>N</i> -acetyltransferase
GERD	gastro-oesophageal reflux disease
GFP	green fluorescent protein
HAT	hydrogen atom transfer
HIV	human immunodeficiency virus
HPAO	<i>Hansenula polymorpha</i> amine oxidase
HRP	horseradish peroxidase
IPTG	isopropylthio-β-D-galactoside
ITCHY	incremental truncation for the creation of hybrid enzymes
kDa	kilodalton
kJ	kilojoule
L	path length
LB	Luria-Bertani broth
MAO	monoamine oxidase

---



## Abbreviations

---

MAO-A	type A monoamine oxidase from <i>homo sapiens</i>
MAO-B	type B monoamine oxidase from <i>homo sapiens</i>
MAO-N	monoamine oxidase from <i>Aspergillus niger</i>
mbar	millibar
MDQ	1-methyldihydroisoquinoline
MTQ	1-methyltetrahydroisoquinoline
Ni-NTA	nickel-nitrilotriacetic acid
OD	Optical density
PAO	polyamine oxidase
PCR	polymerase chain reaction
PEI	polyethyleneimine
PMHS	polymethylhydrosiloxane
PMSF	phenylmethylsulfonyl fluoride
<i>R</i>	gas constant
<i>rac</i>	racemic
RACHITT	random chimeragenesis on transient templates
RNA	ribonucleic acid
SDM	site directed mutagenesis
SDS	sodium dodecylsulfate
SDS PAGE	sodium dodecylsulfate polyacrylamide gel electrophoresis
SET	single electron transfer
StEP	staggered extension process
TAE	tris acetate EDTA
TBME	<i>tert</i> -butyl methyl ether
TPQ	topaquinone
Tris	tris(hydroxymethyl)aminomethane
tRNA	transfer ribonucleic acid
U	units
v/v	volume by volume

## Abbreviations

---

w/v	weight by volume
$\alpha_D$	optical rotation
$\epsilon$	molar extinction coefficient
$\Delta G$	change in free energy
$\Delta G^\ddagger$	change in free energy (transition state)
$\Delta H$	change in enthalpy
$\Delta S$	change in entropy

Contents

Abstract	i
Acknowledgements	iii
Abbreviations	iv
Contents	viii

**1. Introduction**

1.1. Synthesis of optically active chiral amines	1
1.1.1. 1,2-Addition to carbon-nitrogen double bonds	2
1.1.2. Asymmetric reduction of imines	7
1.1.3. Enantioselective reductive aminations	13
1.2. Biocatalysis	16
1.2.1. Kinetic resolutions	16
1.2.2. Dynamic kinetic resolutions	19
1.2.3. Deracemisations	21
1.2.4. Biocatalytic route to optically active amines	26
1.3. Amine oxidases	31
1.3.1. Flavin containing amine oxidases	31
1.3.2. MAO-N	37
1.3.3. Mechanism of FAD oxidation in MAO	37
1.3.4. Synthetic potential of amine oxidases	40
1.3.5. Copper dependent type I amine oxidases	40

---

1.4. Directed evolution	45
1.4.1. Generation of variant libraries	46
1.4.2. Screening methods	54
1.4.3. Progress in directed evolution	61
1.5. Summary and aims	68
<b><u>2. Results and discussion</u></b>	
2.1. Purification and stability studies	71
2.1.1. Ion exchange purification	71
2.1.2. Affinity purification	73
2.1.3. Activity profile during MAO-N purification	75
2.1.4. Stability of MAO-N upon storage	77
2.1.5. Growth and expression of MAO-N	81
2.1.6. Conclusions	86
2.1.7. Future work	87
2.2. Screening of MAO-N wild type and N336S M348K variant against panel of amines	88
2.2.1. The colorimetric peroxidase assay	88
2.2.2. MAO-N wild type and MAO-N <i>I</i> variant amine oxidation screen	89
2.2.3. Enantioselectivity of the MAO-N <i>I</i> enzyme	102
2.2.4. Oxidation of MTQ (amine <b>76</b> )	105
2.2.5. Conclusion	107
2.2.6. Future work	108

---

2.3. Directed evolution of MAO-N	109
2.3.1. Mutation strategy for MAO-N	109
2.3.2. Proposed directed evolution	110
2.3.3. Solid phase assay	111
2.3.4. Screening of MAO-N variant library with MTQ	112
2.3.5. Specificity or expression mutant?	115
2.3.6. Sequencing MAO-N <u>2</u>	118
2.3.7. Kinetic parameters of MAO-N <u>2</u>	119
2.3.8. Screening of MAO-N <u>2</u> variant against a panel of amines	121
2.3.9. Enantioselectivity of MAO-N <u>2</u>	125
2.3.10. Conclusion	127
2.3.11. Future work	127
2.4. Saturation mutagenesis	129
2.4.1. Exploration of the I246M mutation	129
2.4.2. Quikchange site directed saturation mutagenesis	130
2.4.3. Preparation of 246 saturation library for screening	132
2.4.4. Screening of 246 saturation library against amine <b>178</b>	133
2.4.5. Alignment of MAO-N and MAO-B sequences	136
2.4.6. Saturation mutagenesis at aligned active site residues	138
2.4.7. Screening of 384/385 saturation library	141
2.4.8. Quantitative analysis of the selected variants	145
2.4.9. Michaelis-Menten studies of the MAO-N variants	148
2.4.10. Thermodynamic improvements in specificity	156
2.4.11. Error in measuring protein concentration by the Bradford assay	160
2.4.12. Molecular modelling of MAO-N	161
2.4.13. Conclusion	166
2.4.14. Future work	168

---

2.5. Screening of reducing agents for reductions of imines	170
2.5.1. The screening of reducing agents	170
2.5.2. Monitoring the time course of reactive boranes	172
2.5.3. Conclusion	173
2.5.4. Future work	173
2.6. Deracemisation experiments	175
2.6.1. Deracemisation objectives	175
2.6.2. Deracemisation of ( <i>rac</i> )-MTQ with whole cell expressing MAO-N	175
2.6.3. Deracemisation at higher substrate concentrations of ( <i>rac</i> )-amine <b>76</b> with whole cell expressing MAO-N	177
2.6.4. Immobilisation of MAO-N	178
2.6.5. Immobilisation of MAO-N on Eupergit	179
2.6.6. Calculation of the activity of MAO-N activity on the resin	180
2.6.7. Evaluation of immobilised MAO-N stability	181
2.6.8. Preparative deracemisation of ( <i>rac</i> )-amine <b>76</b> (MTQ)	182
2.6.9. Preparative deracemisation of ( <i>rac</i> )-amine <b>76</b> with whole cells	183
2.6.10. Deracemisation of ( <i>rac</i> )-amine <b>209</b>	184
2.6.11. Effect of alternative reducing agents on the deracemisation of ( <i>rac</i> )-amine <b>76</b>	186
2.6.12. Catalytic transfer hydrogenation (CTH) in the deracemisation of amine <b>76</b>	188
2.6.13. Conclusions	190
2.6.14. Future work	193

### **3. Experimental**

3.1. MAO-N assay methods	195
3.1.1. The horseradish peroxidase coupled liquid assay	195

---

3.1.2. Measurement of U-shaped well path length	196
3.1.3. Relative rate calculation	196
3.1.4. CFE rate calculation	197
3.1.5. Michaelis-Menten calculations	197
3.1.6. The solid phase assay	198
3.1.7. Solid phase MAO-N-Eupergit assay	198
3.2. MAO-N purification techniques	200
3.2.1. Q-Sepharose purification	200
3.2.2. Nickel affinity purification	200
3.2.3. PD10 desalting	201
3.2.4. Ammonium sulfate precipitation	201
3.2.5. SDS PAGE protein gel	202
3.2.6. The Bradford assay	202
3.2.7. Estimation of error in the Bradford assay	203
3.2.8. Mass spectrometry characterisation of MAO-N	203
3.2.9. UV-visible spectrum of MAO-N	204
3.3. MAO-N transformation and fermentation methods	205
3.3.1. Transformation of <i>E. coli</i> BL21 (DE3)/BL21 (DE3) star chemically competent cells	205
3.3.2. Transformation of <i>E. coli</i> TOP10 chemically competent cells	205
3.3.3. Electroporation of <i>E. coli</i> XL1-blue electrocompetent cells	205
3.3.4. Transformation of <i>E. coli</i> XL1-red chemically competent cells and preparation of library of variants	206
3.3.5. Fermentation of <i>E. coli</i> BL21 (DE3) expressing MAO-N	207

---

3.3.6. Preparation of CFE	208
3.3.7. Spreading of fermentation onto LB agar +/- ampicillin plates	208
3.3.8. Isolation of plasmid DNA from clones on LB agar plate	208
3.3.9. IPTG induction during fermentation	209
3.4. DNA purification and manipulation	210
3.4.1. DNA plasmid purification	210
3.4.2. DNA agarose gel	210
3.4.3. DNA gel extraction	210
3.4.4. DNA sequencing	211
3.4.5. Quikchange PCR I246 saturation library	212
3.4.6. Quikchange PCR 384/385 saturation library	213
3.4.7. Nick repair and preparation of DNA for screening	214
3.4.8. Verification of representation of the mutagenesis	215
3.5. Reducing agent screening	216
3.5.1. The half reaction reduction screen	216
3.5.2. Measurement of amine <b>76</b> and imine substrate onto palladium catalyst	216
3.5.3. Catalytic transfer hydrogenation of MDQ imine	217
3.5.4. Deracemisation of ( <i>rac</i> )-amine <b>76</b> with various boranes	217
3.6. Deracemisation reactions	218
3.6.1. Stereoinversion of ( <i>S</i> )-amine <b>76</b> with purified MAO-N protein	218
3.6.2. Deracemisation of ( <i>rac</i> )-amine <b>76</b> to ( <i>R</i> )-amine <b>76</b> with whole cells expressing MAO-N	218
3.6.3. Preparative deracemisation of ( <i>rac</i> )-amine <b>76</b> to ( <i>R</i> )-amine <b>76</b> with whole cells expressing MAO-N	219



---

3.6.4. Immobilisation of MAO-N onto Eupergit-C	220
3.6.5. Preparative deracemisation of ( <i>rac</i> )-amine <b>76</b> to ( <i>R</i> )-amine <b>76</b> with MAO-N-Eupergit	220
3.6.6. Deracemisation of ( <i>rac</i> )-amine <b>209</b> to ( <i>R</i> )-amine <b>209</b> with MAO-N-Eupergit	221
3.6.7. Preparative deracemisation of ( <i>rac</i> )-amine <b>209</b> to ( <i>R</i> )-amine <b>209</b> with MAO-N-Eupergit	221
3.6.8. Deracemisation of ( <i>rac</i> )-amine <b>76</b> to ( <i>R</i> )-amine <b>76</b> using CTH and MAO-N-Eupergit	222
3.6.9. Deracemisation of ( <i>rac</i> )-amine <b>76</b> to ( <i>R</i> )-amine <b>76</b> using CTH with palladium catalyst and MAO-N-Eupergit	222
3.7. Analytical methods	224
3.7.1. Chiral HPLC of MTQ	224
3.7.2. CE analysis of MTQ	224
3.7.3. CE analysis of 2-phenylpyrrolidine	225
3.7.4. Reverse phase MDQ analysis	225
3.8. Buffer and reagent recipes	226
References	228
Appendices	238
Publications	245

## 1.1. Synthesis of optically active chiral amines

Chirality is a key issue concerning the production of fine chemicals and in recent years the desire to achieve the efficient synthesis of chiral compounds has increased following the release of the FDA's guidelines<sup>1</sup>. In 1992 the FDA and European Committee for Proprietary Medicinal Products required manufacturers to research and characterise each enantiomer in all chiral drugs proposed to be marketed as a mixture. Worldwide sales of chiral drugs in single enantiomer dosage continue to grow at more than 11.4% annually with the market estimated to be worth \$14.94 billion by the end of 2009<sup>2</sup>. The same survey showed this growth would be realised by a 36% rise in chemocatalysis and 22% in biocatalysis, whilst traditional technology would drop to 41%. To access chirality in industrial transformations several options are available. Enantiopure precursors can be used from the natural 'chiral pool', asymmetric synthesis can be used or a kinetic resolution method maybe undertaken.

Amines constitute an important class of functional group present in many biologically active chiral molecules. Several strategies exist for the preparation of optically active chiral amines which are classified into two main groups<sup>3</sup>. Asymmetric synthesis is the first of these routes. Typically, a prochiral substrate undergoes an asymmetric chemical change to the chiral amine product. This can be achieved by a reductive amination, transamination or a transfer hydrogenation. Secondly a physical separation may be possible where no chemical modification to the substrate is undertaken. Traditional physical separation techniques (distillation, chromatography and crystallisation) cannot be used to separate enantiomers because they have identical physical properties. But if a chiral additive is introduced separation is possible if it can interact with the substrate, this effectively converts it from an enantiomeric to a diastereomeric mixture. Owing to the fact that diastereomers are not chemically equivalent, physical separation becomes possible.

### 1.1.1. 1,2-Addition to carbon-nitrogen double bonds

1,2-Addition of nucleophiles to a C=N imino group in an asymmetric fashion provides a route to enantiomerically enriched amines<sup>4</sup>. The analogous reaction with the keto, rather than imino functionality has been much more widely investigated<sup>5</sup>. Imino groups encounter some general problems that make 1,2-additions more challenging than with the equivalent keto group; the imino group is less electrophilic, can tautomerise to the enamine and can undergo reductive coupling, hampering 1,2-addition reactions.

However, activation of the imino group and selective reagents can be used to help reduce some of these difficulties<sup>4</sup>. Achieving asymmetric synthesis of amines is possible by introducing chirality either into the carbonyl or amine part of the imino substrate, in the nucleophilic reagent or in the external chiral ligands. 1,2-addition reactions to yield chiral amines are not limited to imino functionality, 1,2-additions to hydrazones gives hydrazines, addition to oxime ethers or nitrones leads to hydroxylamines<sup>4</sup>. Hydrazines and hydroxylamines can then be converted to the corresponding optically active amine by reductive cleavage. Oxime ethers are the least useful electrophilic C=N bond component for 1,2-additions because they are less electrophilic and usually comprise of *E/Z* mixtures which can interfere with the design of the asymmetric process. In the case of aldehyde hydrazones they generally are obtained as *E* isomers<sup>6</sup>.

Condensation of commercially available enantiopure amines to a carbonyl compound can be used to prepare *N*-alkyl/arylamines. In the case where the amine possesses a second heteroatom, the transition states are energetically strengthened by chelation and this improves diastereoselectivities. Condensation of *S*-valinol-1 to an aldehyde gave non-enolisable arylamines which were subsequently treated with a metal aryl/benzyl reagent to give the diastereomeric amine-3 with d.e.s >98%. The auxiliary group could be subsequently removed to give the enantiomerically enriched amine. A transition state was proposed with the alkoxy group from the  $\beta$ -amine alcohol coordinating with the metal

and therefore directing nucleophilic attack at the *si*-face of the imine-**2**. Changing the chiral auxiliary to *S*-alaninol lowered the selectivity from *S*-valinol-**1**, showing the importance of the more bulky isopropyl group<sup>7</sup>.

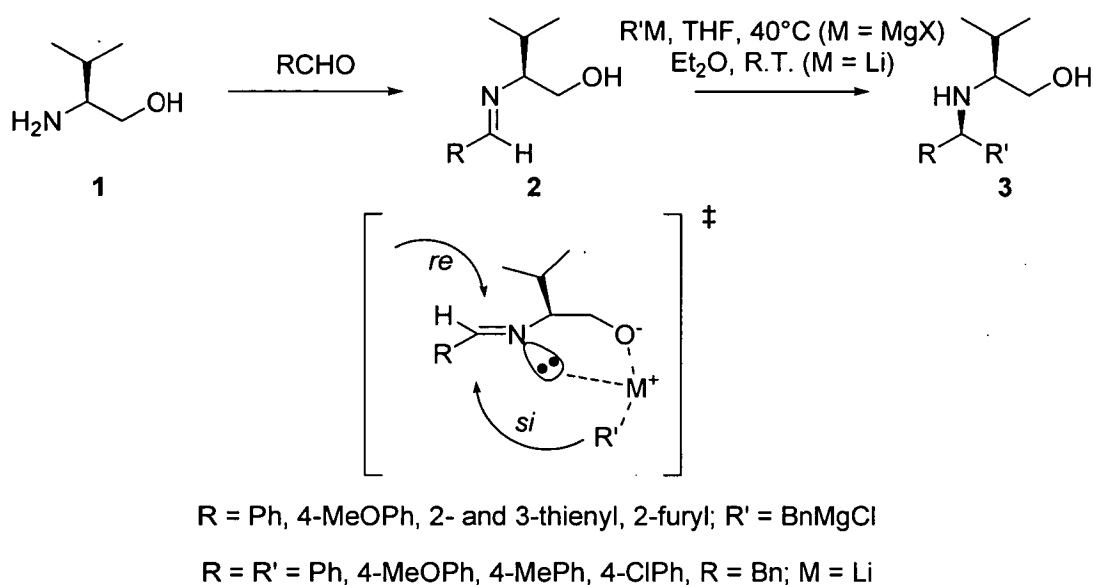
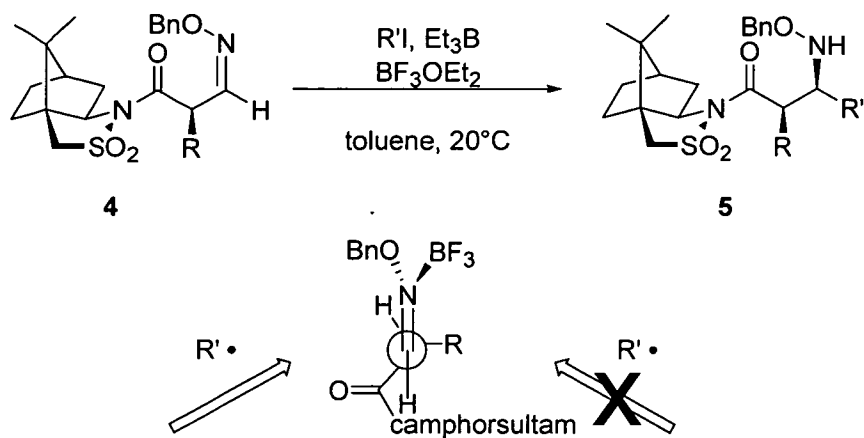


Figure 1.1.1.1. Diastereoselective synthesis of amines-**3** using  $\beta$ -amino alcohols as an auxiliary.

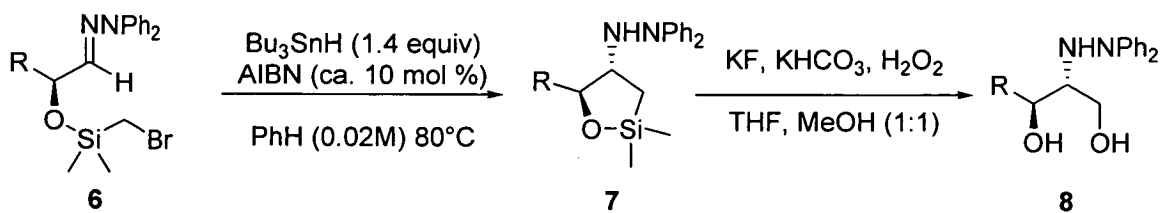
Synthetic applications of radical addition to C=N bonds can give several potential products including unsymmetrical ketones, quaternary C-C bonds and chiral  $\alpha$ -branched amines<sup>8</sup>. Malonate-derived oxime ethers-**4** (as shown in figure 1.1.1.2) gave high diastereoselectivity in the hydroxylamine-**5** product (d.r. > 40:1) for ethyl radical addition reactions. The chiral camphorsultam part of the oxime substrate was not the major stereocontrolling element because the oxime ether analogue with no chirality at the  $\alpha$ -amide carbon (substrate-**5a** in figure 1.1.1.2) showed little stereocontrol<sup>9</sup>.



Substrate	R	R'	Yield	d.r.
5a	Hydrogen	Ethyl	84%	(1.1:1)
5b	Benzyl	Ethyl	99%	(>40:1)
5c	<i>p</i> -Nitrobenzyl	Ethyl	72%	(>40:1)
5d	Propargyl	Ethyl	43%	(>40:1)

Figure 1.1.1.2. Ethyl radical addition to camphorsultam oxime ether substrates.

More recently, the radical addition to chiral hydrazones has allowed chiral acyclic amino-alcohols to be accessed. This offers a complementary route from the ionic method described earlier (figure 1.1.1.1). Bromomethyl or vinyl radical precursors tethered via a temporary silicon connection underwent tin mediated 5-exo radical cyclisation of  $\alpha$ -hydroxyhydrazones. Oxidative removal of the tether provided *anti*-2-hydrazino 1,3-diols in good yield<sup>10</sup>. The Beckwith-Houk model<sup>11</sup> predicts enhancement of diastereoselectivity based upon increasing substituent steric demand in 4-substituted 5-hexenyl radical cyclisations. On the assumption that this 5-exo radical cyclisation undergoes a similar transition state, *A*-values were calculated and appeared to correlate well with the experimentally observed *anti:syn* ratio. The *A*-value is a measure of the free energy difference between the equatorial and axial chair conformers of the monosubstituted cyclohexane.



Substrate	R	Yield	Product ratio ( <i>anti</i> : <i>syn</i> )	<i>A</i> value (kcal/mol)
<b>8a</b>	Methyl	76%	79:21	1.6
<b>8b</b>	<i>i</i> -Butyl	68%	85:15	1.8
<b>8c</b>	<i>i</i> -Propyl	80%	96:4	2.2
<b>8d</b>	Phenyl	57%	>98:2	2.9

Figure 1.1.1.3. Diastereoselective addition of hydroxymethyl using a silicon tether approach for addition of functionalised radicals to  $\alpha$ -hydroxyhydrazones.

The ketene-imine cyclocondensation of the Staudinger reaction is one approach that can be used to prepare  $\beta$ -lactams. Most stereoselective versions use a chiral amine or ketene auxiliary<sup>12</sup>, the first example of a catalytic asymmetric Staudinger reaction was reported by Lectka in 2000<sup>13</sup>. The Staudinger reaction consists of a chiral nucleophile catalyst which activates a ketene towards cycloaddition with an electron deficient imine; the product  $\beta$ -lactams isolated had high e.e.s but only moderate yields. More recently the use of planar chiral nucleophiles as catalysts in the asymmetric Staudinger reaction<sup>14</sup> were effective at catalysing the cycloaddition reaction of symmetric and unsymmetric disubstituted ketenes-**9** with a wide range of tosylimines-**10** (figure 1.1.1.4). Carrying out the reaction at ambient temperature afforded  $\beta$ -lactam-**11** products in high e.e.s (81-98%) with good yields (76-98%).

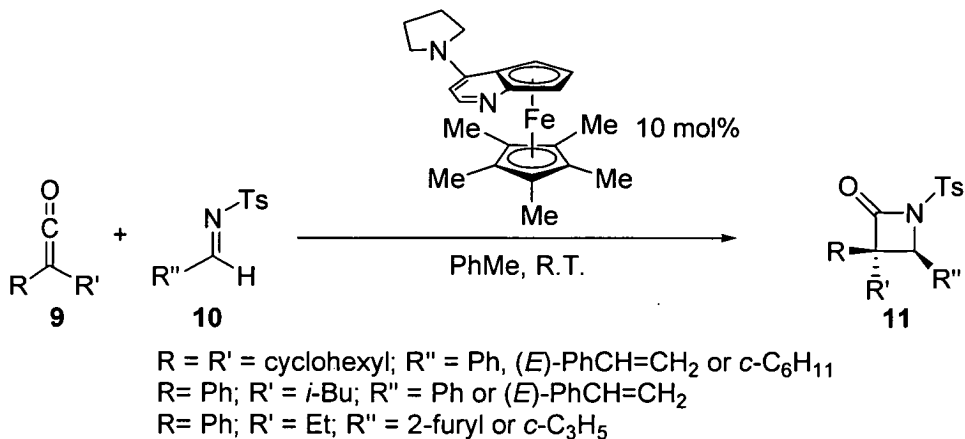


Figure 1.1.1.4. The catalytic asymmetric Staudinger reaction for the preparation of enantiomerically enriched  $\beta$ -lactams by a cycloaddition of a ketene with a tosylimine.

Although, not a 1,2-addition to a C=N bond, enantioselective hydroamination of alkenes is another synthetic method for the preparation of chiral amines. Hydroaminations are catalysed by transition metal and alkali metals.<sup>15</sup> The potential of enantioselective hydroamination of alkenes has been discussed by Roesky and Müller<sup>16</sup>. The enantioselective addition of aniline-**12** to vinylarenes-**13** using palladium catalysts has been carried out at 25°C yielding product-**14** in 81% yield and 81% e.e.<sup>17</sup>. The attractive feature of the Staudinger reaction and the hydroamination of alkenes is that achiral inexpensive substrates are converted into a chiral amine product at without the need for significant heating. Generally the other asymmetric 1,2 C=N bond additions rely on chirality being present in the starting substrates.

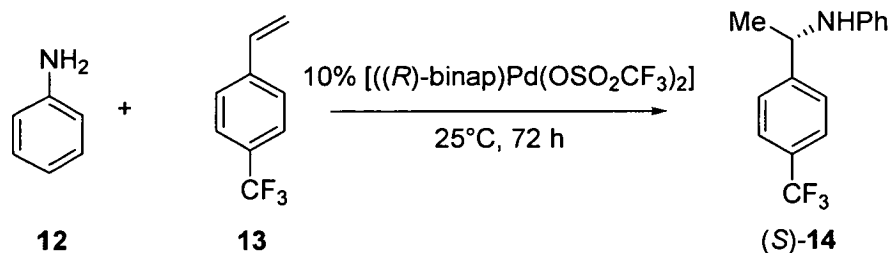


Figure 1.1.1.5. Reaction of aniline-12 with *p*-trifluoromethylstyrene-13 catalysed by [((*R*)-binap)-Pd(OSO<sub>2</sub>CF<sub>3</sub>)<sub>2</sub>]

### 1.1.2. Asymmetric reduction of imines

Imine reductions to the corresponding amine are well documented. Catalytic transfer hydrogenation offers an attractive alternative to hydrogen gas in reductions with the hydrogen source coming from a cheap source such as formate salts<sup>18</sup>, propanol<sup>19</sup> or indoline<sup>20</sup>. The synthesis of chiral non-racemic secondary amines by imine reduction is divided into three main areas: (i) enantioselective hydride reduction, (ii) enantioselective hydrogenation and (iii) enantioselective transfer hydrogenation.

Much of the emphasis in research in asymmetric transfer hydrogenation is based on ketone reduction<sup>21</sup> and has provided the basis to examine the imine reduction. Noyori, *et al*<sup>22</sup> used a ruthenium based catalyst to asymmetrically reduce a cyclic imine-15 using a formic acid – triethylamine mixture. The rate and enantioselectivity of the reaction are delicately influenced by the chiral ligand. The highest efficiency obtained not only relies on the chirality of the *N*-tosylated 1,2-diamine but also the presence of polar functional groups, as well as the alkyl substituents on the *p*-cymene ligand. The NH<sub>2</sub> and ArSO<sub>2</sub> groups play important roles for the high reactivity. The catalyst can be fine-tuned to a particular imine substrate by modification of η<sup>6</sup>-arene ligand substitution. An interesting aspect of this catalyst is that under specific conditions the C=N/C=O chemoselectivity for reduction is in favour of the imine. This ligand was also shown to reduce a variety of acetophenone derivatives in excellent yields and e.e.<sup>23</sup>. The Noyori catalyst-17 has been



shown to be effective for the enantioselective hydrogenation of imines containing a fully substituted nitrogen group along with aniline and bromophenyl ortho-substituted imines<sup>24</sup>. The main limitation of this method is the sensitivity of the catalyst to product inhibition.

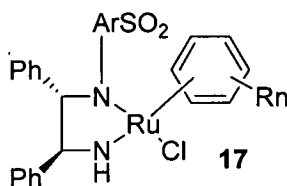
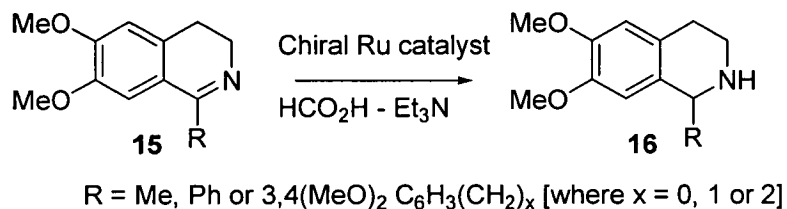


Figure 1.1.2.1. Noyori's ruthenium based catalyst for the asymmetric reduction of a prochiral imine-15

Labelling studies with deuterated propan-2-ol indicated that propan-2-ol could not be used as a hydrogen source for this particular catalytic system. However, Bäckvall had earlier reported the ruthenium-catalysed transfer hydrogenation of imines<sup>25</sup> by propan-2-ol in the presence of base (potassium carbonate). The advantage of formic acid is that it allows the reduction to be done under essentially irreversible conditions, as carbon dioxide is released as the by-product.

Two routes have described the mechanism for transfer hydrogenation: (i) direct hydrogen transfer and (ii) hydridic route. The direct hydrogen transfer process involves a six-membered cyclic transition state in which both hydrogen donor and hydrogen acceptor are held in close proximity to the metal centre.

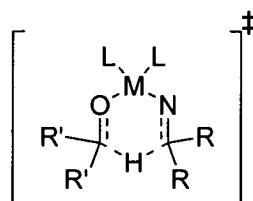


Figure 1.1.2.2. Proposed transfer hydrogenation mechanism – direct hydrogen transfer

The hydridic route proceeds in a stepwise manner by formation of a metal hydride by loss of acetone from propanol hydrogen source. The metal hydride then undergoes hydride transfer with the hydrogen acceptor.

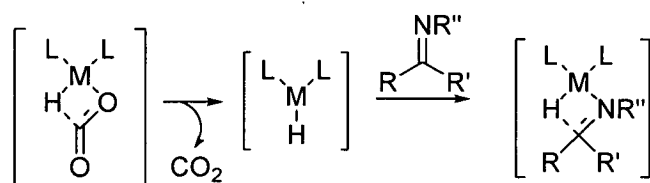


Figure 1.1.2.3. Proposed transfer hydrogenation mechanism in the hydridic route

The first example of optically active hydride reagents for asymmetric reduction was reported in 1951 where lithium aluminium hydride was modified with stoichiometric amount of (+)-camphor. Some of the most successful and general catalysts for hydride reduction are based on the oxazaborolidine structure, developed by Corey<sup>26</sup> following initial work by Itsuno<sup>27</sup>. Itsuno's chiral borane-**22** was prepared by combining borane and a chiral amino alcohol. Successive additions of substrate realised a more effective semicatalytic process<sup>28</sup>. Bolm revealed that the absolute configuration of the reduced products was determined not only by the catalyst but also the geometric structure of the substrates. Namely the *E*-isomer gave the *S*-enantiomer and the *Z*-isomer gave the *R*-enantiomer<sup>29</sup>. Although the mechanism of the asymmetric induction is unclear, it is probably due to differences in steric bulk of the approaching substrate.

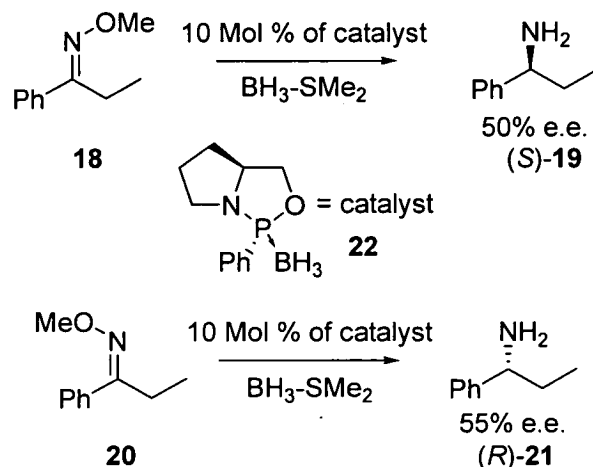


Figure 1.1.2.4. Oxazaborolidine catalysts used in the asymmetric reduction of ketones and imines.

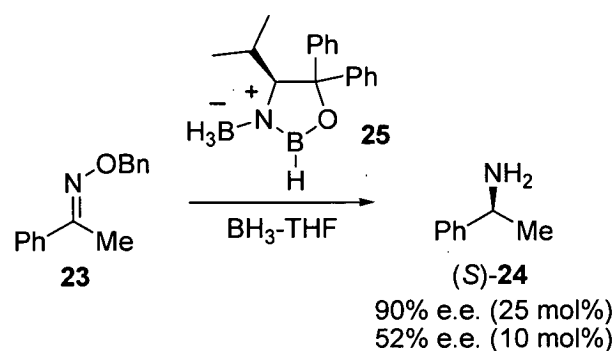


Figure 1.1.2.5. Oxazaborolidine catalysts used in the asymmetric reduction in the synthesis of alpha-methylbenzylamine.

The enantioselective preparation of chiral molecules is most commonly performed with chiral metal complexes<sup>30</sup>. The main advantage of this approach is that stereochemical information of a single chiral ligand can catalytically relay the enantioselection to many thousands of molecules effectively amplifying the chiral information. The origin of the enantioselection from the chiral ligand has been shown in the transition state<sup>31</sup>. Metal complexes also allow both enantiomeric forms of the product to be obtained, provided both chiral ligands are available. BINAP and DuPHOS ligands are capable of hydrogenating ketones in extremely high e.e., but the major drawback is the requirement

for an adjacent heteroatom. A version of DuPHOS called BASPHOS, bearing water solubilising hydroxyl groups, has been shown to hydrogenate 2-acetamido acrylic acid and its methyl ester under aqueous conditions with excellent e.e.s.<sup>32</sup>. Metals other than Noyori's Ru (II) have also been used to asymmetrically reduce prochiral ketones these catalysts are also late transition metal complexes Rh (I) and Ir (I). Other factors that can influence the catalytic reduction include co-catalysts and solvent. The nature of the imine substrate is important as the enantiomeric excess achieved asymmetrically in the reduction of cyclic imines is insensitive to changes in hydrogen pressure, whilst the e.e. of acyclic imines is affected by the hydrogen pressure<sup>33</sup>. The cause of this effect is likely to be the mixture of anti- and syn-isomer of the C=N bond which interconverts during the course of the reaction.

Polymethylhydrosiloxane (PMHS) is another interesting alternative to hydrogen because it is inexpensive, non-toxic and stable to air and moisture<sup>34</sup>. A high throughput screen has allowed the rapid identification of new catalysts for the enantioselective reduction of imines using PMHS as a reducing agent<sup>35</sup>. Reactions were performed in a 96-well microtitre plate which allowed multiple reaction conditions to be evaluated in parallel. The crude reaction mixtures were analysed by GC (conversion) and HPLC (enantioselectivity). New catalysts were identified for the reduction of imine-**26** into amine (*R*)-**27** using PMHS as the reducing agent. Chiral induction was possible using combination of catalysts such as Sn(OTf)<sub>2</sub>, Zn(OTf)<sub>2</sub>, In(OTf)<sub>3</sub> and Cd(CHB)<sub>2</sub> with chiral ligands-**28**, -**29**, -**30**, -**31** and -**32**. A selection of some of the conditions identified is shown in table 1.1.2.1.

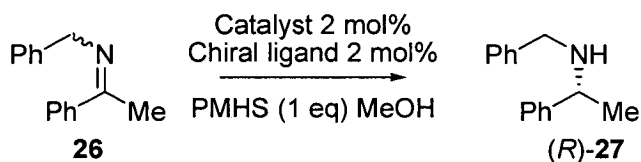


Figure 1.1.2.6. Asymmetric reduction screening of imines with PMHS.

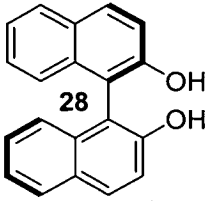
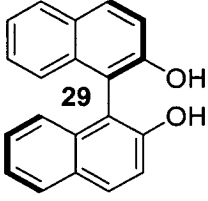
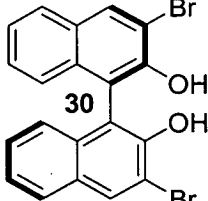
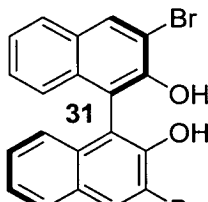
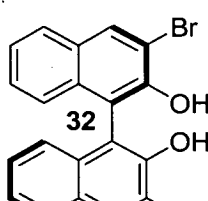
Catalyst	Ligand	Conversion	e.e.
Zn(OTf) <sub>2</sub>	No ligand	87%	0%
Zn(OTf) <sub>2</sub>	 <p>28</p>	>99%	30% ( <i>R</i> )-27
In(OTf) <sub>3</sub>	 <p>29</p>	56%	29% ( <i>R</i> )-27
Sn(OTf) <sub>2</sub>	 <p>30</p>	85%	60% ( <i>R</i> )-27
Zn(OTf) <sub>2</sub>	 <p>31</p>	87%	33% ( <i>R</i> )-27
In(OTf) <sub>3</sub>	 <p>32</p>	50%	36% ( <i>R</i> )-27

Table 1.1.2.1. Yield and enantioselectivities of the reduction of *N*-Benzylphenylethylimine (1mmol) with PMHS (1.2 equivalents), 2 mol% catalyst and 2 mol% ligand in MeOH (reproduced from T. Ireland *et al*<sup>35</sup>).

---

Most of the reported methods for imine reductions are carried out in organic solvents under anhydrous conditions because imines tend to be unstable in the presence of water. Subsequently there is little mention in the literature of imine reductions being carried out under mild aqueous conditions that would be compatible with an enzymatic step such as would be required in the deracemisation strategy used in this project. Water is not an ideal solvent to perform imine reductions as they can be hydrolysed to the ketone/aldehyde. Also, water is rarely used in reductions because of the chemical incompatibility with most reducing agents. There has been some work in this area to address these problems. Imino-acids have been reduced under mild aqueous conditions and neutral pH<sup>36</sup> sodium borohydride, ammonia-borane, ammonium formate with a 10% Pd/C catalyst, with ammonia-borane being the most effective. Zinc powder has been used to reduce imines in water at room temperature using 5% sodium hydroxide<sup>37</sup>.

### 1.1.3. Enantioselective reductive aminations

Being able to achieve an enantioselective reductive amination of an amine and a prochiral ketone is an attractive route to obtaining chiral amines. There is no need to isolate and purify the imine intermediate. There is less attention on enantioselective approaches to accessing these chiral amine products from non-chiral starting materials. One of the first examples of an asymmetric reductive amination was reported by Blaser *et al.*<sup>38</sup> in which a chiral amine grass herbicide was prepared in 78% e.e. from methoxyacetone and 2-methyl-5-ethylaniline. More recently Ir-f-Binaphane catalyst has been used to achieve highly enantioselective reductive aminations of a variety of simple aryl ketones with *p*-anisidine in the presence of Ti(O<sup>*i*</sup>Pr)<sub>4</sub> and I<sub>2</sub><sup>39</sup>.

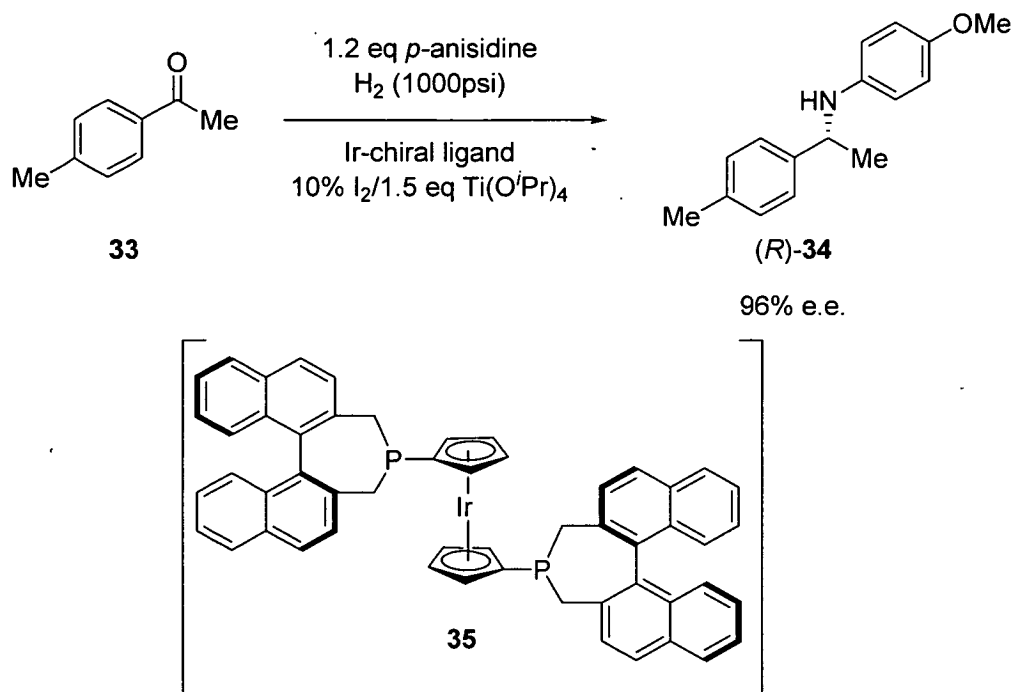


Figure 1.1.3.1. Asymmetric reductive amination of an aryl ketone with *p*-anisidine with (*S,S*)-f-binaphane chiral ligand-**35**.

An enantioselective hydrogen transfer reductive amination reaction was screened against a variety of catalyst types which avoided the use of hydrogen gas<sup>40</sup>. [Rh(C<sub>5</sub>Me<sub>5</sub>)Cl<sub>2</sub>]<sub>2</sub> was the only catalyst that demonstrated acceptable activity in the presence of ammonia and isopropyl alcohol in the reductive amination of acetophenone-**36** (figure 1.1.3.2). Further investigation of Rh, Ir and Ru complexes using ammonium formate showed that Rh and Ir gave poor enantioselectivities compared to Ru. Addition of ammonia was found to slow the reaction but improve enantioselectivities. A series of ketones were examined under the optimised conditions and amines were obtained in good yields with high enantioselectivities (86-98% e.e.). The 2-octanone enantioselective hydrogen transfer reductive amination under these conditions showed full consumption of the starting material but only a trace amount of 2-octylamine was detected. Removing ammonia from the reaction did however give the desired product in 44% yield and 24% e.e.

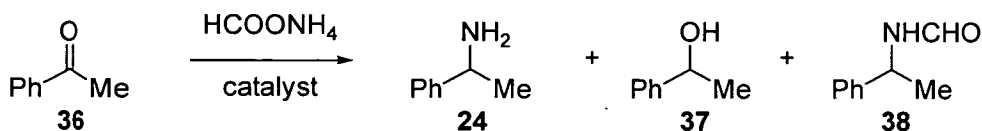


Figure 1.1.3.2. The reductive amination of acetophenone-**36** in the screening of catalytic reaction conditions to affect the asymmetric hydrogen transfer reductive amination to  $\alpha$ -methylbenzylamine-**24**.

Alternatively a chiral amine can be obtained with a reductive amination by the addition of a prochiral ketone to a chiral amine. There are several cheap chiral amines commercially available as both enantiomers which can be used as chiral auxiliaries and this is an attractive route to producing chiral amines. (+) and (-)-norephedrine-**40** have been used as chiral auxiliaries in the preparation of enantiomerically enriched amines from a selection of different ketones-**39**<sup>41</sup> (figure 1.1.3.3). Enantiomerically pure chiral benzocyclic amines were obtained by asymmetric transamination of the corresponding prochiral ketone<sup>42</sup>. In this case (*R*) and (*S*)-phenylethylamine-**24** was used as the chiral auxiliary which was subsequently removed by catalytic hydrogenation.

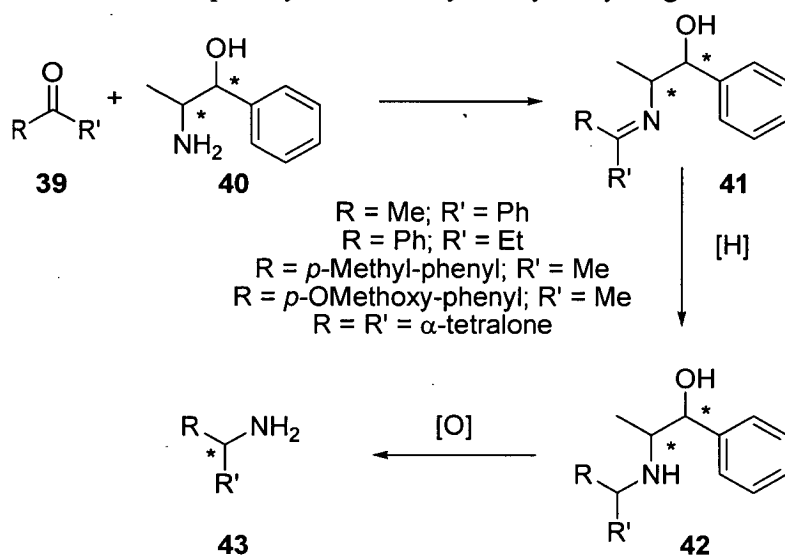


Figure 1.1.3.3. Asymmetric synthesis of amines by the reductive amination of ketones using (+) and (-)-norephedrine-**40** followed by periodate oxidation.



## 1.2. Biocatalysis

Enzymes are protein catalysts that are capable of accelerating reactions under mild conditions. Biocatalysis encompasses catalysis by bacteria, fungi, other microbes or their true catalytic components - enzymes. Biocatalysis is becoming an ever increasingly important tool in the industrial synthesis of bulk chemicals, pharmaceutical and agrochemical intermediates and food ingredients<sup>43</sup>. High enantioselectivities are one of the attractive features associated with biocatalysis. There is much work currently underway to exploit the potential this approach has to offer<sup>44</sup>. Recent scientific breakthroughs in genomics, directed enzyme evolution and exploitation of biodiversity provide exciting opportunities to utilise biocatalysts in many more industrial processes.

The need to find 'greener' routes for producing fine chemicals has become more important in recent years; biocatalysis offers an environmentally friendly alternative to synthetic chemistry. Enzymes are proteins and hence are biodegradable, their immobilisation onto inert supports pose little to no environmental hazard. They generate fewer waste disposal problems and their mild operating conditions require a lower energy input. The lower energy usage saves on cost and the reduction of the energy input lowers emissions of greenhouse gases.

### 1.2.1. Kinetic resolutions

A process where enantiomers are separated is called a resolution. The first resolution was reported by Pasteur in 1848 when he completed the manual resolution of tartrate<sup>45</sup>. A kinetic resolution is the process where one enantiomer is more readily transformed into product than its mirror image (figure 1.2.1.1). The enantioselection is based on the difference of reactions rates ( $k_R$  and  $k_S$ ) during the transformation by a chiral catalyst to

$P_R$  and  $P_S$ . Recovery of the product  $P_R$  and the unreacted enantiomer  $S_S$  in a non-racemic form constitutes a kinetic resolution.

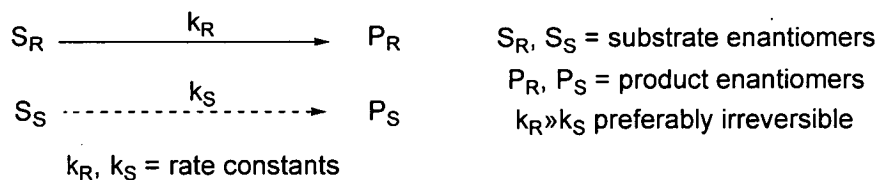


Figure 1.2.1.1. The principle of a classical kinetic resolution.

One of the most common biocatalytic methods to achieve kinetic resolutions is with the class of enzymes called lipases. They are available in bulk quantities from microbial sources and many are commercially available. Their role in nature is in fat cleavage, so it is not surprising that they have been found to be particularly useful for the resolution of esters bearing a chiral alcohol, since their natural glyceride substrates bear a chiral alcohol fragment. General guidelines have been suggested concerning lipase specificity and enantioselectivity<sup>46</sup>. In addition, the stereochemical preference of the most commonly used lipases (e.g. from *Pseudomonas* and *Candida* species) for esters of secondary alcohols follow an empirical model generally referred to as ‘Kazlauskas rule’<sup>47</sup>.

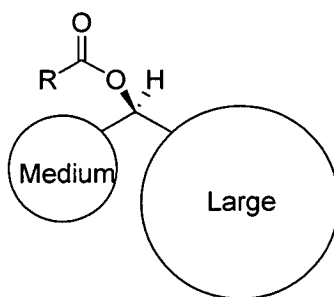


Figure 1.2.1.2. The preferred substrate enantiomer for lipase specificity according to ‘Kazlauskas rule’.

Performing lipase catalysed kinetic resolutions is often easier than chemical resolutions, which normally require a stoichiometric amount of a covalently bound chiral auxiliary.

Lipases have high stability towards organic solvents, which makes them useful in the reverse as well as the forward acylation. 1,1'-Binaphthylamine derivatives are useful chiral ligands of various asymmetric reactions, 2,2'-diamino-1,1'-binaphthyl has been used as the starting material for the synthesis of BINAP which is a chiral ligand used in the asymmetric hydrogenation of ketones<sup>48</sup>. The lipase catalysed acylation was recently reported using LIP-300 (*Pseudomonas aeruginosa* immobilised on Hyflo Super-Cel) and LPL-311 (*P. aeruginosa*) on Toyonite 200-M for the optical resolution of 1,1'-binaphthylamine derivatives-44<sup>49</sup>. The amidation was sensitive to the length of the alkyl chain between the binaphthyl ring and amino group and improved enantioselectivities were observed for increasing alkyl chain length of the R substituent on the acyl donor.

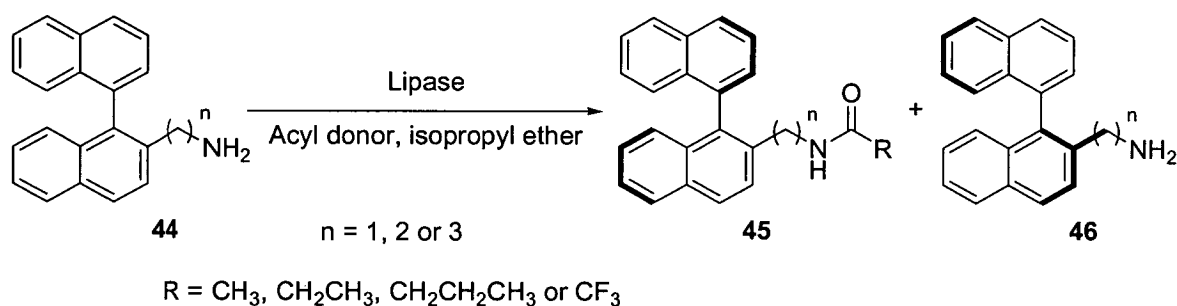


Figure 1.2.1.3. Lipase catalysed amidation of 1,1'-binaphthylamine derivatives.

The reverse of a lipase catalysed acylation is the hydrolysis reaction. Kinetic resolutions have been achieved with *Candida antartica B* lipase (CAL-B) in the hydrolysis of  $\alpha$ -hydroxy esters<sup>50</sup> (figure 1.2.1.4). Interestingly, during this study it was found that the enantioselectivity (*E*-value) varied significantly depending on the immobilisation support used. The enzyme immobilised on cyanogen bromide functionalised resin (CNBr-activated Sepharose 4BCL) gave an *E*-value of 7.4 whilst the PEI (Polyethyleneimine) derivative yielded *E*-value of 67 in the hydrolysis of  $\alpha$ -hydroxy-phenylacetic acid methyl ester-47 under similar conditions. The enantioselectivity dropped for the PEI immobilised CAL-B on reducing the temperature, but the

enantioselectivity increased for other derivatives. The difference in performance between the different derivatives of immobilised CAL-B supported the hypothesis the lipase exists in different structural forms during catalysis. It was suggested that the active site of the lipase is secluded from the reaction medium by a helical oligopeptide lid. This lid can exist either in the closed (inactive) or open (active) form and the interaction between the lipase and the immobilisation support controls the lipase activity causing the varying results amongst different supports.

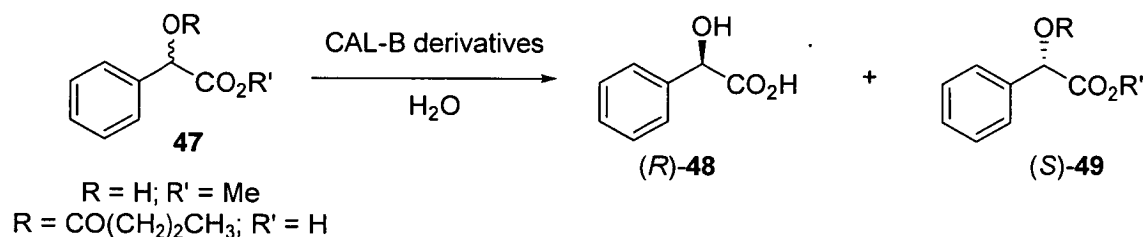


Figure 1.2.1.4. CAL-B catalysed hydrolysis of an  $\alpha$ -hydroxy ester and an  $\alpha$ -acyl acid.

The drawback of a kinetic resolution is that there is a limited 50% yield; close reaction monitoring is required because the process has to be stopped at or near 50% conversion and the product needs to be separated from unreacted substrate. These difficulties can be largely circumvented by a deracemisation. The theoretical yield is now 100% with no requirement for a separation step and monitoring can be simplified because the reaction can be left to run to completion.

### 1.2.2. Dynamic kinetic resolution (DKR)

If a second step is introduced into a kinetic resolution, allowing the two enantiomers to be interconverted, a DKR is possible (figure 1.2.2.1).

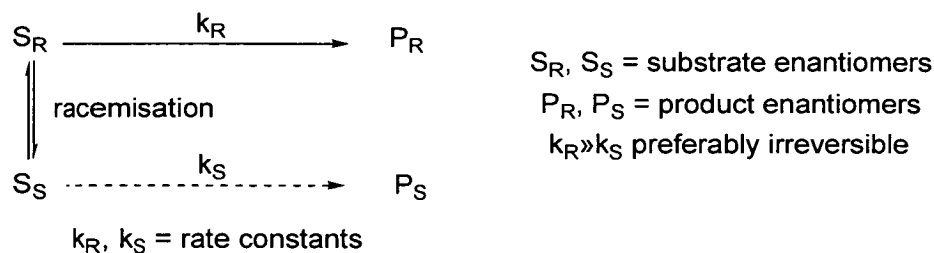


Figure 1.2.2.1. Reaction scheme of a dynamic kinetic resolution (DKR).

To avoid the necessity to undertake a stepwise racemisation and kinetic resolution iterations, an *in situ* racemisation is required. The choice of racemisation strategy falls into two classes; chemo-catalytic and bio-catalytic. The easiest and most widely used method for *in situ* racemisation involves acid/base catalysed enolisation, which is usually used for racemising the  $\alpha$ -position of a carbonyl. For chemically more stable chiral centres, such as *sec*-alcohols or *sec*-amines, direct chemical racemisation is more difficult. Instead chemically labile derivatives of *sec*-alcohols can be prepared such as cyanohydrins, hemiacetals, hemiaminals and hemithioacetals<sup>51</sup>. Alternatively stable *sec*-alcohols and amines can be racemised by an oxidation and reduction sequence with a transition metal catalyst such as Ru, Rh, Ir, Al, or Pd<sup>52</sup>. Bäckvall and co-workers have developed a system based on the use of *p*-chloroacetate as the acyl donor and ruthenium as the catalyst to allow the DKR of secondary alcohols. The acyl donor is compatible with the metal catalyst and no external base was required in the racemisation<sup>53</sup>. *Candida antartica* lipase B (CAL-B) transesterification with *p*-chloroacetate combined with the ruthenium catalysed racemisation gave (*R*)-acylated secondary alcohols-**51** in 72-98% yield and >99% e.e. (figure 1.2.2.2).

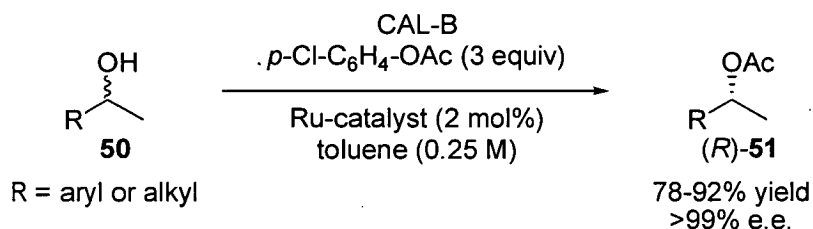


Figure 1.2.2.2. The DKR of secondary alcohols-**50** combining a metal catalysed racemisation step (chemocatalysis) and an enantioselective acylation step (biocatalysis).

The challenge of achieving *in situ* racemisations for DKRs with compounds possessing a stable chiral centre may be overcome by performing a stereoinversion. The stereoinversion relies on one enantiomer being chemically converted to an achiral intermediate. The achiral intermediate is subsequently chemically converted to the opposite enantiomer with a second step. In order to achieve the transformation of a racemate into a single stereoisomer, at least one step in the stereoinversion must be irreversible to compensate for the energetically disfavoured process. In the example shown in figure 1.2.2.3, one enantiomer of a secondary alcohol is selectively oxidised to the corresponding ketone whilst the other remains untouched. The achiral ketone is reduced in a subsequent step with an enzyme displaying the opposite stereochemical preference<sup>54</sup>.

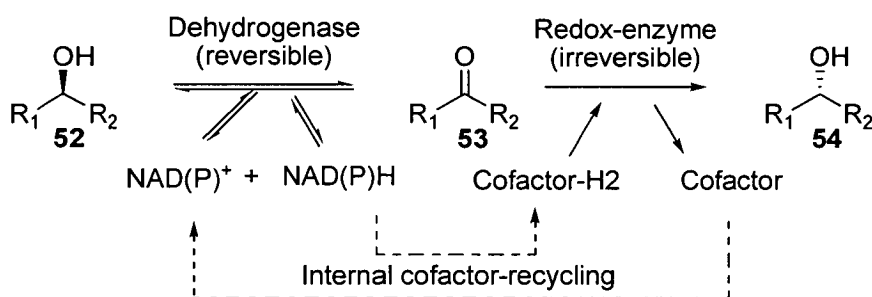


Figure 1.2.2.3. Stereoinversion of *sec*-alcohols via oxidation-reduction steps.

### 1.2.3. Deracemisation

A deracemisation constitutes any process during which a racemate is converted into a non-racemic product in 100% theoretical yield without intermediate separation of materials. According to this definition dynamic kinetic resolution (DKR), dynamic thermodynamic resolution, stereoinversion and enantioconvergent transformations of a racemate are all classified as deracemisation processes. [Examples of DKR and stereoinversion deracemisations are discussed in section 1.2.2].

An enantioconvergent transformation is where enantiomers are converted into the same product enantiomer by two independent pathways. One enantiomer is reacted giving product with retention of configuration and the opposite enantiomer is reacted with inversion of configuration to its counterpart product. An enantioconvergent process can be illustrated with epoxide hydrolase<sup>55</sup>. Epoxide hydrolysis takes place via attack of a nucleophile to either carbon atom of the oxirane ring of the (*S*)-enantiomer of (*rac*)-epoxide-55 with the structure of substrate and the epoxide hydrolase specificity determining the regioselectivity of attack.

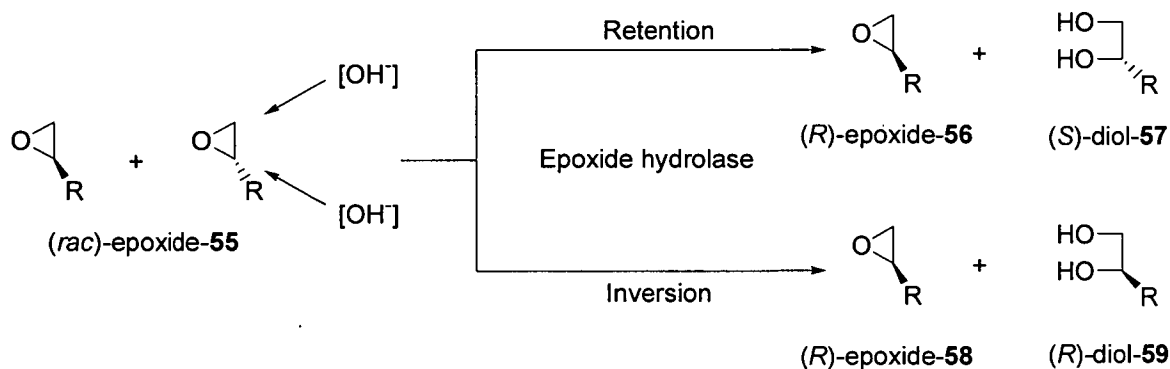


Figure 1.2.3.1. Enzymatic hydrolysis of epoxide-55 in the enantioconvergent of (*S*)-diols.

If the (*S*)-enantiomer-55 is preferentially hydrolysed from the racemate with retention of configuration, kinetic resolution gives the (*S*)-diol-57 and the unreacted (*R*)-epoxide-56. The (*R*)-diol-59 can be prepared by hydrolysis of the (*S*)-epoxide-55 by inversion of configuration. Use of the appropriate epoxide hydrolase allows the enantioconvergent hydrolysis of epoxides, for example racemic styrene oxide-66 has been deracemised by using two different epoxide hydrolases<sup>56</sup>.

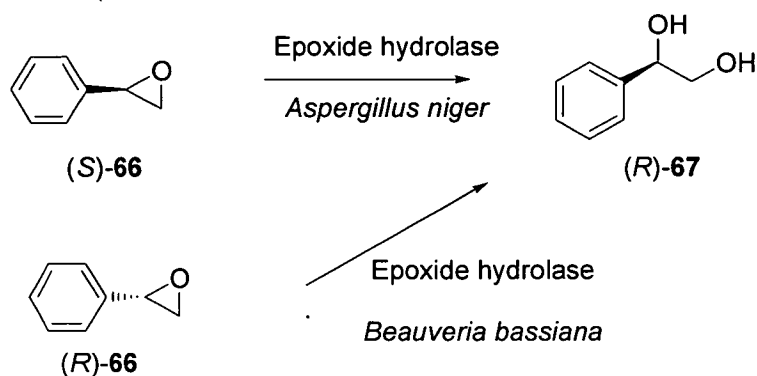


Figure 1.2.3.2. The deracemisation of (*rac*)-styrene oxide-66 through an enantioconvergent conversion of (*rac*)-epoxide with two epoxide hydrolases exhibiting different regioselectivities.

Furthermore, the enantioconvergent synthesis of diols from chiral epoxides is possible with a single biocatalyst. Epoxide hydrolase from *Nocardia* species hydrolyses both enantiomers of *cis*-2,3-disubstituted epoxyalkanes-68 and -69<sup>57</sup>. Enantioconvergence is possible because hydrolysis is performed at the (*S*)-configured oxirane carbon with inversion of configuration yielding the (2*R*, 3*R*)-diol-70 as the product.

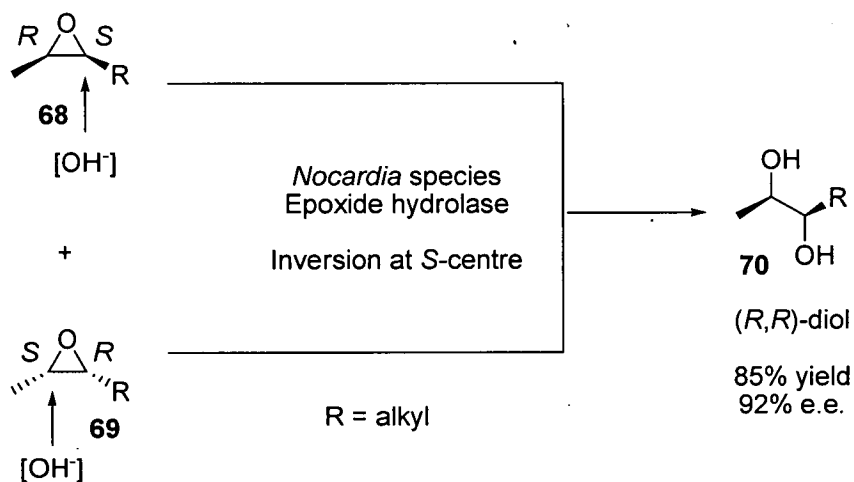


Figure 1.2.3.3. Enantioconvergent synthesis of (2*R*, 3*R*)-disubstituted diols from epoxyalkanes with *Nocardia* species epoxide hydrolase.



A cyclic oxidation and reduction sequence can allow the deracemisation of *sec*-alcohols and *sec*-amines<sup>58</sup>. This process relies on the enantioselective oxidation of the substrate (figure 1.2.3.4  $k_R \gg k_S$ ). One enantiomer of the starting racemate is oxidised to the achiral intermediate, either a ketone or imine. The oxidised product is then converted back to the alcohol or amine by a chemical reduction in a non-selective manner.

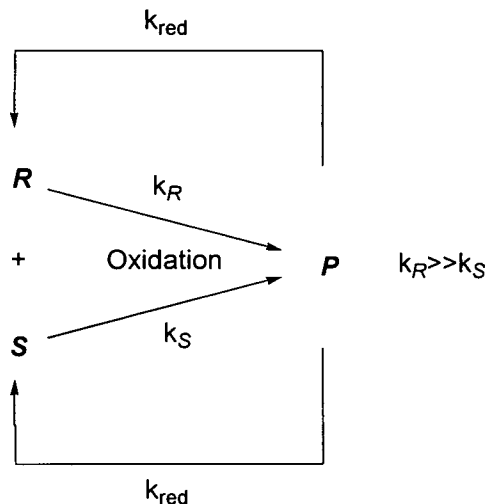


Figure 1.2.3.4. Deracemisation by a cyclic oxidation and reduction sequence.

Hafner and Wellner have reported the generation of *L*-alanine and *L*-leucine from the corresponding *D*-enantiomers with the use of porcine kidney *D*-amino acid oxidase and sodium borohydride<sup>59</sup>. Subsequently Soda *et al* extended this method for the deracemisation of *DL*-proline<sup>60</sup> and *DL*-pipercolic acid<sup>61</sup> also using *D*-amino acid oxidase and sodium borohydride. After 4 oxidation and reduction cycles the e.e. of *L*-amino acid will be over >93% from a starting racemate assuming a completely enantioselective oxidation and non selective chemical reduction.

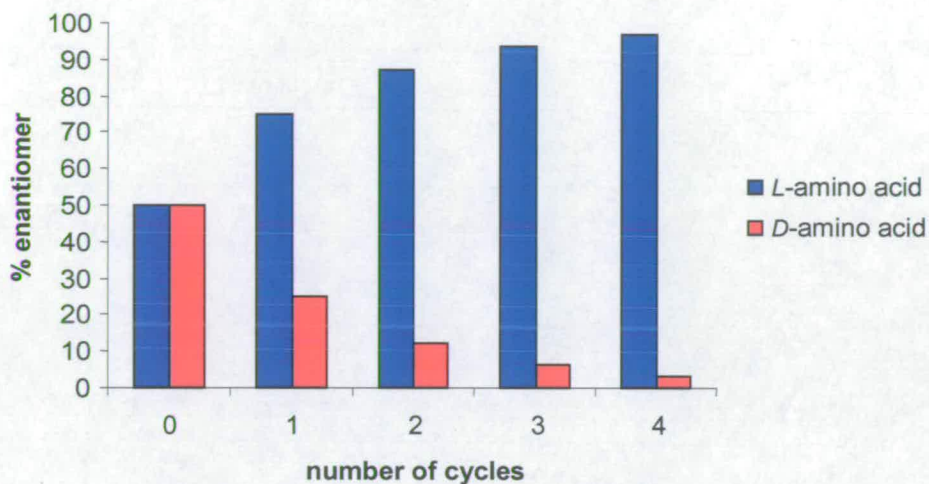


Figure 1.2.3.5. Progression of the deracemisation of racemic amino acid with *D*-amino oxidase.

More recently the deracemisation of amino acids using amino acid oxidase combined with a chemical reducing agent was extended to include cyclic and acyclic substrates, the preparation of  $^2\text{H}$ -labelled L-amino acids and the use of sodium cyanoborohydride in place of sodium borohydride<sup>62</sup>. By switching the reducing agent from sodium borohydride to sodium cyanoborohydride the imino acid intermediate accumulated, indicating that the reduction had become the rate limiting step since some hydrolysis of the imine to the corresponding keto acid was observed. It was also found that fewer equivalents of sodium cyanoborohydride were required than sodium borohydride because borohydride was less stable than cyanoborohydride under the aqueous conditions of the deracemisation. The use of catalytic transfer hydrogenation has also shown to be effective as the reducing agent in the deracemisation of amino acids with L-amino acid oxidase giving (*D*)-amino acids-71<sup>36</sup>. Extension of the deracemisation approach of  $\alpha$ -amino acids has been used in the stereoinversion of  $\beta$ - and  $\gamma$ -substituted  $\alpha$ -amino acids using the chemo-enzymatic oxidation and reduction procedure<sup>63</sup>.

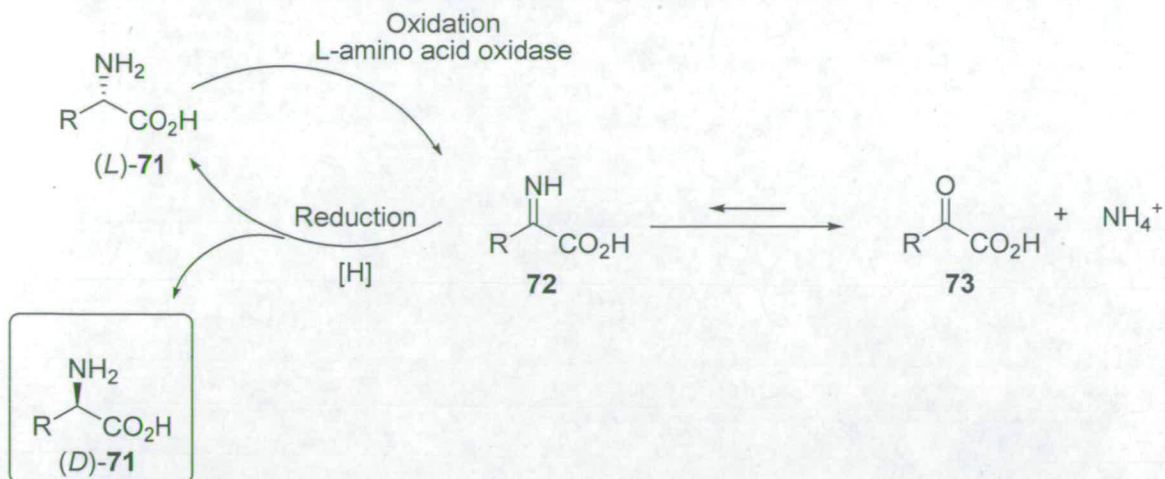


Figure 1.2.3.6. Deracemisation of (*DL*)-amino acids-71 to (*D*)-amino acids-71 using (*L*)-amino acid oxidase combined with a chemical reducing agent.

The concept of deracemisation by an oxidation and reduction sequence has recently been applied to amines. The concept has been successfully validated with the deracemisation of  $\alpha$ -methylbenzylamine-24 in 77% yield and 93% e.e.<sup>64</sup>. Although this result did suffer from a loss of yield primarily as a result of intermediate imine hydrolysis it showed in principle that amines can be deracemised in a similar fashion as has been used previously with amino acids.

#### 1.2.4. Biocatalytic routes to optically active amines

The objective of the work undertaken in this project was to develop a method for the efficient synthesis of optically active amines. There are several existing biocatalytic routes by which optically active amines can be prepared. The aim here is to highlight and provide some examples of different routes by which optically active amines can be prepared using a biocatalytic approach. The application of these routes for the preparation of chiral amines at industrial scale is also discussed.

Unlike the enzyme catalysed acylation of alcohols the corresponding acylation of amines is less explored. In 1993 BASF undertook an extensive screening of lipase catalysed acylations of amines. It was found that 1-phenylethylamine-**24** could be acylated with *Burkholderia plantarii* lipase with esters of methoxyacetic acid-**74** giving optically pure (*S*)-amine-**24** and (*R*)-amide-**75** at 52% conversion<sup>65</sup>. After separation by distillation, the (*R*)-amine was released by basic hydrolysis of the amide without racemisation, in quantitative yield. The attractive feature of this process was the broad substrate tolerance of the catalyst and a wide variety of amines have been resolved, in some cases on a multiton scale<sup>66</sup>, recycling of the undesired enantiomer by racemisation and recovery of the acylating agent help to lower the cost of the industrial process. Reetz has reported the use of an *in situ* racemisation step in the enantioselective acylation of 1-phenylethylamine using palladium on carbon at 50-55°C<sup>67</sup>. This enabled a DKR to take place giving the (*R*)-amide in 64% yield and 99% e.e.

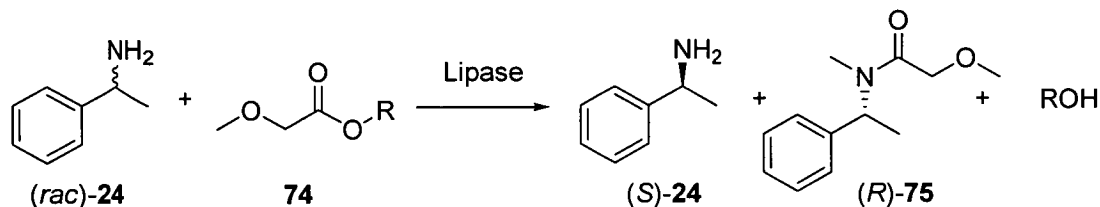


Figure 1.2.4.1. The lipase catalysed resolution of racemic 1-phenylethylamine-**24** with methoxyacetic acid esters-**74** and a lipase.

There are few reported methods for the lipase mediated enantioselective acylation of secondary amines and the resolutions that are reported tend to suffer from poor yields or poor enantioselectivities. The secondary amine 1-methyltetrahydroisoquinoline (MTQ)-**76** is a building block of YH1885-**79**, a potential treatment for GERD (gastro-oesophageal reflux disease) and duodenal ulcers<sup>68</sup>. Accessing both enantiomers was required for the development of the drug and the kinetic resolution was achieved with substituted phenyl allyl carbonates-**77** in the enantioselective acylation of (rac)-MTQ-**77** with *Candida rugosa* lipase<sup>69</sup>.

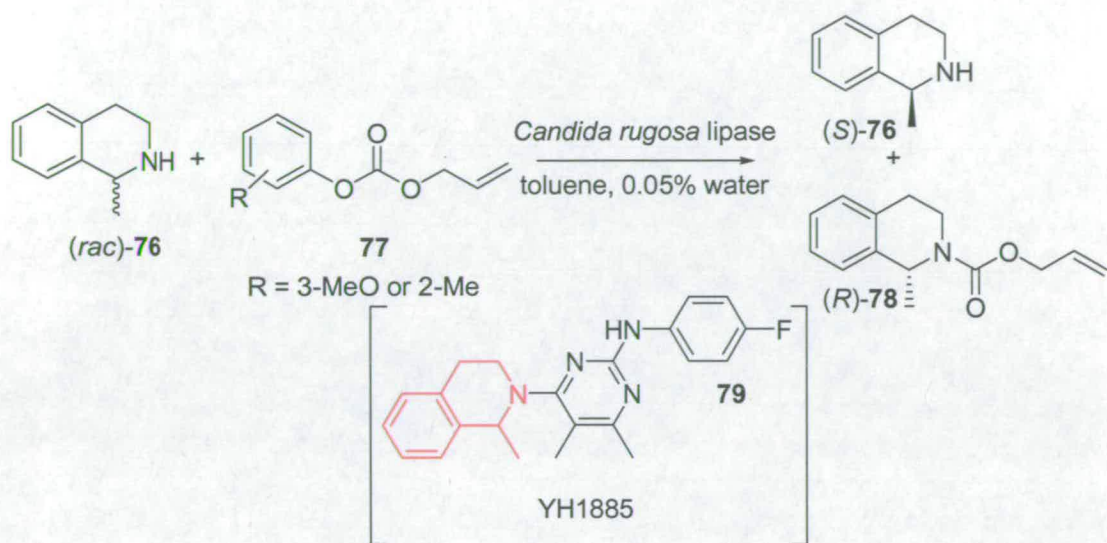


Figure 1.2.4.2. The lipase catalysed kinetic resolution of *(rac)*-MTQ-76 with a phenylallyl carbonate acyl donor-77. MTQ is a building block (shown in red) in the potential drug YH1885-79 (GSK).

Transaminases have also been used in the production of optically active amines. In this process, a carbonyl compound such as a ketone or an  $\alpha$ -keto acid is converted into an amine. The enantioselective transfer is dependent on the transaminase cofactor pyridoxal phosphate. The chemical reaction is normally performed in a two-phase system to shift the equilibrium in favour of the amine product. Celgene have developed both *(S)*- and *(R)*-selective transaminases enabling both enantiomers to be accessed<sup>70</sup>. The reaction can be carried out either as a synthesis or as a kinetic resolution. In the synthetic procedure isopropyl amine provides an amino group which is transferred to a prochiral ketone enantioselectively to give the optically active amine product. The kinetic resolution is essentially the synthesis in reverse, where the racemic amine substrate is enantioselectively converted to the ketone. The amino group is transferred to a low molecular weight aldehyde such as propionaldehyde. If  $\alpha$ -ketoacids are used in place of ketones, amino acids are obtained.

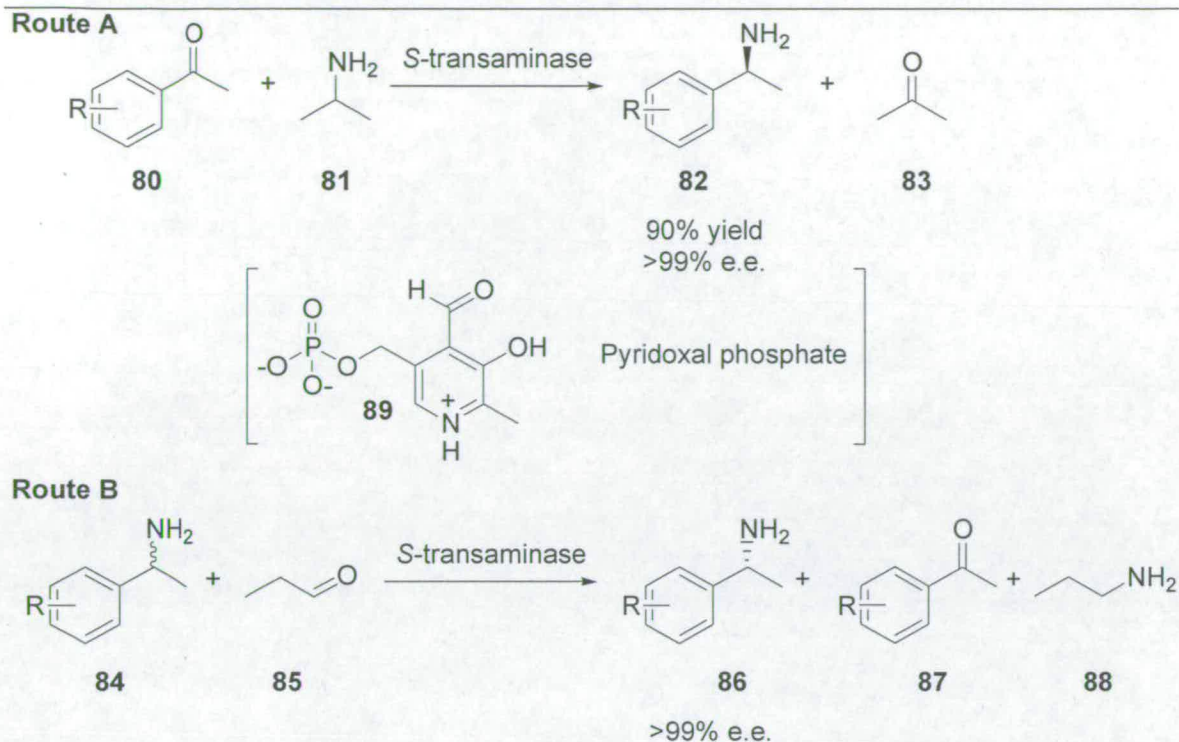


Figure 1.2.4.3. Route A is the synthesis procedure for the transamination of a prochiral ketone-**80** using a (*S*)-transaminase and isopropylamine. Route B is the kinetic resolution procedure of a (*rac*)-amine-**84** to the (*R*)-amine-**86** (Celgene).

Optically active amines can also be accessed by exploiting a class of enzymes known as amidases. Compared to the lipases however, these enzymes are less commercially available but many are found in nature and can be isolated as a microbial culture. Growing micro-organisms in simple growth media containing an amide as the sole carbon and/or nitrogen source for growth selects for amidase active micro-organisms over the remainder of the population. Following successive subculturing, the microbial population becomes enriched in micro-organisms possessing the desired amidase activity. Using this approach with *N*-acetyl-2-butylamine as the amide substrate approximately 60 organisms, predominately *Arthrobacter* species, were isolated<sup>3</sup>. A freeze dried microbial sample (BH2-N1) was shown to exhibit (*S*)-selective amidase

## Introduction

activity in the hydrolysis of racemic amide substrates. (1*S*, 2*R*)-*N*-acetyl-1-aminoindanol-**89** has been accessed by the amidase approach and this is a key intermediate of the HIV protease inhibitor Indinavir-**92** (Crixivan, Merck). This amino alcohol is also a useful ligand in asymmetric catalysis (C. H. Senanayke, *Aldrichimica Acta* (1998) **31**, 3-15).

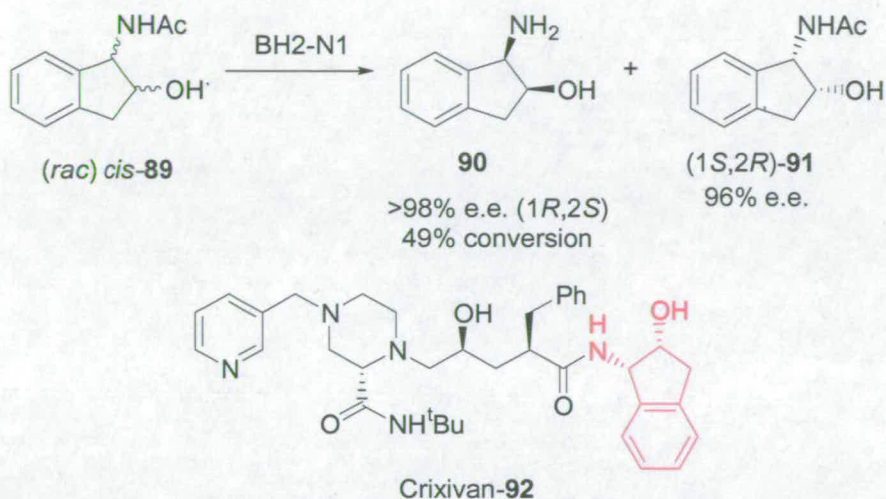


Figure 1.2.4.4. The kinetic resolution of *N*-acetyl-1-aminoindanol by BH2-N1 amidase. The (1*S*,2*R*)-enantiomer of 1-aminoindanol (shown in red) is a key intermediate in Indinavir-**92** (Crixivan, Merck).

### 1.3. Amine oxidases

Amine oxidases catalyse the oxidation of amines to ketones/aldehyde, ammonia and hydrogen peroxide through an imine intermediate (figure 1.3.1). They are classified into two groups according to which cofactor they possess and are widely distributed in nature. Type I are copper dependent and require 2,4,5-trihydroxyphenylalanine quinone (TPQ) as a cofactor, whereas type II are flavin dependent primarily comprising monoamine oxidases (MAO). In lower eukaryotes amine oxidases appear to have a clear role in providing the organism with an assimilable form of nitrogen. In humans, they play an important role in catalysing the oxidative deamination of neurotransmitters and inhibitors of MAO have been used clinically as antidepressants<sup>71</sup> and in the treatment of Parkinson's disease<sup>72</sup>.

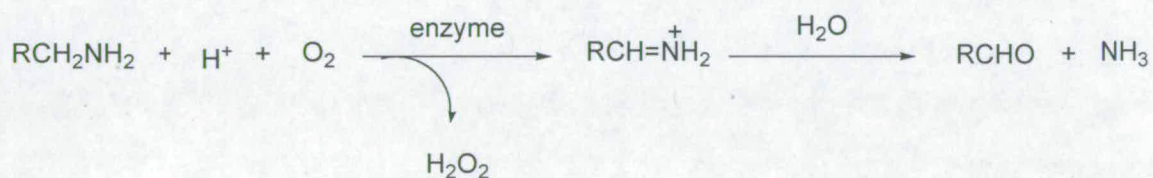


Figure 1.3.1. Reaction scheme of amine oxidation catalysed by amine oxidases.

#### 1.3.1. Flavin containing amine oxidases

MAO was first discovered in 1928 by its ability to catalyse the oxidative deamination of tyramine<sup>73</sup> and is found in a number of different tissue types<sup>74</sup>. MAO plays an important role in regulating levels of neurotransmitters in particular dopamine-**95**, serotonin-**96**, adrenalin-**93** and noradrenalin-**94**. Hence much of the published literature in this area is associated with the potential use of MAO inhibitors as antidepressants because of the relationship of neurotransmitter levels to various psychiatric and neurological disorders. The utility of MAO inhibitors was discovered serendipitously when patients treated for



tuberculosis with isoniazid showed signs of an improvement in mood; isoniazid-99 was subsequently found to work by inhibiting MAO<sup>75</sup>. The two different types of MAO in humans, i.e. type A (MAO-A) and type B (MAO-B) were first discovered pharmacologically<sup>76</sup> as MAO-A is inhibited by clorgyline-98 and MAO-B by deprenyl-7 (figure 1.3.1.1).

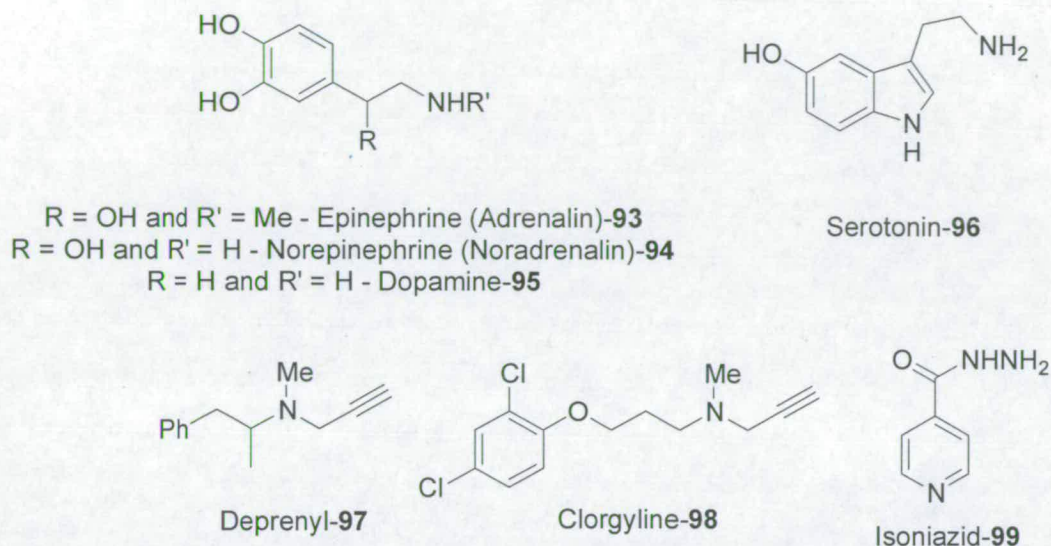


Figure 1.3.1.1. Chemical structures of neurotransmitters and MAO inhibitors.

cDNA cloning of MAO-A and MAO-B from human liver elucidated their amino acid sequences<sup>77</sup>. MAO-A and MAO-B showed high amino acid sequence identity (70%) and subunit molecular weights of 59.7 kDa and 58 kDa respectively. Both contained the pentapeptide Ser-Gly-Gly-Cys-Tyr which covalently binds the FAD cofactor<sup>78</sup>. FAD is bound by Cys-406 in MAO-A and Cys-397 in MAO-B, one cofactor for each subunit of the symmetrical dimer.

MAO-A and MAO-B are integral proteins of the outer membrane of mitochondria, which has made their crystallisation difficult. The high affinity of MAO-B for the outer mitochondrial membrane is demonstrated by the need for digestion of phospholipids for its efficient detergent extraction during enzyme isolation. Studies of MAO-B have been assisted more recently by the development of a high level expression system in *Pichia*

*pastoris*, which allowed larger quantities of purified enzyme to be prepared<sup>79</sup>. Owing to the difficulty in preparing soluble, functional membrane proteins, the three-dimensional structure of MAO-B has only recently been solved<sup>80</sup>. The crystal structure of MAO-B is complemented by the publication of the crystal structure of polyamine oxidase (PAO)<sup>81</sup>. PAO is another type II amine oxidase; it has a non-covalently bound FAD cofactor and is involved in the catabolism of polyamines such as spermine and spermidine. Polyamines are essential for cell growth and differentiation and their metabolism is the subject of research into antiproliferative drugs<sup>82</sup>. PAO and MAO-B share ~20% amino acid sequence identity and comparisons of the two proposed structures of MAO-B and PAO revealed structural similarity<sup>80</sup>. The MAO-B crystal structure has also provided a more accurate template to model the structure of MAO-A<sup>83</sup>. The structure was solved by single crystal isomorphous replacement. The results show the sites that are important for its binding to the outer mitochondrial membrane and reveal the architecture of the catalytic site.

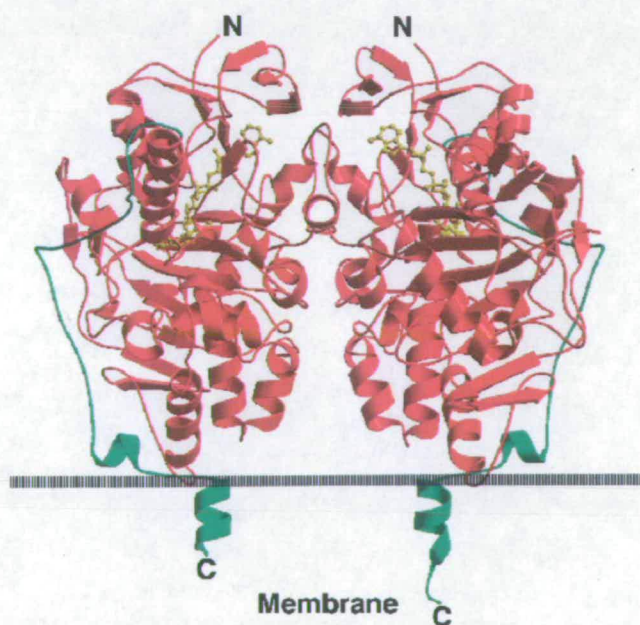


Figure 1.3.1.2. A cartoon representation of the proposed crystal structure of the MAO-B enzyme with the FAD cofactor shown in yellow and the transmembrane region in green<sup>84</sup>.

The crystal structure showed the enzyme to be dimeric with the C-terminus anchored to the outer mitochondrial membrane. The proposed structure is likely to be the quaternary structure *in vivo*, as the dimer was observed in both the orthorhombic and triclinic forms. Pargyline, an analogue of the MAO-B inhibitor deprenyl-97, binds covalently to the N5 of flavin on the *re*-face in a solvent inaccessible environment. The substrate binding is a shallow cavity of volume 420Å<sup>3</sup>, which is lined by a number of aromatic and aliphatic amino acid residues providing a highly hydrophobic environment. Adjacent to the substrate cavity is a separate smaller cavity lined with further aromatic and hydrophobic residues called the 'entrance cavity'. The recognition site for the substrate amino group is an aromatic cage formed by Tyr 398 and Tyr 435 in MAO-B where their aromatic rings are slightly turned towards the flavin<sup>80</sup>. It has been shown that point mutations in MAO-B of either the aromatic cage tyrosines to serine resulted in inactivation, but point mutations to phenylalanine retained activity with an increase in  $K_M$ <sup>85</sup>. Point mutation of the tyrosines to phenylalanine removed the hydroxyl group and the mutation to serine represents the removal of the aromatic part of the side chain.

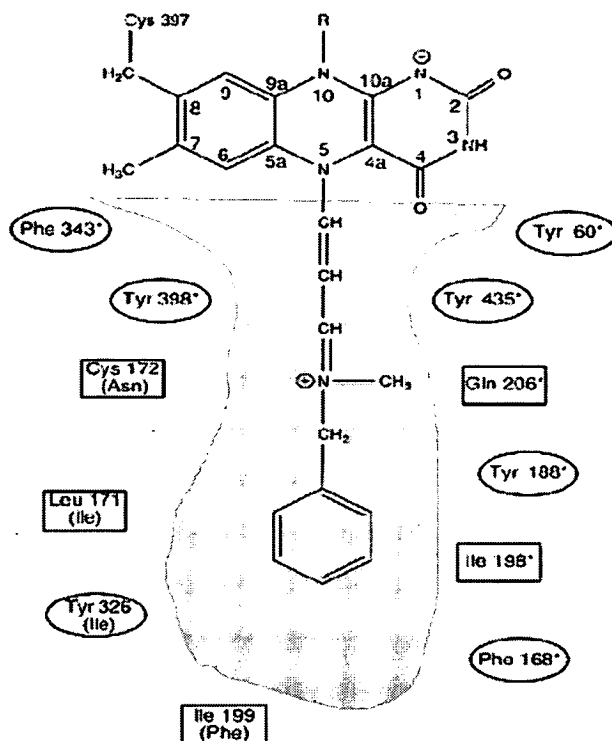


Figure 1.3.1.3. A schematic representation of the pargyline suicide inhibitor covalently attached to FAD and bound at the MAO-B active site<sup>84</sup>. Conserved residues in MAO-A are indicated with an asterisk and for the none conserved amino acids, the MAO-A amino acids are shown in brackets. Aromatic residues are in ellipsoidal frames and other residues in rectangular boxes.

The entrance cavity is shielded from the surface of the protein by a 13 amino acid long loop which is thought to regulate admission into the active site of MAO-B. It has been hypothesised that initial movement of the loop 'gated switch' facilitates binding of the substrate into the entrance cavity. This is followed by a transient movement of 4 residues which separate the entrance and substrate cavities allowing diffusion of the substrate into the substrate cavity<sup>84</sup>.

---

1,4-diphenyl-2-butene was serendipitously discovered as a competitive inhibitor of MAO-B<sup>86</sup> ( $K_I \approx 35 \mu\text{M}$ ). The novel aspect of this inhibitor compared to other inhibitors studied in the crystallisation of MAO-B is that it has two phenyl rings, meaning that one ring can be bound in the entrance cavity whilst the other is bound in the substrate cavity. Comparison of other inhibitors with 1,4-diphenyl-2-butene bound in the crystal structure of MAO-B show that the Ile-199 side chain exists in a different rotamer conformation<sup>87</sup>. The substrate binding site faces the membrane surface and the gated switch loop is partly embedded in the membrane<sup>88</sup>. In addition to the membrane-loop interaction, the membrane may increase the local substrate concentration by a favourable electrostatic attraction between the cationic amine and the anionic phosphate of the phospholipids head group. This may suggest a multifunctional role of the membrane in controlling MAO-B catalysis.

In both PAO and MAO-B crystal structures the normally planar FAD ring is bent around the N5-N10 axis. In PAO Lys-300 is hydrogen bonded to a water molecule which itself is hydrogen bonded to the N5-atom of FAD. Binding studies have shown that this residue participates in catalysis by compensating for the change in FAD protonation state during catalysis<sup>89</sup>. This interaction is conserved in MAO-B where Lys-296 undertakes the same role, it is also seen in (*L*)-amino acid oxidase and sarcosine oxidase<sup>90</sup>. In both PAO and MAO-B two aromatic amino acids form an aromatic sandwich about 8Å apart, perpendicular in orientation to FAD on the *re*-side<sup>80</sup>. Structural models of substrates bound in the active site of MAO-B and PAO suggested that the aromatic sandwich and flavin combine in amino recognition of the substrate. Circular dichroism (CD) spectra of MAO-A indicate that on binding a large inhibitor spectral changes occur that is consistent with alteration of the environment of tyrosine and tryptophan residues<sup>91</sup>. The presumption is that the perturbations of aromatic residues on binding the inhibitor are present in the aromatic cage of the substrate binding cavity in MAO.

### 1.3.2. MAO-N

Schilling<sup>92</sup> identified a novel type II amine oxidase enzyme (MAO-N) which oxidised mono-amine substrates compared to the previously reported di- or polyamines<sup>93</sup>. This enzyme was discovered from butylamine-induced cultures of *Aspergillus niger* and has subsequently been purified to homogeneity using a recombinant MAO-N expressed in *E. coli*<sup>94</sup>. The recombinant enzyme was shown to have a higher turnover of some aliphatic and aromatic amines than the mammalian enzyme. However, the major difference between MAO-N and the human MAO enzymes is that the FAD cofactor is non-covalently bound in MAO-N, as the penta-peptide present in MAO-A and MAO-B to which FAD is attached is missing in MAO-N. The non-covalent FAD attachment offers the opportunity to gain information on FAD-inhibitor adducts and their mechanism of action without the need for proteolytic digestion and purification.

### 1.3.3. Mechanism of FAD oxidation in MAO

There are three principal steps in the catalytic cycle of MAO catalysed oxidation of an amine substrate with the FAD cofactor (figure 1.3.3.1). The first of these steps is the oxidation of the substrate with concurrent reduction of FAD to FADH<sub>2</sub>. Second, is the deamination of the imine intermediate by water giving the corresponding ketone or aldehyde and ammonia (strictly this step is not enzyme catalysed but occurs spontaneously in water). Third, is the reoxidation of FADH<sub>2</sub> to FAD by molecular oxygen, releasing hydrogen peroxide and completing the redox reaction.

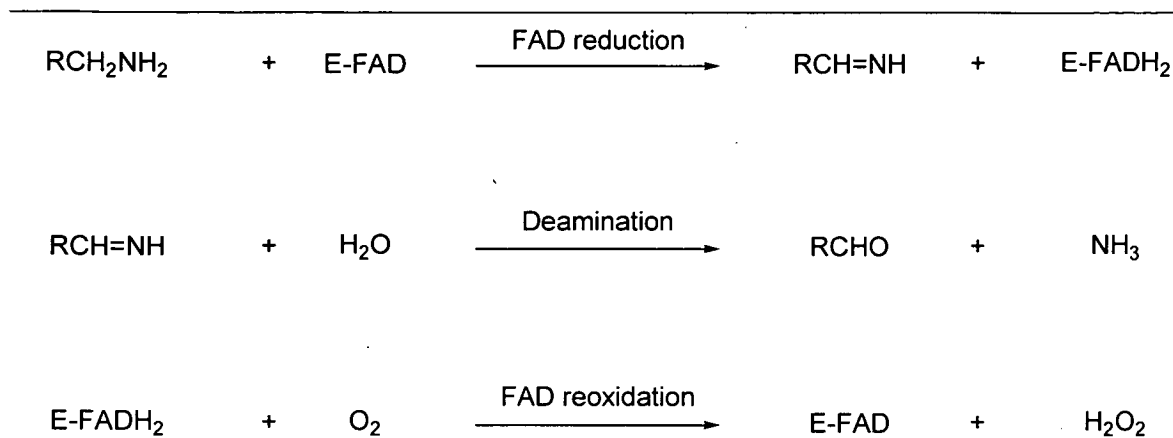


Figure 1.3.3.1. The principal steps in the catalytic cycle of amine oxidation catalysed by MAO.

Three different pathways have been proposed to describe the precise mechanism of FAD reduction and amine oxidation: (1) single electron transfer (SET) pathway, (2) hydrogen atom transfer (HAT) pathway and (3) nucleophilic (polar) pathway. The SET pathway is the generally accepted version for MAO catalysed  $\alpha$ -carbon oxidation of amines according to studies on mechanism-based inactivators<sup>95</sup>. N-cyclopropylamines inactivators initially formed an amine radical cation which is proposed to undergo rapid ring opening to form a highly reactive primary carbon centered radical. The carbon centred radical is thought to be responsible for inactivation of the enzyme. The use of <sup>14</sup>C labelled N-cyclopropylamine showed the compound attaches to MAO in a 1:1 stoichiometric ratio at the flavin or at an active site cysteine residue<sup>96</sup>.

The nature of the substrate has been shown to be important in the reoxidation of FADH<sub>2</sub><sup>97</sup>. It has been shown with stopped flow spectroscopy that a binary or ternary complex is present in the catalytic cycle. The ternary complex consisting of reduced enzyme, oxygen and product or in the presence of benzylamine and 1-methyl-4-phenyl-1,2,3,6-tetrahydropyridine the ternary complex comprised of reduced enzyme, oxygen and substrate<sup>98</sup>. There is recent spectroscopic evidence that a stable tyrosyl radical is

present in the partially reduced MAO-A<sup>181</sup>. It is thought that radical forms following single electron donation to FAD from the substrate and that the tyrosyl radical is in equilibrium with the FAD flavosemiquinone. This evidence further supports the single electron transfer mechanism for FAD catalysed oxidations.

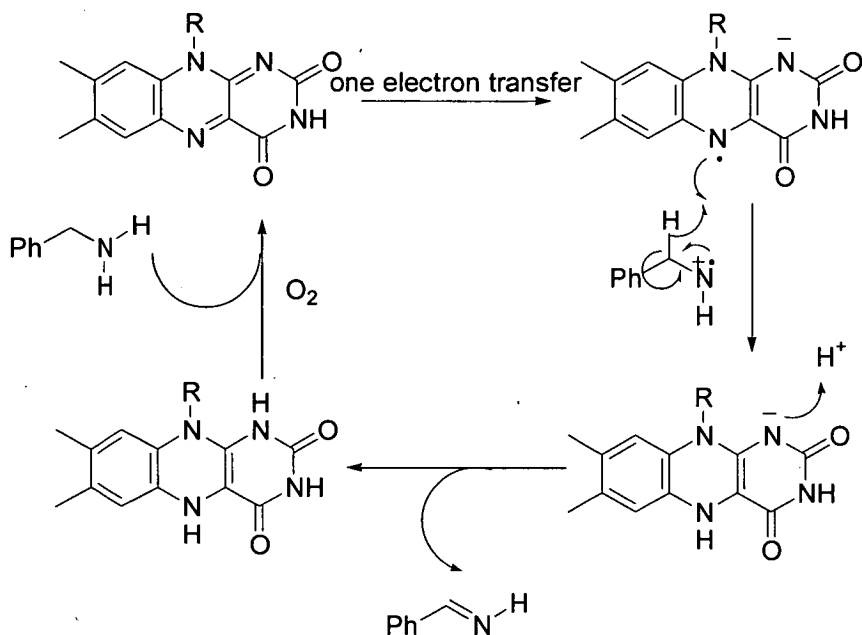


Figure 1.3.3.2. The proposed SET mechanism for amine oxidation catalysed by a FAD dependent MAO enzyme.

Debate had arisen concerning the deamination step, whether the actual product released from the active site of MAO is the imine intermediate or if imine hydrolysis occurs in the reduced enzyme-product complex<sup>99,100</sup>. Direct evidence for the release of imine from the MAO catalysed oxidation was shown with *N*-methylbenzylamine. The amine was oxidised in 1% v/v water in benzene and oxidised products were examined by capillary gas chromatography<sup>101</sup>.



### 1.3.4. Synthetic potential of amine oxidases

Owing to the synthetic potential of amine oxidases<sup>102,103</sup> and that many potential substrates have poor solubility in aqueous medium, investigations into the tolerance of amine oxidases in non-aqueous medium have been performed<sup>104,105</sup>. It was demonstrated that amine oxidases can tolerate high contents of organic solvents; in biphasic systems the enzyme was found to be located in the aqueous phase which avoids unfavourable direct contact with the nonaqueous environment. MAO-B is capable of catalysis in organic solvents containing low concentrations of water although it was unclear whether this is because catalysis is occurring in aqueous globules or dispersed in the organic solvent. Water miscible solvents tended to give very low or no conversion of amine substrate and this is thought to have arisen by loss of essential enzyme hydration by water stripping<sup>106</sup>.

### 1.3.5. Copper dependent type I amine oxidases

Copper containing amine oxidases (CuAO) contain a covalently bound cofactor 2,4,5-trihydroxyphenylalanine quinone (TPQ) cofactor which is derived from the modification of an endogenous tyrosine residue<sup>107</sup>. CuAOs contain a copper ion in the active site which is involved in the biogenesis of TPQ and in the catalytic cycle of the oxidation of amines. Despite the functional differences of CuAOs in different organisms they all share a common chemical pathway in the catalytic mechanism. The catalytic cycle requires three steps (figure 1.3.5.1); firstly the biogenesis of TPQ, secondly the oxidation of amine substrate to generate the reduced state of TPQ and thirdly the reduction of oxygen by the reduced TPQ to complete the catalytic cycle.

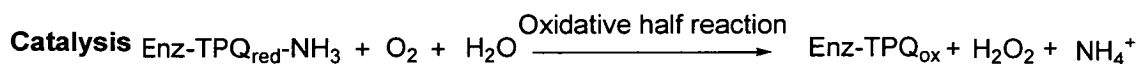
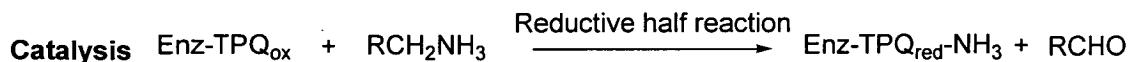
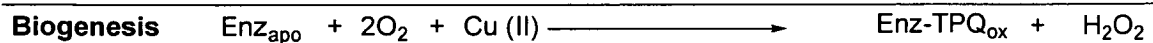


Figure 1.3.5.1. The reactions catalysed by CuAO; biogenesis of the enzyme-TPQ (Enz-TPQ) from the tyrosine precursor. The catalytic cycle is comprised of the reductive and oxidative half reactions.

TPQ formation is a self processing event synthesised with a single turnover using copper and oxygen. To probe the mechanism of TPQ formation, CuAO has been prepared in the absence of copper<sup>108</sup> but the apo-enzyme has high affinity for zinc in the absence of copper and proved extremely difficult to remove. Experimental evidence for the proposed TPQ biogenesis is based on *Hansenula polymorpha* amine oxidase (HPAO) solution studies<sup>109</sup> and x-ray crystallographic data of *Arthrobacter globiformis* amine oxidase (AGAO)<sup>110</sup>. Crystals of holo-AGAO are pink ( $\lambda_{\text{max}} = 480\text{nm}$ ) due to the presence of the oxidised form of TPQ, in contrast apo-AGAO crystals are colourless. This difference in spectral properties gives a handle to monitor the progress of TPQ biogenesis. The proposed reaction mechanism for the biogenesis of TPQ from tyrosine<sup>111</sup> is outlined in figure 1.3.5.2. The rate determining step in this pathway is the first step in which there is a high energetic cost to break the aromaticity of tyrosine by the addition of oxygen.

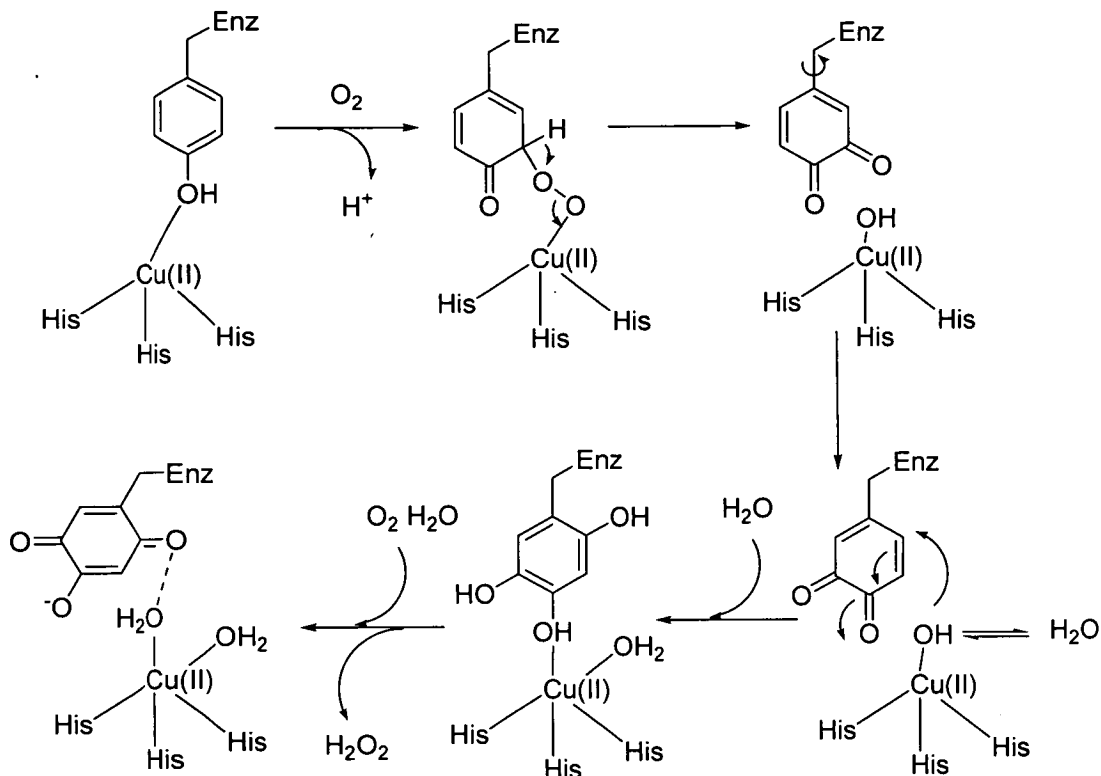


Figure 1.3.5.2. The proposed mechanism for 2,4,5-trihydroxyphenylalanine quinone (TPQ) biogenesis in CuAOs.

The first step in the reductive half reaction for CuAO catalysed oxidation of amines is nucleophilic attack of the amine onto TPQ. This results in the formation of an imine intermediate. The next step is abstraction of a proton by an active site base (a conserved aspartic acid) to give a carbanionic species which rapidly rearranges to give the imine. The aldehyde product is released by hydrolysis of the imine resulting in the TPQ being left in its reduced aminoquinol state, with the amine nitrogen replacing the oxygen at C5 of the cofactor. The TPQ ring has been reduced by two electrons and the chromophoric spectrum associated because the cofactor is now an aminoquinol. This intermediate has been trapped and a 2.4Å resolution of the crystal structure of this intermediate confirmed the existence of the reduced TPQ species. The enzyme crystals were prepared by

bleaching the CuAO anaerobically and reducing it with  $\beta$ -phenylethylamine<sup>112</sup>. This completes the reductive half reaction. To complete the full catalytic cycle in CuAO, TPQ needs to be returned back to its resting state by the oxidative half reaction.

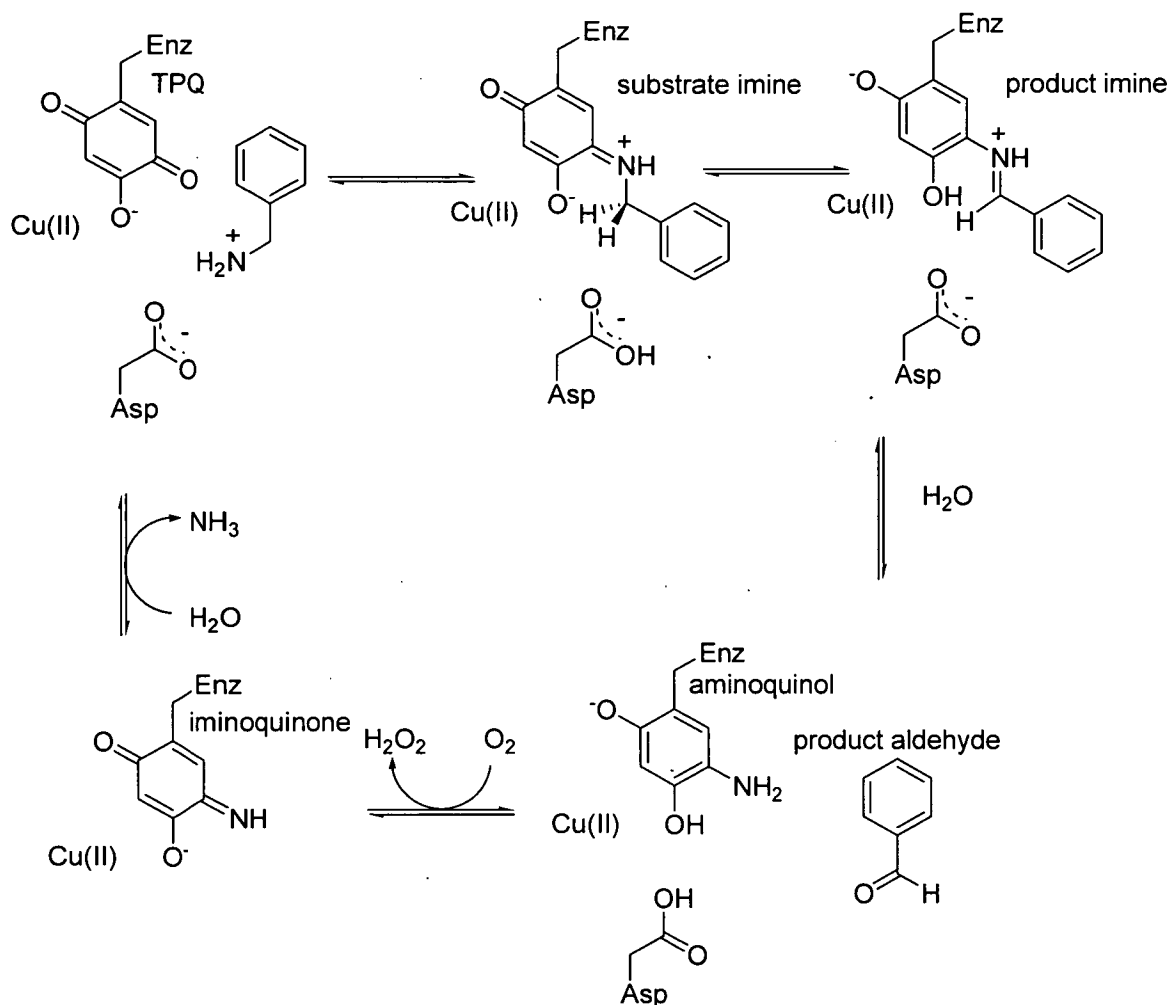


Figure 1.3.5.3. The proposed catalytic cycle of CuAO for the oxidative deamination of benzylamine to benzaldehyde.

The oxidative half reaction is less well understood than the reductive half reaction. Several studies have put forward the hypothesis that copper does not change oxidation state during the oxidative half reaction. A kinetic study with HPAO in which copper was

replaced with cobalt, gave a very similar  $k_{\text{cat}}$  with molecular oxygen even though cobalt is unlikely to participate in this redox reaction<sup>113</sup>. It has been proposed that molecular oxygen does not react with Cu (I) but instead binds in the active site and accepts the first electron from the aminoquinol<sup>114</sup>. Hydrolysis of the iminoquinone completes the catalytic cycle.

## 1.4 Directed Evolution

Enzymes that are used in synthetic chemistry as biocatalysts have evolved over millions of years to be efficient and selective catalysts for the chemical reactions taking place in living systems. Potential industrial applications for these catalysts involve substrates, organic solvents and other reaction conditions that are not encountered in nature.

Directed evolution can be used to change the properties of these natural catalysts to suit the needs of the industrial application.

Directed evolution can be considered as the laboratory equivalent of ‘survival of the fittest’, the Darwinian evolution of biological macromolecules. It comprises mutation of the gene encoding the potential enzyme accompanied by selection on the basis of the desired functional changes. It has emerged as a powerful strategy for improving the characteristics of enzymes to a desired goal. Although directed evolution is a relatively new concept with regards to improving biocatalysts in laboratories the manipulation of biological characteristics by humans has been used for many centuries. For instance, the common black and white Friesian breed of cattle was generated by selective breeding over many centuries for efficient milk production.

There are two crucial aspects to achieving the directed evolution of a biocatalyst – mutation and selection. They are combined to give rise to an improved variant and each will be discussed here in turn. The first step in directed evolution is the generation of genetic diversity and strategies for introducing mutations to give rise to libraries of variant enzymes (1.4.1). Second is the screening of these libraries to identify a variant or variants with the desired characteristic (1.4.2). After an improved variant is found it can be subjected to the directed evolution process again to either further improve the variant or select for another desired function. This concept of directed evolution comprising of iterative cycles of mutation and selection is illustrated in figure 1.4.1.

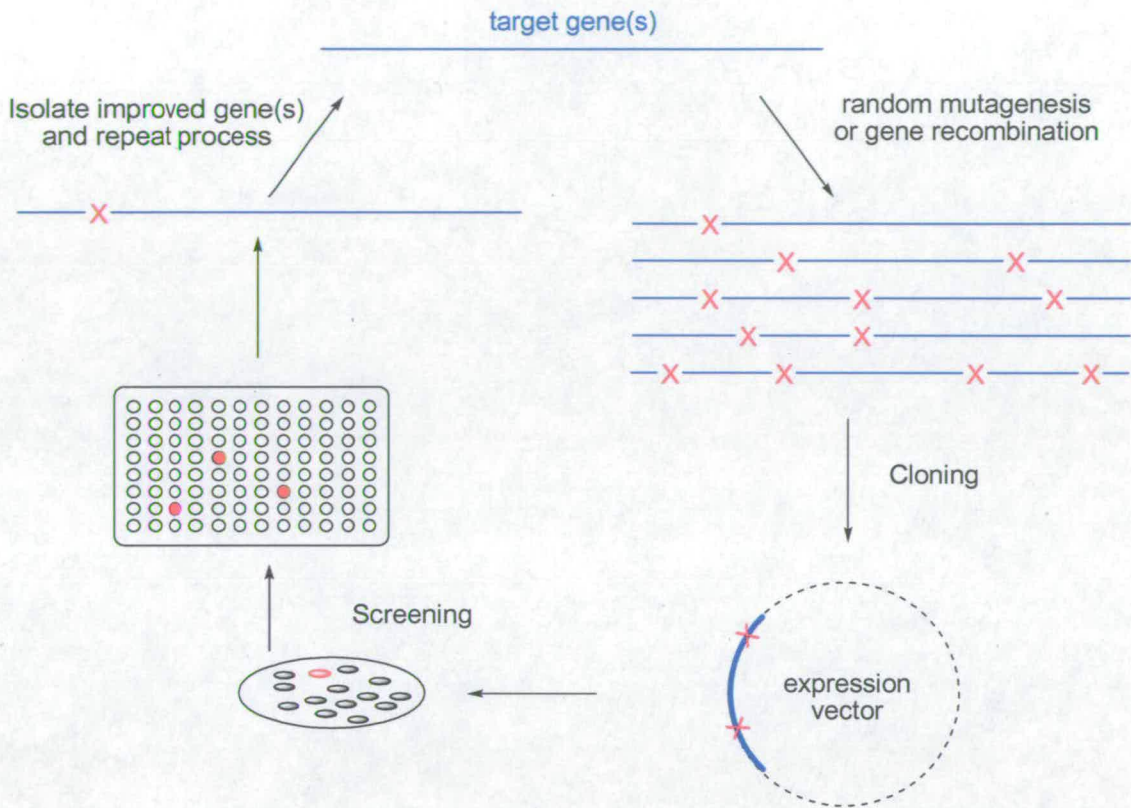


Figure 1.4.1. A schematic representation of directed evolution using genetic diversification of a target gene followed by cloning and screening to identify improved variant(s).

#### 1.4.1. Generation of variant libraries

Many different methods have been developed to generate large libraries consisting of hundreds of thousands, billions or even larger numbers of variant proteins. New approaches continue to be developed to generate more comprehensive and less biased variant libraries. Bias can arise from the uneven representation of particular amino acids in a randomised site in a protein sequence. In contrast to rational design, which generally concentrates on a small number of variants, evolutionary methods for the directed

---

evolution approach for protein engineering rely on the generation of vast molecular diversity by random mutagenesis and recombination. Rational protein design consists of making mutations to a protein that are anticipated to alter the property of the enzyme based on an understanding of the structure of the enzyme. The attractive feature of directed evolution is that there is no requirement for previous knowledge of the structure or function of the biocatalyst or when mutations are difficult to predict from the known protein structure<sup>115</sup>.

One route in which genetic diversity can be produced is from the error prone polymerase chain reaction (epPCR). epPCR was developed by a modification of the standard PCR procedure to decrease the fidelity of the PCR reaction. It is a random mutagenesis technique for generating amino acid substitutions in proteins by introducing mutations into a gene during a PCR. Mutations are deliberately introduced by the error prone DNA polymerases and/or reaction conditions. The mutated PCR products are then cloned into an expression vector and the resulting library can be screened for the desired change in the function of the protein. Increasing the concentration of magnesium or manganese chloride or by unbalancing the concentration of the four dNTPs leads to lower fidelity in the PCR<sup>116</sup>. The presence of  $Mn^{2+}$  along with an over representation of dGTP and dTTP in the amplification reaction leads to error rates of 1 to 10nt/kb in the final library<sup>117</sup>. Commercial kits based on epPCR technologies are available from Clontech (Diversify PCR random mutagenesis kit) and Stratagene (GeneMorph system) which detail instructions of mutagenesis rate required. The ease by which mutations can be generated by epPCR and the control of the mutation rate makes this method appealing as a tool in directed evolution, but a drawback with this approach is the problem of mutational bias. Transitions (purine to purine or pyrimidine to pyrimidine) mutations are more common than transversion (purine to pyrimidine or pyrimidine to purine) and as epPCR only introduces single nucleotide mutations, this can lead to a bias in the amino acid that the mutant DNA encodes. This arises from the degeneracy of the genetic code. For example, single point mutations in a valine codon can encode phenylalanine, leucine, isoleucine,



alanine, aspartate or glycine. To access the codons for the other amino acids, either two point mutations (C, S, P, H, R, N, T, M, E, Y) or even three (Q, W, K) are required. The result of this codon bias is that specific amino acid changes are more likely to occur than others while some are not represented at all in a library constructed by epPCR. The third source of bias is caused by the amplification nature of the PCR. If a mutation is introduced after the first cycle of the PCR then this will be present in 25% of the product daughter molecules. The mutated daughter molecules are amplified during the remaining PCR cycles and therefore any molecule that is copied early in the amplification process will be over represented in the final library compared with a mutation that is introduced towards the end of the PCR. This problem can be reduced by a combination of multiple reactions and reducing the number of amplification cycles. Another encumbrance with epPCR is the DNA products need to be cloned into a vector prior to screening.

Stratagene has developed a highly efficient, rapid and reproducible method for introducing random mutations into a cloned gene<sup>118</sup>. This method involves propagating the cloned gene in an *E. coli* strain called XL1-red which is deficient in three of the primary DNA repair pathways in *E. coli*, namely *mutS*, *mutD* and *mutT*. DNA polymerase is efficient in correcting many errors made during DNA replication, however a significant number of errors remain uncorrected after replication has been completed. The mismatch repair pathway is another system of repair after DNA replication. *MutS* is one of the genes responsible for correcting mismatched DNA base-pairs; its role is to recognise a base pair mismatch and to recruit other proteins involved in the mismatch repair pathway. DNA polymerase III has a subunit  $\epsilon$ , which is responsible for proof-reading (3'-5' exonuclease activity) this subunit is encoded by the *mutD* gene. The role of 8-oxodGTPase (the gene product of *mutT*) is to clean the cellular pool of dNTPs preventing the incorporation of 8-oxodGTP into DNA<sup>119</sup>. The advantage of using XL1-red for random mutagenesis is that the mutation rate can be carefully controlled and there is no cloning involved. The main disadvantage is that the XL1-red strain of *E. coli* is its genetic instability resulting in damage to the bacterial DNA. Other potential

problems can arise from introduction of mutations elsewhere because of the indiscriminate nature of the mutagenesis. Mutations on the plasmid outside the gene can also affect the screening because if they occur at a promoter region it may influence the recruitment of the RNA polymerase and therefore the expression of the recombinant protein. This leads to expression variants which can either increase or decrease the amount of protein produced.

Rather than introducing random mutations along a section DNA, another approach is to target specific positions in the target gene. These techniques are based on the incorporation of synthetic DNA within the coding sequence. The synthetic DNA can be designed to be randomised at particular positions, which can then be incorporated into the target gene. This strategy comprises of two components, firstly the preparation of the randomised DNA and secondly incorporating this DNA into the gene. Oligonucleotide based mutagenesis is reliant on the chemistry of DNA synthesis. The synthesis of oligonucleotides is a well established technique<sup>120</sup> and libraries of synthetic oligonucleotides can be prepared by mixing any combination of the four bases at the required position to generate diversity. Bias problems can occur with this approach if the mixtures of reagents do not react to the same degree giving rise to the greater incorporation of one reagent over another. Another bias problem is the triplet nature of the genetic code. To randomise a codon to all of the possible 20 amino acids, a mixture of four bases is required at the first and second positions of the codon. Also there are six times as many codons represented by serine than tryptophan or methionine in the genetic code which further skews the bias towards particular well represented amino acids. The solution to this problem is to simply synthesise the DNA separately for each mutation, but this approach is only appropriate for limited small libraries, i.e. one codon. It is not necessary to fully randomise all three bases of a codon to represent all twenty amino acids. If an NNS codon is prepared (where N is any of the four DNA bases and S is either C or G) each amino acid is represented at least once, whilst reducing the number of stop codons. The other benefit with the NNS codon approach is that it decreases the

number of variants to be screened at the randomised position. Alternatively, trinucleotide phosphoramidites can be used so that 20 codons (one to represent each amino acid) are introduced into the oligonucleotide. Trinucleotide phosphoramidites are not straightforward to synthesis and this adds to the cost of preparing oligonucleotides by this route<sup>121</sup>.

The MAX system relies on the annealing of oligonucleotides to specific regions of a gene, with a completely randomised codon (NNN) at the desired target<sup>122</sup> (figure 1.4.1.1). If all 20 amino acids are required then the 20 primers for each position are synthesised, one codon for each amino acid. These primers are annealed to the template according to their adjacent complementary sequence. The ligated primers are converted to dsDNA ready to be incorporated into the full gene. The advantage of this is that the attractive features of the trinucleotide phosphoramidite approach can be used without the significant costs. Although a relatively large number of primers are required, the maximum number of primers required to randomise each amino acid is 20 and the library size required to be screened is reduced compared to conventional libraries with codon bias.

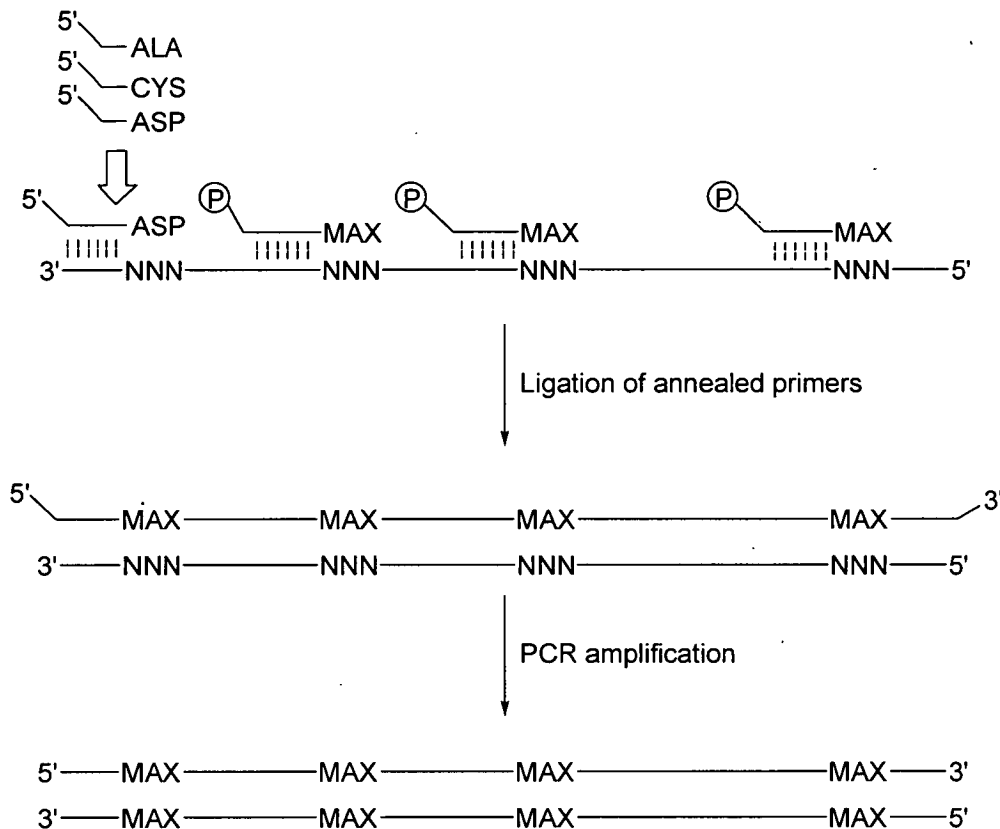


Figure 1.4.1.1. MAX method of library generation. The template contains the NNN sites (where N is G, C, T or A) selected to be randomised. A selection of primers for each position is added to represent each amino acid once (denoted as MAX). Primers are annealed, ligated and finally converted into dsDNA ready to be incorporated back into the gene.

Incorporation of the randomised oligonucleotide into the gene is necessary to prepare the library of variants. The basic requirement for a successful cloning of the mutated DNA into the gene is that a low level of wild type sequence is present in the cloned library. A high incidence of wild type in the cloned DNA library would suggest either the cloning or mutagenesis was unsuccessful. A range of straightforward techniques are available for incorporating DNA into full length genes such as the PCR-based techniques overlap extension and megaprimer protocols<sup>123,124</sup>.



Natural evolution exploits recombination to bring together advantageous mutations and separate out deleterious mutations. DNA shuffling was the first laboratory recombination technique that was used for directed evolution<sup>125,126</sup>. DNA shuffling allows the recombination of a collection of genes containing different point mutations or a pool of genes with sequence similarity from different sources. In DNA shuffling, the genes are digested with DNase to give gene fragments which can then be shuffled. The number of crossover points can be controlled by selecting the degree to which the genes are digested. The mixtures of DNA fragments are then subjected to repeated cycles of melting, annealing and extension. The product DNA is PCR amplified to generate adequate quantities of DNA for transformation to allow screening. More recently the DNA shuffling method has progressed with a number of other similar techniques emerging based on linking gene fragments together<sup>117</sup> a few examples of which are discussed below.

One such approach is the staggered extension process (StEP) which also relies on repeated cycles of melting, annealing and extension to build up the full length gene<sup>127</sup>. In StEP fragments of the gene are added to a growing strand of DNA. This is made possible by preventing the growing strand completing the gene extension, by use of a very short extension time in the PCR. Partial elongation of the gene results, which is then melted and re-annealed to a different template leading to a crossover. Balancing the yield and recombination can be challenging in StEP. If the extension step is too long, full length template is produced and if extension times are too short the yield of mutated DNA can be reduced<sup>117</sup>.

Random chimeragenesis on transient templates (RACHITT) is a further variation of DNA shuffling<sup>128</sup>. The fragments in this case are brought together to form one product strand. The fragments are then reassembled by annealing together on a parental strand, mismatched sections are removed, the fragments extended and ligated to give full length recombined genes. Large numbers of crossovers are possible with this method. The

drawbacks with the RACHITT technique is that the overlapping regions between fragments need to be removed by exonuclease digestion and the RACHITT method is limited to incorporation of sequence elements that are similar to the template. The principles of DNA shuffling, StEP and RACHITT are shown in figure 1.4.1.2.

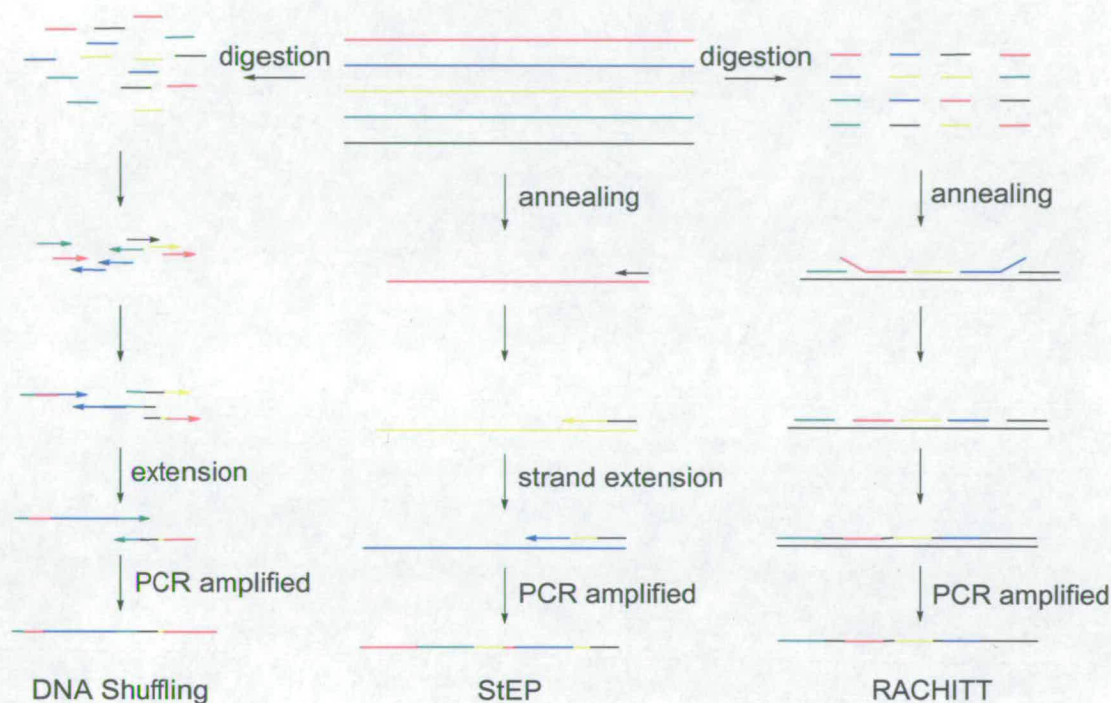


Figure 1.4.1.2. Gene recombination methods for creating mutant libraries of genes. All originate from a selection of parental genes.

It is more challenging to generate recombination events when the sequence homology between genes selected to be recombined is low. DNA shuffling techniques suffer from the inherent necessity that they require strand extension and annealing to a template. Incremental truncation for the creation of hybrid enzymes (ITCHY) was developed for shuffling parental genes with low sequence homology<sup>129</sup>. It is based on the direct ligation of libraries of fragments generated by the truncation of two DNA template

sequences. One fragment is digested with exonuclease III and S1 nuclease from the 5'-end of the gene and are ligated to fragments of a second template that have been digested from the 3'-end. The ligation is introduced at arbitrary sites and because the two ends required no template, there is no requirement for any homology. The initial ITCHY method was further developed to the thio-ITCHY, where the phosphates of the DNA are replaced with phosphothioate bonds. This was necessary as the exonuclease digestion to prepare the truncated templates was difficult to control and optimise. Incorporation of random exonuclease resistant phosphorothioate linkages into the DNA determine the length of the truncated fragments to be ligated<sup>130</sup>. The other benefit with the thio-ITCHY method is that this method has been developed to remove the inherent problem of out-of-frame shifts ligation products.

One of the crucial issues with recombination events in shuffling DNA fragments between genes is deciding on the location of the crossover site. Arnold and coworkers have reported the approach of using crossover points that have minimal interaction with the rest of the protein<sup>131</sup>. By scanning the known three dimensional structure of a protein for local networks of interactions, favourable recombination points between proteins that minimise the disruption of favourable steric and electrostatic interactions can be located. In one example the resultant libraries of  $\beta$ -lactamase variants were shown to contain a higher proportion of functional proteins than by using random crossover points<sup>132</sup>.

### **1.4.2. Screening methods**

To determine whether each individual candidate has the desired property of the target biocatalyst, the DNA library is assayed using biochemical or biophysical methods; this process constitutes a screen. There are three main types of a selection in a screen, a life or death selection, a colorimetric/fluorometric screen or a microbial screen. A life or death selection has the advantage compared to the other screens that only those variants showing the desired enzyme function are represented since those variants not meeting

the selection requirements are not viable. The disadvantage with a life or death selection is that this often requires 'knock-out' strains of the host organism to be engineered which adds to the effort and time for the screen. A colorimetric screen has the advantage that the host organism requires no genetic engineering, each variant is assayed for activity based on the detection of a chemical response arising from a hit variant. A microbial screen is where each variant is analytically examined requiring detection of product by HPLC, GC, capillary electrophoresis, mass spectrometry, NMR or other analytical techniques. The throughput of the microbial screen is normally the lowest of the three selection strategies since each member needs to be individually analytically examined. This often needs expensive instrumentation and involves at least some degree of human handling, both of which limit the throughput of the screen. The advantage with a microbial screen is that should a colorimetric/fluorimetric or life and death selection not be possible a microbial selection is normally possible.

The potential number of candidates that can be generated in a variant DNA library can be vast, so it is imperative that the highest throughput screen as possible be employed. Often the screen is the limiting factor in assessing the number of library members of a variant library. A high quality screen should be flexible and versatile so that experimental conditions of the screen can be changed to allow selection of variants with the desired improvements. Typically, improvements which may be observed are for example, activity of variants in a non-natural environment or improvement of activity to novel substrates. It is preferable for screening to be carried out in parallel and within a short time frame to accelerate the throughput of the screen and thus enable greater numbers of variants to be assessed. Some of the different approaches used in screening are discussed below.

Most high throughput assays are based on chromogenic and fluorogenic substrates or sensors. For example, umbelliferone-**104** is a fluorogenic phenol and is strongly fluorescent due to the blue emission of the phenolate anion. The  $pK_a$  of umbelliferone is



low ( $pK_a \sim 7$ ) and so the substrate fluoresces in buffer at pH 6.5 or lower, although esters and ethers of umbelliferone are not fluorescent. This has been used to assay lipase and esterases to detect ester hydrolysis by release of umbelliferone<sup>133,134,135</sup> (figure 1.4.2.1). The same concept of release of a chromogenic product by ester hydrolysis is used with *p*-nitrophenol rather than umbelliferone, where rather than releasing a fluorogenic substrate, a yellow chromogenic product is released.

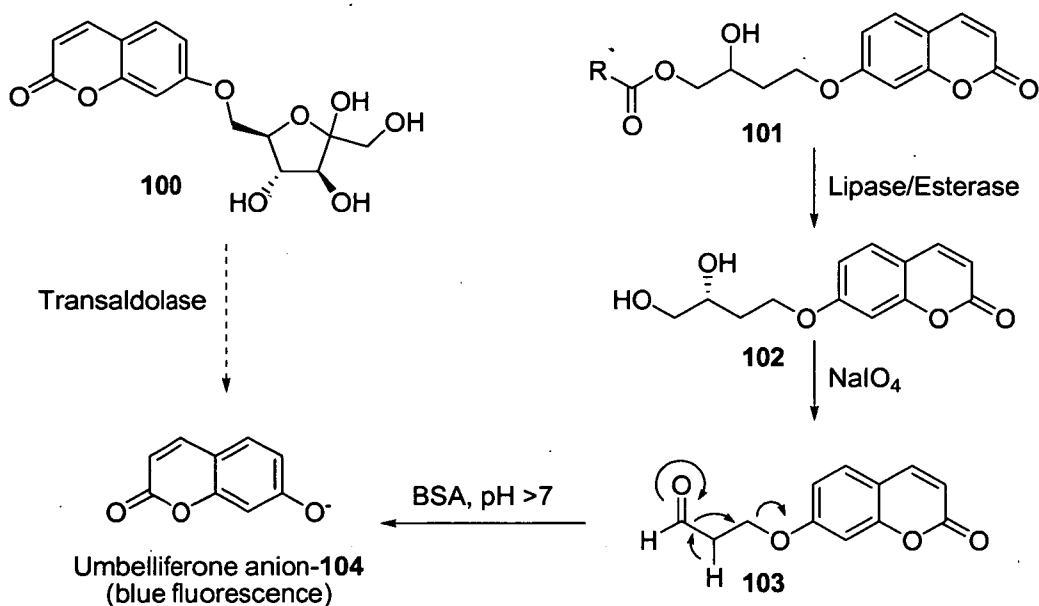


Figure 1.4.2.1. Umbelliferone-104 can be used to monitor enzyme activities by  $\beta$ -elimination of the enzymatic product. The diol product-102 generated by enzymatic cleavage of the ester-101 is oxidised to an aldehyde-103 by sodium periodate which eliminates to give the fluorescent product.

Fluorescein and 4-nitrobenzofurazane derivatives are other fluorogenic labels that can be used to monitor rates of enzyme mediated reactions. Fluorescein fluorescence autoquenches between different substrate molecules when they are fixed in close proximity. This feature was employed to follow the proteolysis of fluorescein isothiocyanate derivatised casein where fluorescence occurs upon release of the

fluorescein from casein<sup>136</sup>. For 4-nitrobenzofurazane the nature of the substituent strongly influences the fluorescent properties of the chromophore. Amide hydrolysis by acylases has been monitored with 7-chloro-4-nitrobenzofurazane-**107**<sup>137</sup>. Alternatively, 7-hydrazino-4-nitrobenzofurazane-**111** allowed the monitoring of acetaldehyde-**110** release from a vinyl ester-**109** by hydrolysis with lipases<sup>138</sup> (figure 1.4.2.2).

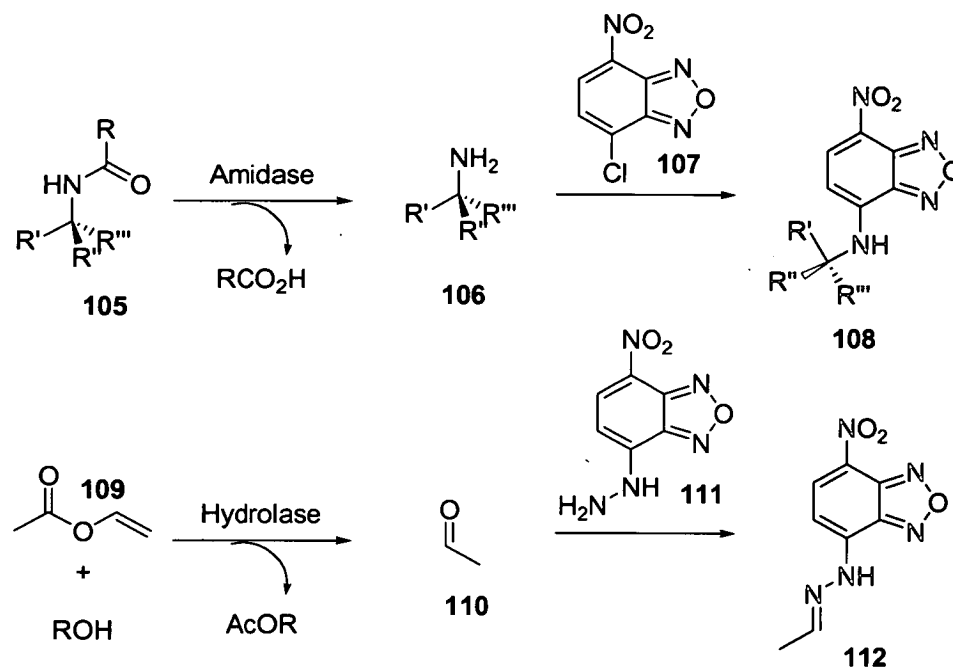


Figure 1.4.2.2. Fluorescent 4-nitrobenzofurazane derivative assays for the detection of the production of amines and aldehydes.

In addition to colorimetric screening a new digital imaging spectrophotometer called Kcat Technology (KAIVOS Scientific Inc.) has been developed. Kcat Technology allows the high throughput solid phase assay of microbial libraries expressing variant enzymes undergoing directed evolution (figure 1.4.2.3). Each microcolony is analysed simultaneously at a single pixel resolution (75 $\mu\text{m}$ /pixel). This allows nearly confluent plates with microcolonies densities of 500 colonies/ $\text{cm}^2$  to be screened. The benefit of this technology is that for each pixel it is possible to plot a kinetic profile and thereby

rank in order the relative performance of hits identified in the screen, which is not facile with a regular plate based screen.

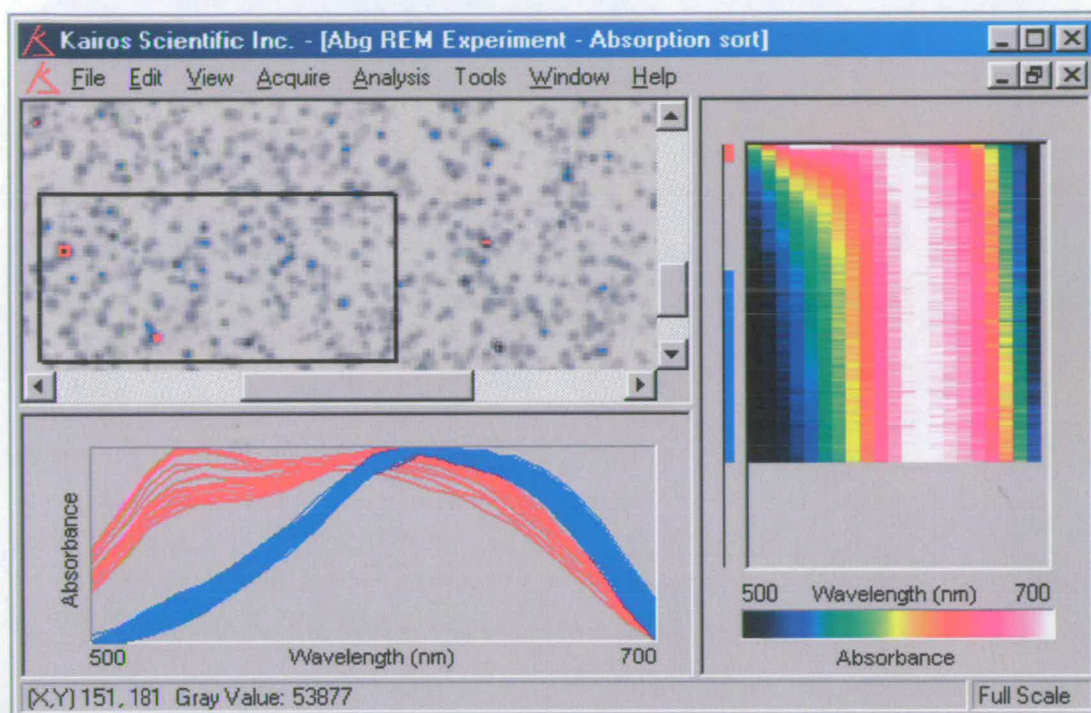


Figure 1.4.2.3. The graphical interface of the Kcat instrument with an enlarged plate based assay. Pixels with microcolonies responding in the assay are further categorised by their catalytic velocity<sup>139</sup>.

Isotopic labels have also been used to determine enantioselectivity of nitrilase enzymes<sup>140</sup> (figure 1.4.2.4). The reaction of <sup>15</sup>N-labelled 3-hydroxyglutaronitrile-113 pseudo-prochiral enantiomers can be used to assay the enantioselectivity of nitrilases using mass spectrometry. Isotopically labelled pseudo racemic substrates have also been used in high throughput screening using <sup>1</sup>H-NMR<sup>141</sup> and FT-IR<sup>142</sup>.

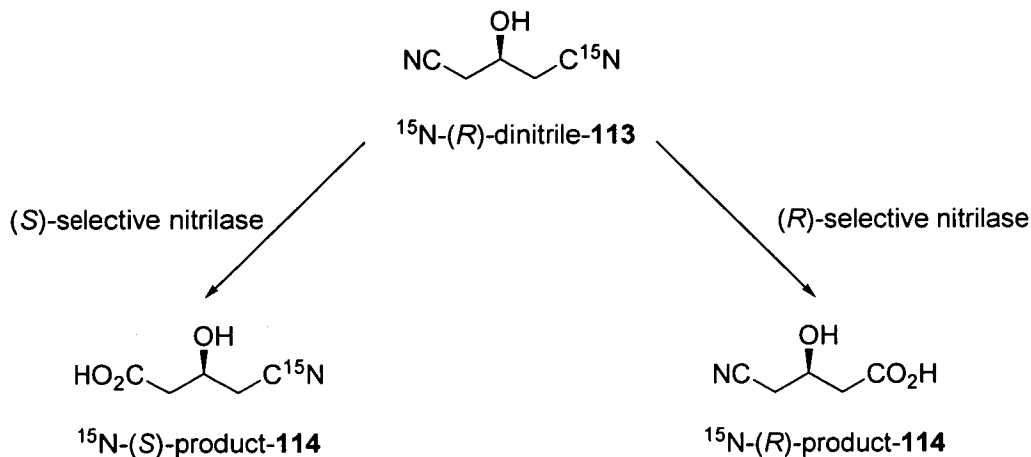


Figure 1.4.2.4. Determination of the enantioselectivity of nitrilase enzymes using isotopically labelled pseudo-enantiomers of a prochiral substrate.

Although many of these fluorogenic and chromogenic screens are amenable to automation and can be performed in parallel on microtitre or agar plates, these screening technologies are only able to screen a limited number of mutants, typically not exceeding several hundred thousand. Sophisticated approaches to analyse protein-ligand interactions have become available, in particular fluorescence activated cell sorting (FACS). Using flow cytometry, much larger libraries of variant enzymes can be screened (up to  $10^9$  variants) to detect expression levels, stability, ligand binding and catalysis<sup>143</sup>. Flow cytometry is a means of measuring certain physical and chemical characteristics of cells or particles by optical density or fluorescence as they travel in suspension one by one past a sensing point. As well as measuring optical properties, it is possible to measure physical characteristics such as cell size, shape and internal complexity. If a cell of interest is detected, the cytometer waits until the cell has travelled to a point in the flow where it has become a droplet and the instrument then charges the stream. The sorted cell droplet now carries a charge that is different to the rest of the stream and this either reflected or attracted to the correct holder by an electrical field. Using this

approach FACS is capable of sorting at a rate of 30,000 cells per second<sup>143</sup> so is a particularly high throughput (figure 1.4.2.5).

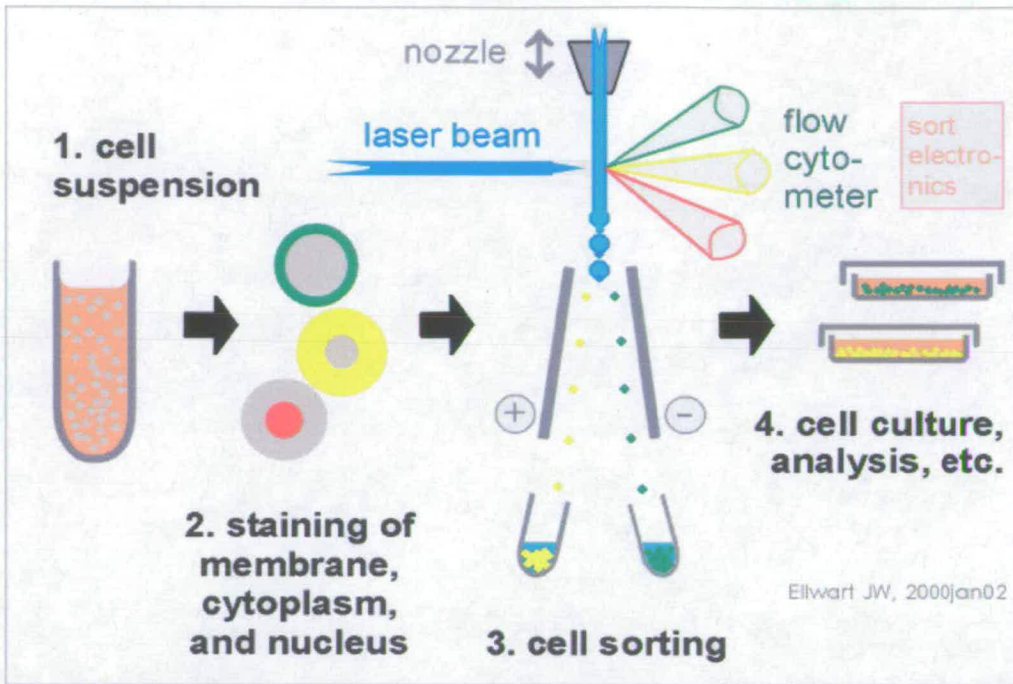


Figure 1.4.2.5. The FACS principle for sorting cells in solution<sup>144</sup>.

The use of GFP (green fluorescent protein) is another popular way of monitoring enzyme activity by FACS. Schultz and co-workers have described the application of GFP and FACS to identify the introduction of unnatural amino acids into proteins<sup>145</sup>. This work evolved aminoacyl-tRNA synthetase to accept unnatural amino acids to charge tRNA molecules to translate the unnatural amino acids into proteins. FACS was used to screen synthetase variants to identify variants that were able to accommodate *p*-isopropylphenylalanine, *p*-aminophenylalanine, *p*-carboxylphenylalanine or *O*-allyltyrosine from a mutant library of  $10^9$  clones. The screen relied on the ability of the synthetase to incorporate an unnatural amino acid at a stop codon during the translation of GFP.

---

To discover a GAT enzyme a search of *Bacillus* species incubated with glyphosate and acetyl CoA was performed<sup>146</sup>. The acetylation of glyphosate was measured by mass spectrometry. *Bacillus licheniformis* was identified as the optimal strain which accumulated the greatest reproducible levels of *N*-acetylglyphosate. The gene responsible for the acetylation was isolated by assaying recombinant genomic DNA fragments and the active fragments contained a 438 base pair open reading frame that had similarity with other *N*-acetyltransferase enzymes. Three parental GAT enzymes were identified by BLAST search and analysis. The ability of each to acetylate glyphosate was found to be in range  $k_{cat}$  of 1.0 to 1.7  $\text{min}^{-1}$  with a  $K_M$  of 1.2 to 1.8mM at pH 6.8 and 21°C. The average enzyme efficiency ( $k_{cat}/K_M$ ) was 0.81  $\text{min}^{-1}\text{mM}^{-1}$  which was too inefficient to be used as a GAT enzyme to protect transgenic crops from glyphosate; however it provided a starting point for directed evolution by gene shuffling.

The *gat* coding regions were PCR amplified, fragmented and reassembled in a primerless PCR reaction<sup>147</sup>. Shuffled variants were assayed and those that accumulated more *N*-acetylglyphosate than the parental controls had their genes shuffled again in iteration. Several GAT enzymes from the third iteration showed ~100 fold improvement in  $k_{cat}/K_M$  compared with the parent enzymes. This was sufficient to allow the recombinant *E. coli* to grow in 5mM glyphosate. However, this improvement was still insufficient to enable transgenic plants to grow in the presence of glyphosate. Further rounds of gene shuffling resulted in continual improvements in  $k_{cat}$  but the  $K_M$  failed to decrease below 0.5mM. An epPCR approach to create variant libraries was used to find a variant with a lower  $K_M$  without success. To solve this problem a dual method was engaged. Firstly, a functional prescreen was used which allowed the screening of  $10^6$  variants (compared with 5000 using the mass spectrometry screen) eliminating all but those containing highly active variants. The prescreen was based on a life or death selection, recombinant *E. coli* expressing GAT variants were treated with glyphosate and only those that survived were further assayed. Secondly, the genetic diversification in the further iterations of DNA shuffling was increased by using the natural genetic variability

In concluding there are various screening technologies available that can be used in a screen. Each method has benefits and drawbacks and the most appropriate method should be selected individually for each case to best suit the conditions of the screen. Furthermore it is imperative that the method chosen is high throughput and is sensitive enough to monitor the production of product or products to maximise the numbers of candidates that can be examined.

### 1.4.3. Progress in directed evolution

Directed evolution has emerged as an efficient way to develop new biocatalysts. A few examples are discussed below which demonstrate the application of directed evolution in discovering and enhancing biocatalysts.

Glyphosate-**115** (Monsanto's Roundup®) is a herbicide which inhibits the enzyme enolpyruvylshikimate-3-phosphate synthase (EPSPS). This enzyme is important because it is involved in the biosynthesis of aromatic acids making glyphosate a potent herbicide. Plants can gain tolerance towards herbicides by metabolic detoxification through chemically modifying the plant toxin. Glyphosate tolerance crops have been engineered to withstand glyphosate treatment, but the glyphosate remains in the plant where it can interfere with reproductive development and can lower crop yield. If glyphosate is *N*-acetylated, the *N*-acetylglyphosate-**116** is not herbicidal and is not an effective inhibitor of EPSPS. If a glyphosate *N*-acetyltransferase (GAT) enzyme could be found it could provide a route to detoxification of glyphosate, which would allow spraying during reproductive development and give more robust tolerance (figure 1.4.3.1).

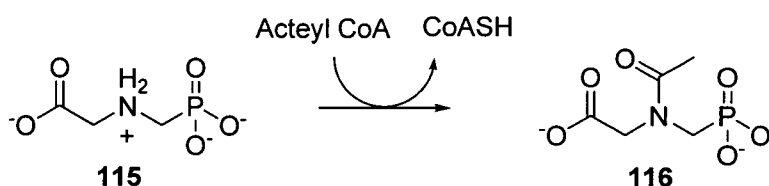


Figure 1.4.3.1. The *N*-acetylation of glyphosate-**115** with a GAT enzyme.

in related hypothetical proteins. Synthetic libraries from predicted *B. subtilis* and *B. cereus* sequences, based on the best GAT variant of the 4<sup>th</sup> generation, were incorporated as templates to increase diversity. The resultant fifth iterative library produced a variant with a  $K_M$  of 0.05mM. The rounds of iterations were continued until after the eleventh round where the most efficient GAT variant was discovered. The improved GAT variant was found to have a  $k_{cat}$  of 416min<sup>-1</sup> and a  $K_M$  of 0.05mM for the *N*-acetylation of glyphosate, which is nearly a 10,000 fold improvement in  $k_{cat}/K_M$  over the parental GAT enzymes. This variant was 76-79% identical to the original native GAT enzymes and was introduced into tobacco plants. Treatment with a 6X glyphosate spray demonstrated that the plant suffered no adverse symptoms compared to the control plants (figure 1.4.3.2).

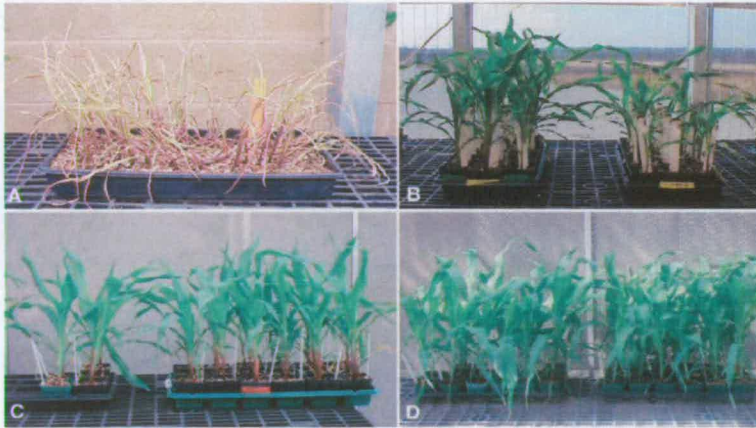


Figure 1.4.3.2. Transgenic maize expressing GAT<sup>146</sup>. (A) The control maize (untransformed) 10 days after spraying with glyphosate spray. (B to D) Plants on the right are shown 10 days after glyphosate treatment, the plants on the left are untreated (B) Transformed maize expressing a fifth iteration *gat* variant were tolerant to a 4X dose but suffered a setback in growth. (C) Transformed maize expressing a seventh iteration *gat* variant showed no symptoms or growth setback at up to 4X glyphosate compared to unsprayed controls. (D) Transformed maize expressing tenth and eleventh iteration *gat* variants had tolerance up to 6X glyphosate with no visual damage or growth damage.



Furthermore, there are numerous examples of lipases being used to control the enantioselectivity of the hydrolysis of esters. The lipase catalysed hydrolysis of racemic *p*-nitrophenol esters has been used as a model reaction to evolve *Pseudomonas aeruginosa* lipase to enhance the enantioselectivity of a hydrolytic kinetic resolution<sup>148</sup>. The choice of the *p*-nitrophenol ester substrate allowed the direct monitoring of the ester hydrolysis by the production of the yellow *p*-nitrophenol product (figure 1.4.3.3).

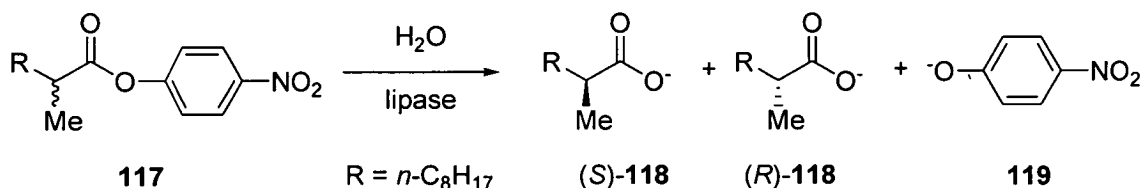


Figure 1.4.3.3. The lipase catalysed hydrolysis of a *p*-nitrophenol ester-117 to give the acid-118 and the yellow *p*-nitrophenolate anion-119.

The wild type enzyme had a poor *E*-value of 1.1 and this proved a good starting point for improvement through a directed evolution process. epPCR was employed to generate variants to be screened at a mutation rate averaging one amino acid substitution per enzyme molecule. After the first round, the most enantioselective variant was isolated and the corresponding gene used as a template in the next round of epPCR. After four cycles of mutagenesis and screening the selectivity factor in the hydrolytic kinetic resolution of the *p*-nitrophenol chiral ester increased from *E* = 1.1 to *E* = 11.3 in favour of the (*S*)-enantiomer. An *E*-factor of 11.3 was obtained as a result of four amino acid changes, but the epPCR method to identify these four residues was not optimised. This assumption is reasonable because the size of the screen was smaller (2000-3000 variants in each round) than the theoretical number of variants (see section 1.4.1 for discussion on epPCR bias). It was assumed that these sites were 'hot spots' therefore saturation mutagenesis was undertaken at these points. This led to a new variant<sup>149</sup> with an *E*-value of 20 and by a further round of epPCR a significantly improved variant was identified that had an *E*-factor of 25.

DNA shuffling was considered to further evolve the optimized lipase variant but it was decided that a higher gene diversification was required. epPCR was repeated on the wild type gene but at three times the previous mutation rate, which gave two new variants with  $E$ -factors of 3 and 6.5 after one cycle<sup>150</sup>. These two variants, along with the optimized variant resulting from the low mutation rate epPCR, were subjected to DNA shuffling giving rise to a yet further increase in  $E$  to 32. By using extended combinatorial multiple-cassette mutagenesis the variants isolated from the high frequency epPCR were fragmented. To the mixture of these fragments was added a mutagenic oligocassette which allowed two 'hot spots' to be randomized and incorporated into the product gene variants (figure 1.4.3.4). The optimized variant generated by this method exhibited an  $E$ -value of >51.

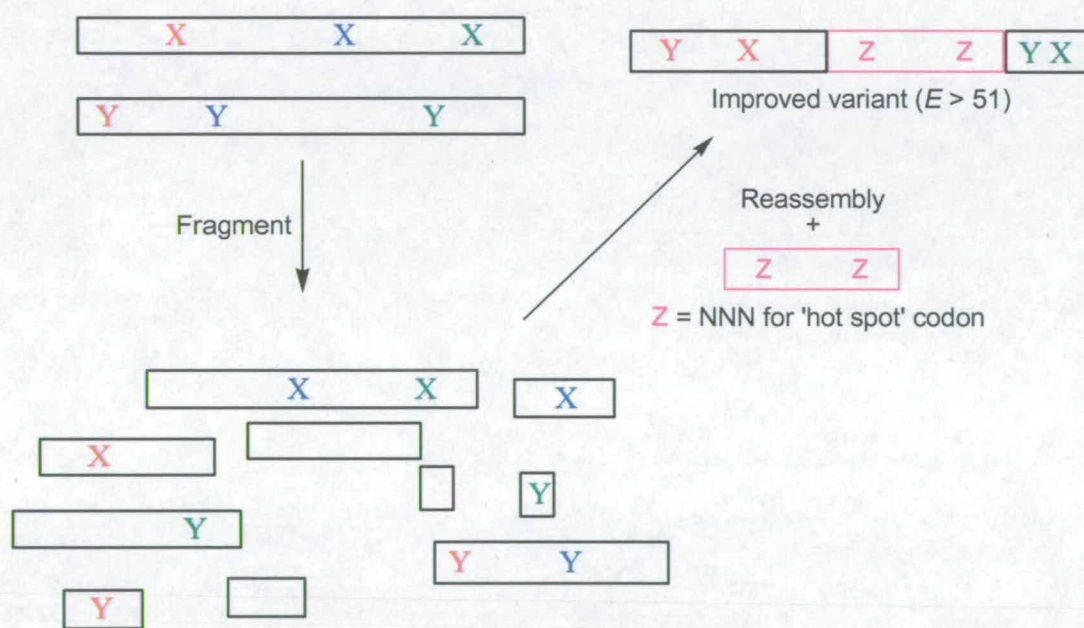


Figure 1.4.3.4. Extended combinatorial multiple cassette mutagenesis in the evolution of an ( $S$ )-selective lipase. The mutagenic oligocassette is shown in pink with the two hotspots denoted by Z, both being randomized by NNN incorporation.

---

Using the high mutation frequency the (*S*)-selective lipase was converted to an (*R*)-selective lipase with an *E*-value of 2.0. Further epPCR rounds of directed evolution gave *E* = 7.0 and then by subsequent DNA shuffling gave *E* = 30 for (*R*)-enantiomer hydrolysis<sup>151</sup>. The (*R*)-selective variant had eleven amino acid substitutions in different positions to the (*S*)-selective variants. The ability of directed evolution to increase and also reverse enantioselectivity of *Pseudomonas aeruginosa* lipase was obtained without prior knowledge of the 3D structure of the enzyme and its mechanism.

Detailed molecular modeling has subsequently been undertaken to rationalise what has caused these changes in catalysis by the lipase<sup>152</sup>. The modeling concluded that the rise in enantioselectivity was caused by a disruption of the hydrogen bonding network arising from the mutations which allows histidine 83 to adopt different conformers. Changes in histidine 83 conformations affect the enantioselectivity during catalysis since it is involved in the proton shuttle of the catalytic triad of this serine esterase. It was shown that the side chain movement of histidine 83 provided additional stabilization of the oxyanion hole for the (*S*)-ester by a new hydrogen bond. In contrast, the (*R*)-ester doesn't have this stabilization, it has a steric repulsion which further helps to increase the enantioselectivity for the (*S*)-selective variants.

In conclusion, these two examples demonstrate that directed evolution can be used to engineer transgenic crops to self-protect against a potent herbicide by enzymatic degradation of the toxin. The wild type enzyme alone was insufficient to fulfill this task without substantial improvements (10,000 fold compared to wild type) of the parent gene by directed evolution. Lipases have been evolved by directed evolution to increase enantioselectivity of ester hydrolysis. Combinations of epPCR and DNA shuffling were used to invert the enantioselectivity allowing either enantiomer of an ester to be selectively hydrolysed. There appears not to be a single preferred method by which genetic diversification is best prepared. In practice, it is seen that the preferred choice of

variant library preparation is case specific, with the optimal methods often combining several approaches such as epPCR, gene shuffling and saturation mutagenesis.

## 1.5. Summary and aims

The number of different approaches for the preparation of optically active amines has increased in recent years. Chiral amine functionality is important in many fine chemical intermediates, therefore there is much commercial and academic interest in discovering novel routes to provide cheaper and more efficient routes. A biocatalytic approach offers many attractive features to achieve this goal.

The project outlined here is based upon work initially reported for the deracemisation of cyclic amino acids<sup>60</sup>. Prior to undertaking the work described here, progress had been made in applying a similar principle for the deracemisation of chiral amines. The previous studies selected MAO-N as the parent gene in the search for an enantioselective amine oxidase. A variant MAO-N enzyme (N336S) was discovered by directed evolution that had improved activity towards  $\alpha$ -methylbenzylamine<sup>153</sup>. It was shown to have high (*S*)-enantioselectivity and has been employed in the deracemisation of (*rac*)- $\alpha$ -methylbenzylamine achieving high e.e. and moderate/good yields<sup>154</sup>.

The goal in this project was firstly to establish a method for the purification of recombinant MAO-N expressed in *E. coli*. Once MAO-N had been purified and isolated, the next task was to screen the improved MAO-N N336S M348K variant against a variety of amines to evaluate the feasibility of using this enzyme as a biocatalyst for the deracemisation of other chiral amines. The MAO-N was passed through a further round of directed evolution, this time screening for activity towards a secondary amine, in an attempt to increase the range of substrates that the amine deracemisation principle can be applied to. The ultimate aim being to obtain a 'toolbox' selection of MAO-N biocatalysts that could be chosen depending on the type of substrate to be deracemised

---

(*e.g.* primary, secondary or tertiary amine) and which enantiomer was required (either (*R*) or (*S*)).

A second MAO-N variant was identified which incorporated a mutation in the protein sequence that introduced secondary amine activity. The mutated site was randomised and then screened again against secondary amines to select for the optimal amino acid residue. Subsequently, further saturation mutagenesis of other residues in MAO-N which appeared to perform specific contacts with the substrate at the active site was undertaken. The postulation of the specific contacts between the substrate and the enzyme was based upon a homology model. The MAO-N sequence was aligned with MAO-B and employing the published three dimensional crystal structure of MAO-B with an inhibitor bound at the active site<sup>84</sup> gave the basis of the homology model. The variant libraries generated by saturation mutagenesis were screened using a solid phase assay to identify variants that had improved secondary amine oxidation rates.

A range of reducing agents was screened for their performance in the reduction of imines, which allowed them to be categorized into those that should perform more efficiently under deracemisation conditions. The reducing agent screening was critically important to highlight those that efficiently reduced imines under aqueous buffer conditions thereby maximising the efficiency of the deracemisation cycle and minimising loss of substrate by imine hydrolysis. Finally, optimised MAO-N biocatalysts and the more efficient reducing agents were combined to investigate the viability of the preparative deracemisations of chiral amines using both whole cell recombinant *E. coli* expressing MAO-N and purified MAO-N immobilised on resin.

During the results and discussion section each MAO-N variant is referred to by number. The assigned numbers for each variant have the mutations incorporated as indicated in table 1.5.1.

---

MAO-N variant	Mutations incorporated
<u>1</u>	N336S M348K
<u>2</u>	I246M N336S M348K
<u>3</u>	I246M N336S M348K T384S D385N
<u>4</u>	I246M N336S M348K T384N D385S

Table 1.5.1. The number assigned with each MAO-N variant and the mutated residues of the variant.

## 2.1. Purification and stability studies

### 2.1.1. Ion exchange purification

Separation of crude protein mixtures in ion exchange chromatography depends upon the reversible adsorption of charged solute molecules to immobilised ion exchange groups of a resin that have an opposite charge. Most ion exchange experiments are performed in five main stages as shown in figure 2.1.1.1. There are two methods of ion exchange, either anion where the medium is positively charged or by cation exchange where the medium is negatively charged. The protein is then eluted by application of a salt gradient (3.2.1). Substances are separated based on their charge, charge density and the distribution of charge on the surface of the substance. The interaction of protein and ion exchanger can be varied according to the conditions used during the purification in particular the ionic strength and pH are particularly important.

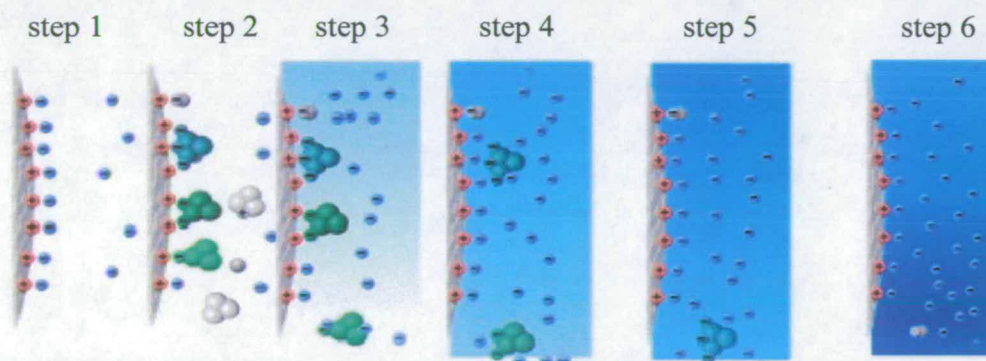


Figure 2.1.1.1. The principle of salt gradient elution in ion exchange chromatography for the purification of proteins. The example shown here is anion exchange chromatography step 1 = equilibration, Step 2 = sample application and wash, step 3 = gradient elution (protein with -1 net charge), step 4 = gradient elution (protein with -2 net charge), step 5 = gradient elution (protein with -3 net charge) and step 6 = regeneration (illustration taken from Amersham biosciences).



---

The first step is the loading of the crude mixture onto the column; the desired protein is bound to the pre-equilibrated resin. Desorption then can proceed, this elutes substances that have a lower strength of attraction to the resin. This is normally achieved by raising the ionic strength which disrupts the ionic interaction between resin and substrate. After all substances have been desorbed, the resin is regenerated ready for re-use.

Purification of recombinant MAO-N *I* variant by the modification of the reported method<sup>94</sup> using Resource Q resin rather than with another ion exchange resin (DEAE-sepharose) gave better resolution of proteins<sup>153</sup>. Resource Q chromatography gave MAO-N protein of approximately 75% purity as determined by SDS-PAGE<sup>153</sup>. Resource Q is an anion exchange purification technique, so the buffer pH should be higher than the protein's pI to allow the ionic interaction between the protein (net negative charge) and exchanger (net positive charge). Cell free extract (CFE) 50ml was adsorbed onto a HiLoad 26/10 50ml Q Sepharose column and a linear salt gradient 0-1.0 M over 20 column volumes was applied. All fractions were assayed (3.1.1) and MAO-N activity was found in three fractions (35-37) corresponding to 238-277mM sodium chloride (3.2.1). The efficiency of the purification was measured by the total activity recovered in the purified protein relative to the activity measured in the CFE.

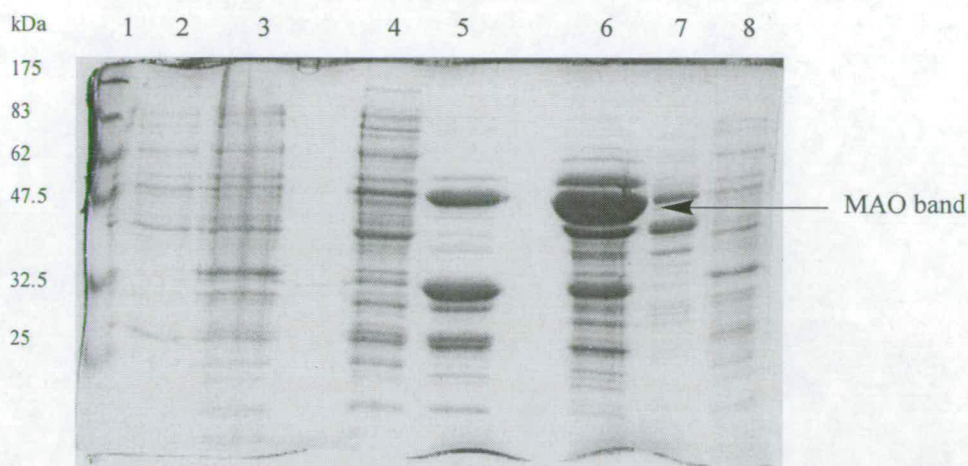


Figure 2.1.1.2. Separation of eluted fractions obtained by Resource Q chromatography in a SDS polyacrylamide gel followed by Coomassie blue staining. Lane 1, Molecular weight protein markers (NEB); lane 2 and 3, cell pellet before sonication; lane 4, CFE; lane 5, fraction 35; lane 6, fraction 36 and lane 7, fraction 37.

### 2.1.2. Affinity Purification

Affinity chromatography separates proteins on the basis of a reversible interaction between a protein (and group of proteins) and a specific ligand coupled to a chromatography matrix. The His-tag is a commonly used tag to facilitate the purification of recombinant proteins. A chelating matrix with  $\text{Ni}^{2+}$  metal ions selectively binds proteins if complex forming amino acid residues, in particular histidine, are exposed on the protein surface. Application of an increasing imidazole gradient causes proteins that are bound non-specifically to be eluted.

Owing to the pET-16b recombinant expression system that was used in the expression of recombinant MAO-N protein, an N-terminal histidine peptide ( $\text{His}$ )<sub>6</sub> tag was attached. This allowed purification of the protein to >95% purity. Optimisation of the affinity

purification protocol to determine the maximum imidazole concentration required for the MAO-N to remain bound on the resin was determined to be 60mM. This was used in the wash step to remove weakly associated proteins from the host organism that were non-His tagged proteins. The same investigation was used to determine the minimum concentration of imidazole required to elute the His-tagged MAO-N protein, this was found to be 200mM imidazole (3.2.2).

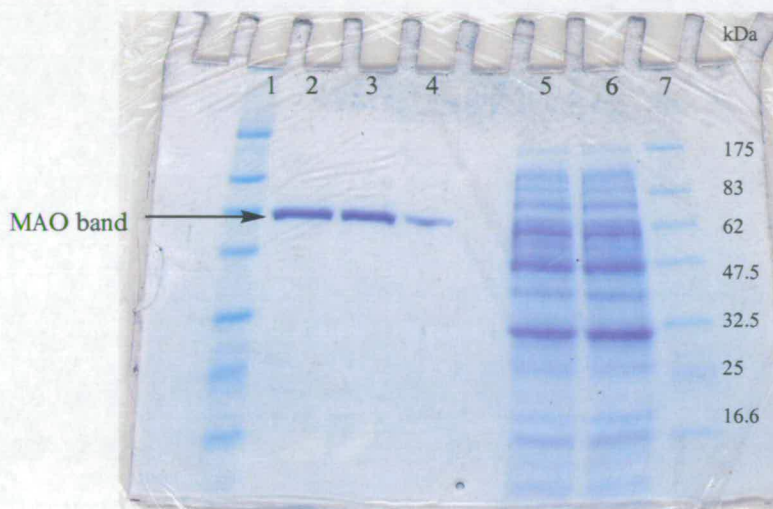


Figure 2.1.2.1 Analysis of eluted fractions of nickel affinity chromatography purified protein samples by SDS polyacrylamide gel electrophoresis followed by staining with Coomassie blue staining (3.2.5). Lanes 1 and 7, molecular weight protein markers (NEB); lanes 2, 3 and 4, fractions from eluted nickel affinity chromatography; lanes 5 and 6, CFE.

Typically, storage of the purified protein overnight led to protein precipitation and complete loss of soluble protein as determined by the Bradford assay (3.2.6).

Furthermore, agitation of the stored protein sample caused flakes of protein to be visible indicating the loss of soluble protein. Attempts to improve the purified protein stability were tried. It was suggested that the instability of the purified protein may be caused by the high concentration of imidazole required to elute the protein in the affinity

---

purification technique (elution buffer 200mM imidazole, Tris-HCl pH 7.8, 300mM NaCl, 1 mM DTT and 0.1 mM PMSF). To investigate if this was the case a purified sample of protein was exchanged into the same buffer used for MAO-N purification by nickel affinity chromatography lacking imidazole. A freshly purified protein sample was applied to a Vivaspin centrifugal filter and spun to concentrate the sample (method followed was according to manufacturer's guidelines). The concentrated protein sample was then diluted in buffer used to purify the protein, lacking imidazole (25 mM Tris-HCl pH 7.8, 300mM NaCl, 1 mM DTT and 0.1 mM PMSF). The reconstituted protein sample was passed through several repetitions of concentration and dilution to exchange the buffer into 25 mM Tris-HCl pH 7.8, 300mM NaCl, 1 mM DTT and 0.1 mM PMSF. However, the serial concentration and dilution of the sample led to the protein being absorbed onto the spin-column membrane. Overnight dialysis was attempted instead. Dialysis into the same purification buffer, lacking imidazole, did not prevent loss of activity. Storage at 4°C, -20°C and -80°C led to a loss of MAO-N activity, these storage conditions did not alleviate the stability problem so a more rigorous investigate of protein storage conditions was required (2.1.4).

### **2.1.3. Activity profile during MAO-N purification**

The activity profile of MAO-N through the two purification methods, ion exchange and nickel affinity chromatography, is summarised in table 2.1.3.1. It showed that the ion exchange method gave an overall better yield of purified MAO-N activity with 88% recovery from CFE compared with 21% for the nickel affinity method. The differences in specific activity of the CFE arise from the fact that the two purifications were performed on different batches of cells and were caused by differences in the expression level of recombinant MAO-N during the fermentation. The specific activity of the purified protein was significantly higher for the ion exchanged purified protein than for the nickel affinity purified protein. Normally, the specific activity would rise from the CFE to the purified protein, but the opposite occurs for the nickel affinity purified

MAO-N protein. This results from the instability of the purified MAO-N protein by the nickel affinity procedure [this problem is addressed later (2.1.4)].

Purification method	Total activity of CFE (OD/sec)	Total activity of purified protein (OD/sec)	Specific activity of CFE (Umg <sup>-1</sup> )	Specific activity of purified protein (Umg <sup>-1</sup> )
Resource Q (Ion exchange)	1676	1476	0.36	0.81
Ni-NTA (Nickel affinity)	5407.5	1112	0.20	0.062

Table 2.1.3.1. Activity profile during MAO-N I purification; comparison of ion-exchange and affinity chromatography methods [1 U = 1  $\mu$ mol/min].

The positive ion mode electrospray mass spectrum of MAO-N wild type was recorded showing clearly the presence of FAD with  $M+H^+ = 786$  and  $M+Na^+ = 808$  (see appendices). The sample was also analysed by LCMS and showed a charge envelope characteristic of a peptide (3.2.7). MaxEnt transformation of the charge envelope gave several mass peaks in the 51-61kDa region. The molecular weight of MAO-N wild type was calculated to be 55581.3Da (monoisotopic mass) in addition to this was the histidine tag which increased the molecular weight to 56935.3Da. There was no mass peak corresponding to either of these exact masses (see appendices) although the mass peaks did occur within 5% of the calculated mass of MAO-N wild type.

---

The UV-visible spectrum of MAO-N wild type was recorded to identify the presence of FAD cofactor in the purified protein sample (3.2.8). Two maximums were observed in the spectrum at 361nm and 458nm. This is consistent with reported UV-visible spectrum of MAO-N<sup>94</sup> and the based on the absorbance at 458nm (abs = 0.468 units) it was possible to calculated the FAD content in the protein sample. The FAD content was determined to be 0.04372mM based on the reported extinction coefficient<sup>94</sup>  $\epsilon_{458nm} = 0.7\text{mM}^{-1}\text{cm}^{-1}$  which gave the concentration of holo-enzyme of MAO-N wild type to be  $2.4\text{mgml}^{-1}$ . The protein concentration measured by absorbance at 458<sub>nm</sub> ( $2.4\text{mgml}^{-1}$ ) matched well with the protein concentration measured by the Bradford assay (3.2.6) ( $2.5\text{mgml}^{-1}$ ).

#### 2.1.4. Stability of MAO-N upon storage

MAO-N was purified to homogeneity with nickel affinity chromatography as judged by SDS PAGE analysis. The benefit of this single step affinity purification to give pure protein was considered to be an improvement over the previously described Resource Q Sepharose purification<sup>94</sup>. However, the problem of loss of activity during storage needed to be addressed to make this technique a viable route for the preparation of MAO-N as a biocatalyst in a deracemisation. To examine this, purified protein was stored in different buffers at different temperatures, 4°C, -20°C or -80°C. The purified protein was buffer exchanged into the desired buffer by PD10 desalting immediately after affinity purification (3.2.3). At various time intervals (24 hours, 48 hours, 72 hours, 168 hours and 6 weeks) the samples were thawed on ice and the activity of MAO-N was measured against amylamine (amine 1) (using the protocol as described in 3.1.1). The CFE was also assayed to test its stability upon storage to determine whether MAO-N was more stable stored in CFE rather than purified.

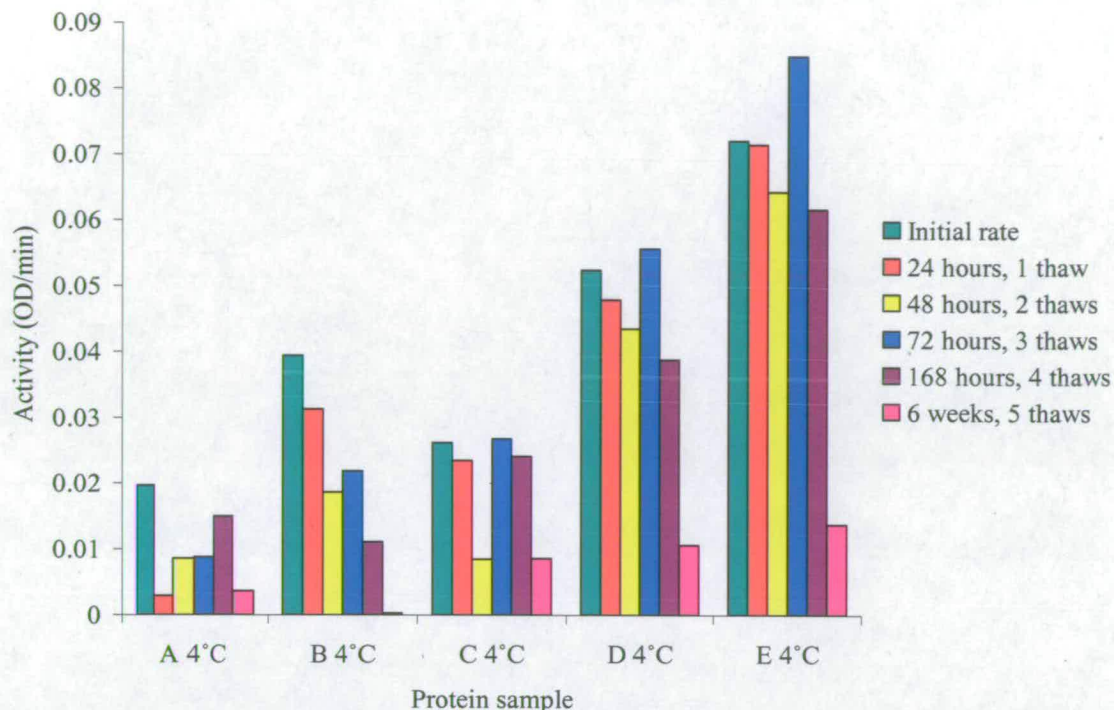


Figure 2.1.4.1. Stability studies of purified MAO-N stored in various buffers at 4°C.

A = 1:1 (v/v) 25mM Tris/HCl pH 7.6, 300mM NaCl, 1mM β-mercaptoethanol and 1mM PMSF (nickel affinity chromatography purification buffer lacking imidazole): glycerol

B = Purification buffer lacking imidazole

C = 1:1 (v/v) 0.1M potassium phosphate buffer pH 7.6: glycerol

D = 0.1M potassium phosphate buffer pH 7.6

E = CFE sample in 25mM Tris/HCl pH 7.6, 300mM NaCl, 1mM β-mercaptoethanol and 1mM PMSF.

The highest MAO-N activities for the purified protein stored at 4°C were seen in buffer D (figure 2.1.4.1). These showed the best maintenance of MAO-N activity upon storage. The samples stored in purification buffer lacking imidazole (buffer B) showed the lowest MAO-N activities. Addition of glycerol in both buffer A and C lowered the measured MAO-N activities compared to the same sample without glycerol, this was due to the dilution of the sample with glycerol which was not taken into account. Had

## Results and Discussion

the dilution difference been included, the difference in activity between the samples with and without glycerol is negligible. The addition of glycerol seemed to have no effect on the rate at which the MAO-N activity was lost on storage. Some of the samples seem to show a recovery in activity after a further period of storage. This may be caused by slight inaccuracies in the assay. All the samples showed significant loss of MAO-N activity after 6 weeks storage and 5 thaws.

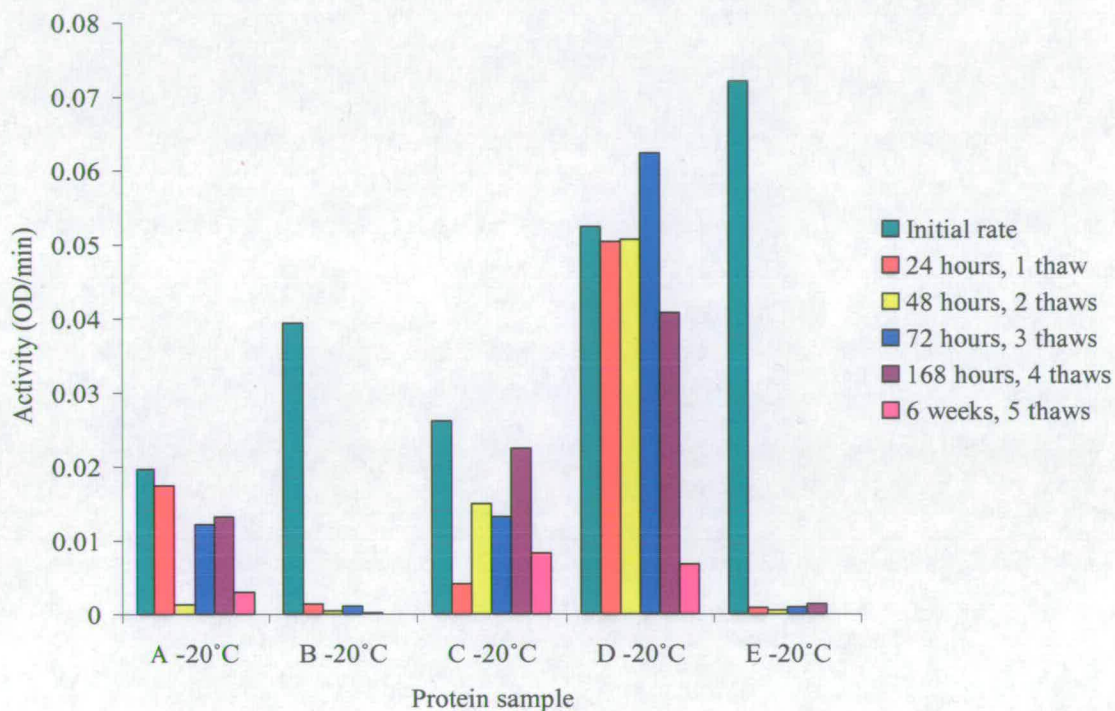


Figure 2.1.4.2. Stability studies of purified MAO-N stored in various buffers at  $-20^{\circ}\text{C}$ . Composition of storage buffers as in figure 2.1.4.1.

Storage at  $-20^{\circ}\text{C}$  generally was worse for activity loss with time than storage at  $4^{\circ}\text{C}$  (figure 2.1.4.2). The CFE and the samples stored in purification buffer lacking imidazole (buffer B) lost almost all activity upon storage. Addition of glycerol to the purification buffer lacking imidazole (buffer A) appeared to stabilise MAO-N over 24 hours. The best conditions were the samples stored in 0.1M potassium phosphate buffer pH 7.6 without glycerol (buffer D). There appears to be some erroneous rates measured were



the activity appears to be lost but then recovers (e.g. 48 hours in buffer A compared to longer storage in the same buffer).

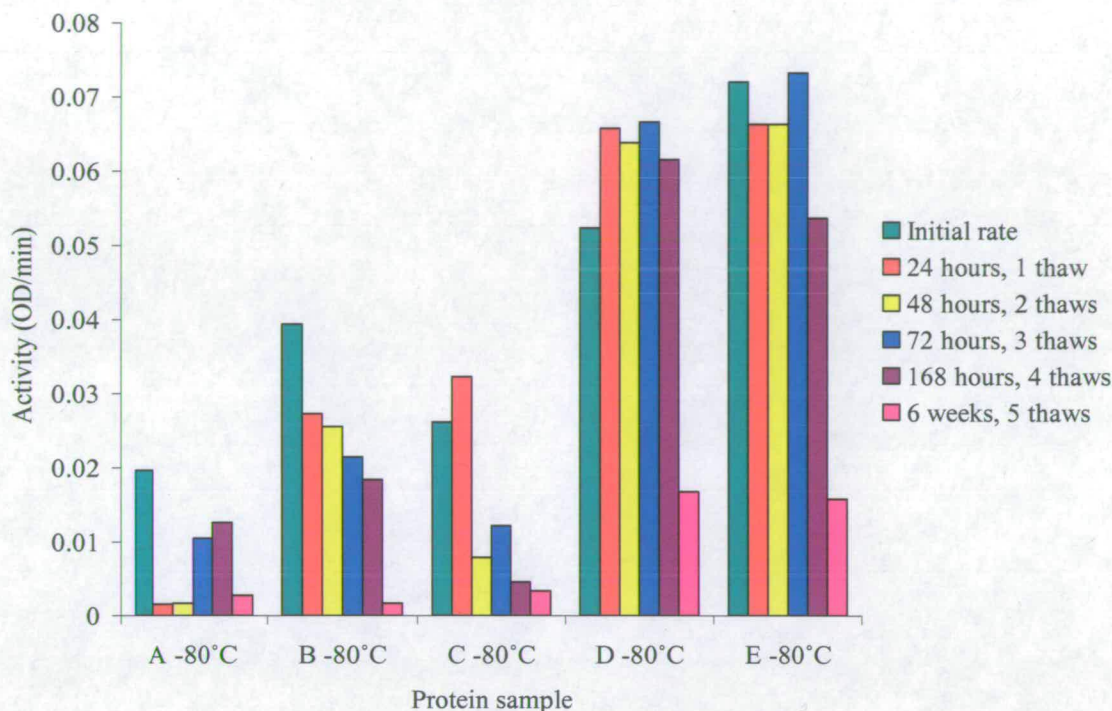


Figure 2.1.4.3. Stability studies of purified MAO-N stored in various buffers at -80°C. Composition of storage buffers as in figure 2.1.4.1.

The best storage conditions for -80°C was the same as for 4°C and -20°C (figures 2.1.4.1 and 2.1.4.2) where the samples were stored in 0.1M potassium phosphate without any glycerol added. CFE also showed good preservation of MAO-N activity upon storage. Samples stored in the presence of glycerol (buffers A and C) both suffered the greatest losses of MAO-N activity.

Several conclusions can be made from this investigation into the effects of storage conditions on MAO-N activity. Firstly, the freeze/thaw cycles on purified MAO-N generally appeared to lower the activity. After six weeks storage and five thaws MAO-N

---

activity had significantly reduced in all samples. The best overall stability over the five freeze/thaw cycles examined was for MAO-N stored at -80°C in 0.1M potassium phosphate buffer without glycerol (buffer D). The phosphate buffer (buffer D) generally gave better storage conditions than for the Tris buffer (buffer B) under these conditions for MAO-N storage.

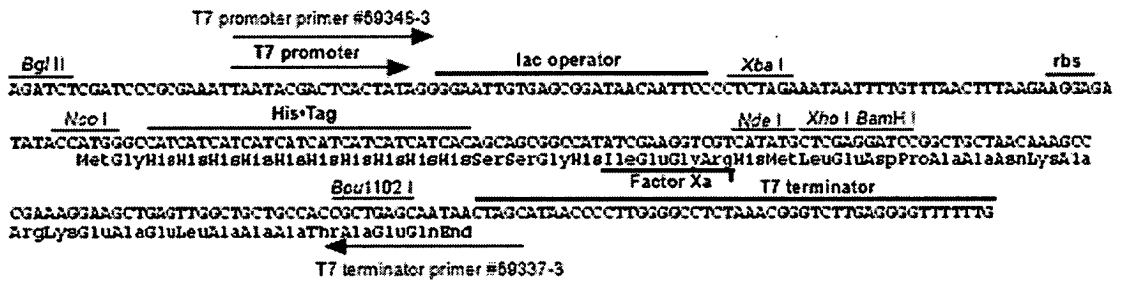
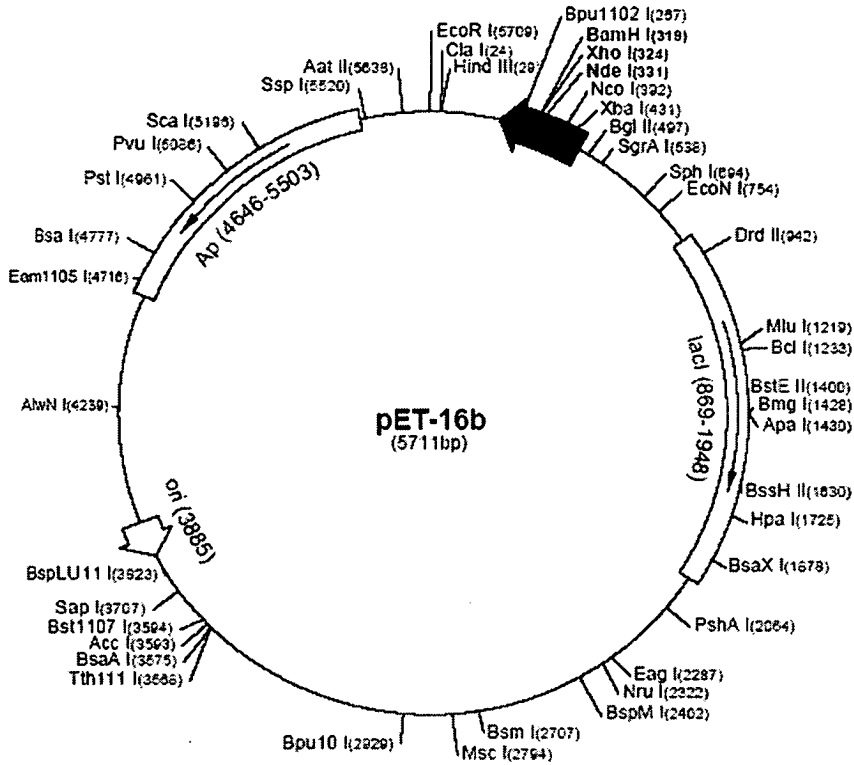
An alternative way of storing purified MAO-N is by precipitation of the protein. Ammonium sulphate precipitation of purified MAO-N with 60% saturation led to total loss of MAO-N from solution after centrifugation to give a bright yellow pellet. When the pellet was redissolved in 0.1M potassium phosphate buffer pH 7.6, it maintained the same activity as the freshly purified enzyme.

### 2.1.5. Growth and Expression of MAO-N

The *mao* gene had been constructed in pET-16b which adds an N-terminal histidine tag to the MAO-N protein, allowing nickel affinity chromatography purification to be employed in one step. It was shown that the level of MAO-N expression was found to be five times higher than the previous pECME3 construct<sup>153</sup>.

The *mao* gene was cloned downstream of a bacteriophage T7 transcription site. A *lac* operator sequence is located downstream of the T7 promoter, so in  $\lambda$ DE3 lysogens the expressed *lac* repressor acts to repress transcription of the target gene. The *lac* repressor also interacts with *lac UV5* promoter in the host chromosome to repress transcription of the T7 RNA polymerase by the host polymerase. The benefit of this expression system is that the expression of the target gene can be regulated so that expression can occur once induction has occurred. Upon induction with IPTG the *lac UV5* promoter transcribes the T7 RNA polymerase gene. The T7 RNA polymerase can then transcribe the target DNA in the plasmid. However, the inherent leakiness of the *lac* promoter allows some degree

of transcription in the uninduced state. This allows expression of genes whose products are harmless to the host cells growth.



**pET-16b cloning/expression region**

Figure 2.1.5.1. Novagen's pET-16b vector map with cloning sites and expression regions indicated.

Leaky expression of the MAO-N pET-16b construct was seen in the bacterial host *E. coli* BL21 (DE3)<sup>153</sup>. To increase levels of MAO-N expression further IPTG induction was performed. Novagen suggest that a final concentration of 1mM IPTG gives maximum induction and is recommended during the exponential phase of cell growth, OD<sub>600nm</sub> 0.4-1.0<sup>155</sup>. MAO-N 1 variant was grown in 10ml LB containing 100µg/ml ampicillin overnight and 1ml was used to inoculate two duplicate 1 litre baffled flasks each containing 100ml LB containing 100µg/ml ampicillin. Once the cells had reached OD<sub>600nm</sub> of 0.4 one of the cultures was induced with IPTG. At various intervals 1ml samples were taken post-induction and frozen prior to assay for MAO-N activity (3.3.9).

Sample growth	Point of induction	1 hour post induction (OD/sec)	2 hours post induction (OD/sec)	4 hours post induction (OD/sec)	18 hours post induction (OD/sec)
IPTG	0	$6.81 \times 10^{-3}$	$1.79 \times 10^{-2}$	$6.62 \times 10^{-2}$	$2.49 \times 10^{-3}$
No IPTG	0	0	0	$1.65 \times 10^{-4}$	$6.82 \times 10^{-3}$

Table 2.1.5.1. Comparison of MAO-N expression with and without IPTG induction. The rate of MAO-N activity of frozen/thawed samples measured against amylamine (amine 1) using the peroxidase assay (3.1.1).

MAO-N expression improved significantly with IPTG induction. The best expression was measured 4 hours post induction. Without induction of protein expression, MAO-N activity was first detected at the 4 hour time point. The rate of activity for this sample was nearly 10 times less than the activity measured after 4 hours post induction in the induced sample. The trend of the activity in the assay profile (table 2.1.5.1) was matched in the SDS PAGE (figure 2.1.5.2).

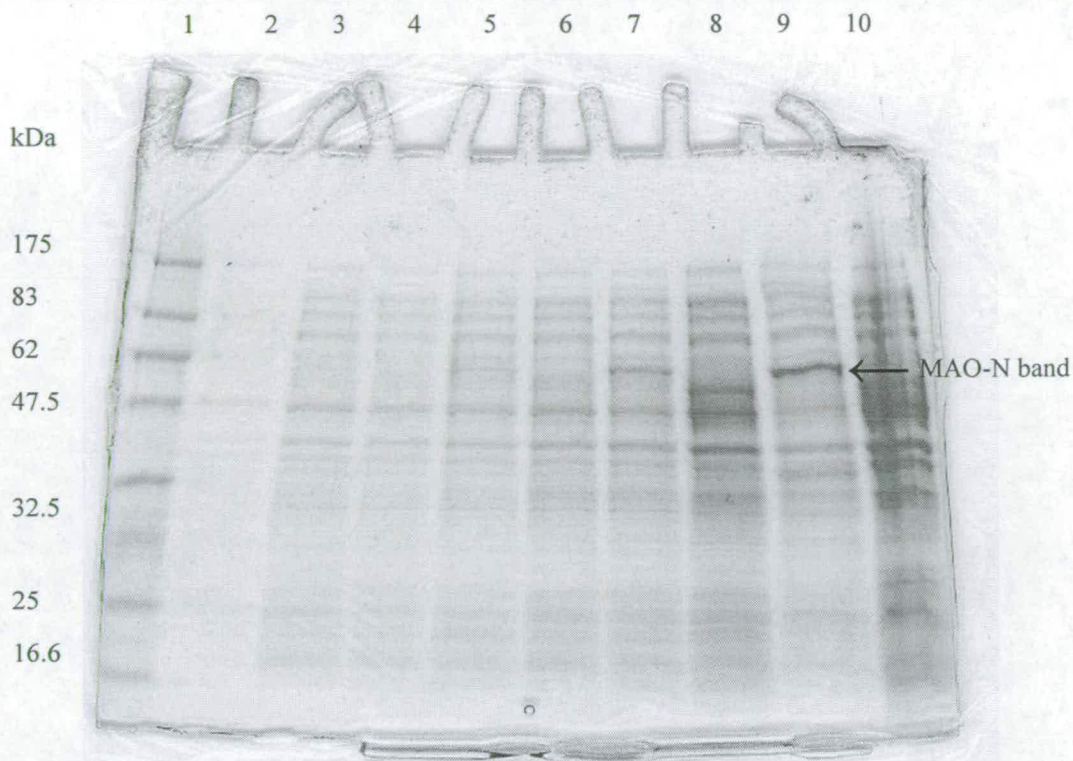


Figure 2.1.5.2. SDS PAGE with Coomassie blue staining analysis of the soluble protein from BL21 (DE3) samples expressing MAO-N with and without IPTG induction (3.2.5). [Lanes 4, 6, 8 and 10 are non-induced samples at 1, 2, 4 and 18 hours respectively. Lanes 3, 5, 7 and 9 are IPTG induced samples at 1, 2, 4 and 18 hours respectively. Lane 2 is the 0 hour sample, the point of induction and lane 1 is the molecular weight protein markers].

Repeated shake flask experiments and using 10 litre fermentations (3.3.5.3) with these improved conditions (IPTG induction) gave poor reproducibility. Induction at  $OD_{600nm}$  of between 0.4-1.0 with IPTG followed by harvesting 4 hours post induction produced inconsistent MAO-N expression. Often there was no apparent enhancement in the total MAO-N expression compared to a non induced fermentation which was harvested at stationary phase. Furthermore, the  $OD_{600nm}$  was seen to drop post induction on repeated fermentations. These unfavourable effects were shown to be particularly noticeable from inoculations where the starter cultures had an  $OD_{600nm} > 1.0$ . This empirical observation

---

may arise from plasmid instability in the expression host. If the *mao* gene product is detrimental or toxic at high levels to the host (*E. coli*) then during the fermentation the population containing the plasmid DNA could be reduced as cell divisions of *E. coli* containing plasmid DNA is retarded or stopped. Another factor causing this effect could be the antibiotic selection. The pET vectors have been engineered to encode for ampicillin resistance so only cells containing the plasmid DNA are viable in media containing ampicillin. During the fermentation, *E. coli* containing the MAO-N pET-16b construct can either receive a copy of the plasmid or not. Under antibiotic conditions, those not containing the plasmid will not be viable because they do not have ampicillin resistance. However, during the fermentation  $\beta$ -lactamase is excreted into the media degrading the antibiotic. Therefore once ampicillin levels had fallen to a sufficiently low level, cells not containing the plasmid DNA can survive in the fermentator. The population could proportionately rise to contain more non-plasmid containing cells. This effect would be magnified should the growth rate of cells containing plasmid DNA be decreased or stopped as cellular metabolic energy is directed into MAO-N production rather than cell division.

In order to determine if this was the case a stationary phase culture was diluted and spread onto 2 LB agar plates, one containing ampicillin and the other with no antibiotic (3.3.7). There was a two fold excess of colonies on the LB only plate indicating that half of the colonies do not contain the ampicillin selection in this culture suggesting that a significant proportion of the *E. coli* population did not contain plasmid DNA. [There were 23 colonies on the LB only plate and 11 colonies on the LB containing 100 $\mu$ g/ml ampicillin plate]. However, this level of plasmid retention within the host is deemed acceptable<sup>156</sup>.

The reproducibility problems of the IPTG induction and the observation of loss of plasmid from the host meant that routine fermentations for the production of MAO-N protein in this project were performed with no induction. Relying on just the leaky

---

expression of the pET-16b without induction meant that the potential yields of MAO-N were probably lower; but the fermentation performance was more robust and less likely to incur the problems of cell lysis and variable expression levels. To ensure maximal retention of the plasmid in the organism, the medium was inoculated with a single colony from a fresh transformant and the subculturing minimised. Inoculums were washed with fresh LB containing 100µg/ml ampicillin to remove excreted β-lactamase and the β-lactam antibiotic changed to carbenicillin to improve the selection. It has been shown that carbenicillin is less prone to degradation by β-lactamase than ampicillin<sup>157</sup>. Based on this effect, replacement of ampicillin with carbenicillin as the antibiotic selection for the fermentation may help alleviate the suggested problem of degradation of the antibiotic selection. Recombinant MAO-N fermentations were performed in the same manner as previously described (3.3.5) but with the replacement of ampicillin with carbenicillin at the same concentration (100µg/ml) throughout the fermentation. After several attempts using carbenicillin, rather than ampicillin, no improvement in MAO-N expression was observed.

#### **2.1.6. Conclusions**

Recombinant MAO-N has been purified as a functional soluble protein. The previously reported ion exchange chromatography has been changed to the nickel affinity purification technique affording higher purity of protein. The stability problems associated with the purified protein have been addressed and an improved storage buffer (phosphate) was found to increase the stability of the protein over the post purification buffer (Tris). Induction with IPTG during the fermentation has been shown to raise the expression of MAO-N compared with no induction. Problems with the lack of reproducibility of the induction method meant that it was not used when carrying out fermentations. The amount of protein obtained from a non-induced fermentation gave sufficient quantities to allow the kinetic and biotransformation experiments to be undertaken.

### 2.1.7. Future work

The stability problem of purified MAO-N (2.1.4) was addressed, but with only a moderate degree of success. Other storage conditions could be investigated including alternative buffers, lyophilisation of the purified protein and storage as an ammonium sulfate pellet. MAO's flavin is non-covalently bound, so storing the purified protein with addition of flavin cofactor may assist the stability of the protein. The problems associated with the current vector (pET-16b) could be investigated by using other expression systems.

Should higher levels of MAO-N be required in the future then further investigation into improving expression would be required. Enriched media would probably give higher final OD<sub>600nm</sub> at stationary phase than the currently used LB media, yielding a higher biomass on harvest. Different growth media may also improve expression and solubility of the MAO-N protein. Other adjustments that could be tried to improve the fermentation yield include lowering the temperature, also addition of cofactor and/or substrate may help to increase the overall yield of functional soluble MAO-N enzyme. As the *mao* gene product is from a eukaryotic organism, *Aspergillus niger*, then switching the expression host from prokaryote (*E. coli*) to a eukaryote system such as *Saccharomyces* or *Pichia* may also be beneficial.



## 2.2. Screening of MAO-N wild type and N336S M348K variant against panel of amines

The substrate specificity of MAO-N from *Aspergillus niger* had been studied to a degree prior to this work<sup>154</sup> and existing work had only demonstrated the deracemisation of  $\alpha$ -methylbenzylamine (amine **24**) with the MAO-N I variant. In order to determine the potential application of MAO-N wild type and the MAO-N I variant in the deracemisation of other chiral amines a more thorough substrate screening exercise was undertaken. For the amines that were found to be active in this screen a further investigation into the enantioselectivity was undertaken. For MAO-N to be used as a biocatalysis in the deracemisation of a racemic amine substrate, enantioselectivity and activity are crucial. The deracemisation concept of cycles of oxidation and reduction is reliant on an enantioselective oxidation to achieve high e.e. for the final amine product.

### 2.2.1. The colorimetric peroxidase assay

A key aspect of amine oxidation by MAO-N that allows the facile and accurate assay of catalytic activity is that the by-product of the amine oxidation is hydrogen peroxide. This by-product is generated by the reduction of molecular oxygen with water to give hydrogen peroxide in the regeneration of FAD to its oxidised form in the final stage of the MAO-N catalytic cycle (1.3). Horseradish peroxidase catalyses the reduction of hydrogen peroxide to water with simultaneous oxidation of a proton donor (figure 2.2.1.1). The proton donor in this case was 4-aminoantipyrine-**120**, which subsequently reacted chemically with 2,4,6-tribromohydrobenzoic acid-**122** to give a soluble red dye which can be quantified by absorbance at 510nm. This direct measurement of hydrogen peroxide production was used to calculate MAO-N activity in the following experiments (3.1.1).

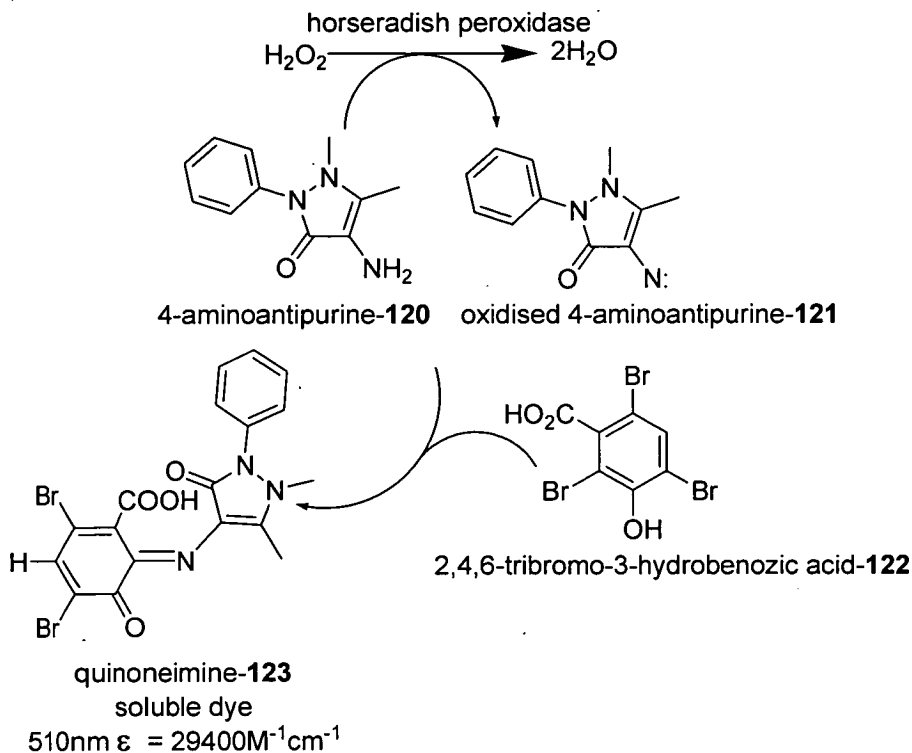
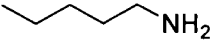
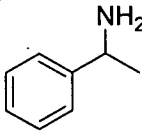
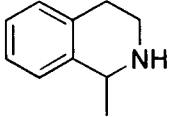


Figure 2.2.1.1. The peroxidase coupled assay producing a soluble quinoneimine-123 dye.

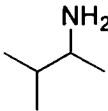
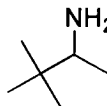
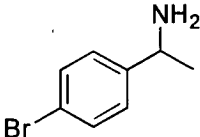
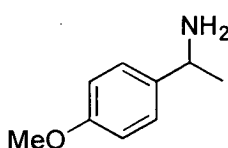
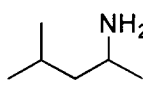
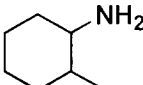
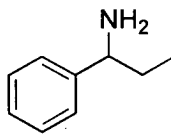
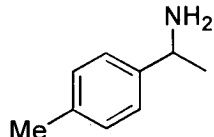
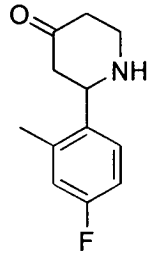
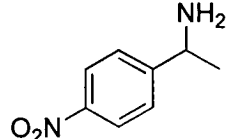
### 2.2.2. MAO-N wild type and MAO-N I variant amine oxidation screen

Existing work had shown the deracemisation of (*rac*)-amine **24** with the MAO-N I variant<sup>64</sup>. To examine the potential use of MAO-N to deracemise chiral amines other than (*rac*)-amine **24**<sup>154</sup> MAO-N wild type and the MAO-N I variant were screened for activity. The M348K mutation in MAO-N N336S has previously been reported to be an expression mutant of the MAO-N N336S variant and is not involved in the improvement of MAO-N catalysis in amine oxidation<sup>153</sup>. The initial difficulties with isolating and storing stable pure protein (2.1.4) made detailed kinetic analysis difficult, therefore amine rates were measured relative to amine **24** (3.1.3). Each screening experiment included (*rac*)-amine **24** so that variability in the oxidation rate resulting from enzyme instability was eliminated. Amine activities were measured as percentages with activity

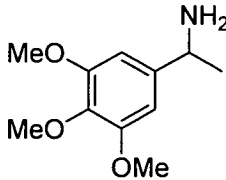
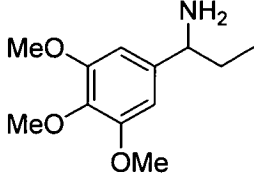
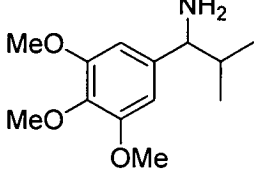
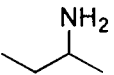
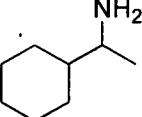
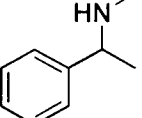
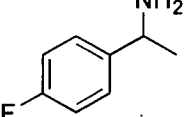
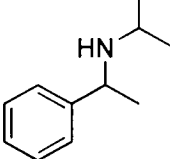
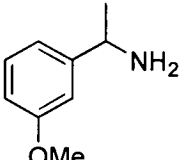
of (*rac*)-amine **24** set at 100%. To facilitate the screening of large numbers of substrates, the assays were carried out using a 96-well microtitre plate. The use of a 96-well microtitre plate to measure MAO-N activity offers advantages over the single (cell) cuvette method, as multiple samples can be measured in parallel saving time and money. The additional advantage is that it increases the through put of the screening and should it be desired, it can be automated. To allow the measured assay rates between substrates to be comparable, all amines were prepared at 10 mM in the assay mixture. Negative control assays were also carried out in the absence of MAO-N so that any non-enzymatic production of the coloured product could be discovered and false positives eliminated from the screen. It was found that some of the commercial amines had impurities that caused a false positive response; often these impurities could be removed by Kugelrohr distillation of the amine. However after purification it was often found that the substrate became impure again after storage, reflecting the unstable nature of some of the amines in the free base form. Generally, amines supplied as the hydrochloride salts proved to be more stable than the corresponding free base amine and hence tended not to give false positives. Table 2.2.2.1 details the results of the screening. Each substrate has been allocated a number and its structure is indicated. All the rates were measured using racemic substrates (for those that were chiral) and were measured as relative percentages of the rate observed with  $\alpha$ -methylbenzylamine (amine **24**).

Amine	Wild type activity (%)	MAO-N <i>I</i> variant (%)	Structure
<b>124</b>	4417	1307	
<b>24</b>	100	100	
<b>76</b>	0	9.1	

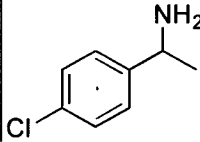
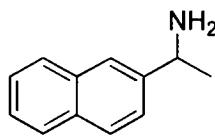
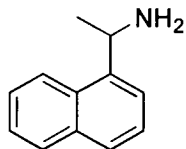
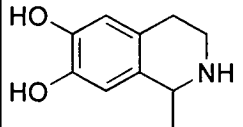
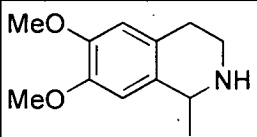
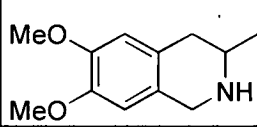
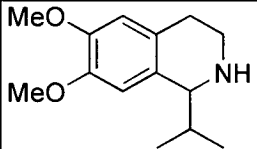
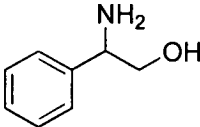
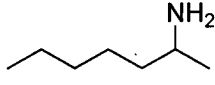
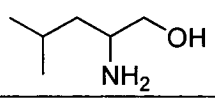
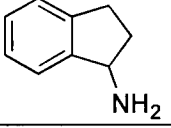
## Results and discussion

125	0.4	54.4	
126	0.2	89.3	
127	0.9	9.6	
128	0	12.7	
129	0	190	
130	0	18.6	
131	0.4	0	
132	0	2.4	
133	1.1	0	
134	1.6	22.6	

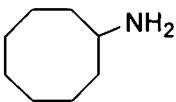
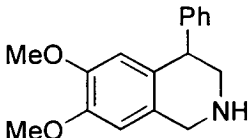
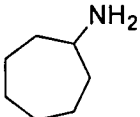
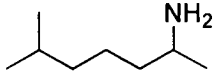
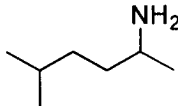
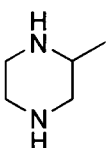
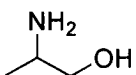
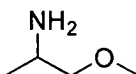
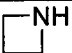

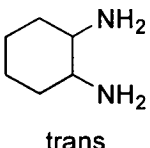
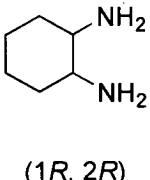
Results and discussion

135	0	0	
136	0	4	
137	0	5	
138	0	2.7	
139	67.2	915	
140	2.9	4.5	
141	0.1	101	
142	0	0	
143	Impure	Impure	

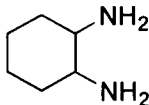
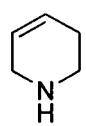
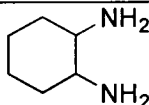
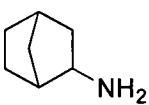
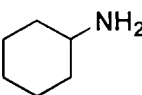
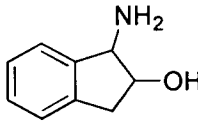
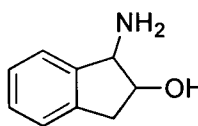
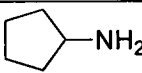
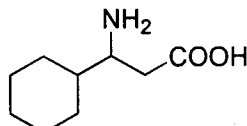
Results and discussion

144	0	29.9	
145	0	9.1	
146	Impure	Impure	
147	0	0	
148	0	7.6	
149	0.1	0.1	
150	0.7	0.1	
151	0	49.5	
152	0.3	24.1	
153	0	7.8	
154	Impure	Impure	

Results and discussion

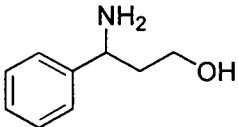
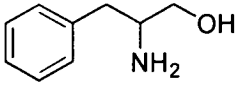
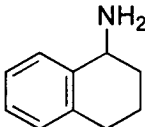
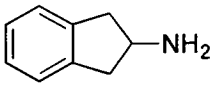
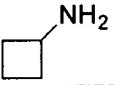
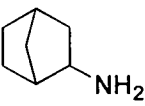
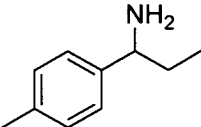
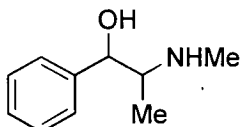
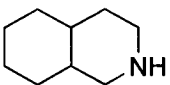
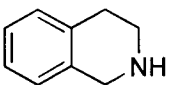
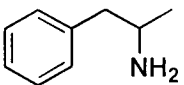
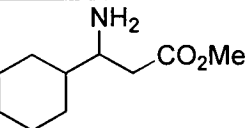
155	5.4	36.6	
156	0	0.1	
157	13.7	161	
158	0.4	16.3	
159	4.4	141	
160	0	0.7	
161	0	2.2	
162	0.4	1.4	
163	0.5	0.2	
164	0	0	
165	0	0.6	
166	1.2	0.2	

Results and discussion

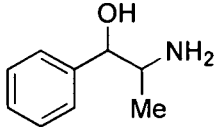
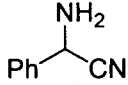
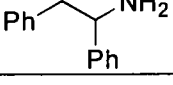
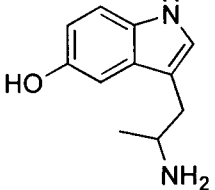
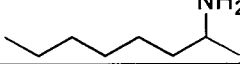
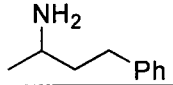
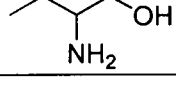
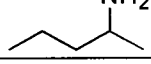
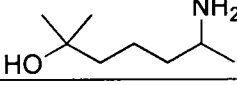
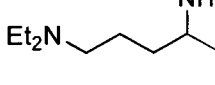
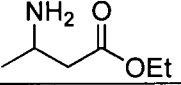
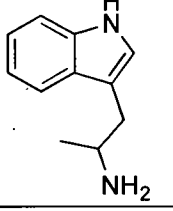
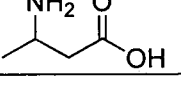
167	0.7	4.1	 (1 <i>S</i> , 2 <i>S</i> )
168	12.5	0.4	
169	1.2	0.7	 <i>cis</i>
170	512	183	 predominately <i>endo</i>
171	0	11.4	
172	0	0.9	 (1 <i>R</i> , 2 <i>S</i> )
173	0	0	 (1 <i>S</i> , 2 <i>R</i> )
174	0	6.7	
175	0	0	



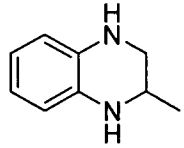
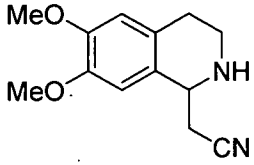
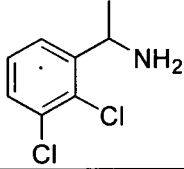
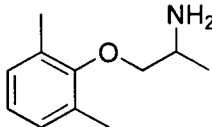
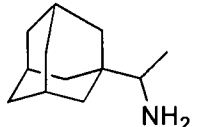
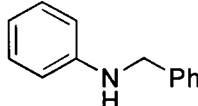
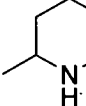
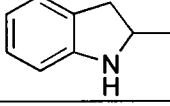
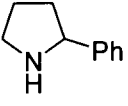
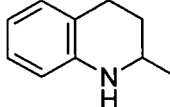
Results and discussion

176	0	7.2	
177	0	0.1	
178	0	2.2	
179	0	0.9	
180	0	0	
181	1	2.5	 exo
182	0	0	
183	0.5	0.2	
184	13.6	3.7	
185	1321	60.3	
186	0.6	1.4	
187	0.2	0.1	

Results and discussion

188	0	0	
189	0	0	
190	5.8	1.7	
191	0.5	0.1	
192	9.7	0.8	
193	0	2.7	
194	0	0	
195	3	39.6	
196	0	0	
197	0	0.1	
198	0	0	
199	0.2	0	
200	0	0.1	

Results and discussion

201	Impure	Impure	
202	2.2	0.8	
203	0.6	4.6	
204	0	0	
205	68.3	175	
206	0	0	
207	0	1.0	
208	0	0.4	
209	499	4080	
210	0	0	

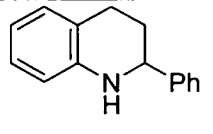
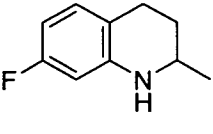
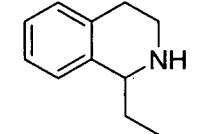
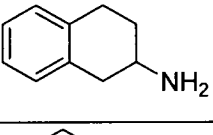
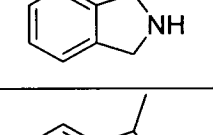
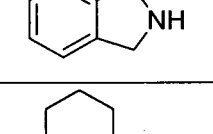
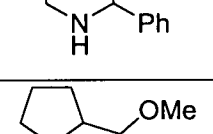
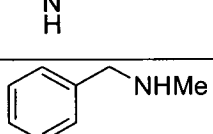
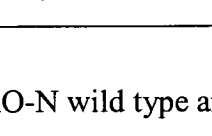
211	0	0	
212	0	0	
213	Impure	Impure	
214	3.2	1.2	
215	Not determined	2053	
216	Not determined	111	
217	14	9.4	
218	Not determined	187	
219	Not determined	2447	

Table 2.2.2.1. Percentage relative rate of amines screened against MAO-N wild type and MAO-N *I* variant.

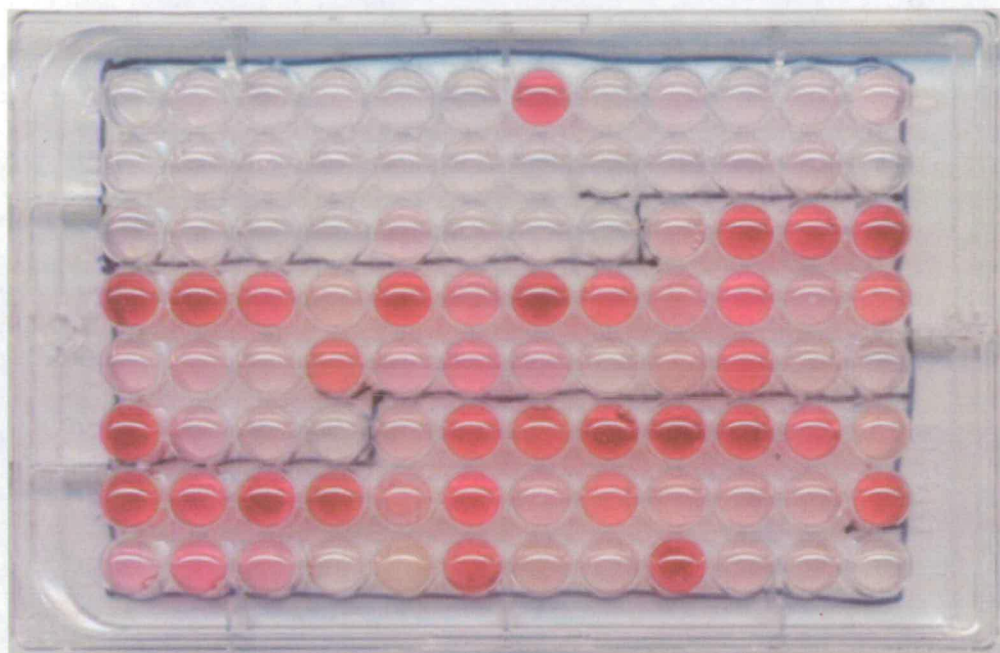


Figure 2.2.2.1. 96-well microtitre plate based screening of various amines with the MAO-N I variant.

The results indicated an improvement in activity for a significant number of the amines (49 amines) for the MAO-N I variant compared to the wild type and only 19 amines tested were found to have greater activity with the wild type. This data shows that the N336S substitution has caused an improvement in MAO-N activity towards many more amines than  $\alpha$ -methylbenzylamine-**24** (this substrate was used for the generation of this variant through directed evolution).

Although a 3-dimensional structure of the enzyme was unavailable at the time, the substrate specificity changes due to the N336S M348K substitutions have been summarised (figure 2.2.2.2). The wild type enzyme has activity towards simple achiral amines such as benzylamine and amylamine, but the N336S substitution has changed MAO-N specificity so that amines with  $\text{NH}_2\text{CH}_2$  and  $\text{NHMe}$  functionality at the amino

position were active in the assay. The MAO-N I variant continues to be capable of oxidising amine substrates with the NH<sub>2</sub> functional group. The changes in MAO-N resulting from the N336S substitution have enabled hydrophobic alkyl and aryl groups at the R-position of the amine substrates to be tolerated. In particular, cyclohexyl and adamantyl type R-groups were both excellent substrates against the MAO-N I enzyme. The results of the MAO-N specificity broadening for the amines that were screened in the MAO-N wild type and the MAO-N I variant assays is summarised in table 2.2.2.2. Based on the relative rates measured (below 5% being considered as non-active substrates) the wild type showed activity against 13 amines and MAO-N I variant showed activity against 36 amines from the total 93 amines screened (excluding the 5 impure substrates).

Percentage rates relative to ( <i>rac</i> )-amine <b>24</b>	>5%	5-25%	25-100%	100-200%	>200%
Wild type	76	7	2	0	4
MAO-N <u>I</u> variant	57	16	6	9	5

Table 2.2.2.2. Distribution of activities of amines from screening

The MAO-N enzymes tend to have a preference for hydrophobic alkyl and aryl groups at the R-position. For the other position  $\alpha$  to the amino group the amine screening has identified substrates that have groups other than methyl, as in the case of amine **24**, that can be oxidised by the MAO-N I enzyme. The specificity of the MAO-N I variant is broadened, enabling substrates having CH<sub>2</sub>OH (amine **151**) and CH<sub>2</sub>CH<sub>2</sub>OH (amine **176**) to be oxidised. However, the majority of substrates screened continued to show preference for  $\alpha$ -methyl substrates, as these had the highest activities of the amines that were screened. It was interesting to observe that although the MAO-N I variant was selected during directed evolution experiments to have activity towards amine **24**,

activity has been found to increase towards most of the amines tested compared to wild-type with some chiral amines displaying higher activity than amine **24**.

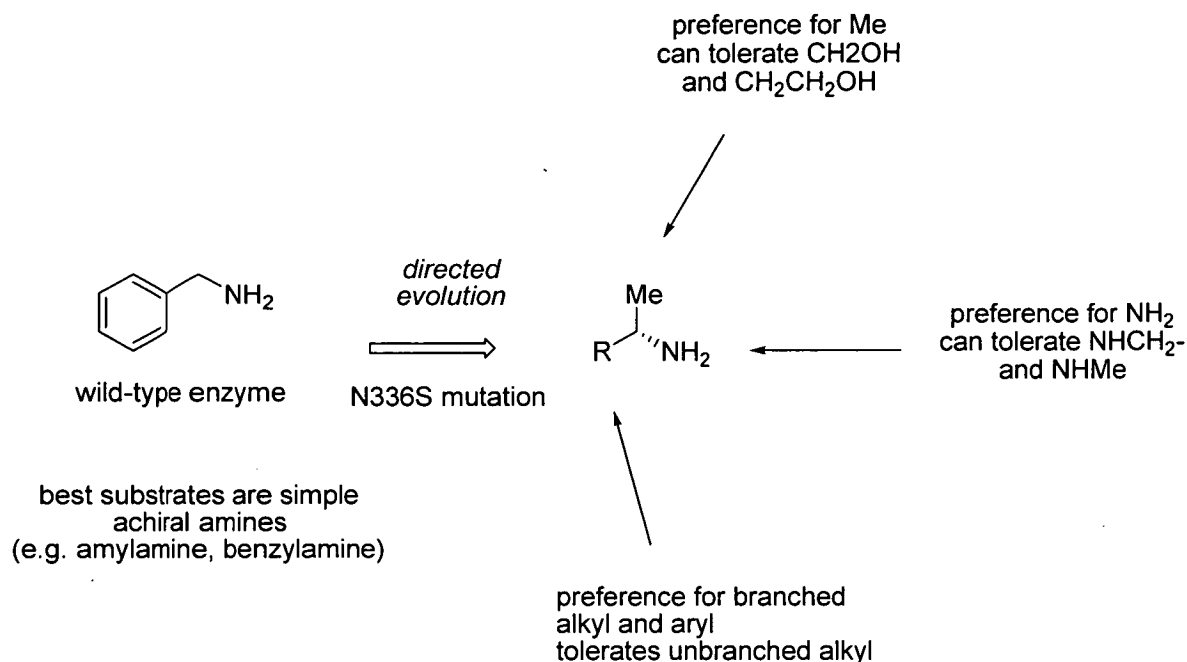


Figure 2.2.2.2. Summary of MAO-N specificity changes arising from the N336S mutation in MAO-N. (N.B. the M348K mutation was shown to improve expression but not specificity of MAO-N<sup>153</sup>)

### 2.2.3. Enantioselectivity of the MAO-N I enzyme

The screening of MAO-N I variant against the amine panel identified numerous active chiral amines. If they were to be considered as substrates for deracemisation then the enantioselectivity of the MAO-N I enzyme in the oxidation of these substrates needed to be examined. The deracemisation principle used in this project relies on the enantioselective oxidation of a single enantiomer of a racemic substrate. If the enzyme displays poor enantioselectivity it will be unsuitable as a biocatalyst in the deracemisation. Substrates that showed activity in racemic form (table 2.2.2.1) and where the single enantiomers were commercially available, the individual enantiomers

were assayed to evaluate enantioselectivity. Each enantiomer was assayed at a concentration of 10mM and the oxidation rates were measured in the same manner as the previous experiment (table 2.2.2.1). All the rates were measured relative to (*S*)-amine **24**, which was set at 100% activity (3.1.3) (table 2.2.3.1).

Amine	( <i>R</i> )-activity %	( <i>S</i> )-activity %	( <i>S</i> )/( <i>R</i> )
<b>24</b>	0.5	100	200
<b>76</b>	0.2	3.1	15.5
<b>125</b>	0.7	96.8	138
<b>126</b>	1.3	126	96.9
<b>127</b>	0.3	21.8	72.7
<b>128</b>	0.2	38.7	194
<b>134</b>	0.6	55.3	92.2
<b>139</b>	26.3	353	13.4
<b>141</b>	1.1	312	284
<b>144</b>	0.2	23.1	116
<b>151</b>	35.1	0.1	351

Table 2.2.3.1. Oxidation rates of amine enantiomers based on the peroxidase assay for MAO-N 1 enzyme. The enantioselectivity is calculated by (*S*)-activity/(*R*)-activity (except amine **151** where enantioselectivity = (*R*)-activity/(*S*)-activity).

Of the eleven amines tested in single enantiomer form, all showed high levels of enantioselectivity. Amine **151** showed the highest enantioselectivity in the MAO-N 1 catalysed oxidation, based on the ratio of the oxidation rates of the (*R*)- and (*S*)-enantiomers. Amine **139** had the lowest enantioselectivity. The poor enantioselectivity of amine **76** arises because of the inherent poor activity of the (*S*)-enantiomer compared to other substrates; generally the observed high enantioselectivities for the other substrates was caused by increased (*S*)-enantiomer activity compared to wild type (data not shown). Amine **139** was a very active substrate in racemic form (table 2.2.2.1) and



had the highest (*S*)-activity out of the amines tested, but its poor enantioselectivity with the MAO-N 1 enzyme catalysed oxidation results from the (*R*)-enantiomer having significant activity. The high enantioselectivity of the amines screened are shown below (figure 2.2.3.1) it shows the percentage rates of each enantiomer for the total activity of the substrate.

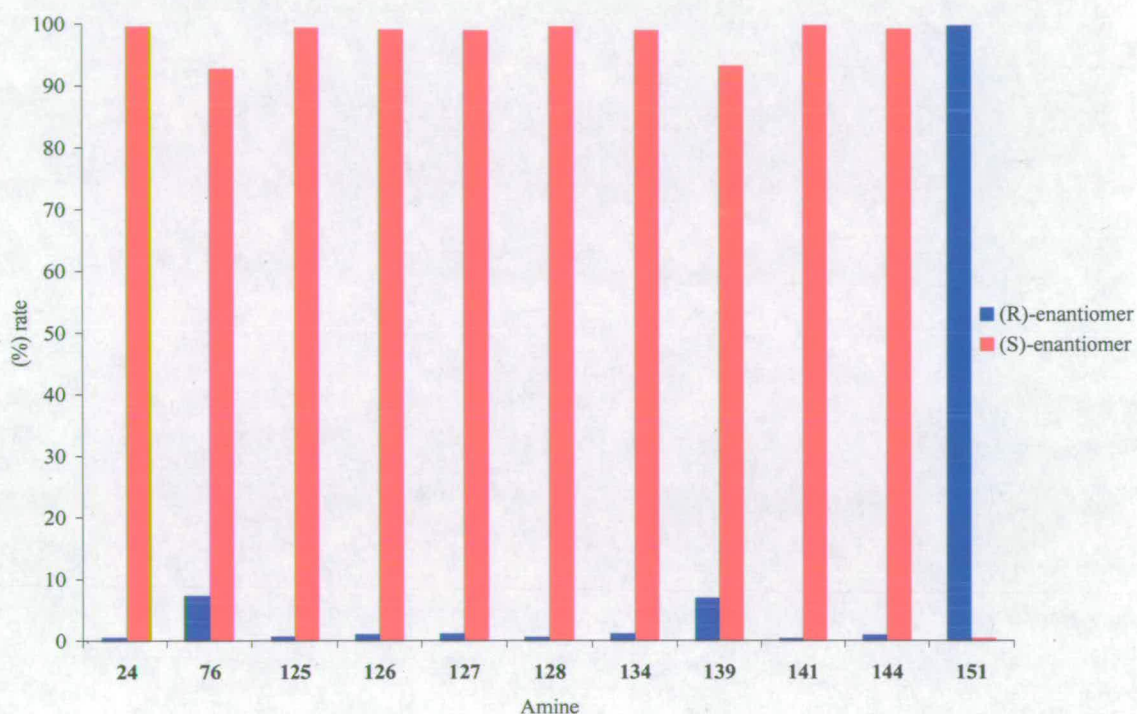


Figure 2.2.3.1. The composition of substrate activity for the enantioselective oxidation with the MAO-N 1 enzyme.

Amine **151** had the highest enantioselectivity of those tested, but with reversal of enantioselectivity to the (*R*)-enantiomer. The reversal of enantioselectivity is caused by the change in priority in the assignment of stereochemistry. The priority of the  $\alpha$ -methyl carbon is raised relative to the other  $\alpha$ -carbon (phenyl) by the hydroxyl substitution on the  $\alpha$ -carbon. If it was assumed that the amino group and the R-group (phenyl) were important groups in substrate binding at the MAO-N active site then the face of

oxidation of amine **151** and amine **24** are the same, maintaining enantioselectivity. The reversal of enantioselectivity becomes more obvious with the Newman projection of the chiral centre, as shown in figure 2.2.3.2, with the coloured numbering of the constituents around the chiral centre indicating the change in the assignment of absolute stereochemistry.



Figure 2.2.3.2. Assignment of stereochemistry of the active enantiomer for amine **24** (*(S)*-selective) and amine **151** (*(R)*-selective).

#### 2.2.4. Oxidation of MTQ (amine 76)

It has been shown that MTQ (amine **76**) was an active substrate in the oxidation catalysed by the MAO-N I enzyme and examination of the enantioselectivity of this oxidation showed high (*S*)-selectivity, making it a good candidate for deracemisation. Oxidation of MTQ results in a cyclic imine product; this is less likely to become hydrolysed under the aqueous deracemisation reaction conditions since the reduction in degrees of freedom compared to an acyclic imine stabilise the water labile bond. This should enable higher yields to be achieved in the deracemisation of this substrate than the 77% yield (93% e.e.) achieved with  $\alpha$ -methylbenzylamine (amine **24**).

Although the MAO-N I variant catalyses an enantioselective oxidation of MTQ, the mechanism of the oxidation needed to be examined to investigate whether it gave an achiral imine product. There is a choice of regioselectivity for MTQ oxidation as there are two routes by which amine **76** can be oxidised by MAO-N (as shown in figure

2.2.4.1). For primary amines there is only one route because there is only a single proton  $\alpha$  to the amino group available. For secondary amines there are two choices of  $\alpha$ -protons that can be removed to give the imine and tertiary amines have three  $\alpha$ -protons which would mean that there are 3 possible imine products.

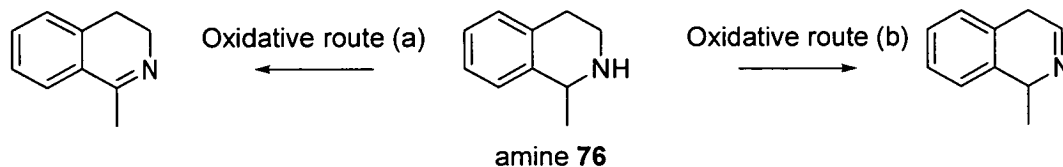


Figure 2.2.4.1. Two possible routes for amine **76** oxidation by MAO-N.

If oxidative route (a) is performed by MAO-N an achiral product is generated. If oxidative route (b) is followed the imine still contains a chiral centre and deracemisation of this substrate is not possible. The availability of the (*S*)-enantiomer of MTQ allowed a stereoinversion experiment to be performed. A stereoinversion of (*S*)-MTQ can determine whether the MAO-N I enzyme follows oxidative route (a) or (b). Freshly prepared enzyme, ammonia borane and (*S*)-MTQ were left to react for 90 hours at 30°C (3.6.1). The reaction was then analysed by chiral HPLC (3.7.1.A) (figure 2.2.4.2) (work carried out by T.S.C. Eve, University of Edinburgh). The analysis showed the presence of (*R*)-MTQ which indicated that, to some degree, oxidative route (a) was occurring; therefore a deracemisation of MTQ should be possible. By the end of the reaction there was no soluble protein left in the stereoinversion reaction (soluble protein measured by the Bradford assay) and precipitated protein was visible in the reaction tube.

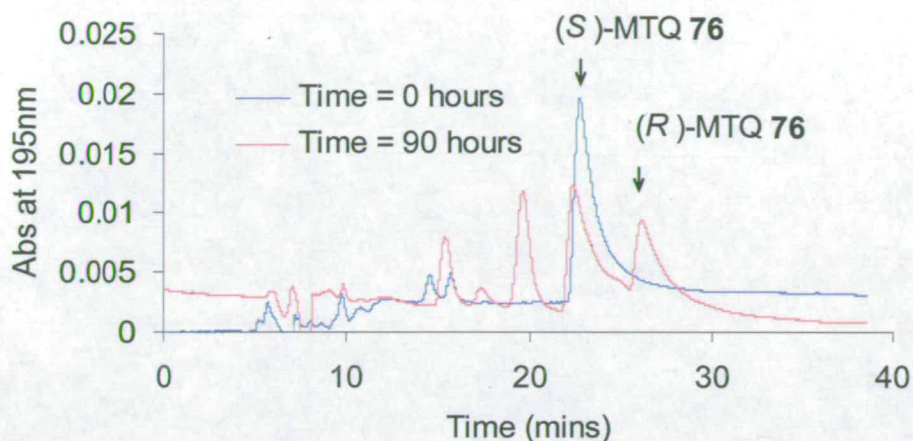


Figure 2.2.4.2. Chiral HPLC monitoring of the stereoinversion of (*S*)-MTQ with purified MAO-N I enzyme and ammonia borane (courtesy of T.S.C. Eve, University of Edinburgh).

### 2.2.5. Conclusion

The instability of purified MAO-N meant that measuring specific activities of amine oxidation rates was unreliable. Instead a relative rate screen of amine oxidation rates was performed, with all the rates measured relative to (*rac*)-amine **24** ( $\alpha$ -methylbenzylamine). The MAO-N I enzyme was shown to have a broadened substrate specificity compared to the wild type enzyme. MAO-N I specificity has been summarised and shown to accept large bulky hydrophobic R-groups, with a preference for  $\alpha$ -methyl and primary amino groups. The MAO-N I enzyme has high (*S*)-enantioselectivity which is important in the deracemisation reaction, where high enantioselectivity is crucial to achieve a high e.e. For the secondary amine **76**, high enantioselectivity was observed and the oxidation by MAO-N was shown (at least to some degree) to proceed by a route which could allow its deracemisation.

### **2.2.6. Future work**

The amine panel screening can be continually updated as new substrates are identified, allowing the identification of further substrates that would be suitable for deracemisation by MAO-N. For substrates that react in the peroxidase assay, the enantioselectivity of the MAO-N catalysed oxidation will need to be tested. If necessary, the enantioselectivity could be determined by analytical techniques other than spectrophotometrically with the peroxidase assay, using chiral separation techniques such as chiral HPLC, chiral GC and CE. If secondary and tertiary amines are identified in the amine screen the route by which MAO-N catalyses the oxidation will need to be examined, to determine whether they can be deracemised.

## 2.3. Directed evolution of MAO-N

### 2.3.1. Mutation strategy for MAO-N

There are several protocols by which a mutant library can be generated as discussed, (1.4.1). The Epicurian coli, mutator strain XL1-Red<sup>158</sup> was chosen as the choice for introducing mutations in *mao* because this was the successful approach that had led to the discovery of the MAO-N N336S variant<sup>153</sup>. Experience in our laboratory meant that the handling and use of this technique was well understood. The XL1-Red strain provides a highly efficient, rapid and reproducible method for introducing random mutations. The major advantage of this method is that it is not labour intensive and is less time consuming than other methods. It has been experimentally measured that in pBluescript the mutation rate was 1 mutation per 2kb after 30 generations<sup>159</sup>. In XL1-Red the mutation rate is typically 1 mutation/ $5 \times 10^6$  bp/generation/cell and because of the damaging effect this has on *E. coli*, the doubling time for this strain is lowered to approximately 90-120 minutes, compared to 20 minutes for wild type *E. coli* (Stratagene). Random mutations are introduced throughout the entire genome and include transitions, transversions and single base deletions/insertions.

The *mao* gene is 1489 base pairs in length, so assuming an error rate comparable with the rate observed with pBluescript then it would take 22.3 generations for the introduction of a single mutation (assuming a doubling time of 120 minutes this would mean that a total of 44.6 hours would be required). The efficiency of the XL1-Red mutator strain has been calculated with pUC18, based upon screening for knocking out of  $\beta$ -galactosidase activity. After 48 generations 1.2% of the colonies screened were found to no longer have  $\beta$ -galactosidase activity<sup>153</sup>.

---

XL1-Red competent cells were transformed with the *mao I* gene in pET-16b DNA using a modified version of the manufacturer's protocol (3.3.4). The transformed cells were used to inoculate 10ml of LB containing 100µg/ml ampicillin. The cells were grown for 18 hours and 20µl of this overnight growth was added to a further 10ml of LB containing 100µg/ml ampicillin. After the inoculum had grown for 24 hours, 1ml was removed for isolation of the plasmid DNA (3.4.1). This procedure gave the first generation library of mutants. The plasmid DNA of the first generation mutants was then used in a second transformation of XL1-red competent cells; inoculation, growth and purification of plasmid DNA was repeated as before, giving a second generation library of mutants. This process was repeated four times until a fourth generation of mutants had been prepared. The extent to which *mao* was mutated was limited to the fourth generation mutant library because this level of mutagenesis with XL1-red had led to identification of the N336S mutation from the wild type<sup>153</sup>.

### 2.3.2. Proposed directed evolution

The existing MAO-N *I* variant had good activity towards chiral primary amines but showed only low activity towards secondary amines. Although the MAO-N *I* variant had been shown to be active towards the secondary amine MTQ (amine **76**) the rate was low at ca. 9% relative to  $\alpha$ -methylbenzylamine (amine **24**) (2.2.2), making this amine a good target substrate for directed evolution of MAO-N to improve activity. Amine **76** was selected as a candidate for screening the fourth generation MAO-N mutant library for a MAO-N variant that was more capable of oxidising a secondary amine. If a MAO-N variant could be discovered, the deracemisation of this substrate compared with the acyclic amines might be higher yielding because the corresponding imine product is more stable. A further reason for selecting amine **76** was that gram quantities of the amine were available in racemic, (*S*)- and (*R*)-enantiomer form. The proposed directed evolution of MAO-N towards amine **76** is outlined in figure 2.3.2.1.

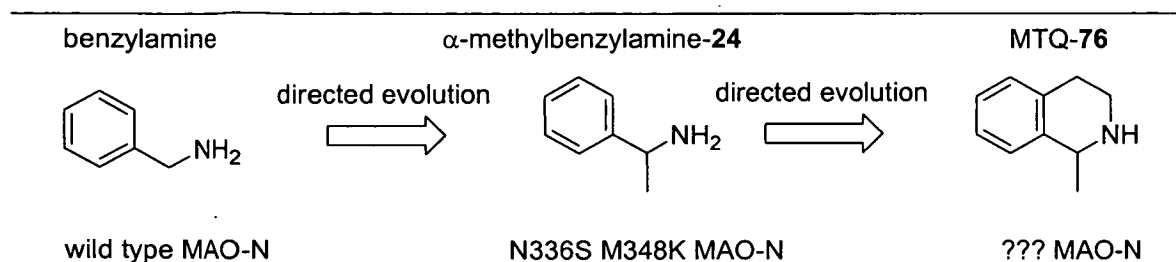


Figure 2.3.2.1. Proposed directed evolution of MAO-N I variant to identify a MAO-N variant with improved activity towards amine **76**. The first round of directed evolution of MAO-N wild type to the MAO-N I variant is shown.

### 2.3.3. Solid phase assay

The solid phase assay used in the screening of MAO-N variant libraries is based on a similar approach to the liquid assay used in the earlier screen (2.2.1). Horseradish peroxidase (HRP) catalyses the reaction of hydrogen peroxide with another substrate. The hydrogen peroxide is produced as a by-product from the amine oxidation catalysed by MAO-N. However, rather than using aminoantipurine as in the liquid assay (figure 2.2.1.1) an alternative substrate was used for the HRP step. The change of substrate for HRP was necessary because the product from the 4-aminoantipurine dye product was found to diffuse through the solid phase matrix resulting in a loss of resolution<sup>153</sup>. Switching to 3,3'-diaminobenzidine DAB as the HRP substrate gave rise to a brown oxidation product which was less soluble giving higher definition and greater contrast between the matrix and colony. The appearance of a brown halo surrounding an *E. coli* colony on the plate indicates MAO-N activity towards the amine substrate being screened. This colony is regarded as being a 'hit'. The mechanism by which the DAB dye product is generated is shown in figure 2.3.3.1.



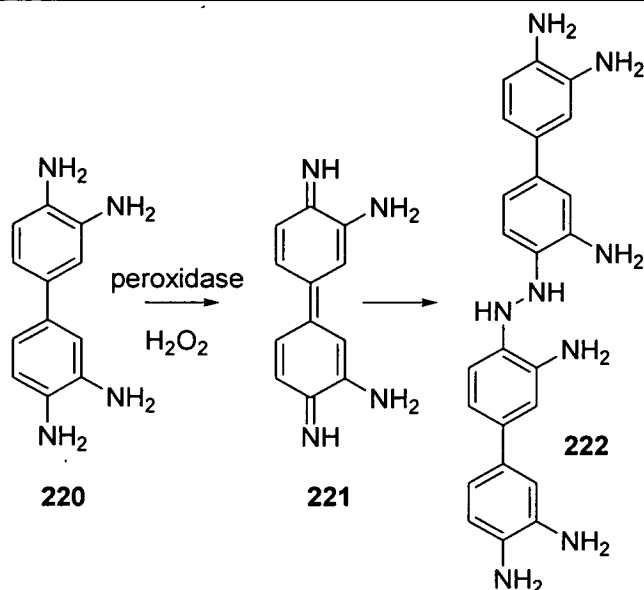


Figure 2.3.3.1. Peroxidase coupled reaction of hydrogen peroxide and DAB in the solid phase assay.

#### 2.3.4. Screening of MAO-N variant library with MTQ

Plasmid DNA from the fourth round of mutagenesis generated by XL1-Red was used to transform BL21 (DE3) star *E. coli* competent cells, which were then plated on to nitrocellulose membranes on LB agar plates containing 100µg/ml ampicillin. The colonies were left to grow for 16 hours resulting in a library of ca. 12000 variants (3.1.1). The membranes were subjected to a freeze-thaw cycle to partially lyse the cells and allow the MAO-N activity to be accessible for the assay. The (*rac*)-MTQ (amine 76) assay mixture was poured directly onto the nitrocellulose membranes containing the partially lysed cells and the assay left to develop at room temperature (3.1.6). It was apparent that a single colony (MAO-N 2) was visible after 24 hours which was more darkly coloured compared to the other colonies. MAO-N 2 was picked along with several other colonies (1a, 1b, 1c and 1d) which were randomly selected from the library and grown in 5ml of LB containing 100µg/ml ampicillin along with a control colony of a MAO-N 1 variant from which the library was generated. After 16 hours growth, 1ml of

## Results and discussion

the cells was used for purification of plasmid DNA (3.4.1), the remainder of the cells were used for further characterisation of MAO-N 2 and the other selected colonies. The cell suspensions (10µl in each assay) were assayed against amylamine (amine **124**), (*rac*)- $\alpha$ -methylbenzylamine (amine **24**) and (*rac*)-MTQ (amine **76**) in a 96-well microtitre plate using the previously described assay (3.1.1). After 2 hours monitoring on the plate reader there was no change in OD<sub>510nm</sub> so the microtitre plate was covered and left to react for 60 hours (figure 2.3.4.1). The results, as judged by colour formation supported the previous observation that MAO-N 2 had improved MTQ (amine **76**) activity compared to the MAO-N 1 variant. The activity in the (*rac*)- $\alpha$ -methylbenzylamine (amine **24**) assays did not show significant production of colour as might have been expected. All the amylamine (amine **124**) assays gave a positive response; the discrepancy seen with (*rac*)- $\alpha$ -methylbenzylamine (amine **24**) may be influenced by the fact that this is a whole cell assay. Other factors which could account for the poor response of the (*rac*)- $\alpha$ -methylbenzylamine (amine **24**) assays include diffusion of product across the cell membrane and possibly an endogenous *E. coli* enzyme interfering with the coupled assay.

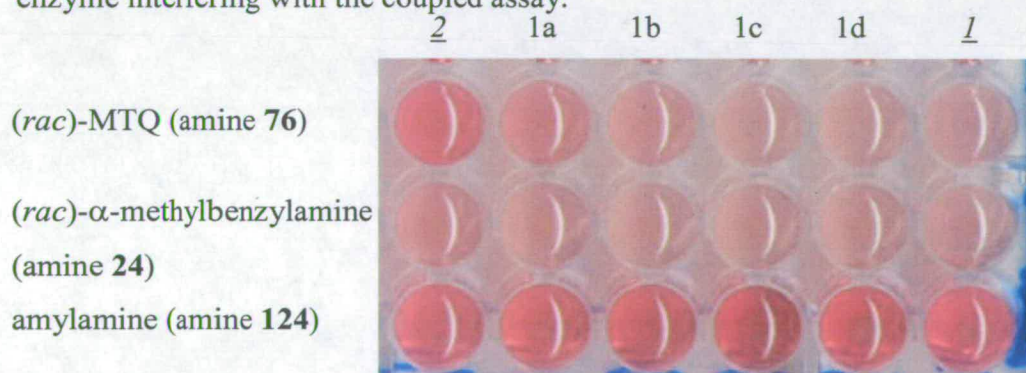


Figure 2.3.4.1. Liquid phase peroxidase assay of MAO-N 2, MAO-N 1 variant and random colonies (1a, 1b, 1c and 1d) from variant library activities towards amylamine (amine **124**),  $\alpha$ -methylbenzylamine (amine **24**) and MTQ (amine **76**) after 60 hours.

To further examine and validate whether MAO-N 2 had improved MTQ (amine **76**) activity 50µl of the 16 hours growth of MAO-N 2 and the MAO-N 1 variant were spread

## Results and discussion

on nitrocellulose membranes on LB agar containing 100 $\mu$ g/ml ampicillin and left to grow for a further 16 hours. The membranes were freeze/thawed and the solid phase assay repeated using racemic, (*R*)- and (*S*)- $\alpha$ -methylbenzylamine (amine **24**) and MTQ (amine **76**) (3.1.6). The nitrocellulose membranes from each were divided into quarters allowing each variant to be measured in each solid phase assay in duplicate. This removed any discrepancies that could arise between each of the solid phase assay plates.

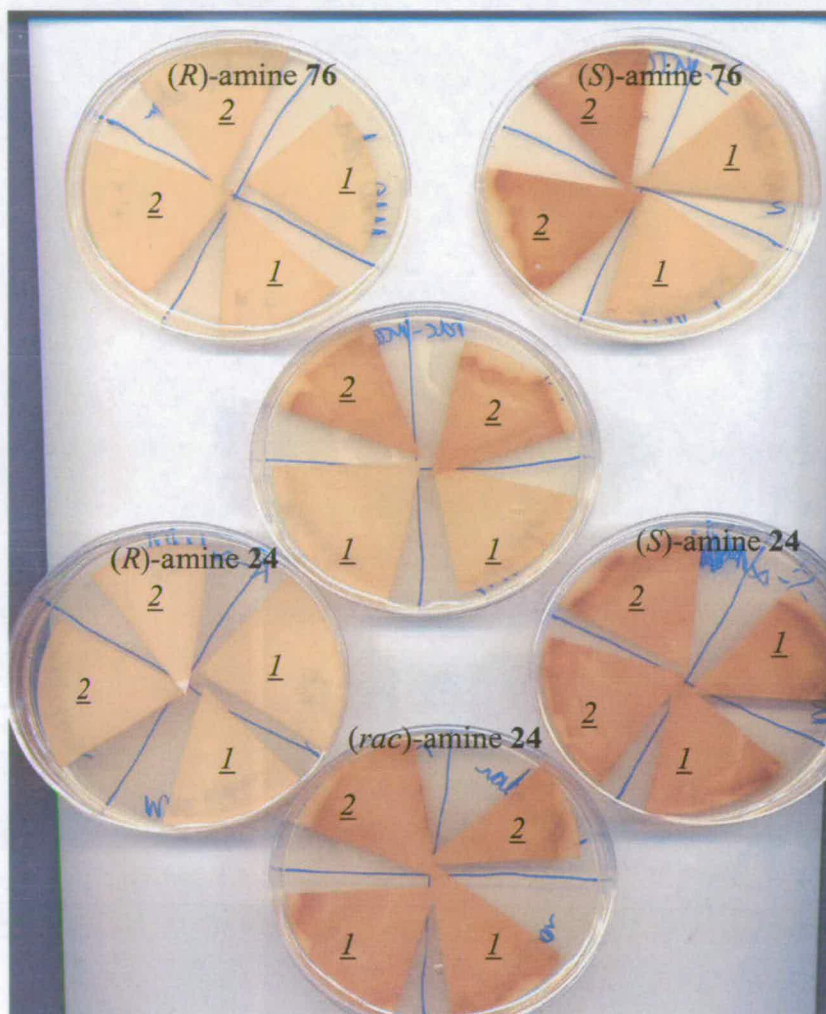


Figure 2.3.4.2. Solid phase assay of MAO-N 1 variant and MAO-N 2 variant against (*R*)-amine **24**, (*S*)-amine **24**, (*rac*)-amine **24**, (*R*)-amine **76**, (*S*)-amine **76** and (*rac*)-amine **76**.

It is evident from the solid phase assay that there is an improvement in MAO-N 2 (*S*)-MTQ (amine **76**) activity when compared with the parent MAO-N 1 variant. There appears to be little difference in the solid phase assay in  $\alpha$ -methylbenzylamine (amine **24**) activities. Encouragingly, the improvement in activity was only seen in the (*S*)-enantiomer which was promising for potential use as a biocatalyst in a deracemisation reaction where high enantioselectivity is vital. MAO-N 2 plasmid DNA, isolated from the overnight growth, was transformed into BL21 (DE3) cells and 50 $\mu$ l spread onto a fresh nitrocellulose membrane on LB agar containing 100 $\mu$ g/ml ampicillin. This gave single isolated colonies and verified the same result as seen in figure 2.3.3.3 with (*S*)-amine **76** and (*rac*)-amine **76** reacting faster with the MAO-N 2 than the MAO-N 1 variant in the peroxidase/DAB solid phase assay (3.1.6).



Figure 2.3.4.3. Single colony solid phase of MAO-N 2 (right hand segment of nitrocellulose membrane) and MAO-N 1 variant (left hand segment of nitrocellulose membrane) against (*R*)-amine **76** (left plate) and (*S*)-amine **76** (right plate).

### 2.3.5. Specificity or expression mutant?

The solid phase screen had identified a variant that possessed improved activity towards MTQ (amine **76**) with retention of high (*S*)-enantioselectivity. The solid phase screening does not distinguish between mutations that lead to an increase in expression of the enzyme or a change in the catalytic activity. The MAO-N 1 variant had been shown to

---

have a low, but measurable, activity towards MTQ (amine **76**) so an improved expression could potentially cause the result observed in the solid phase assay, without changing the catalytic performance of the parent enzyme. To test whether a specificity or expression variant had been generated, a 96-well assay was performed on the cell free extract (CFE). A single freshly transformed BL21 (DE3) colony containing the MAO-N 1 plasmid or MAO-N 2 plasmid was grown to stationary phase overnight. CFE was prepared and an assay of the amine was carried out (3.1.4). The 96-well microtitre plate was divided into 3-sections, each having 32 wells, one for MAO-N 2, one for the MAO-N 1 variant and one third for as a control (i.e. no addition of MAO-N). From the original screening carried out on the MAO-N 1 variant (2.2.2) 32 substrates were selected to provide a structurally diverse selection of amines to assess the specificity of MAO-N 2. If ranking the 32 substrates, in order of reactivity, was the same in the assays for the two variants of MAO-N, then it is probable that the MAO-N 2 is an expression variant. An expression variant can arise from a silent mutation of an amino acid codon to a degenerate codon which is more effectively translated in *E. coli* or by an effect elsewhere in the plasmid altering the level of transcription of the *mao* gene (e.g. the promoter region). The rate of oxidation for the screened substrates was measured relative to  $\alpha$ -methylbenzylamine (amine **24**) (normalised to 100%). Those substrates showing activity <10% relative activity to amine **24** are not represented in figure 2.3.5.1. Amines **124**, **126**, **129** and **139** rates were not measurable in this screen as the oxidation rate was too fast and levelled off before the microtitre plate could be read in the plate reader.

## Results and discussion

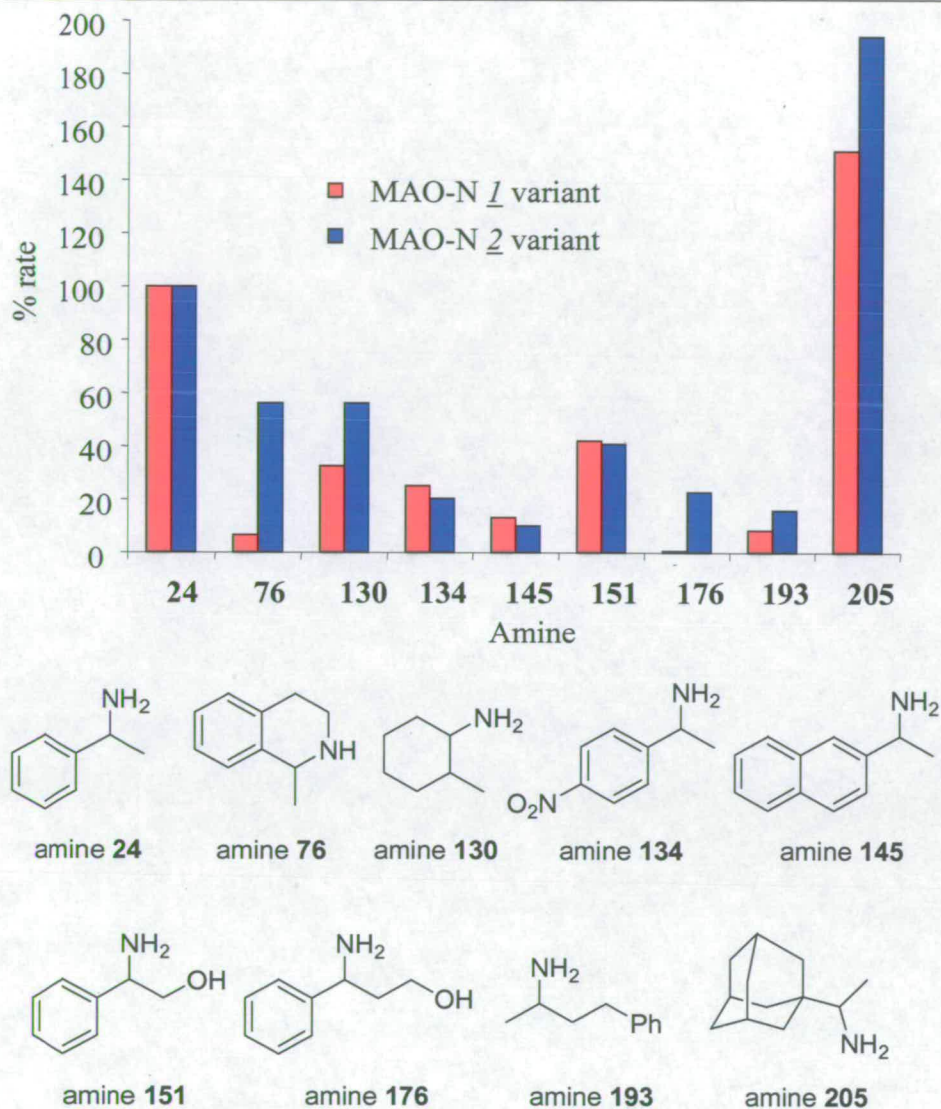


Figure 2.3.5.1. Relative rate activities of MAO-N 2 variant compared with MAO-N 1 variant towards a range of amines.

The relative rates were found not to be the same between the two variants indicating that there was indeed a change in specificity of MAO-N 2 against these substrates tested. Five of the amines (amines **76**, **130**, **176**, **193** and **205**) showed improved activity towards MAO-N 2 variant and three amines (amines **134**, **145** and **151**) had less activity. MTQ (amine **76**) had improved activity for MAO-N 2 compared with MAO-N 1 variant

---

with an 8.5 fold improvement. Amine **176** showed the greatest improved activity in the rate of amine oxidation from the MAO-N 1 to MAO-N 2 variant, with over a 39-fold improvement. CFE analysis by SDS PAGE showed no noticeable difference in the MAO-N band between the two variants further supporting the evidence that the change in MAO-N 2 is a specificity change and not an expression mutant.

### 2.3.6. Sequencing MAO-N 2

The MAO-N 2 plasmid was transformed into *E. coli* (TOP10) competent cells and a single colony from the transformation was picked and grown overnight in 10ml LB containing 100µg/ml ampicillin (3.3.2). Plasmid DNA was purified and the full *mao* gene sequenced. In order to sequence the complete gene five separate sequencing reactions were performed (3.4.4). Two commercial external primers were used which were complementary to the pET-16b plasmid sequence. Three internal sequencing primers were required to complete the sequencing within the *mao* gene.

Sequencing results revealed a single nucleotide change A to G at position 738. This corresponded to the amino acid residue 246 in *mao*. In the wild type enzyme the codon is ATA which encodes for an isoleucine residue. The A to G transition mutation for this codon in the MAO-N 2 changes the codon to ATG which encodes for methionine. This is a conservative change in amino acid at 246 both isoleucine and methionine are uncharged residues under physiological conditions and both are hydrophobic with methionine having a larger side chain volume than isoleucine. This conservative change in amino acid complements the overall change that the MAO-N 2 has undergone with regards to amine specificity. Of the amines screened there was no dramatic alteration of specificity just a general overall improvement in catalysis whilst maintaining the high level of (*S*)-enantioselectivity. On a molecular level, in the MAO-N enzyme it could be speculated that the I246M mutation has subtly altered the active site enabling improved catalysis for amine **76**. The change from isoleucine to methionine results in removal of a

$\beta$ -methyl branch in the amino acid side group. This removal of steric interference could improve the non-bonding van der Waals contacts between enzyme and ligand. Enzyme specificity for substrate can be driven by hydrophobic exclusion and Van der Waals interactions between the enzyme's active site and the substrate. For example aminoacyl tRNA synthases have the ability to discriminate subtle changes in amino acid side groups. Isoleucyl tRNA synthase has to select between isoleucine and valine. Valine, being shorter by one methylene group than isoleucine binds to isoleucyl tRNA synthase, but 150 times more weakly<sup>160</sup>.

### 2.3.7. Kinetic parameters of MAO-N 2

The mutation introduced in MAO-N 2 was found to generally improve activity for the majority of the amines screened (2.3.8) and maintained the high enantioselectivity (2.3.9) compared to what was seen for the MAO-N 1 variant. To quantify more precisely the changes between MAO-N 2 and the parent MAO-N variant the  $k_{cat}$  and  $K_M$  for amylamine (amines **124**),  $\alpha$ -methylbenzylamine (amine **24**) and MTQ (amine **76**) was measured. Michaelis-Menten kinetic constants were calculated for these three substrates for both variants. Specific activity measurements were measured in the range 16.7mM to 10 $\mu$ M (over these data points: 16.7mM, 10mM, 8mM, 6mM, 4mM, 2mM, 1mM, 0.8mM, 0.6mM, 0.4mM, 0.2mM, 0.1mM, 50 $\mu$ M, 20 $\mu$ M and 10 $\mu$ M) and data analysed using SigmaPlot Enzyme Kinetic module (3.1.5).

MAO-N variant	amylamine (amine <b>124</b> )		<i>(rac)</i> - $\alpha$ -methyl benzylamine (amine <b>24</b> )		<i>(rac)</i> -MTQ (amine <b>76</b> )	
	$k_{cat}$	$K_M$	$k_{cat}$	$K_M$	$k_{cat}$	$K_M$
<u>1</u>	47.8 min <sup>-1</sup> ( $\pm$ 1.16)	0.359 mM ( $\pm$ 0.04)	4.13 min <sup>-1</sup> ( $\pm$ 0.07)	1.26 mM ( $\pm$ 0.07)	0.69 min <sup>-1</sup> <sup>1</sup> ( $\pm$ 0.02)	0.034 mM ( $\pm$ 0.008)
<u>2</u>	45.0 min <sup>-1</sup> ( $\pm$ 1.1)	0.462 mM ( $\pm$ 0.05)	6.40 min <sup>-1</sup> ( $\pm$ 0.3)	2.41 mM ( $\pm$ 0.23)	4.57 min <sup>-1</sup> <sup>1</sup> ( $\pm$ 0.17)	0.234 mM ( $\pm$ 0.04)

Table 2.3.7.1. Kinetic constants for amines **1**, **24** and **76** with MAO-N 1 and 2.



There are small changes in the amylamine (amine **124**)  $k_{cat}$  and  $K_M$  between the MAO-N 2 variant and the MAO-N 1 variant. However, for  $\alpha$ -methylbenzylamine (amine **24**) the differences are larger, the  $k_{cat}$  has increased 1.5 fold for MAO-N 2 from the MAO-N 1 and the  $K_M$  has risen by a similar order of magnitude. For MTQ (amine **76**) the same trend is observed with an increase in the  $k_{cat}$  and an increase in the  $K_M$  for MAO-N 2. But the scale of the increases is significantly greater for amine **76** than amine **24**, a 6.6 fold improvement in  $k_{cat}$  and a 6.9 fold rise in  $K_M$ . This shows the changes in MAO-N 2's substrate specificity have affected the activity in the order amine **124**<amine **24**<amine **76**.

MAO-N variant	Amine <b>124</b> $k_{cat}/K_M$	( <i>rac</i> )-amine <b>24</b> $k_{cat}/K_M$	( <i>rac</i> )-amine <b>76</b> $k_{cat}/K_M$
<u>1</u>	133 min <sup>-1</sup> mM <sup>-1</sup>	3.28 min <sup>-1</sup> mM <sup>-1</sup>	20.29 min <sup>-1</sup> mM <sup>-1</sup>
<u>2</u>	97.4 min <sup>-1</sup> mM <sup>-1</sup>	2.66 min <sup>-1</sup> mM <sup>-1</sup>	19.53 min <sup>-1</sup> mM <sup>-1</sup>


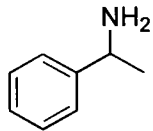
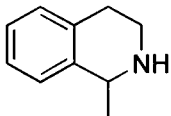
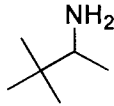
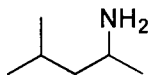
Table 2.3.7.2. Specificity constants ( $k_{cat}/K_M$ ) for amine **124**, (*rac*)-amine **24** and (*rac*)-amine **76** with MAO-N 1 and 2 variants.

The increases seen in both  $k_{cat}$  and  $K_M$  mean that the specificity constant ( $k_{cat}/K_M$ ) is largely unchanged. MAO-N 2 has slightly lower specificity constants compared to the parent enzyme. However, the higher  $k_{cat}$  for amine **76** should mean that the deracemisation should proceed faster.  $K_M$  is defined as the concentration of substrate at half  $V_{max}$ . The change in  $K_M$  from the MAO-N 1 variant to MAO-N 2 is significant because the increase in  $K_M$  will mean that the reaction will decelerate sooner for the MAO-N 2 variant. However, as the  $k_{cat}$  is 6.6 times higher for MAO-N 2 than the parent variant, even when the substrate concentration falls to the  $K_M$  the reaction is still operating 3 times faster. For example, at a concentration of 0.234mM of amine **76** the rate would have fallen to half the  $V_{max}$  for MAO-N 2 and at 0.0338mM of amine **76** the  $V_{max}$  will have halved for the MAO-N 1 variant. The effect of the mutation in the MAO-

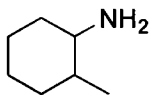
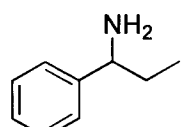
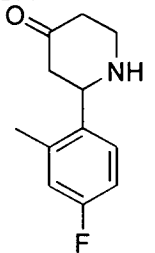
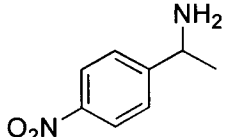
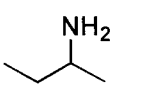
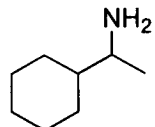
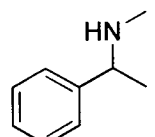
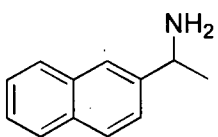
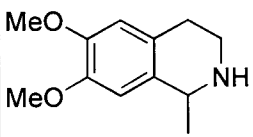
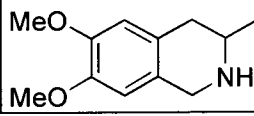
N 2 is to improve the turnover whilst lowering the affinity of the enzyme for the substrate.

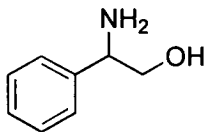
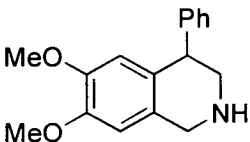
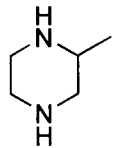
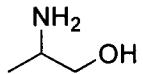
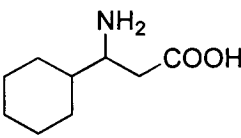
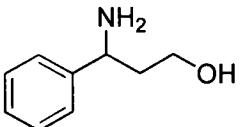
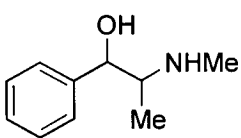
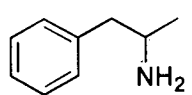
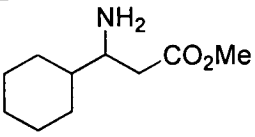
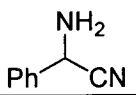
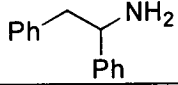
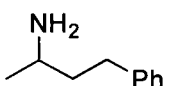
### 2.3.8. Screening MAO-N 2 variant against a panel of amines

To investigate the catalytic change in the MAO-N 2 variant, the protein was purified and its activity assessed against a range of amines and compared to the activity of the parent enzyme (MAO-N 1). MAO-N 2 protein was purified as described previously (3.2.2). By using purified MAO-N 2 a more accurate comparison of the changes in catalytic activity from the parent can be made, than with CFE (2.3.5), because it is not affected by other component enzymes from *E. coli*. Amine rates were measured relative to the rate measured for (*rac*)-amine **24** as described earlier (2.2.2). The relative rate for MAO-N 2 variant was divided by the relative rate measured for the same substrate with MAO-N 1 variant to indicate the change in specificity between the two variants.

Amine	MAO-N <u>1</u> variant (%)	MAO-N <u>2</u> variant (%)	Ratio = (2)/(1)	Structure
<b>124</b>	1307	653	0.5	
<b>24</b>	100	100	1	
<b>76</b>	9.1	47	5.1	
<b>126</b>	89.3	298	3.3	
<b>129</b>	190	489	2.6	

Results and discussion

130	18.6	69.3	3.7	
131	0	0	*	
133	0	1.1	*	
134	22.6	31.0	1.4	
138	2.7	3.1	1.2	
139	915	1984	2.2	
140	4.5	6.8	1.5	
145	9.1	1.5	0.2	
148	7.6	8.5	1.1	
149	0.1	1.8	18	

151	49.5	67.0	1.4	
156	0.1	1.0	10	
160	0.7	0.6	0.9	
161	2.2	0.6	0.3	
175	0	0.6	*	
176	7.2	24.7	3.4	
183	0.2	0.9	4.5	
186	1.4	3.5	2.5	
187	0.1	0	*	
189	0	0	*	
190	1.7	0	*	
193	2.7	10.1	3.7	

197	0.1	0	*	
199	0	0.2	*	
205	175	364	2.1	
206	0	0	*	
207	1.0	0	*	
208	0.4	0.1	0.3	
209	4080	2629	0.6	
210	0	0	*	
211	0	0	*	
212	0	0	*	

Table 2.3.8.1. Percentage relative rate screening of amines with MAO-N 2 variant and its rate ratio compared with the MAO-N 1 variant. \* = ratio not calculated when relative rate = 0% for either variant

---

The results from the screening of the MAO-N 2 variant against a panel of amines (figure 2.3.5.1) further support the earlier indications that the MAO-N 2 variant's activity has been altered with respect to the parent variant enzyme. The ratio of the MAO-N 2: MAO-N 1 variant would be 1 if MAO-N 2 was an expression mutant, but the ratios deviate from 1 indicating a specificity change. There are six substrates (amines 1, 24, 39, 40, 87 and 88) with ratios less than 1 indicating that the mutation introduced into the MAO-N 2 enzyme is detrimental for amine oxidation compared with MAO-N 1. There are 17 substrates that have an improved activity with MAO-N 2 compared to the MAO-N 1 variant, showing that for the majority of amines tested MAO-N 2 performed as a better catalyst in the oxidation. Amines that were shown to have good rates of oxidation with the MAO-N 1 variant are mostly shown to have an even higher activity with MAO-N 2, e.g. the rate measured for amine 139 with MAO-N 1 enzyme was 915% and this is increased to 1984% with MAO-N 2. The rate of oxidation measured for amine 76, the substrate that MAO-N 2 variant was selected from in the directed evolution experiment had an improvement of 5 times that of the MAO-N 1 mutant. In conclusion, the MAO-N 2 variant has generally improved rates for the oxidation of the amines that were screened; typically this improvement is 2-3 fold compared with the MAO-N 1 variant for substrates that previously were shown to be active.

### 2.3.9. Enantioselectivity of MAO-N 2

The change in MAO-N 2 resulted in a general improvement in the rate of amine oxidation which will be beneficial for the use of this MAO-N enzyme as a biocatalyst in the deracemisation of amines. However, it is important that the new variant enzyme maintains enantioselectivity in the deracemisation process. The enantioselectivity of MAO-N 2 enzyme was therefore assessed against a panel of amines and compared to the enantioselectivity of the parent MAO-N 1 enzyme. Single enantiomers were assayed at 10mM amine concentrations and rates were measured relative to (*S*)-amine 24 as previously described (2.2.3).

Amine	( <i>R</i> )-activity %	( <i>S</i> )-activity %	Enantioselectivity	Enantioselectivity of MAO-N <u>1</u>
<b>124</b>	0	100	>200	200
<b>76</b>	0.7	51.2	73	16
<b>125</b>	2.5	220	88	138
<b>126</b>	6.1	271	44	97
<b>134</b>	0	54.7	>200	92
<b>139</b>	64	2374	37	13
<b>142</b>	4.3	12.6	3	Not determined
<b>145</b>	0.3	22.8	76	Not determined

Table 2.3.9.1 Rates of amine enantiomers based on peroxidase assay for MAO-N 2 and its enantioselectivity.

The enantioselectivity of MAO-N 2 maintains the high (*S*)-enantiomer preference as was observed for MAO-N 1. For the oxidation of MTQ (amine **76**) by MAO-N 2 the enantioselectivity has risen to 73.1 from 15.5 compared with the MAO-N 1 variant, this is primarily caused by the increased in (*S*)-enantiomer reactivity. MAO-N 2 also shows improvements in the enantioselective oxidation of amine **139** which has risen to 37.1 from 13 of the parent, again caused primarily by an increase in (*S*)-enantiomer reactivity rather than a change in (*R*)-enantiomer reactivity. In the MAO-N catalysed oxidation of the (*R*)-enantiomer of amine **139** reactivity has increased to 64% with MAO-N 2, compared with 26.3% for the MAO-N 1 variant. Despite this increase in the oxidation of (*R*)-amine **139** by MAO-N the enantioselectivity has still risen since the rate of oxidation of the (*S*)-enantiomer by MAO-N 2 has increased over six times. The enantioselectivity for the MAO-N 2 catalysed oxidation of amine **142** showed the poorest selectivity.

### 2.3.10. Conclusion

XL1-red was chosen as the mutation strategy for further evolving MAO-N 1 towards amine **76**. The solid phase assay, a high throughput screen, was employed in the screening of 12,000 colonies to identify MAO-N 2. The evidence from the kinetic characterisation of MAO-N 2 in the amine screening showed it to be a specificity mutant whilst maintaining high (*S*)-enantioselectivity of the parent. There was an increase in  $k_{cat}$  for amine **24**, but the greatest increase was seen for amine **76** with a 6.6 fold improvement from the parent to MAO-N 2. The  $K_M$  has risen for both substrates as well as the  $k_{cat}$ , meaning that the catalytic efficiency of the enzyme slightly decreased. Sequencing of the *mao* gene identified the mutation in MAO-N 2 to be a transition of A to G at nucleotide 738. This translates to amino acid residue 246 in the protein sequence, which is encoded by ATA (isoleucine) in the parent and ATG (methionine) in MAO-N 2. In concluding, the MAO-N 1 enzyme has been evolved for increased activity for a secondary amine by the introduction of the I246M change.

### 2.3.11. Future work

Directed evolution can be used to make other improvements to MAO-N. It may be desirable to find a MAO-N variant that has other desirable features such as thermal stability, tolerance to organic solvents, reversal of enantioselectivity or activity towards novel substrates (i.e. tertiary amines). Preparation of the library of variants is reasonably straightforward and the mutation rate can be control by the number of times the gene is propagated in the XL1-red Mutator strain. Techniques such as replica plating and/or isolation of plasmid DNA from a positive colony could be used when selecting for a MAO-N variant when the *E. coli* itself may not be viable. Directed evolution is rapid with the discovery of new variants taking a matter of a few weeks compared to natural selection which takes thousands of years<sup>161</sup>.



As mentioned in section 2.2.6, further examination of amines screening of MAO-N 1 variant should also be carried out for the MAO-N 2 variant because of their differences in substrate specificity.

Thus far, all MAO-N variants are (*S*)-selective, to broaden the scope of this deracemisation technology it would be advantageous to have an (*R*)-selective variant. This would allow the (*S*)-enantiomer product to be produced from the deracemisation of a racemic substrate. The requirement to produce an (*R*)-selective MAO-N would be desirable but a challenging task. Another approach which removes the necessity for an (*R*)-selective MAO-N is if an 'amine racemase' could be discovered (i.e. an amine oxidase with low enantioselectivity combined with a chemical reduction). This would allow the dynamic kinetic resolution and (*S*)-product could be isolated in a theoretical 100% yield and 100% e.e. (figure 2.3.11.1).

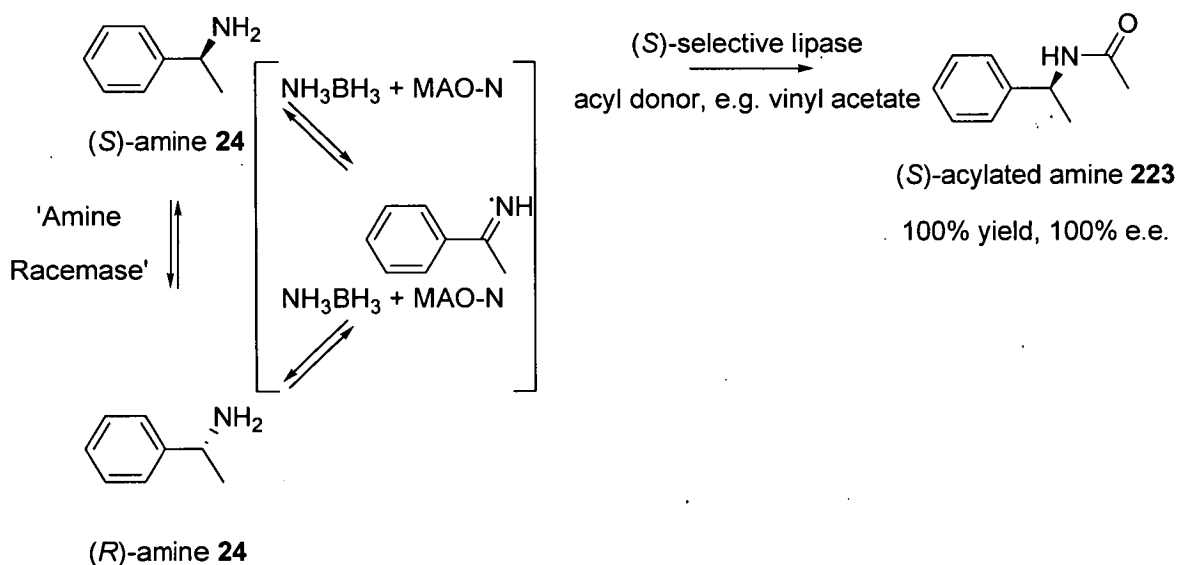


Figure 2.3.11.1. Principle of a dynamic kinetic resolution of amine **24** with an 'amine racemase' and an (*S*)-selective lipase acylation.

## 2.4. Saturation mutagenesis

### 2.4.1. Exploration of the I246M mutation

The mutation producing the improvement of activity in the parental MAO-N *I* enzyme towards amine **76** was generated by introduction of a single nucleotide change in the *mao* gene. This mutation changed the amino acid residue in the protein sequence at position 246 from isoleucine to methionine. But is methionine the optimal amino acid at 246 to improve MAO-N catalysis? The directed evolution approach used to identify this mutation was based on a library screen of 12000 colonies. The mutation rate of *E. coli* XL1-red mutator strain used to generate this library, should, on average, introduce a single mutation per gene. This will result in a proportion of the library being non-mutated parental MAO-N owing to silent mutations and the statistical spread of genes where no mutations have been incorporated. The library size that would be required to fully randomise each nucleotide within *mao* would be  $4^n$  (with  $n = 1489$ , the length of the *mao* gene). This is an astronomically large number which is vastly beyond the screening capabilities of the current screening method. Even if the library just fully randomised each amino acid, rather than each nucleotide, then a vast library size would be required  $20^n$  (with  $n = 495$ , the number of amino acids in the MAO-N protein sequence). The enormous library sizes required to represent all possible mutations means that in the previous 12000 library screen, the other nineteen amino acid residues that can arise at 246 were unlikely to have been represented.

To explore the 246 amino acid mutation in MAO-N more thoroughly, a site directed mutagenesis approach was used. The 3 nucleotides that encode position 246 would be substituted for NNS, where N represents any of the 4 DNA bases and S either G or C. The S substitution reduces the occurrences of stop codons, whilst each of the amino acids is still represented. This does affect the degeneracy of the genetic code when an

---

NNS substitution is made. For instance isoleucine is represented three times in the genetic code by ATT, ATC and ATA but with the NNS substitution only the ATC codon is represented. The other advantage of using NNS rather than NNN is the library size to statistically represent each codon falls from 64 to 32. This reduces the library size required for screening. For a 99% probability of statistically representing each possible codon combination in a library is given by the equation in figure 2.4.1.1. The number of colonies required for a NNS single site directed saturation mutagenesis is calculated from this to be 147 colonies, based on a 99% probability with  $V = 32$  ( $4 \times 4 \times 2$ ).

$$P = 1 - e^{-N/V}$$

where P = % probability

N= number of colonies required

V = total possible number of combination

Figure 2.4.1.1. Calculation of the percentage probability of representing all possible mutations in a total combination size of V.

#### 2.4.2. Quikchange site directed saturation mutagenesis

Preparation of the 246 site directed saturation mutagenesis was performed using Stratagene's Quikchange kit (3.4.5). The advantage with this method is there is no need to gel purify the mutated fragment of DNA from the PCR reaction and has the added benefit of no requirement for ligating PCR products into a plasmid. Firstly, two oligonucleotide primers are designed to encode the NNS sequence along with flanking regions of complementary sequence to allow hybridisation of the primer to the template, figure 2.4.2.1.

Forward primer: 5'-GGATGCATGGACTGCTTGNSAGTTATAAGTTCAAGG-3'

Reverse primer: 5'-CCTTGAAGTTATAACTSNNCAAGCAGTCCATGCATCC-3'

Figure 2.4.2.1. Oligonucleotide primers designed for the NNS saturation mutagenesis library at amino acid residue 246 in MAO-N.

The next stage is the PCR where the oligonucleotide primers are extended with PfuTurbo DNA polymerase completely around the plasmid. The template is subjected to *Dpn* I endonuclease digestion to selectively digest the template (parental) DNA. *Dpn* I endonuclease specifically digests the methylated strand of hemimethylated DNA. The template DNA used the PCR is methylated by the *dam* gene from *E. coli* and therefore susceptible to digestion by *Dpn* I endonuclease. The nucleotides added during the PCR are unmethylated and therefore are not digested. The nicked circular plasmid DNA incorporating the 246 saturation library was used to transform XL1-blue competent cells which covalently closed the nicked DNA and repaired and propagated the plasmid library. The DNA was then ready to be screened and was used to transform the BL21 (DE3) expression strain of *E. coli*.

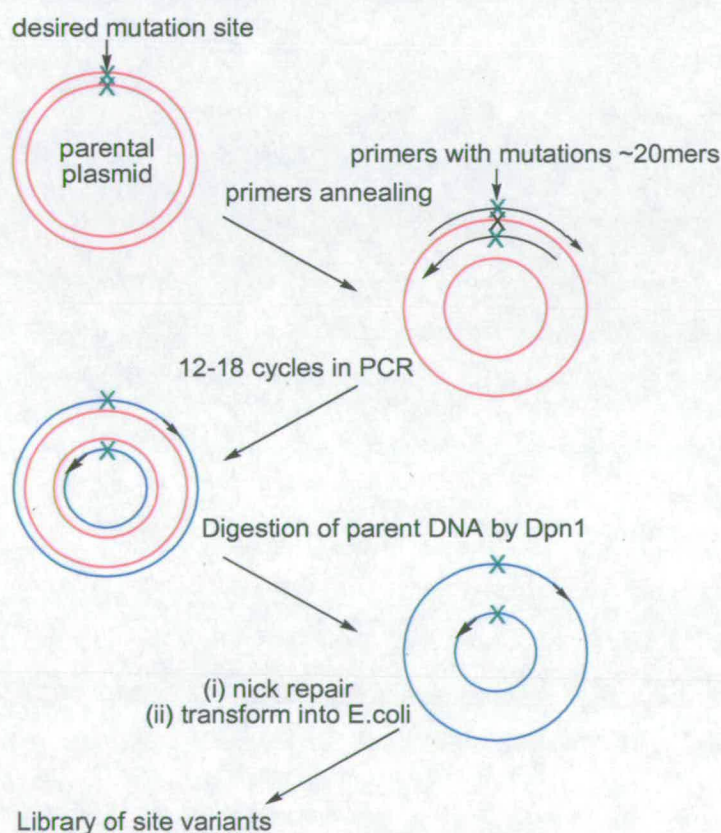


Figure 2.4.2.2. Summary of the Quikchange method for generating a saturation library at 246 in MAO-N. Parental (methylated) DNA is represented in red, PCR product in blue and saturation mutagenesis site as a green cross.

### 2.4.3. Preparation of 246 saturation library for screening

After transformation of the nicked DNA into XL1-blue, 12 colonies were selected at random (clones 2a-2l) and the nucleotide sequence at 246 analysed by DNA sequencing to verify that the library was representative and without bias (3.4.8). Sequencing showed a good representation of codons and only one ATG (methionine) from the parent was observed, showing that the mutagenesis at 246 was successful, table 2.4.3.1. The third nucleotide of all the codons sequenced was either G or C as designed in the mutagenic NNS oligonucleotide primer, further validating the success of the mutagenesis.

Clone	246 codon	amino acid
2a	GGC	Gly
2b	TCG	Ser
2c	TAC	Tyr
2d	CCC	Pro
2e	AAG	Lys
2f	TTG	Leu
2g	CGG	Arg
2h	ACG	Thr
2i	ACC	Thr
2j	TGC	Cys
2k	GTC	Val
2l	ATG	Met

Table 2.4.3.1. Random sequencing of 12 clones (2a – 2l) of 246 saturation mutagenesis library generated by the Quikchange kit.

---

*E. coli* XL1-blue competent cells were transformed with the crude DNA product yielding 200 colonies from a 1ml transformation (3.4.7). This exceeded the number required to statistically give a 99% probability of representing all 32 possible NNS codons. The repaired plasmid DNA was recovered and was used in the transformation of *E. coli* BL21 (DE3) competent cells giving 220 colonies when spread onto nitrocellulose membranes on LB agar containing 100µg/ml ampicillin. The membranes were then assayed against (*rac*)-amine 76 (MTQ) (3.1.6). After 16 hours, 8 colonies appeared to be browner than the rest of the colonies. The 8 colonies were picked and grown in LB containing 100µg/ml ampicillin along with the parent MAO-N 2 variant. The plasmid DNA was purified from each of the 8 'hits' and the sequencing of the 246 site in these mutants all gave the same codon ATG, encoding for methionine. Further confidence that the screen was representative of the mutagenesis was obtained by the observation that the remainder of the library was significantly slower to react in the solid phase assay than the 8 'hits' identified. The ATG codon has a 1 in 32 chance of occurring amongst the NNS library; therefore in the library size screened here it should be expected to occur on average  $(1/32) \times 220 = 6.9$  times. This frequency of average codon occurrence matches well with the frequency of the 'hits' that were identified from the screen.

#### 2.4.4. Screening of 246 saturation library against amine 178

The screening of the 246 saturation library against (*rac*)-amine 76 (MTQ) showed that ATG methionine was the optimal residue in MAO-N for catalysing the oxidation of amine 76. The first round of evolution generated an improved (*S*)-amine 24 MAO-N enzyme (N336S variant) and the second round of evolution generated an improved (*S*)-amine 76 MAO-N enzyme (I246M variant); amine 24 and amine 76 are related to each other by a core  $\alpha$ -methyl benzylamine unit. Amine 76 could be considered to be conformationally restricted version of amine 24 by the presence of the amino group being locked in a 6 membered ring. Based on this substrate similarity and to further probe the active site changes that have occurred with the 246 mutation, other

conformationally locked versions of  $\alpha$ -methyl benzylamine were examined. Three other amines can be drawn based on this concept, each containing the  $\alpha$ -methyl benzylamine core along with some degree of conformational restriction (figure 2.4.4.1). Amine **178** was shown from the amine screening to be more active than amine **217**, so this was selected as the substrate to further screen the 246 saturation library.

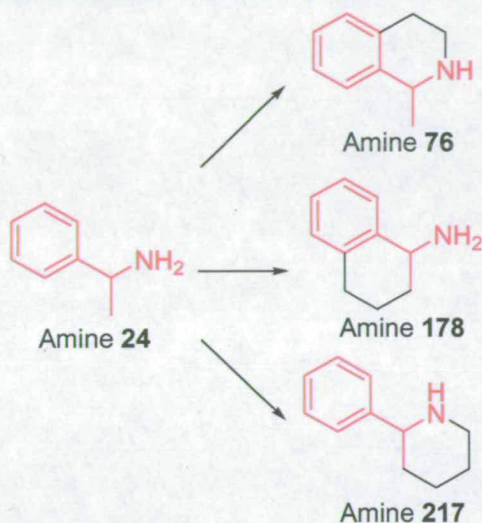


Figure 2.4.4.1. Conformationally restricted versions of amine **24**. The  $\alpha$ -methyl benzylamine core is shown in red and additional bonds that reduce the degrees of freedom are shown in black.

Attempts to screen the library with (*rac*)-amine **178** failed to show any clones with a fast enough rate of amine oxidation to be identified. The DAB based peroxidase assay would slowly oxidise over several days, so slow reacting colonies would not be detectable as their response is not sensitive enough against the background. The exercise was repeated with 10 mM (*S*)-amine **178** rather than 10 mM (*rac*)-amine **178** to improve the activity of any potential clones having a distinguishable improvement in amine oxidation. From a library of around 2000 clones many appeared to be reacting, albeit much slower than the corresponding screening performed with (*rac*)-amine **76**. The 10 clones (3a-3j) that appeared to be browner than the rest were picked and grown in 10 ml LB containing

100µg/ml ampicillin. After overnight growth, the 10 clones had their plasmid DNA recovered and sequenced. The results of the sequencing are shown in table 2.4.4.1.

Clone	246 codon	amino acid
3a	CGC	Arg
3b	ATG	Met
3c	ATG	Met
3d	ATC	Ile
3e	ATC	Ile
3f	ATG	Met
3g	ATC	Ile
3h	ATC	Ile
3i	ATC	Ile
3j	CGC	Arg

Table 2.4.4.1. Sequencing results of the 10 hits (3a-3j) from (*S*)-amine **178** screened against the 246 saturation mutagenesis library.

The sequencing results showed a new active residue at the 246 position, arginine (CGC), but the majority of those picked as being the most reactive was methionine (ATG) and isoleucine (ATC). This suggests that at the 246 amino acid position the methionine and isoleucine residues are the optimal for amine **178** oxidation by MAO-N. The appearance of arginine in this list of hits may arise from the low sensitivity of the screen because of the inherent low activity of MAO-N variants for amine **178** oxidation. This reduced the resolution of this qualitative assay.



### 2.4.5. Alignment of MAO-N and MAO-B sequences

The human mono-amine oxidase MAO-B is the most closely related enzyme to MAO-N which has a three-dimensional structure available. There is 24% sequence identity and 43% sequence similarity between the two amino acid sequences and the comparison between the two proteins gave a basis for evaluating the changes that have been introduced by the directed evolution approach used here. Previously a sequence alignment of MAO-B and MAO-N had been carried out by M. Alexeeva<sup>153</sup>.

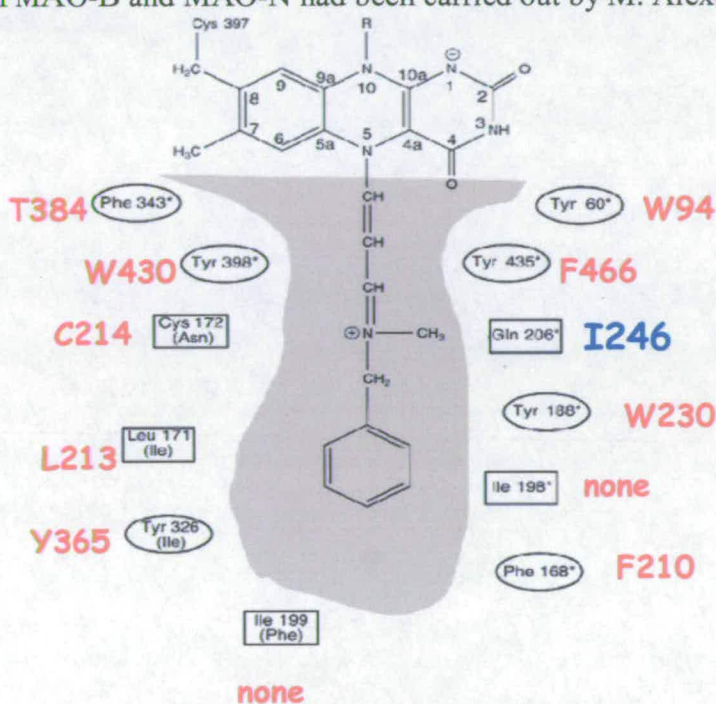


Figure 2.4.5.1. Schematic representation of pargyline suicide inhibitor covalently attached to FAD and bound in the active site of MAO-B<sup>84</sup>. MAO-B active site residues are shown in black (aromatic side chains in ellipsoidal frame and others in rectangular boxes). Aligned amino acids in MAO-N are shown in red and the 246 aligned residue is shown in blue.

The prediction from the alignment of the amino acids at the active sites of MAO-B and MAO-N indicates that isoleucine 246 in MAO-N (shown in blue) aligns with glutamine

in MAO-B. The directed evolution of MAO-N towards secondary amine activity led to the I246M change in the enzyme. Based on the homology model of MAO-N and MAO-B the 246 residue in MAO-N is proposed to be located in the substrate binding cavity of the enzyme. The proposed 246 location within MAO-N supports the directed evolution of MAO-N towards amine **24** since mutating this residue affected the enzyme's specificity. This helps to validate the reliability of the alignment between MAO-N and MAO-B. Further confidence of the alignment's accuracy can be provided by the 'hot spot' variants identified by M. Alexeeva (table 2.4.5.1). Several of these 'hot spots' mutations were found at sites that align in MAO-B to have crucial roles in MAO-B activity<sup>153</sup>, in particular, the MAO-N M337 'hot spot' aligns to lysine 296 in MAO-B.

MAO-N variant	( <i>S</i> )-amine <b>24</b> ( $k_{cat}/\text{min}^{-1}$ )	( <i>R</i> )-amine <b>24</b> ( $k_{cat}/\text{min}^{-1}$ )	( <i>S</i> )-amine <b>24</b> relative rate (%)
wild type	$3.0 \times 10^{-2}$	$2.0 \times 10^{-3}$	100
G541S R494C	$4.0 \times 10^{-2}$	$1.0 \times 10^{-3}$	133
D385G	0.1	$2.0 \times 10^{-3}$	333
G451S	$3.0 \times 10^{-2}$	$9.0 \times 10^{-4}$	100
M337R	0.2	$1.7 \times 10^{-3}$	667
D385A	$5.0 \times 10^{-2}$	$1.0 \times 10^{-3}$	167
G403E	$8.0 \times 10^{-2}$	$7.0 \times 10^{-4}$	267
A289V	$1.5 \times 10^{-2}$	$7.0 \times 10^{-4}$	50
R260K	$2.0 \times 10^{-2}$	$4.0 \times 10^{-4}$	67
E145K	$3.5 \times 10^{-2}$	$7.0 \times 10^{-4}$	117
N336S	4.5	$1.0 \times 10^{-2}$	15000
N336S M348K	4.0	$1.0 \times 10^{-2}$	13333

Table 2.4.5.1. 'Hot spot' variants generated from XL1-red mutagenesis selected from the screening of amine **24**<sup>153</sup>.

Intriguingly, the lysine 296 in MAO-B this has been shown to compensate for change in flavin protonation state and aid catalysis<sup>162</sup>. Recent saturation mutagenesis studies at 336 and 337 in MAO-N have shown that the optimal residues at 337 are basic amino acids (Toni Fleming personal communication) supporting the hypothesis that the 337 residue performs a similar role in MAO-N, as 296 in MAO-B. The N336S M337K substitutions gave the greatest improvements in  $k_{cat}$  for (*S*)-amine **24** in this study and the aligned residue for 337 in MAO-B (296) is also lysine, which is responsible for the assistance in flavin catalysis. It is important to note that residue 337 is adjacent to residue 336, which is the site at which the first generation of MAO-N were mutated (2.2.2).

Residues at 336/337 in MAO-N variants	Genotype	<i>(S)</i> -amine <b>24</b>			
		$V_{Max}$ ( $\mu\text{mol}/\text{min}/\text{mg}$ )	$k_{cat}$ ( $\text{min}^{-1}$ )	$k_{cat}$ mutant/ $k_{cat}$ wild type ( $\text{min}^{-1}$ )	$K_M$ (mM)
Ser/Tyr	TCC/TAC	$7.4 \times 10^{-2} \pm 3 \times 10^{-3}$	$4.11 \pm 0.18$	28	$11.53 \pm 0.96$
Ser/Lys	TCG/AAG	$0.131 \pm 6 \times 10^{-3}$	$7.28 \pm 0.32$	50	$11.37 \pm 0.93$
Ser/Asn	TCG/AAC	$7.3 \times 10^{-2} \pm 2 \times 10^{-3}$	$4.06 \pm 0.11$	28	$13.96 \pm 0.65$
Ser/Arg	AGC/CGG	$8.2 \times 10^{-2} \pm 3 \times 10^{-3}$	$4.55 \pm 0.16$	31	$10.12 \pm 0.67$ )
Ser/Met	AGT/ATG	$2.2 \times 10^{-2} \pm 1 \times 10^{-3}$	$1.10 \pm 4 \times 10^{-2}$	8	$16.05 \pm 1.08$
(wild type) Asn/Met	AAT/ATG	$3 \times 10^{-3} \pm 0$	$0.15 \pm 1 \times 10^{-2}$	1	$14.43 \pm 2.74$

Table 2.4.5.2. Optimal residues at 336 and 337 in site directed mutagenesis studies (Courtesy of T. Fleming).

#### 2.4.6. Saturation mutagenesis at aligned active site residues

The sequence alignment prediction shows that previous mutations in MAO-N have a role of forming intimate contacts with the pargyline substrate in MAO-B. It was decided to investigate whether a rationalised approach could be employed for further directed evolution of MAO-N.

---

It has been shown that threonine 384 in MAO-N aligns with phenylalanine 343 in MAO-B. Phenylalanine 343 in MAO-B contributes towards the hydrophobic nature of the active site and shelters the aromatic cage. Aspartate 385 in MAO-N has already been identified as a hot spot (see table 2.4.5.1) and it has been postulated that its mutation effected the active site organisation in MAO-N with respect to the aromatic cage. To further investigate this claim and to utilise the apparent reliability of the sequence alignment, a double amino acid saturation library was made at residues 384 and 385 in MAO-N. Preparation of a 384/385 saturation library has the advantage that because these residues are adjacent in sequence, only a single Quikchange reaction is needed to produce the variant libraries as both NNS codon changes can be introduced in a single oligonucleotide primer. An NNSNNS library is more challenging to screen than a NNS library as a larger library of clones is required to statistically represent all possible combinations.  $V$  (total possible number of combinations) is increased from 32 for a single amino acid change to 1024 for a double amino acid change. To have a 99% probability of representing all possible combinations, 4695 clones are required (figure 2.4.1.1.). The size of the library to be screened could be reduced should a single amino acid change be made at one site and the optimal residue/residues be used as the parental template for the introduction of the second NNS change. The disadvantage with this approach is that the two libraries (albeit smaller) need to be screened rather than one and synergic benefits between the two sites could be missed. Although a larger library of variants are required for the NNSNNS compared to an NNS library, the solid phase assay screen can easily handle this increase.

Two oligonucleotide primers were designed to incorporate the NNSNNS changes in the nucleotide sequence corresponding to residues 384 and 385 in MAO-N (figure 2.4.6.1.). The Quikchange reaction was carried out following the same method as the 246 saturation library with some changes in concentration of primers and templates to improve yield of DNA product (3.4.6). Examination of the DNA purity by gel agarose

## Results and discussion

electrophoresis after *DpnI* digestion showed the majority of DNA product corresponding to DNA of 10-8 kilobase pairs on the DNA ladder. The DNA product band corresponded well to the parental lane indicating the success of the PCR (3.4.2) (figure 2.4.6.2.). There appeared to be several other bands present in the Quikchange product, probably arising from the digested fragments of the parental template by *DpnI*.

Forward primer: 5'-GGTGTGTTTCGGG**NNSNNS**GCGAATCATATCCAGC-3'

Reverse primer: 5'-GCTGGATATGATTTCGC**SNNSNN**CCCGAAACACACC-3'

Figure 2.4.6.1. Oligonucleotide primers designed for NNSNNS saturation mutagenesis library at 384/385 in MAO-N.

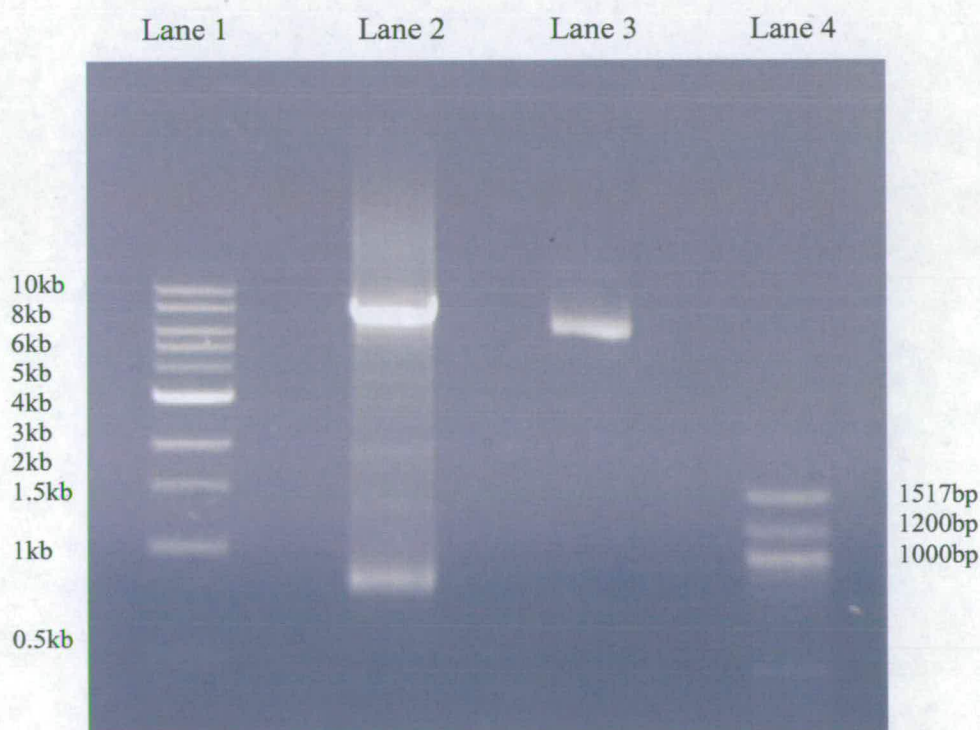


Figure 2.4.6.2. Quikchange 384/385 saturation mutagenesis DNA product after digestion with *DpnI*. Lane 1 corresponds to 1 kilobase pair DNA marker, Lane 2 Quikchange DNA product, Lane 3 parental DNA template and Lane 4 100 base pair marker.

### 2.4.7. Screening of 384/385 saturation library

In order to maximise the transformation efficiency in the next stage of the library generation, the major band corresponding to the nicked plasmid was purified from the DNA gel electrophoresis (3.4.3). Electrocompetent XL1-blue cells were transformed with the purified DNA (3.3.3) but gave no transformants. However, transformation into supercompetent cells gave an average of 600 colonies per plate (3.4.7). Colonies were collected from 20 plates containing on average 600 colonies and the plasmid DNA was isolated (3.3.8). Combining all 20 plasmid preparations gave a DNA library size of 12000 variants which is higher than the 4695 required to statistically give a 99% representation of the library. Prior to transformation of *E. coli* BL21 (DE3) competent cells with the variant library of DNA, 20 XL1-blue colonies were picked at random (clones 4a-4t) and plasmid DNA sequenced to verify that the mutagenesis had been successful, see 3.4.8 (table 2.4.7.1).

BL21 (DE3) competent cells were transformed with plasmid DNA from the 384/385 SDM library (3.3.1) giving a transformation efficiency of 800 colonies per plate. Six plates containing 800 clones were screened for (*rac*)-amine 76 (MTQ) activity and after 24 hours the solid phase assay was examined and the thirteen colonies (5a-5m) deemed to be most active were picked (figure 2.4.7.1). The thirteen colonies were grown in 10 ml of LB containing 100µg/ml ampicillin and plasmid DNA was extracted (3.4.1).

clone	384 codon	384 amino acid	385 codon	385 amino acid
4a	CTG	Leu	CGC	Arg
4b	CCC	Pro	TTC	Phe
4c	CAC	His	ACG	Thr
4d	CGC	Arg	CAC	His
4e	GCC	Ala	AGC	Ser
4f	CCC	Pro	ACG	Thr
4g	ACC	Thr	GTC	Val
4h	TCC	Ser	GAC	Asp
4i	CGC	Arg	CGC	Arg
4j	TAC	Tyr	TGC	Cys
4k	CAC	His	CGC	Arg
4l	GTC	Val	CTC	Leu
4m	GGC	Gly	AGC	Ser
4n	AGG	Arg	CTC	Leu
4o	GCG	Ala	CCG	Pro
4p	AGC	Ser	CTG	Leu
4q	GGG	Gly	*	-
4r	ACC	Thr	CGC	Pro
4s	ACC	Thr	CCC	Arg
4t	CAG	Gln	GTC	Val

Table 2.4.7.1. Sequencing of 20 random clones (4a-4t) of the 384/385 saturation mutagenesis library (\* poor resolution of chromatography gave unreliable sequence data).

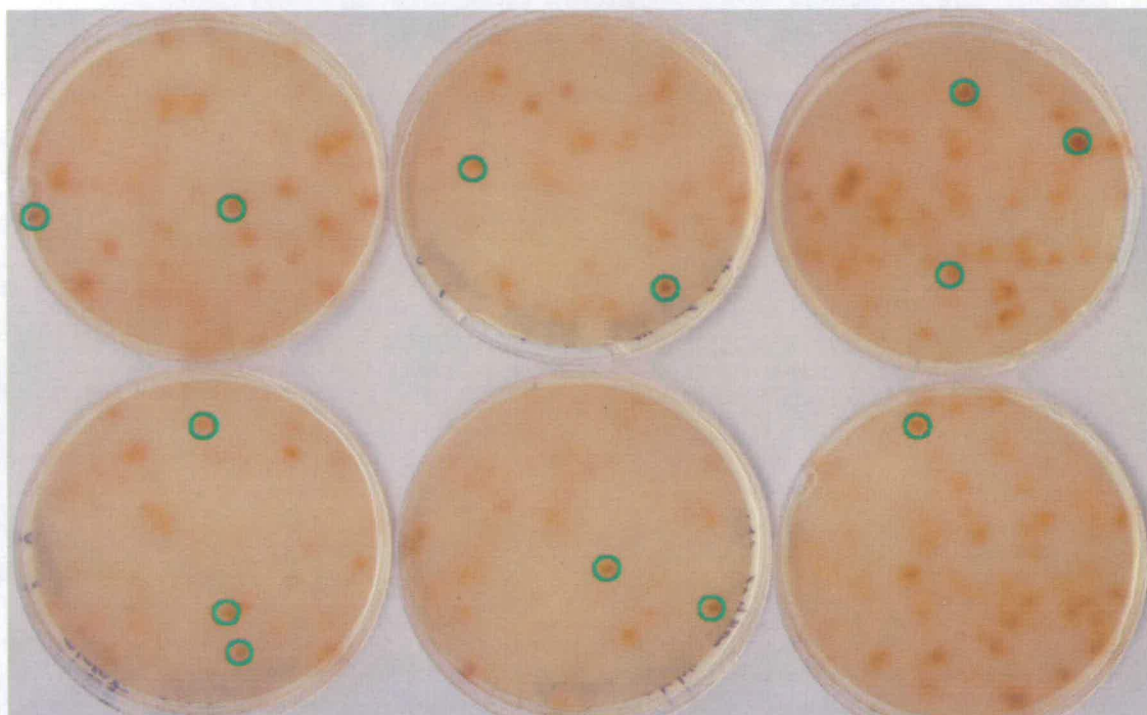


Figure 2.4.7.1. Screening of 384/385 SDM library against (*rac*)-amine **76**. Colonies circled in green were chosen as the most active and picked for further analysis (hits 5a-5m).

To verify the activity of the hits which was observed in the initial screen and to ensure a single colony was picked, plasmid DNA was isolated from the 13 fermented hits (5a-5m). This was used to transform *E. coli* BL21 (DE3) competent cells and the screen repeated. A control transformation of *E. coli* BL21 (DE3) competent cells with the parent gene enabled a qualitative assessment of whether the hits show improved amine **76** activity. At this stage, both enantiomers of amine **76** were assayed separately in the solid phase assay (figure 2.4.7.2).



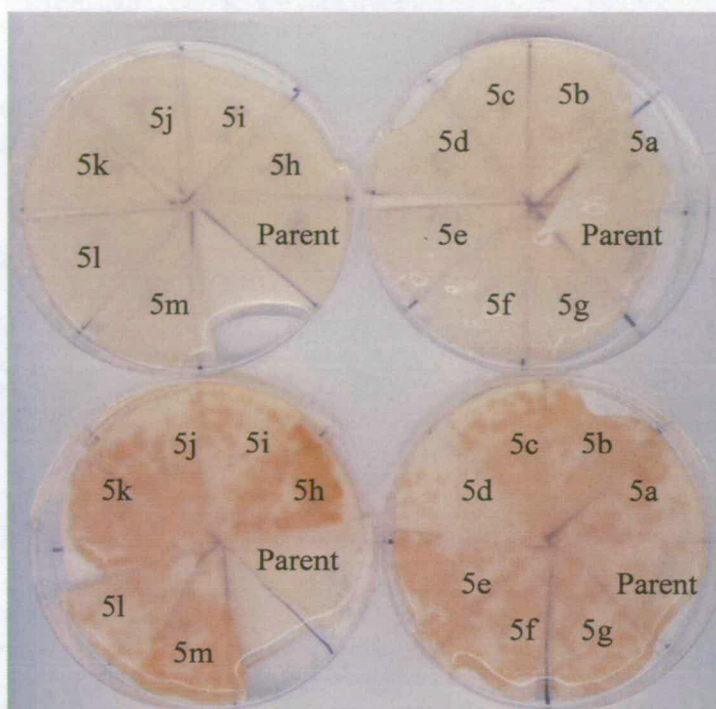


Figure 2.4.7.2. Validation screen of the 13 hits (5a-5m), including the parent gene in one eighth membrane segments. Top two plates are (*R*)-amine **76** solid phase assays and lower two plates (*S*)-amine **76** solid phase assay.

The screen showed each of the hits maintained the high degree of (*S*)-enantioselectivity observed in the parent. The qualitative result obtained from the assays showed that the hits were all more active than the parent gene. The hit plasmids were sequenced to discover the amino acid changes at the 384 and 385 in the *mao* gene (3.4.4). The sequencing results showed all the hits to be variants at both the 384 and 385 positions from the parent gene as expected (table 2.4.7.2). At the 384 position there was representation of 4 different amino acids, 2 of the 4 are represented in many of the hits. There is a preference for serine and asparagine at 384. At 385 there is less of a distinctive choice of amino acid with 5 being represented and less bias towards

particular amino acids than at the 384 position. Although the amino acids alanine, histidine and serine are all represented in several of the hits at the 385 position.

hit	384 codon	384 amino acid	385 codon	385 amino acid
5a	TCG	Ser	GCG	Ala
5b	TCG	Ser	CAC	His
5c	AGC	Ser	TCG	Ser
5d	AAC	Asn	AGC	Ser
5e	AAC	Asn	CAC	His
5f	TCG	Ser	GCG	Ala
5g	AAC	Asn	CAC	His
5h	GGC	Gly	GCC	Ala
5i	AGC	Ser	AAC	Asn
5j	TCG	Ser	GCG	Ala
5k	AAC	Asn	GCC	Ala
5l	TTC	Phe	CGC	Arg
5m	TCG	Ser	AGC	Ser
Parent	ACG	Thr	GAT	Asp

Table 2.4.7.2. Sequence of hits (5a-5m) and the parent gene at the 384/385 codons in the *mao* gene.

#### 2.4.8. Quantitative analysis of the selected variants

To quantify the improvements made at the 384 and 385 positions and to select the best variants for Michaelis-Menten analysis a liquid phase colorimetric assay was undertaken. Plasmid DNA from each hit was used to transform *E. coli* BL21 (DE3)

## Results and discussion

competent cells, each hit was grown in LB containing 100 $\mu$ g/ml ampicillin and the cells harvested then lysed (3.3.5.1 and 3.1.4). The CFE of the lysate was assayed towards (*rac*)-amine 209, (*S*)-amine 24, (*R*)-amine 24, (*S*)-amine 76 and (*R*)-amine 76.

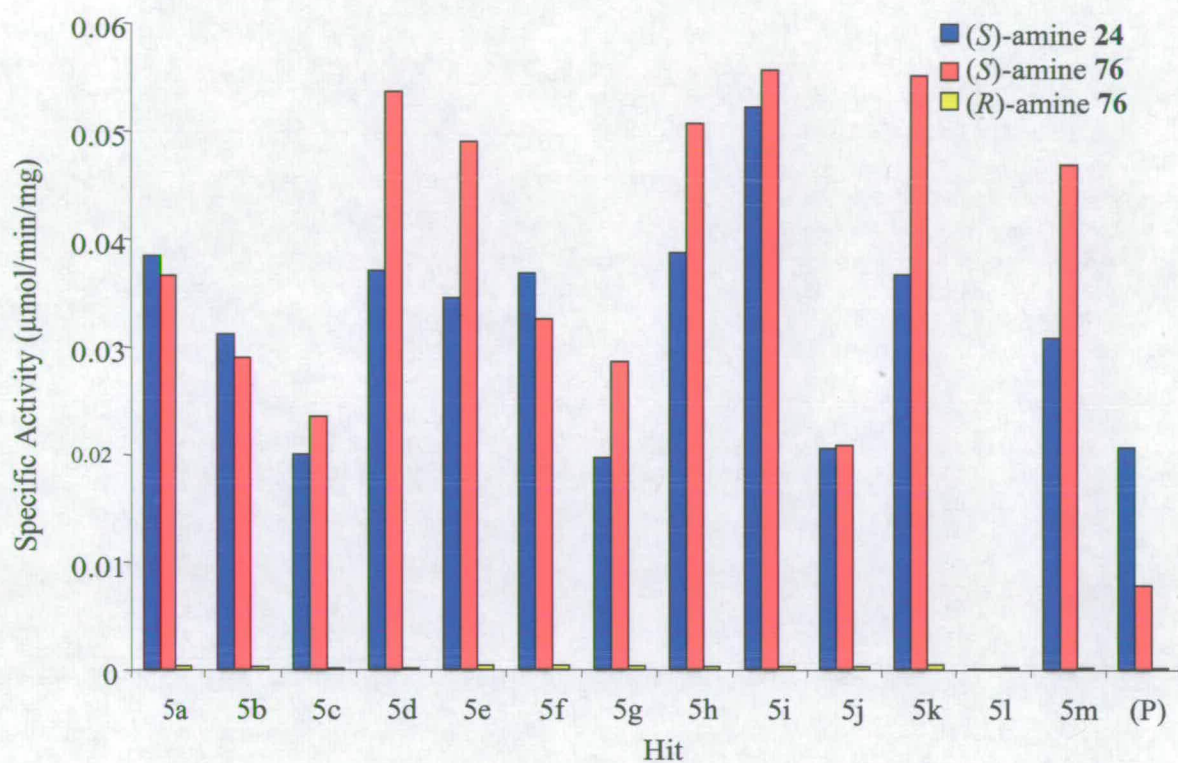


Figure 2.4.8.1. CFE screening of (*S*)-amine 24, (*S*)-amine 76 and (*R*)-amine 76 against the 384/385 library hits (5a-5m) and (P) = Parent gene.

hit	( <i>rac</i> )-amine <b>209</b> ( $\mu\text{mol}/\text{min}/\text{mg}$ )	hit	( <i>rac</i> )-amine <b>209</b> ( $\mu\text{mol}/\text{min}/\text{mg}$ )
5a	0.290	5h	0.301
5b	0.270	5i	0.373
5c	0.201	5j	0.201
5d	0.260	5k	0.272
5e	0.240	5l	0.0094
5f	0.303	5m	0.317
5g	0.151	Parent	0.267

Table 2.4.8.1. CFE screening of (*rac*)-amine **209** against the 384/385 library hits (5a-5m) (rates shown are in  $\mu\text{mol}/\text{min}/\text{mg}$ ).

Figure 2.4.8.1 shows an overall general improvement in (*S*)-amine **76** oxidation with some variants now showing a higher rate of oxidation against amine **76** than with amine **24**. SDS PAGE analysis of the CFEs for the hits, showed no noticeable difference in expression of the MAO-N protein (except hit 5l where no band corresponding to MAO-N appeared to be present in the CFE). Assaying (*rac*)-amine **209** showed improvements in the oxidation rates amongst the hits although they were generally more modest with the best improvement being 1.4 fold rather than the 7.1 fold improvement seen with (*S*)-amine **76** (table 2.4.8.1). Hit 5d and hit 5i were selected to investigate the  $V_{\text{Max}}$ ,  $K_{\text{M}}$  and  $k_{\text{cat}}$  constants against a panel of selected amines. The hits were chosen because they are the most active against (*S*)-amines **24** and **76**, with both showing higher specific activities in the CFE assay for amine **76** than amine **24**, which has not been previously observed. Interestingly, these two amines genotypes are the same AGC (serine) and AAC (asparagine) for the two hits, they differ in the fact that hit 5d is 384 asparagine and 385 is serine and vice-versa for hit 5i. In order to assess the progress in evolution

---

from the wild type MAO-N strain, this exercise was also performed on the MAO-N wild type, the MAO-N 1 and the MAO-N 2 variants.

#### 2.4.9. Michaelis-Menten studies of the MAO-N variants

To minimise the possibility of discrepancies in the kinetic studies, MAO-N enzyme was freshly purified using the previous protocol with a slight modification (3.2.4). The modification in the purification procedure was introduced to help stabilise the purified enzyme (2.1.4). Each enzyme variant of MAO-N was prepared from fermented *E. coli* and the protein purified following identical procedures (3.3.5.2 and 3.2.4). The assays were carried out in unison on a 96-well microtitre plate and specific activities calculated for each of the substrate concentrations (substrate range 50mM, 30mM, 20mM, 10mM, 8mM, 6mM, 4mM, 2mM, 1mM, 0.8mM, 0.6mM, 0.4mM, 0.2mM, 0.1mM, 50 $\mu$ M, 20 $\mu$ M, 10 $\mu$ M, 5 $\mu$ M and 1 $\mu$ M). Specific activities for each substrate concentration (measured in triplicate) were plotted in the SigmaPlot enzyme kinetics module to determine the  $V_{\text{Max}}$  and  $K_{\text{M}}$  (3.1.5). Protein concentration was measured using the Bradford assay (3.2.6) and the  $k_{\text{cat}}$  was determined by multiplication of the  $V_{\text{Max}}$  by the molecular weight of the protein (55.6 kDa). Seven amines were selected for characterisation, (*rac*)-amine **209** and **24**, (*R*)-amine **76** and **24** and (*S*)-amine **76** and **24**.

Substrate	$V_{Max}$ ( $\mu\text{mol}/\text{min}/\text{mg}$ )	$k_{cat}$ ( $\text{min}^{-1}$ )	$K_M$ (mM)
<i>(rac)</i> -amine <b>209</b>	0.23 $\pm$ 0.30	12.7 $\pm$ 16.5	0.30 $\pm$ 0.02
<i>(R)</i> -amine <b>76</b>	6.2 $\times 10^{-4}$ $\pm$ 9.5 $\times 10^{-5}$	3.4 $\times 10^{-2}$ $\pm$ 5.3 $\times 10^{-4}$	7.6 $\pm$ 3.0
<i>(S)</i> -amine <b>76</b>	1.48 $\times 10^{-3}$ $\pm$ 1.1 $\times 10^{-4}$	8.2 $\times 10^{-2}$ $\pm$ 6 $\times 10^{-3}$	0.14 $\pm$ 6.1 $\times 10^{-2}$
amine <b>124</b>	3.0 $\pm$ 8.3 $\times 10^{-2}$	167 $\pm$ 4.6	0.37 $\pm$ 7.1 $\times 10^{-2}$
<i>(rac)</i> -amine <b>24</b>	5.5 $\times 10^{-3}$ $\pm$ 1.8 $\times 10^{-4}$	0.31 $\pm$ 1.0 $\times 10^{-2}$	4.6 $\pm$ 0.5
<i>(R)</i> -amine <b>24</b>	1.4 $\times 10^{-3}$ $\pm$ 5.3 $\times 10^{-5}$	7.9 $\times 10^{-2}$ $\pm$ 2.9 $\times 10^{-3}$	4.3 $\pm$ 0.5
<i>(S)</i> -amine <b>24</b>	1.3 $\times 10^{-2}$ $\pm$ 2.3 $\times 10^{-4}$	0.72 $\pm$ 1.3 $\times 10^{-2}$	1.9 $\pm$ 0.1

Table 2.4.9.1.  $V_{Max}$ ,  $k_{cat}$  and  $K_M$  results for MAO-N wild type.

Substrate	$V_{Max}$ ( $\mu\text{mol}/\text{min}/\text{mg}$ )	$k_{cat}$ ( $\text{min}^{-1}$ )	$K_M$ (mM)
<i>(rac)</i> -amine <b>209</b>	2.7 $\pm$ 4.3 $\times 10^{-2}$	150 $\pm$ 2.4	0.38 $\pm$ 3 $\times 10^{-2}$
<i>(R)</i> -amine <b>76</b>	1.0 $\times 10^{-3}$ $\pm$ 7.3 $\times 10^{-5}$	5.6 $\times 10^{-2}$ $\pm$ 4.1 $\times 10^{-3}$	0.70 $\pm$ 0.30
<i>(S)</i> -amine <b>76</b>	2.0 $\times 10^{-2}$ $\pm$ 6 $\times 10^{-4}$	1.10 $\pm$ 3 $\times 10^{-2}$	6 $\times 10^{-2}$ $\pm$ 1 $\times 10^{-2}$
amine <b>124</b>	1.3 $\pm$ 2.9 $\times 10^{-2}$	72.1 $\pm$ 1.6	0.69 $\pm$ 9.1 $\times 10^{-2}$
<i>(rac)</i> -amine <b>24</b>	0.108 $\pm$ 2.3 $\times 10^{-3}$	6.01 $\pm$ 0.13	1.11 $\pm$ 0.11
<i>(R)</i> -amine <b>24</b>	1.82 $\times 10^{-3}$ $\pm$ 1.2 $\times 10^{-4}$	0.101 $\pm$ 7 $\times 10^{-3}$	3.56 $\pm$ 0.88
<i>(S)</i> -amine <b>24</b>	9.6 $\times 10^{-2}$ $\pm$ 1 $\times 10^{-3}$	5.34 $\pm$ 5.8 $\times 10^{-2}$	1.17 $\pm$ 5.0 $\times 10^{-2}$

Table 2.4.9.2.  $V_{Max}$ ,  $k_{cat}$  and  $K_M$  results for MAO-N 1.

The wild type enzyme had poor activity to all of the amines screened other than amine **124**, the natural achiral substrate, demonstrating the limited amine specificity of the wild type enzyme (2.2.2). Introduction of the N336S M348K changes in MAO-N improves the  $k_{cat}$  several fold for all the substrates excluding the natural achiral substrate, where a fall in activity is observed. There are very small increases in the (*R*)-enantiomer turnover numbers but the large improvements are seen for the (*S*)-enantiomer where a 7.4 (*S*)-

amine **24**) and a 13.8 ((*S*)-amine **76**) fold raise was observed. This improvement is less for amine **24** than was previously reported<sup>153</sup>. The improvement in (*S*)-amine **24** activity is likely to have been underestimated in this case because the kinetic measurements for the (*S*)-amine **24** and (*R*)-amine **24** were measured on purified protein that had been stored for a week at -20°C. During the storage the enzyme may have lost some of its initial activity. The  $k_{cat}$  of (*rac*)-amine **24** was measured on the freshly prepared purified protein and was raised 20 fold from wild type, supporting the assumption that the (*S*)-amine **24**  $k_{cat}$  had been underestimated, because of the loss of enzyme activity with storage.

Substrate	$V_{Max}$ ( $\mu\text{mol}/\text{min}/\text{mg}$ )	$k_{cat}$ ( $\text{min}^{-1}$ )	$K_M$ (mM)
( <i>rac</i> )-amine <b>209</b>	$1.18 \pm 3 \times 10^{-2}$	$65.5 \pm 1.8$	$0.68 \pm 9 \times 10^{-2}$
( <i>R</i> )-amine <b>76</b>	$1.39 \times 10^{-3} \pm 8 \times 10^{-5}$	$7.7 \times 10^{-2} \pm 5 \times 10^{-3}$	$9.5 \times 10^{-2} \pm 0.12$
( <i>S</i> )-amine <b>76</b>	$0.103 \pm 2 \times 10^{-3}$	$5.74 \pm 9 \times 10^{-2}$	$0.261 \pm 2.2 \times 10^{-2}$
amine <b>124</b>	$1.29 \pm 3 \times 10^{-2}$	$71.9 \pm 1.5$	$2.22 \pm 0.17$
( <i>rac</i> )-amine <b>24</b>	$0.108 \pm 3 \times 10^{-3}$	$6.00 \pm 0.15$	$3.36 \pm 0.30$
( <i>R</i> )-amine <b>24</b>	$4.5 \times 10^{-3} \pm 9 \times 10^{-5}$	$0.25 \pm 5 \times 10^{-3}$	$3.34 \pm 0.25$
( <i>S</i> )-amine <b>24</b>	$0.25 \pm 3 \times 10^{-3}$	$14.1 \pm 0.1$	$1.98 \pm 7 \times 10^{-2}$

Table 2.4.9.3.  $V_{Max}$ ,  $k_{cat}$  and  $K_M$  results for MAO-N 2.

The addition of the I246M mutation does not produce the large changes in turnover numbers seen from MAO-N wild type to MAO-N 1. But the activity of MAO-N 2 enzyme for (*S*)-amine **76** was improved over 5 times from the MAO-N 1 variant.

Comparison of the absolute values measured between those measured here and those in section 2.3.6 vary slightly. This could be due to a number of issues including the error in fitting the specific activities measured into the Michaelis-Menten type curve by the enzyme kinetics module, the error in measurement of the soluble protein concentration (2.4.10) and the differences in the preparation of the MAO-N protein (3.2.3 and 3.2.4). Previously it had been observed that the  $K_M$ s for the substrates examined rose from the MAO-N 1 enzyme to the MAO-N 2 enzyme (2.3.6.1). In agreement with this, all of the

$K_M$  values have risen apart from (*R*)-amine **24** with the I246M mutation with respect to the parent (MAO-N 1 enzyme).

Substrate	$V_{Max}$ ( $\mu\text{mol}/\text{min}/\text{mg}$ )	$k_{cat}$ ( $\text{min}^{-1}$ )	$K_M$ (mM)
( <i>rac</i> )-amine <b>209</b>	$3.3 \pm 5 \times 10^{-2}$	$182 \pm 2.6$	$0.70 \pm 5 \times 10^{-2}$
( <i>R</i> )-amine <b>76</b>	$4.0 \times 10^{-3} \pm 2 \times 10^{-4}$	$0.225 \pm 1.3 \times 10^{-2}$	$0.819 \pm 0.20$
( <i>S</i> )-amine <b>76</b>	$0.371 \pm 8 \times 10^{-3}$	$20.6 \pm 0.4$	$0.69 \pm 6 \times 10^{-2}$
amine <b>124</b>	$2.0 \pm 5 \times 10^{-2}$	$111 \pm 3$	$2.0 \pm 0.2$
( <i>rac</i> )-amine <b>24</b>	$0.284 \pm 3 \times 10^{-3}$	$15.8 \pm 0.1$	$2.95 \pm 9 \times 10^{-2}$
( <i>R</i> )-amine <b>24</b>	$1.4 \times 10^{-2} \pm 3 \times 10^{-4}$	$0.83 \pm 2 \times 10^{-2}$	$5.34 \pm 0.34$
( <i>S</i> )-amine <b>24</b>	$0.835 \pm 1.1 \times 10^{-2}$	$46.4 \pm 0.6$	$2.64 \pm 0.11$

Table 2.4.9.4.  $V_{Max}$ ,  $k_{cat}$  and  $K_M$  results for MAO-N 3 (hit 5i).

Substrate	$V_{Max}$ ( $\mu\text{mol}/\text{min}/\text{mg}$ )	$k_{cat}$ ( $\text{min}^{-1}$ )	$K_M$ (mM)
( <i>rac</i> )-amine <b>209</b>	$5.96 \pm 0.11$	$331 \pm 6$	$0.93 \pm 7 \times 10^{-2}$
( <i>R</i> )-amine <b>76</b>	$2.3 \times 10^{-2} \pm 3 \times 10^{-3}$	$1.26 \pm 0.15$	$2.12 \pm 0.88$
( <i>S</i> )-amine <b>76</b>	$1.99 \pm 4 \times 10^{-2}$	$111 \pm 2$	$1.7 \pm 0.1$
amine <b>124</b>	$6.69 \pm 9 \times 10^{-2}$	$372 \pm 5$	$2.2 \pm 0.1$
( <i>rac</i> )-amine <b>24</b>	$0.81 \pm 1 \times 10^{-2}$	$45.3 \pm 0.5$	$3.55 \pm 0.12$
( <i>R</i> )-amine <b>24</b>	$2.56 \times 10^{-2} \pm 1 \times 10^{-3}$	$1.42 \pm 6 \times 10^{-2}$	$4.73 \pm 0.59$
( <i>S</i> )-amine <b>24</b>	$1.61 \pm 2 \times 10^{-2}$	$89.7 \pm 0.9$	$3.3 \pm 0.1$

Table 2.4.9.5.  $V_{Max}$ ,  $k_{cat}$  and  $K_M$  results for MAO-N 4 (hit 5d).

Much more significant improvements were seen with the MAO-N 3 variant and even greater improvements with the MAO-N 4 variant than was seen with the introduction of the I246M mutation into N336S M348K. The MAO-N 4 (*S*)-amine  $k_{cat}$  values had increased even higher than the MAO-N 3 variant. For the first time the MAO-N 4



variant has a  $k_{\text{cat}}$  for (*S*)-amine **76** is higher than (*S*)-amine **24**. There are a 3.4 and 18.5 fold improvements in turnover for (*S*)-amine **76** for the MAO-N 3 and 4 variants respectively. The trend that was observed with the I246M mutant is also continued with these two 384/385 mutants, with the  $K_M$  rising for both of the (*S*)-amines.

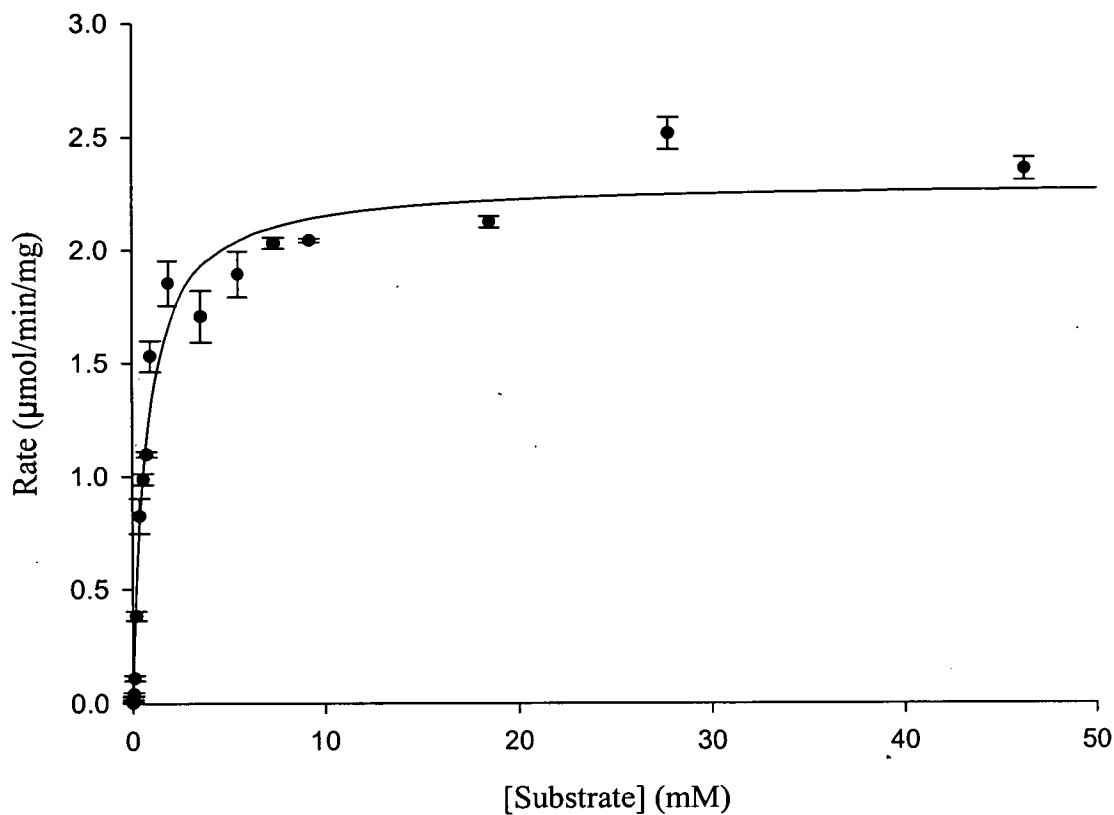


Figure 2.4.9.1. A typical Michaelis-Menten plot. The example shown here is the activity of the MAO-N 2 variant towards (*rac*)-amine **209**.

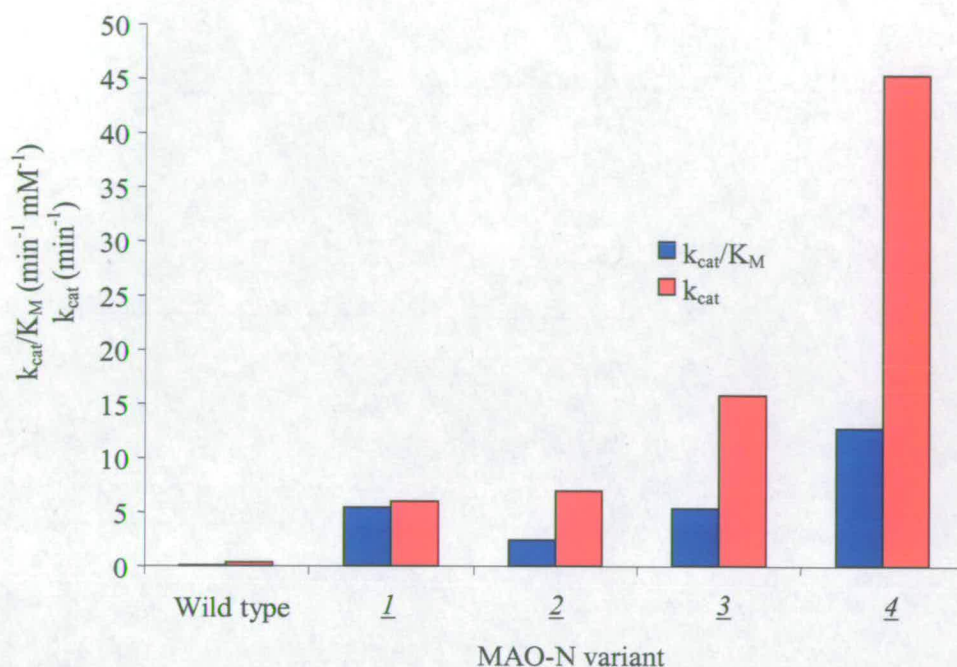


Figure 2.4.9.2. Improvement in the turnover number ( $k_{cat}$ ) and the catalytic efficiency ( $k_{cat}/K_M$ ) in the evolution of MAO-N for (*rac*)-amine **24** oxidation.

The catalytic efficiency ( $k_{cat}/K_M$ ) is increased between the MAO-N variants during directed evolution, but there are much more significant improvements in the turnover numbers (shown in red in figure 2.4.9.2) for (*rac*)-amine **24** oxidation. It is advantageous to have a higher turnover number because this should allow a deracemisation reaction to be completed more rapidly and at higher substrate concentrations. The lower improvements in the catalytic efficiency should not significantly effect the rate of the deracemisations (for substrate concentrations >10mM) as most of the  $K_M$ s measured are in the low mM range. In a biotransformation the  $K_M$  can be considered as the degree to which the biotransformation decelerates. Since  $K_M = V_{Max}/2$ , the higher  $K_M$  the faster the rate of deceleration. For instance, if a deracemisation reaction is conducted at 100-200mM or greater, the biocatalyst will be operating at  $V_{Max}$  (its maximum velocity) until

it starts to approach the  $K_M$ . Therefore if the biocatalyst's  $K_M$  is low, e.g. 1-2 mM, the rate of oxidation will only start falling near the end of the reaction where it is essentially completed. Each of these variants has been examined and shown to maintain a high degree of (*S*)-enantioselectivity. This is beneficial for utilising the optimised MAO-N enzyme as a biocatalyst in a deracemisation.

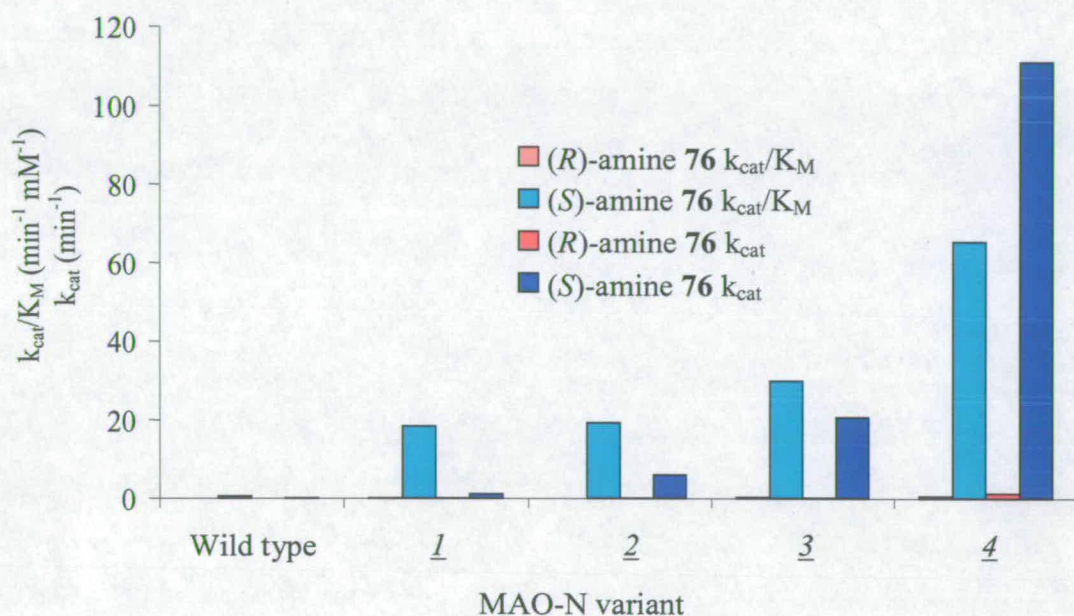


Figure 2.4.9.3. Improvement in the turnover number ( $k_{cat}$ ) and the catalytic efficiency ( $k_{cat}/K_M$ ) in the evolution of MAO-N for (*R*)-amine **76** and (*S*)-amine **76** oxidation.

A similar trend amongst the MAO-N variants in the turnover numbers and catalytic efficiency is seen for amine **76** as was observed for (*rac*)-amine **24**. The improvement in catalytic efficiency from the first 1 variant to the optimal MAO-N 4 variant is more modest than the much larger gains in the turnover number. But as explained previously, as long as the  $K_M$  remains in the low mM range the increases in the turnover numbers is more desirable (rather than improvements in the catalytic efficiency) in order to use this

enzyme as a biocatalyst in a deracemisation. The optimal variant now has a significantly higher level of activity for (*R*)-amine **76** oxidation than the wild type with a catalytic efficiency now higher than the level measured for the (*S*)-amine **76** with the wild type enzyme. However, this increase in (*R*)-amine activity should not be a problem in the deracemisation of this substrate since the rate of oxidation with the optimal MAO-N variant is still heavily in favour of the (*S*)-enantiomer, with an *E*-value of over 100. The *E*-factor can now be calculated for amine **24** and amine **76** because the catalytic efficiency ( $k_{cat}/K_M$ ) of each enantiomer is known<sup>163</sup>. From the *E*-factor an estimated e.e.p. (predicted enantiomeric excess) can be determined<sup>163</sup> based on the relationship that  $e.e.p. = (E-1)/(E+1)$ . As shown in table 2.4.9.6, all the MAO-N mutants will be expected to give an excellent final e.e. (>97.5%) in a deracemisation, assuming the deracemisation is rapid.

MAO-N	wild type	<u>1</u>	<u>2</u>	<u>3</u>	<u>4</u>
amine <b>24</b> <i>E</i> -factor	20.6	161	87.4	113	90.5
( <i>R</i> )-amine <b>24</b> e.e.p	90.8%	98.8%	97.7%	98.2%	97.8%
amine <b>76</b> <i>E</i> -factor	131	229	1788	109	110
( <i>R</i> )-amine <b>76</b> e.e.p	98.5%	99.1%	99.9%	98.2%	98.2%

Table 2.4.9.6. Predicted enantiomeric excesses (e.e.p) using MAO-N biocatalysts in the deracemisation of amines **24** and **76** calculated from the measured *E*-values.

#### 2.4.10. Thermodynamic improvements in specificity

The specificity of an enzyme for a substrate is determined by the specificity constant ( $k_{\text{cat}}/K_M$ ). This is the ability of an enzyme to discriminate a particular substrate from a mixture of substrates. In deracemisation reactions where the two substrates are chemically equivalent, but opposite enantiomers of a racemate, the specificity is determined by the  $E$ -factor. Transition state theory suggests that the energy barrier that needs to be overcome to achieve catalysis is given by  $\Delta G^\ddagger$ . Enzymes normally achieve rate accelerations compared to the uncatalysed reaction by lowering the transition state energy of the high energy intermediate. It is catalytically advantageous for the enzyme's active site to be complementary to the structure of the transition state because it lowers the free energy of this species, thus reducing  $\Delta G^\ddagger$ . If the enzyme's active site is complementary to the structure of the substrate prior to conversion, the free energy of the ES complex is lowered, thereby increasing  $\Delta G^\ddagger$ .

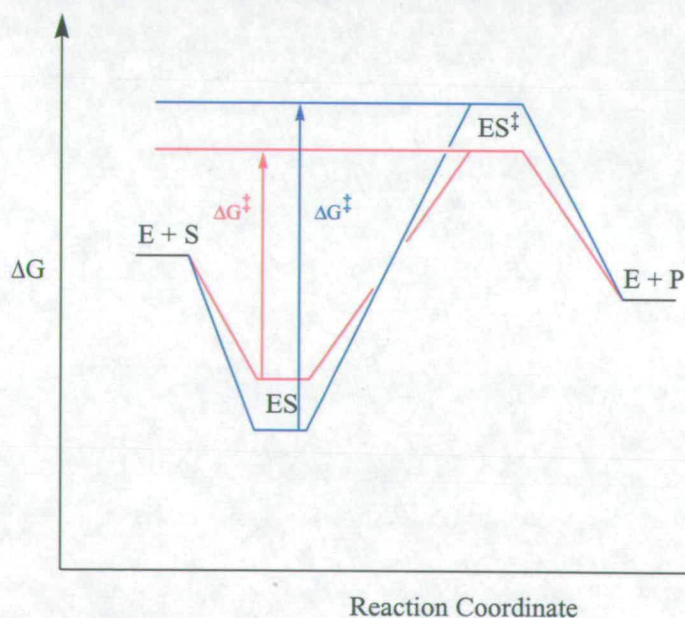


Figure 2.4.10.1. Gibbs free energy changes when the enzyme's active site is complementary to substrate (blue line) and to transition state (red line).

Enzymes can generate differences in substrate specificity by selectively binding the  $ES^\ddagger$  complex of a substrate more efficiently than the opposite enantiomer which reduces the free energy of  $ES^\ddagger$  thus reducing  $\Delta G^\ddagger$ . This substrate selectivity generated by enzymes is shown in figure 2.4.10.1. In red the free energy of  $ES$  is raised and  $ES^\ddagger$  lowered, to lower  $\Delta G^\ddagger$  and hence increasing specificity and in blue the free energy of  $ES$  is lowered and  $ES^\ddagger$  is raised, thereby increasing  $\Delta G^\ddagger$ . The free energy barrier of the transition state is given by:  $\Delta G^\ddagger = \Delta G_{\text{binding}} + \Delta G_{\text{Act}}^\ddagger$  (figure 2.4.10.2).  $\Delta G_{\text{binding}}$  is the energy contribution on binding the substrate and  $\Delta G_{\text{Act}}^\ddagger$  is the activation energy required to reach the free energy of the transition state  $ES^\ddagger$ . The  $\Delta\Delta G^\ddagger$  between two enantiomers ( $A$  and  $B$  of a racemate) is given by:

$$E = [(k_{\text{cat}}/K_M)_A / (k_{\text{cat}}/K_M)_B] = \exp(-\Delta\Delta G^\ddagger / RT)$$

$\Delta\Delta G^\ddagger$  can be considered as the difference in free energy required for catalysis between the 2 enantiomers, i.e. the enantioselectivity of an enzyme.

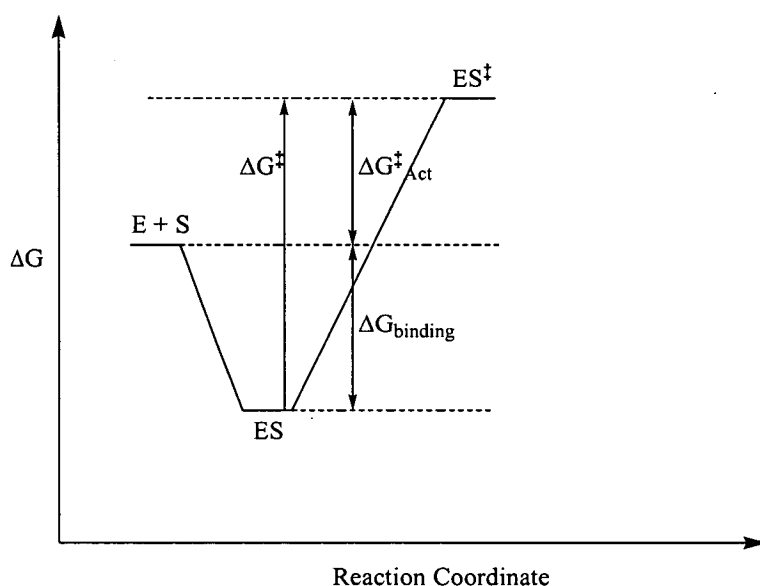


Figure 2.4.10.2. The free energy ( $\Delta G^\ddagger$ ) of an enzyme catalysed reaction is contributed by the binding energy ( $\Delta G_{\text{binding}}$ ) and activation energy ( $\Delta G_{\text{Act}}^\ddagger$ ).

It is possible to estimate the contribution of binding energy<sup>164</sup> of the ES complex using the  $K_M$  value;  $\Delta G_{\text{binding}} = -RT \ln K_M$ . If this is performed on both enantiomers of a racemate then the difference in binding energy ( $\Delta\Delta G_{\text{binding}}$ ) between enantiomer *A* and enantiomer *B* is given by:

$$\Delta\Delta G_{\text{binding}} = -RT \ln [K_M(A)/K_M(B)]$$

Using these relationships the differences in free energy and the kinetic constants  $k_{\text{cat}}$  and  $K_M$  allows the  $\Delta\Delta G_{\text{binding}}$  and  $\Delta\Delta G^\ddagger$  to be calculated between the (*S*)-enantiomer (*A*) and (*R*)-enantiomer (*B*) of amine **76** for the MAO-N variants. [N.B. *E*-factor =  $(k_{\text{cat}}/K_M)_A/(k_{\text{cat}}/K_M)_B$ ]. Note that the errors have not been included in the calculated values shown in table 2.4.10.1. If errors are calculated based on the error values of  $k_{\text{cat}}$  and  $K_M$  measured in tables 2.4.9.1, 2.4.9.2, 2.4.9.3, 2.4.9.4 and 2.4.9.5 then the  $\Delta\Delta G_{\text{binding}}$  and  $\Delta\Delta G^\ddagger$  errors are larger than the values shown.

MAO-N variant	<i>E</i> -factor for amine <b>76</b>	$K_M(A)/K_M(B)$	$\Delta\Delta G_{\text{binding}}$ (kJ/mol)	$\Delta\Delta G^\ddagger$ (kJ/mol)
wild type	131	0.0184	+10.1	-12.3
<u>1</u>	229	0.0857	+6.2	-13.7
<u>2</u>	1788	2.75	-2.6	-18.9
<u>3</u>	109	0.842	+0.434	-11.8
4	110	0.802	+0.556	-11.8

Table 2.4.10.1. Differences in energy of binding ( $\Delta\Delta G_{\text{binding}}$ ) and activation energy ( $\Delta\Delta G^\ddagger$ ) for the (*S*)-enantiomer and (*R*)-enantiomer of amine **76** amongst the MAO-N variants. ( $RT = 2.521$  kJ/mol at 30°C, the assay temperature).

The difference in activation energy ( $\Delta\Delta G^\ddagger$ ) between the (*S*)-amine **76** and (*R*)-amine **76** for all the MAO-N variants is between -11.8 and -18.9 kJ/mol. On a molecular level, this

difference of activation energy between the MAO-N catalysed oxidation of the amine **76** enantiomers is slightly less than the strength of an average hydrogen bond (hydrogen bonds are typically  $\sim 20$  kJ/mol in strength<sup>165</sup>). The MAO-N 2 variant has the greatest difference in activation energy between the enantiomers but is the only variant to show a negative value for  $\Delta\Delta G_{\text{binding}}$ . The negative value for  $\Delta\Delta G_{\text{binding}}$  results from the  $\Delta G_{\text{binding}}$  being lower for the (*S*)-enantiomer than the (*R*)-enantiomer. The other MAO-N variants have positive values for  $\Delta G_{\text{binding}}$  which contributes to the enantioselectivity for these variants. The enantioselectivity observed for the MAO-N 2 variant does not result from the contribution of  $\Delta\Delta G_{\text{binding}}$  but entirely from  $\Delta\Delta G^\ddagger$  and relative stabilisation of the  $ES^\ddagger$  complex for (*S*)-amine **76**.

The wild type enzyme shows the highest degree of difference in energies of binding ( $\Delta\Delta G_{\text{binding}}$ ) between the enantiomers of amine **76** with the ES complex for the (*R*)-enantiomer being greater than 10 kJ/mol more stable than for the (*S*)-enantiomer. The enantioselectivity seen in wild type MAO-N is largely generated by poorer specificity of the active site for the (*S*)-enantiomer which raises the ES free energy and therefore reducing  $\Delta G^\ddagger$  relative to the (*R*)-enantiomer. The differences in energies in enantiomer binding in the ES complex for the quintuple MAO-N variants are small. Enantioselectivity for these two variants is mainly created by stabilisation of the (*S*)-amine **76** transition states.

MAO-N variant	$k_{\text{cat}}/K_M$	$K_M$	$\Delta\Delta G_{\text{binding}}$ (kJ/mol)	$\Delta\Delta G^\ddagger$ (kJ/mol)
<u>1</u>	18.3	0.06	+3.70	-0.46
<u>2</u>	22.0	0.26		

Table 2.4.10.2. The  $\Delta\Delta G_{\text{binding}}$  and  $\Delta\Delta G^\ddagger$  between MAO-N 1 and MAO-N 2 variants for the (*S*)-amine **76** catalysed oxidation.

The final two columns of table 2.4.10.2 shows the  $\Delta\Delta G_{\text{binding}}$  and  $\Delta\Delta G^\ddagger$  for the MAO-N 1 variant when the I246M mutation is introduced. The I246M mutation gave an



improvement in (*S*)-amine **76** catalysis compared to MAO-N 1 variant by less efficient binding of the substrate. There is a slight decrease in  $\Delta G^\ddagger$  which assists in (*S*)-amine **76** catalysis, but the main contribution is from the  $\Delta G_{\text{binding}}$  which can be considered to be a result of destabilisation of the ES complex caused by the I246M change.

#### 2.4.11. Error in measuring protein concentration by the Bradford assay

It is important to consider the potential errors that may have arisen in calculating Michaelis-Menten constants for the MAO-N variants, one source of error being the measuring of the protein concentration in the assays. The error in measuring the protein concentration by the Bradford assay can be estimated by taking multiple readings of a sample (3.2.7). The estimation of error for a measured  $V_{\text{Max}}$  based on the error in measuring the protein concentration can be calculated using the upper and lower error limits of the measured protein concentration. 95% confidence that the true value of the protein concentration can be estimated to be within 2 standard deviations from the mean. The mean protein concentration is calculated to be 0.236 mg/ml  $\pm$  two standard deviations ( $2 \times 0.047$ ) for the MAO-N 4 variant. Recalculation of the  $V_{\text{Max}}$  with the lower and upper protein concentrations gives the values shown in table 2.4.11.1.

Soluble protein (mg/ml)	Estimate	$V_{\text{Max}}$ ( $\mu\text{mol}/\text{min}/\text{mg}$ )
0.142	Lower estimate	4.26
0.236	Mean estimate	5.96
0.330	Upper estimate	9.91

Table 2.4.11.1. Upper and lower error limits of the  $V_{\text{Max}}$  measured for the (*rac*)-amine **209** catalysed oxidation by the MAO-N 4 variant.

---

The error in measuring the protein concentration using the Bradford assay generates a much higher error than is caused by the fitting of the rates by SigmaPlot's enzyme kinetics module. N.B. the  $K_M$  remains unaffected by errors in measuring the protein concentration.

#### 2.4.12. Molecular modelling of MAO-N

To gain a greater insight into the changes that have occurred within the structure of MAO-N during the evolution from wild type to the optimised MAO-N 4 a homology model was developed (G. Grogan, York). The basis of this homology model is taken from the three dimensional structure of MAO-B where the crystal structure has been solved<sup>84</sup>. The related MAO-N sequence is then overlaid over this model and a force field applied to minimise the potential energy of the system, in this case the CHARMM (Chemistry at HARvard Molecular Mechanics) force field was used.

The predicted model generated by this approach (shown in figure 2.4.12.1) has been coloured to highlight the location of the mutated residues that have led to changes in MAO-Ns catalytic performance. The residues that have been shown to affect catalysis are shown in green, the FAD cofactor in red and the remaining residues are shown in white. From the model of the overall enzyme structure it becomes apparent that all of the mutated residues that influence MAO-N catalysis are in the vicinity of the part of the enzyme where catalysis is carried out, i.e. near the FAD cofactor.

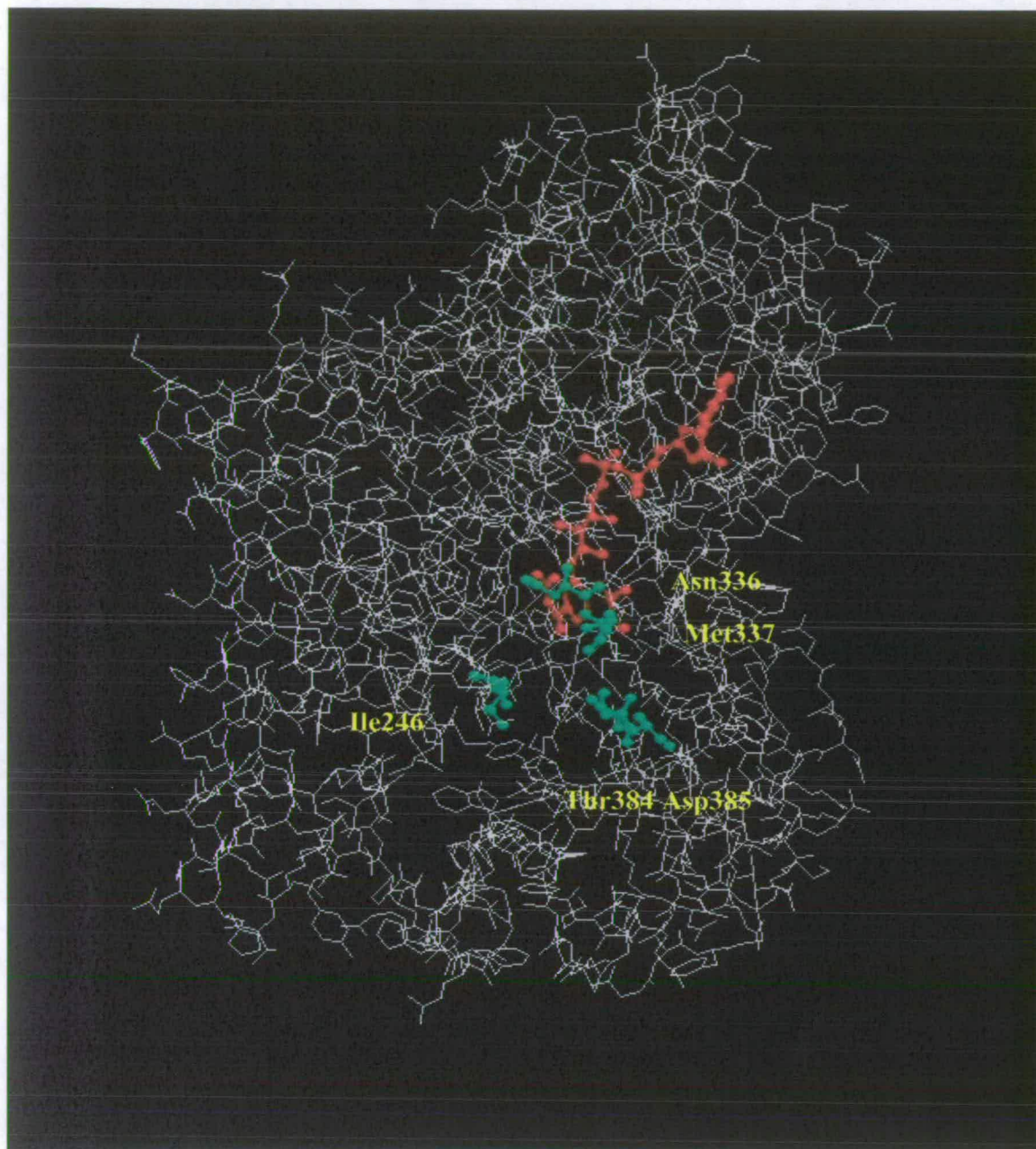


Figure 2.4.12.1 The CHARMMED model of MAO-N from *Aspergillus niger* with residues in green identified to influence the catalytic properties of MAO-N and the flavin cofactor is shown in red.

---

It became apparent when viewing the model in three dimensional perspective (using Insight II Accelrys on a Silicon graphics computer) that there were two important features that regulate catalysis in MAO-N. The active site was identified as being immediately adjacent to and beneath the isoalloxazine ring of flavin. Isoleucine 246 was an integral part of the residues that comprise the active site. The other important feature was a cavity leading from the surface of the enzyme through to the active site. This appeared to be an access channel which could allow a substrate molecule to pass from the bulk solvent to the active site. An access channel for substrate admittance into an enzyme active site is a feature exhibited by some enzymes to regulate their activity. Cytochrome P450s have been shown to have a channel opening mechanisms which are adjusted to the physiochemical properties of the substrate, which can kinetically modulate protein-substrate specificity<sup>166</sup>. In particular the catalytic activity of cytochrome P450 BM3 has been shown to be highly regulated by amino acid residues which flank the surface and heme end of the enzyme access channel. The F87V active site mutation in cytochrome P450 BM3 converted the activity to a regioselective and stereoselective arachidonic acid epoxygenase<sup>167</sup>.

Threonine 384 and aspartic acid 385 are not in the vicinity of the active site and so cannot directly alter the active site specificity; however it became evident that these two residues were at the entrance site of the access channel. The 384 and 385 residues were found to be on a loop structure and not involved in structurally important secondary structure of the protein such as an  $\alpha$ -helix or a  $\beta$ -sheet. There found to be several of these loop features immediately surrounding the access channel. The residues that constitute these loops may give further potential for exploring the access channel because if they are involved in regulating substrate access into the active site it is reasonable to expect that mutation of these residues would influence catalysis.

The suggestion that the 246 residue is at the active site could explain the effect that the I246M variant had on amine catalysis. The I246M variant generated specificity for (*S*)-amine **76** whilst for amine **124** and amine **24** the improvements in catalysis were only marginally improved. The change with the 246 mutation specifically benefits (*S*)-amine **76** oxidation. The mutation and screening of the 384/385 saturation library identified variants with improved (*S*)-amine **76** catalysis. Subsequent kinetic characterisation showed the optimal variants not only having improved activity for (*S*)-amine **76**, but also to the other amines examined (2.4.9). This evidence supports the hypothesis that the 384/385 residues are controlling substrate access since improvement of substrate access would be more likely to be beneficial to more substrates.

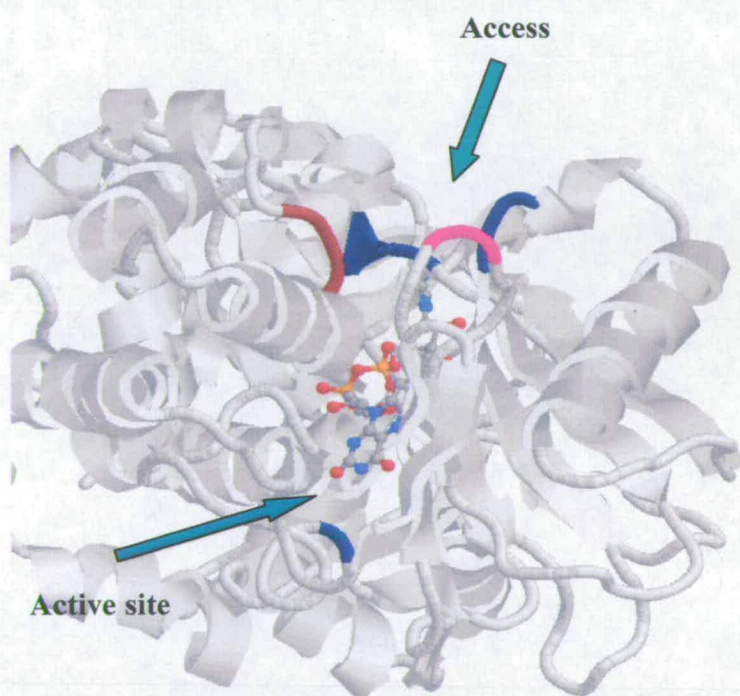


Figure 2.4.12.2. The locations of the active site and substrate access channels in the MAO-N model. The loop regions located at the entrance of the access channel shown in red, pink and blue. The lower blue loop corresponds to the 246 residue and flavin is shown in ball and stick.

---

Energy minimisation manual docking of (*S*)-amine **76** structures into the model allowed further insight into how the mutation of 246 from isoleucine to methionine could cause improvement in catalysis for this substrate. The amino group of (*S*)-amine **76** was fixed within 5Å of N-5 of flavin since it would need to be within this locality during oxidation. It was evident that the methyl branch of the isoleucine side chain was within van der Waals contact distance of the methyl group of (*S*)-amine **76**. Mutation of residue 246 to methionine may accommodate the methyl group of (*S*)-amine **76** more efficiently than isoleucine of the wild type enzyme because methionine lacks substitution at the  $\beta$ -position of its side chain. Other naturally occurring amino acids also lack  $\beta$ -substitution in the side chain but they were not identified as improving (*S*)-amine **76** catalysis during the screening experiment (2.4.3). Presumably this is due to the necessity to maintain a hydrophobic environment at the active site which would exclude hydrophilic residues (1.3.1) and the remaining hydrophobic residues (Gly, Ala, Leu and Pro) have side chains that are either too small or are somehow detrimental to the organisation at the active site.

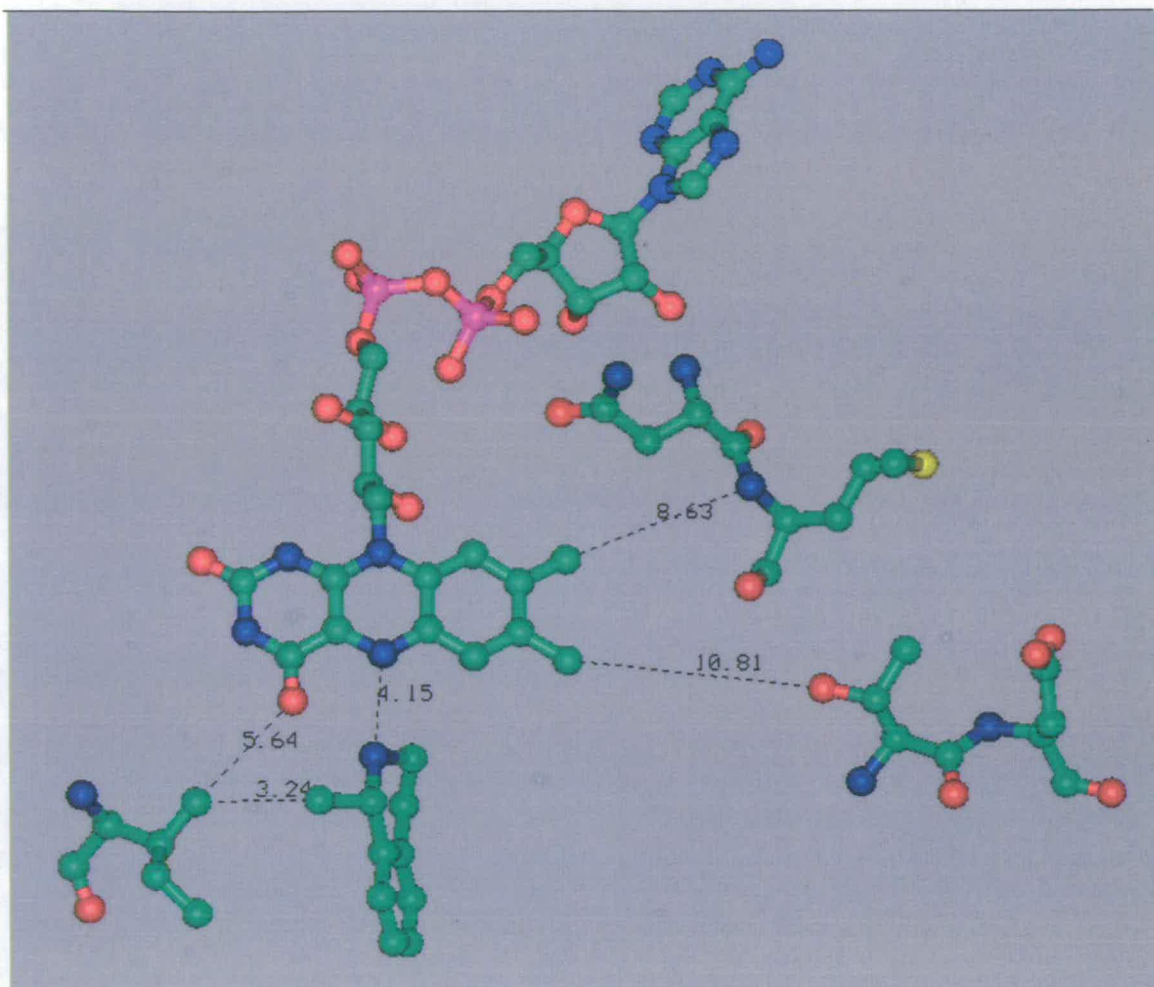


Figure 2.4.12.3. MAO-N model with (*S*)-amine **76** docked. Locations of residues 246, 336, 384, 385 and flavin shown with all other residues removed for clarity. Interatomic distances shown (Å).

### 2.4.13. Conclusion

Exploration by site directed mutagenesis of the 246 amino acid in MAO-N was necessary because of the limitations in screening with the XL1-red generated DNA

---

libraries. Saturation mutagenesis found the methionine variant at 246 in MAO-N discovered by the random approach (2.3.3) was actually the optimal residue when the saturation library was screened against (*rac*)-amine **76**. Screening of the same DNA library against amine **178** showed that methionine as well as isoleucine and arginine were selected as hits in this substrates screen. Alignment of the MAO-N and MAO-B sequences showed that the 246 position in MAO-N aligns to be glutamine 206 in MAO-B. The published crystal structure shows that glutamine 206 in MAO-B to be located at the active site of this enzyme.

The 384 amino acid residue in MAO-N is also aligned to be at the active site (phenylalanine 343 in MAO-B) so a 384/385 site directed mutagenesis saturation DNA library was prepared. After initial difficulties in obtaining enough transformants to represent the library, 13 hits were selected from screening variants against amine **76**. CFE screening of the hits showed improvements amongst all the hits in amine **24** and amine **76** catalysis, whilst still maintaining the high (*S*)-enantioselectivity (except hit L which failed to express MAO-N during fermentation). Hits 5d and 5i were selected for further examination and characterisation by Michaelis-Menten kinetics. Improvements in  $k_{\text{cat}}$  were found to be 19.3 and 3.6 times higher for (*S*)-amine **76** turnover for hit 5d (MAO-N 4 variant) and hit 5i (MAO-N 3 variant) respectively compared to the MAO-N 2 parent. The optimal MAO-N variant for amine **76** oxidation (variant 4) has over a 1300 fold improvement for (*S*)-amine **76** turnover compared to MAO-N wild type. By measuring the  $k_{\text{cat}}$  and  $K_{\text{M}}$ , the *E*-factor can be calculated and based on these values MAO-N should be expected to give high to excellent enantiomeric excesses to the (*R*)-amine product in a deracemisation reaction. The changes in activation energy ( $\Delta G^\ddagger$ ) and free energy of substrate binding ( $\Delta G_{\text{binding}}$ ) have been investigated. The thermodynamic causes of the changes amongst the MAO-N mutants' enantioselectivity and catalytic performance for the enantioselective oxidation of amine **76** have been suggested. Modelling of the MAO-N sequence onto the published MAO-B structure suggests that



---

the mutated residues are either positioned at the active site or control access into the active site of the enzyme. Investigation into the accuracy of the Bradford assay showed there to be a high level of error using this method to measure the soluble protein concentration.

#### 2.4.14. Future work

The 246 saturation library was screened against amines **76** and **178** giving methionine as the optimal amino acid residue for amine oxidation by MAO-N. Is methionine the optimal residue for other amine substrates or if this library were to be tested against other amines would a different optimal residue occur? The crystal structure alignment prediction between MAO-N and MAO-B has several residues, that when mutated in MAO-N, cause a change in MAO-N specificity and in its catalytic performance. It is therefore reasonable to assume that by using the active site alignment model (figure 2.4.5.1) those other residues that are located at the MAO-B active site in the crystal structure could be used to identify MAO-N active site residues. Optimisation of MAO-N catalysis for the 384/385 saturation library should be carried out for different substrates in a similar fashion to the 248 saturation library (2.4.7). A relative rate screening exercise should be undertaken for the MAO-N 4 variant to establish whether this variant enzyme has similar substrate specificity as the earlier versions of variant MAO-Ns?

It would be interesting to see where or if there are limitations in the capability of the directed evolution strategy for improving MAO-N for use as a biocatalyst in deracemisations. In the work conducted here, a 1300 fold improvement in turnover from wild type to the optimised enzyme has been achieved for the (*S*)-amine **76** oxidation, could a similar achievement be possible with a substrate that currently has very poor

specificity? In future work it will probably be better to use an alternative method to measure the soluble protein concentration such as  $OD_{280nm}$  or using the absorbance of MAO-N's cofactor flavin because of the large inaccuracies in the Bradford assay (2.4.11).

## 2.5. Screening of reducing agents for reductions of imines

In order to achieve the efficient deracemisation of a racemic amine using a cyclic oxidation and reduction sequence the oxidised product imine must undergo a chemical reduction to return the imine intermediate to the amine. Previous work in the area of amine deracemisation used ammonia borane to undertake this reduction<sup>64</sup>. Although this approach gave moderate degrees of success, it was apparent that the imine intermediate in the deracemisation reaction underwent a competing hydrolysis reaction. An investigation into the reduction of imines was carried out to evaluate other reducing agents that could be used in place of ammonia borane. The goal was to identify reducing agents that could rapidly reduce an imine and thus minimise hydrolysis. The advantage of examining the reduction step independently in the deracemisation cycle of oxidation and reduction was that the performance of the reducing agents can be directly measured which is not possible in a deracemisation. The imine 1-methyldihydroisoquinoline **224** (MDQ) corresponding to the oxidation of amine **76** was commercially available and therefore this substrate was selected for investigation.

### 2.5.1. The screening of reducing agents

To compare the relative reactivity of various reducing agents a 10mM solution of imine substrate **224** (MDQ) in aqueous buffer was screened against a selection of reducing agents (figure 2.5.1.1). Ten equivalents of the reducing agent were added to each reaction and for reducing agents which did not completely dissolve in aqueous buffer; a minimum amount of cosolvent was added to assist in dissolution (3.5.1).

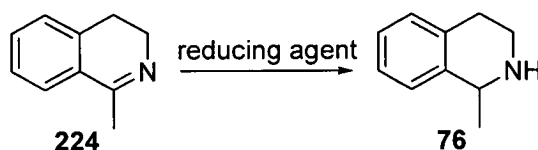


Figure 2.5.1.1. The screening of reducing agents for the reduction of MDQ imine **224**.

The amount of imine remaining after 24 hours was measured by reverse phase HPLC (3.7.4). The reducing agents were classified into two groups depending on their performance in the screen; those that reacted slowly and those that reacted quickly. The amount of imine convert to MTQ (amine **76**) after 24 hours is given in table 2.5.1.2 for the slowly reacting group of reducing agents.

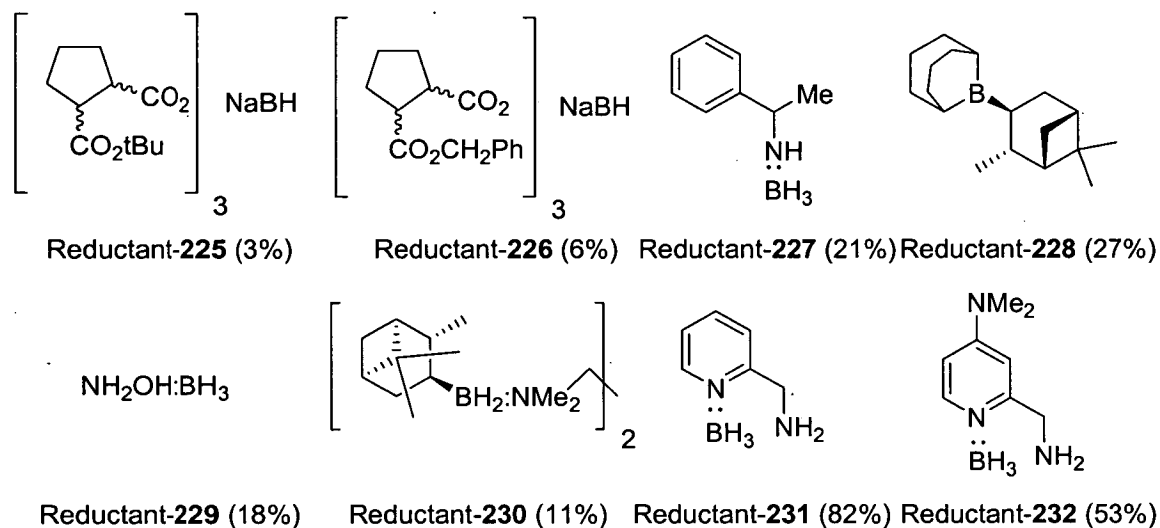


Figure 2.5.1.2. Conversion to MTQ (amine **76**) after 24 hours with 10 equivalents of the reducing agent.

The reducing agents shown in figure 2.5.1.2 were found to react slowly with the imine substrate. These will not be useful in the deracemisation because the rate of reduction is too slow and therefore they were not investigated any further. However, the set of boranes shown in figure 2.5.1.3 are faster and showed complete imine reduction in 24 hours under the same reaction conditions. For these reducing agents the reactions were monitored by regular sampling in order to follow the rate of imine reduction and to evaluate which of these reducing agents produced the fastest rate of imine reduction.

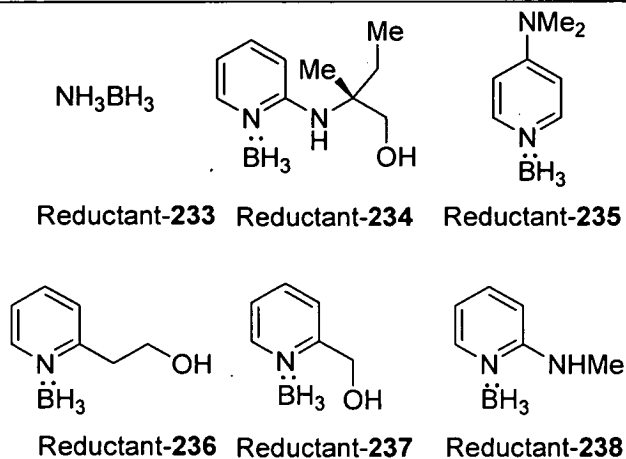


Figure 2.5.1.3. Chemical structures of the reducing agents showing fast imine reductions.

### 2.5.2. Monitoring the time course of reactive boranes

Figure 2.5.2.1 shows that there are 2 amine boranes (reductants **235** and **236**) that have superior rates of imine reduction than the previously reported ammonia borane (reductant-**233**) that was used in the deracemisation of (*rac*)-amine **24** (M. Alexeeva *et al*, *Angew. Chem.*, (2002) 41, 3177-3180). There appears to be an effect in the chemistry of the reductants, with the only differences in the structure of reductant **232** and **237** being the 2-position of the pyridine which is changed from aminomethyl to hydroxymethyl. The increased electronegativity from nitrogen and oxygen or the difference in pKa between the two functional groups may give rise to the improvement in chemical reactivity in the reduction. Further studies within the group<sup>168</sup> have shown that as little as 0.7 equivalents of reductant-**235** afforded the complete reduction of 10mM imine **224** in just 30 minutes. Although ammonia borane showed a lower reactivity than reductant-**235**, complete imine reduction was observed in 24 hours with 1 equivalent of the reducing agent<sup>168</sup>.

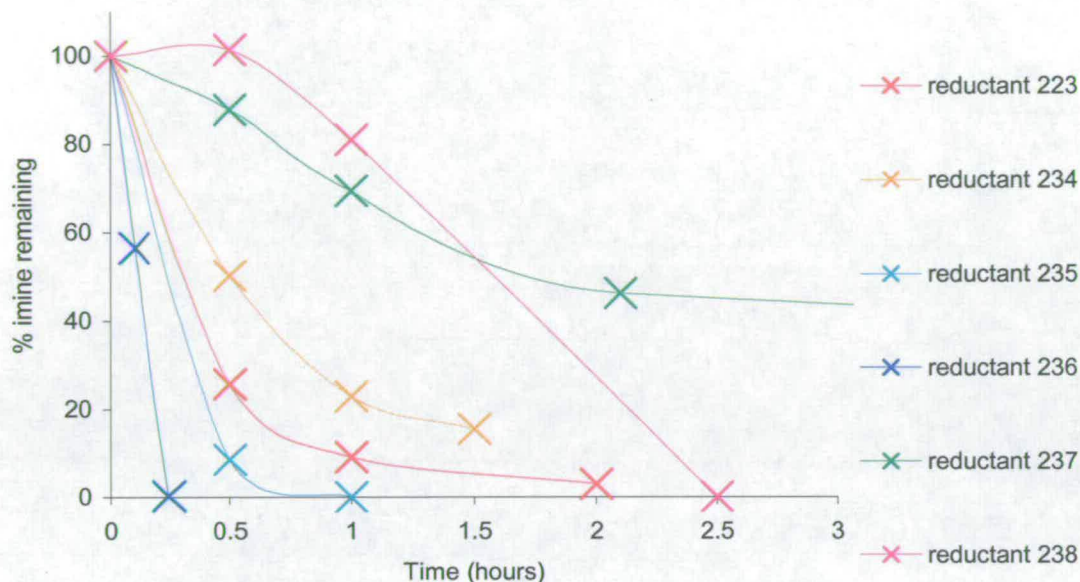


Figure 2.5.2.1. Time course monitoring of the rate of imine reduction with the fast reacting group of reducing agents (reductant **237** shown complete imine reduction in 24 hours).

### 2.5.3. Conclusion

To investigate the inherent problem of hydrolysis in the deracemisation a reducing agent screening was carried out. The reducing agents were classified into two main groups fast and slow reacting depending on the amount of imine remaining in the reduction after 24 hours. The fast reacting group were further examined by time course monitoring and two other boranes were shown to react faster (reductants **235** and **236**) than the previously reported reductant-**233** (ammonia borane).

### 2.5.4. Future work

Other reducing agents could be incorporated into the screening for the chemical reduction of imines (2.5.1) to see if any faster reducing agents could be found. Future

screens could examine the stoichiometry of reducing agents required in order to reduce the inhibitory effect of the amine boranes in MAO-N catalysed amine oxidations (2.6.11) whilst not compromising the imine reduction efficiency. There are few imines commercially available and this is partially due to their inherent instability, but it would be useful to perform the screening on other imines, especially for imines corresponding to amine substrates that are already known to be active towards current MAO-N variants.

It maybe advantageous to look for a biological route to achieve the chemical reduction because the likelihood is that an enzymatic reduction of the imine would not inhibit the MAO-N oxidation as the reductant is not present in the bulk solvent. There is a precedent for this in keto-reductions; fungal oxidoreductases have been used for the asymmetric reduction of  $\beta$ -ketoesters to the corresponding chiral alcohol<sup>169</sup>. Early work has been conducted in employing the anaerobic bacterium *Acetobacterium woodii* in a dynamic combinatorial library to discover new imine reductase activity<sup>170</sup> (figure 2.5.4.1). An imine reductase could offer the opportunity to engineer the compatibility of the enzyme by directed evolution to suit substrate specificity and enantioselectivity.

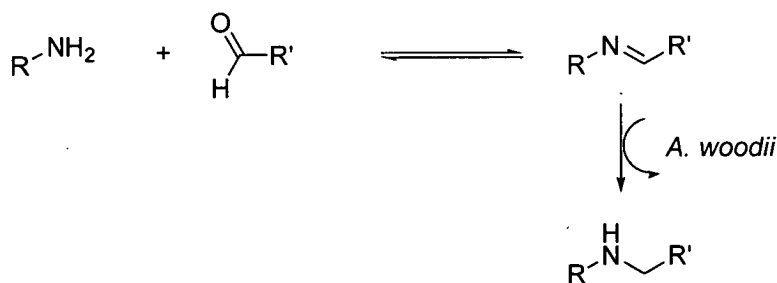


Figure 2.5.4.1. The discovery of novel imine reductase activity by *Acetobacterium woodii* using a dynamic combinatorial library.

## 2.6. Deracemisation experiments

### 2.6.1. Deracemisation objectives

Directed evolution has been used to engineer MAO-N towards the desired goal of achieving successful amine deracemisations. To evaluate the success of the improvements in MAO-N for deracemisation purposes, a series of deracemisation experiments were conducted. Prior to the work described here, only (*rac*)-amine **24** had been deracemised with a high e.e. but in a moderate yield, due principally to the unstable imine being hydrolysed<sup>64</sup>. The early amine **24** deracemisation had been attempted at a low substrate concentration (1mM substrate) and had only been monitored analytically by chiral HPLC. Could the deracemisation of amines be conducted at higher substrate concentrations and preparatively? Unless indicated during the deracemisation studies conducted here the MAO-N 2 variant was used. The selection pressure used in the directed evolution of MAO-N to identify the I246M change was made by its ability to oxidise MTQ (amine **76**) enantioselectively, therefore this substrate appeared the best candidate to conduct preliminary deracemisations. The advantage with using this substrate rather than  $\alpha$ -methylbenzylamine (amine **24**) is the hydrolysis problem associated with amine **24** should not affect MTQ (amine **76**) to the same degree because the imine intermediate is more stable.

### 2.6.2. Deracemisation of (*rac*)-MTQ with whole cell expressing MAO-N

To investigate the deracemisation of (*rac*)-MTQ (amine **76**) a trial reaction was attempted using whole cells. The advantage of a whole cell reaction is there is no requirement to purify the enzyme post-fermentation. It is merely a case of adding the required portion of the harvested cell pellet required for the reaction. The disadvantage is that fermentation variability in the recombinant protein expression can lead to



differences in the level of performance of a whole-cell biotransformation. However, due to the simplicity of a whole cell reaction this was a simple starting point to investigate the deracemisation of (*rac*)-amine **76**. A solution of 10ml of 10mM (*rac*)-MTQ (amine **76**) was successfully deracemised over 24 hours at 30°C with 0.5 g of freshly thawed whole cells (3.6.2). Analysis by chiral HPLC (3.7.1.B) determined the deracemisation to be >99% e.e. with a yield of 69% for (*R*)-MTQ (amine **76**).

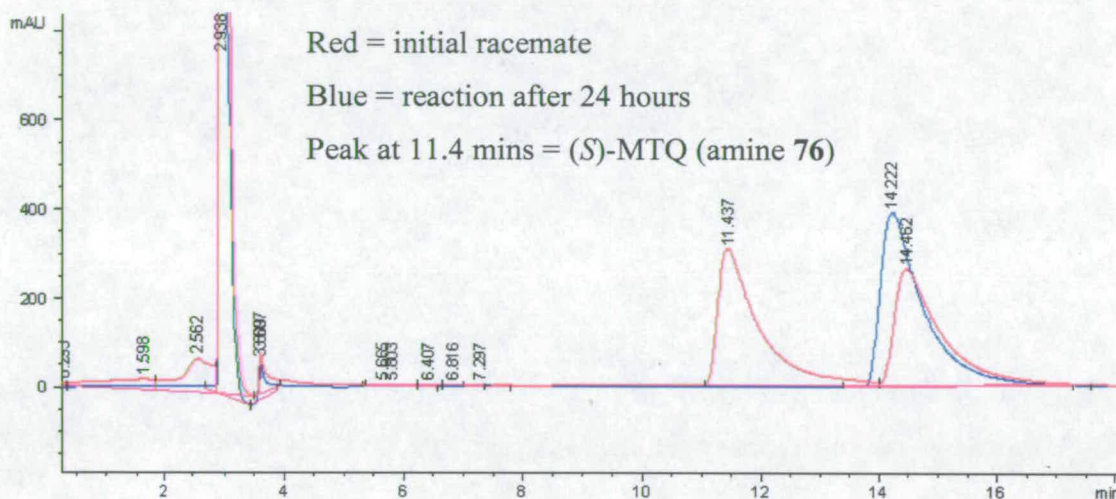


Figure 2.6.2.1. Chiral HPLC trace of the whole cell deracemisation of (*rac*)-MTQ (amine **76**). Red line is the  $t = 0$  hour sample and the blue line is the  $t = 24$  hour sample.

Time course monitoring of the deracemisation showed the reaction to decelerate towards the end of the reaction as expected (figure 2.6.2.2). The  $K_M$  for this enzyme is 0.31mM for (*S*)-amine **76** so once the substrate concentration falls to this concentration the enzyme will be operating at half its maximum velocity ( $V_{Max}$ ). In a 10mM deracemisation when the (*S*)-amine **76** is at a concentration of 0.31mM this corresponds to a 93.8% e.e. of the (*R*)-enantiomer in the reaction, although in reality, the turnover of the enzyme will start falling before it reaches the  $K_M$  concentration. After 48 hours the (*R*)-MTQ (amine **76**) e.e. has risen to >99.5% with a yield of 84.9%, compared to a 98.5% e.e. and 97.6% yield after 29 hours.

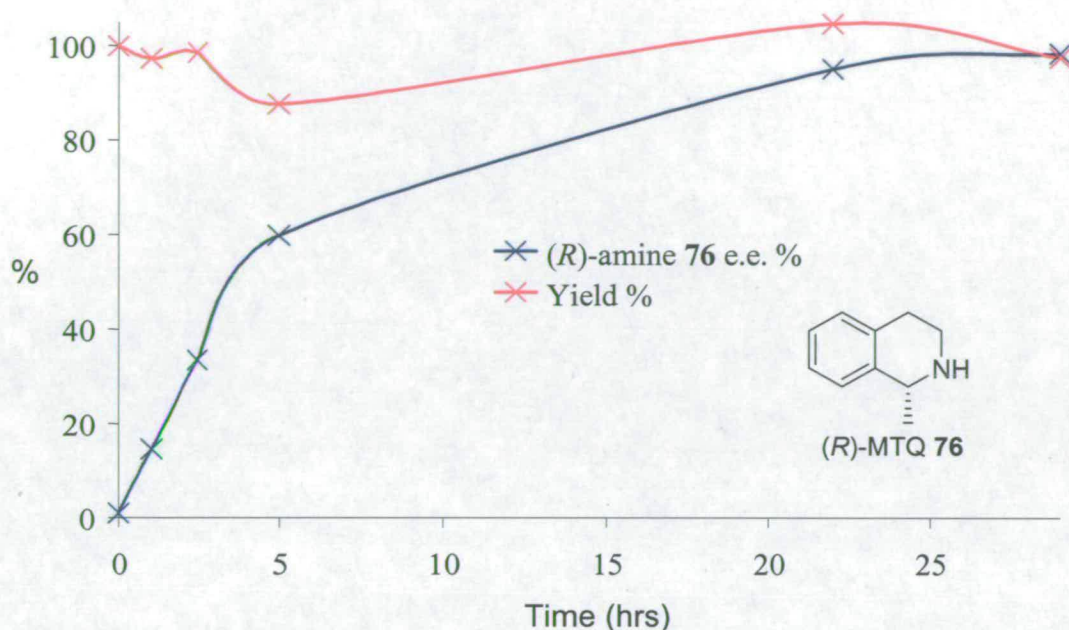


Figure 2.6.2.2. Time course monitoring of the deracemisation of 10mM (*rac*)-MTQ (amine 76) to (*R*)-MTQ (amine 76).

### 2.6.3. Deracemisation at higher substrate concentrations of (*rac*)-MTQ (amine 76) with whole cell expressing MAO-N

The deracemisation of (*rac*)-MTQ (amine 76) was achieved at 10mM substrate concentration, the next objective was to determine what concentration of substrate can be deracemised under similar conditions (3.6.2). In this study the amount of whole cells added to each of the deracemisations was varied to see whether this improved the e.e. of the deracemisation. This experiment was performed as described (method 3.6.2) but with adjustments in the amount of cells and substrate used as indicated (figure 2.6.3.1). As seen in figure 2.6.3.1 the deracemisation of (*rac*)-MTQ (amine 76) at 10mM was virtually completed with 0.59g of whole cells. The e.e.s for the 20mM deracemisations improved from 0.33g and to 0.59g with a complete deracemisation with 1.2g of whole

cells. The 40mM reaction also showed a similar improvement but the e.e. did not improve from the 93% observed with 1.2g of whole cells.

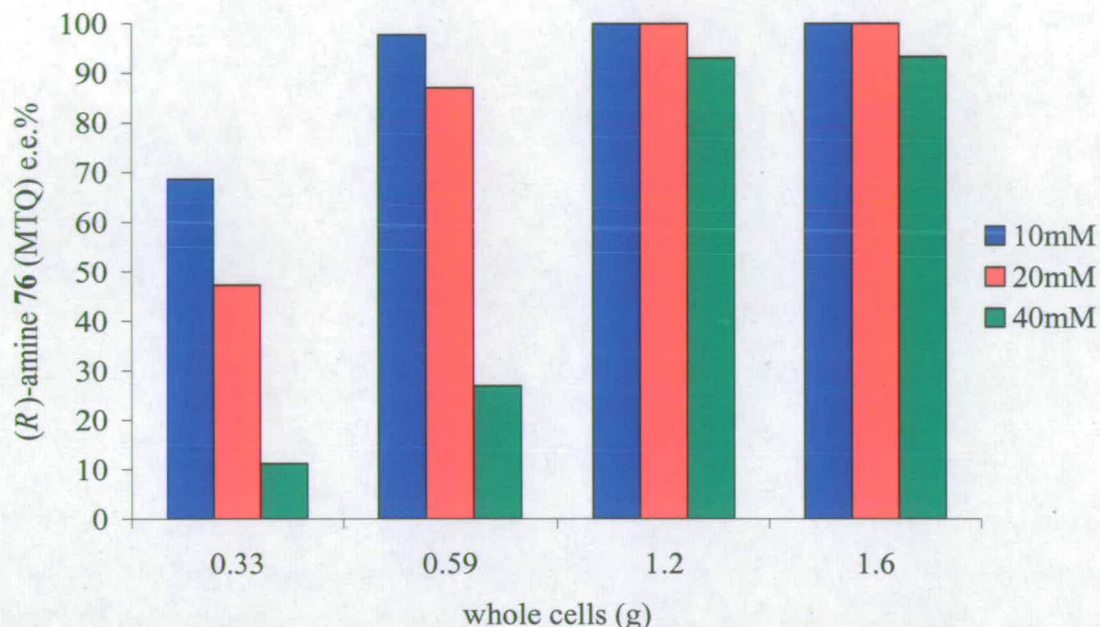


Figure 2.6.3.1. The deracemisation of higher (*rac*)-MTQ (amine 76) concentrations with various amounts of whole cells after 40 hours.

#### 2.6.4. Immobilisation of MAO-N

Early results indicated that the deracemisation of (*rac*)-MTQ (amine 76) worked well using the MAO-N in whole cell form from the fermentation harvest of recombinant *E. coli*. However, the use of whole cell in a biotransformation has several drawbacks which maybe alleviated with an immobilised enzyme. An immobilised enzyme can avoid the problems of diffusion limitations of substrate and loss of product by side activity that can occur with a whole cell process. Whole cell processes tend to pose difficulties with the workup of the reaction, emulsions can occur upon extraction of the aqueous reaction into an organic solvent. If an immobilised enzyme were to be used it could be recovered

---

and potentially reused. The other attractive features about an immobilised enzyme are that often it stabilises the protein and lengthens the life of the biocatalyst. As a simple protocol has been developed for purifying MAO-N (2.1.3) it was decided to investigate the immobilisation of purified MAO-N protein.

Within the group Eupergit had previously been used and it was available in the lab this was selected to be the immobilisation method attempted. Successful applications of other immobilised enzymes has been reported with Eupergit, including an enzyme from the same species as MAO-N, *Aspergillus niger*<sup>171</sup>. The matrix of Eupergit is formed from the copolymerisation of methacrylamide, N,N'-methylene-bis(methacrylamide) and monomers containing oxirane groups. The oxirane groups are the reactive chemical groups that irreversibly attach to the protein via a covalent linkage with the proteins amino and sulfhydryl groups.

#### **2.6.5. Immobilisation of MAO-N on Eupergit**

In order to establish the efficiency of MAO-N immobilisation on Eupergit the uptake of enzyme onto the resin was monitored by the loss of enzyme activity from the buffer solution. This gave a quick and convenient method to follow the progression of the immobilisation. Table 2.6.5.1 gives a typical immobilisation of MAO-N on Eupergit. The MAO-N was assayed towards amine **124** because MAO-N has a high level of activity for amine **124** oxidation making the monitoring of the progression of immobilisation more rapid and reliable. The assay was carried out as described (3.1.7). During each immobilisation reaction a control immobilisation was performed with a protein sample that had no Eupergit added. Typically in a 30ml immobilisation volume, a 100 $\mu$ l aliquot was removed and placed in the blood rotator alongside the immobilisation. Therefore if loss of MAO-N resulted from denaturation, loss of cofactor or proteolysis, this could be monitored through the control reaction.

Time (hours)	Control		Immobilisation	
	0	0.0208 OD/sec	100%	-
24	0.0200 OD/sec	96%	0.00795 OD/sec	38%
42	0.0198 OD/sec	95%	0.00122 OD/sec	6%

Table 2.6.5.1. Monitoring of MAO-N immobilisation onto Eupergit by monitoring the loss of amine 124 activity in solution.

Once the residual MAO-N activity in the immobilisation had fallen below <5% of the initial activity the resin was capped with 3M glycine pH 8.5 to react any unfunctionalised oxirane groups on the resin (3.6.4).

#### 2.6.6. Calculation of the activity of MAO-N activity on the resin

To monitor the immobilisation the loss of MAO-N activity from solution was measured. However, does the loss of MAO-N activity from solution translate to a complete recovery of activity to the resin? Often during an immobilisation procedure the overall enzyme activity will fall to varying degrees as a result of attachment of enzyme to the resin; this can impede the substrates access to the active site and/or cause detrimental global changes in the conformational structure of the enzyme. The method by which the enzyme is attached to Eupergit is by accessible nucleophilic side chain residues in MAO-N that chemically react with the epoxide group on the resin. This process is not selective and will inevitably cause some loss in enzyme activity. There is also the physical change that can affect the biocatalytic properties of the enzyme (diffusion and substrate permeability effects) from going from solution to solid phase.

To account for these changes a solid phase assay was developed to measure the MAO-N activity on Eupergit (3.1.7). Initial attempts at a continuous assay approach that had been

used previously in the solution phase (3.1.1) failed because of the problem of product diffusion. In a 1ml cuvette, the resin would sink to the bottom of the cuvette and the colourimetric red product would sit just above the resin as a dark pink band. As the colourimetric product was not evenly distributed through the cuvette the rate of amine oxidation could not be accurately measured. Instead, a discontinuous assay was required. A weighed portion of the resin, typically 1-4 mgs, in a 1ml eppendorf tube was assayed after 4 minutes, 3 x 200 $\mu$ l of the assay mixture was removed and the OD<sub>510nm</sub> measured. Division of the mean OD of the three measurements by 240 gave the rate in OD/sec; this is then used to calculate a specific activity for the resin (3.1.7). In table 2.6.6.1 is an example of the resin specific activity measured in the preparation of the immobilisation from table 2.6.5.1.

Amount of resin	Mean OD <sub>510nm</sub>	Specific Activity
0.0017g	$0.186 / 240 = 7.75 \times 10^{-4}$ Au/sec	1.752 $\mu$ mol/min/g

Table 2.6.6.1. Measurement of the specific activity of MAO-N-Eupergit activity towards 10mM amine **124**

From the measurement of the immobilised MAO-N activity the percentage recovery of MAO-N activity from the immobilisation can be calculated and was determined to be 2%. [This based on the total rate of the freshly purified being 521.7 OD/sec for the 30ml sample and a total activity of 10.41 OD/sec for the total mass of resin used in the immobilisation (22.88 g)]. This efficiency of immobilisation appeared to be poor; however it was used in subsequent deracemisation experiments.

### 2.6.7. Evaluation of immobilised MAO-N stability

During initial studies with immobilised MAO-N it became apparent that activity was being lost upon storage. To establish the amount of activity being lost and to find the optimal conditions for MAO-N-Eupergit storage a stability study was undertaken.

MAO-N-Eupergit samples from the same preparation were stored at room temperature, 4°C and -20°C. Samples were stored with and without 0.1M potassium phosphate buffer pH 7.0 to determine whether this influenced the longevity of MAO-N activity. Activity was measured after 4 weeks storage (3.1.7) and residual activity is determined by comparison to the specific activity of the freshly prepared MAO-N-Eupergit (1.752  $\mu\text{mol}/\text{min}/\text{g}$ ). The results (table 2.6.7.1) seem to indicate that the best storage temperature is at 4°C and the addition of buffer to the resin made little difference to improve stability. Room temperature and -20°C storage were both worse. Disappointingly, the best storage conditions at 4°C still gave a significant fall in the residual activity. Subsequent preparations of MAO-N-Eupergit throughout these studies were stored at 4°C with no addition of a storage buffer.

MAO-N-Eupergit sample	Specific activity ( $\mu\text{mol}/\text{min}/\text{g}$ )	Residual activity
Room temp (-buffer)	0.137	8%
Room temp (+buffer)	0.244	14%
4°C (-buffer)	0.849	48%
4°C (+buffer)	0.816	47%
-20°C (-buffer)	0.432	25%
-20°C (+buffer)	0.551	31%

Table 2.6.7.1. Measurement of MAO-N-Eupergit activity after 4 weeks storage under different conditions.

### 2.6.8. Preparative deracemisation of (*rac*)-amine 76 (MTQ)

Deracemisation of (*rac*)-MTQ (amine 76) with MAO-N-Eupergit was carried out in a similar fashion to the whole cell deracemisation used previously (3.6.5). 20mM substrate with 5 equivalents of ammonia borane was added to 5.68 g of MAO-N-Eupergit in a 100ml reaction volume. The MAO-N-Eupergit had a specific activity determined to be

4.16  $\mu\text{mol}/\text{min}/\text{g}$ , giving the Units (1 Unit =  $1\mu\text{mol}/\text{min}$ ) of MAO-N activity used in this deracemisation to be 23.6 Units. After 4.5 days the (*R*)-MTQ (amine **76**) e.e. was determined to be >99.5% and the reaction was worked up giving the HCl salt in 100% yield (3.6.5). Satisfyingly, the crude reaction mixture was shown to be pure by  $^1\text{H-NMR}$  and required no further purification after the organic extraction. The optical rotation matched well with previously documented values<sup>172</sup> it was measured at  $\alpha_{\text{D}} +42^\circ$ , compared to the published  $\alpha_{\text{D}} +42^\circ$ .

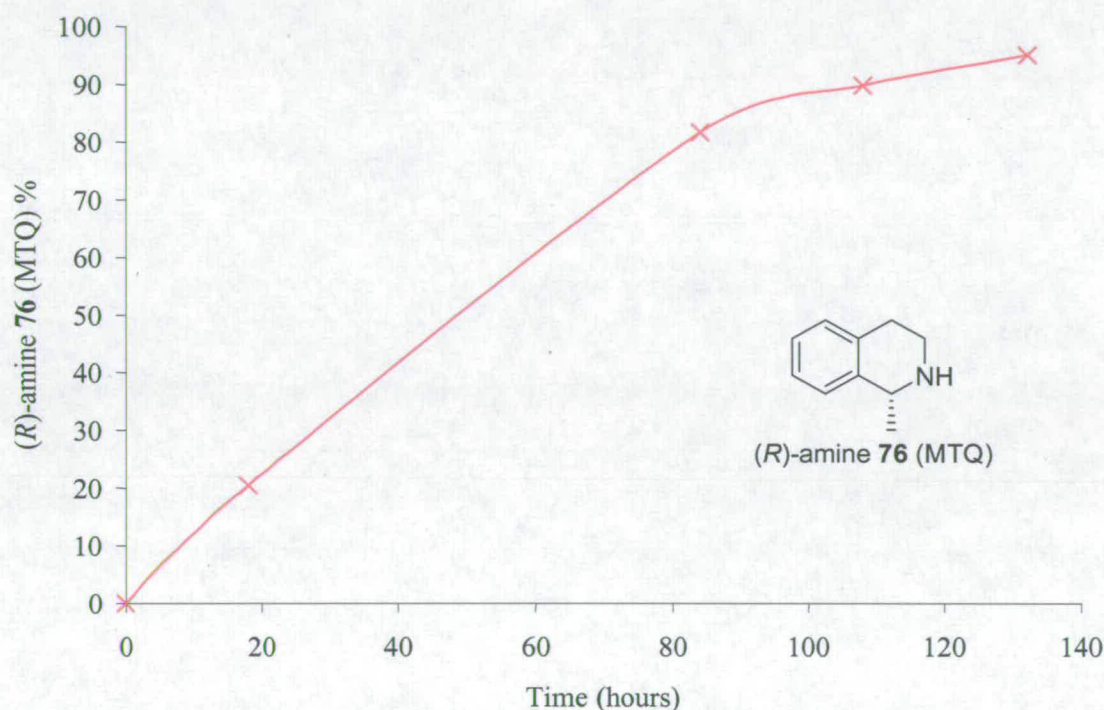


Figure 2.6.8.1. Monitoring of the preparative deracemisation of (*rac*)-amine **76** (MTQ) with immobilised MAO-N-Eupergit.

### 2.6.9. Preparative deracemisation of (*rac*)-MTQ (amine **76**) with whole cells

Although the deracemisation of (*rac*)-MTQ (amine **76**) to (*R*)-MTQ (amine **76**) gave an excellent e.e. and yield the reaction was slow, taking 108 hours to reach an e.e. >99%. It



---

had been shown that the whole cell deracemisation was completed within a day (2.6.2). In order to complete the whole cell deracemisation preparatively the earlier analytical reaction with whole cells was repeated but with a greater quantity of cells to allow more substrate to be deracemised. The reaction was repeated but scaled-up to a 100ml volume (3.6.3). After 18 hours chiral HPLC analysis (3.7.1.B) showed the e.e. >99% and the reaction was worked up. The extraction of product during the workup was problematic addition of TBME gave poor partitioning of the aqueous and organic phases. Even after several hours the phases failed to separate and the crude mixture tended to remain as an emulsion. To alleviate this problem the whole cells were removed by centrifugation, the supernatant basified (pH > 10) and then filtered (0.2 $\mu$ m) to remove any precipitated protein during the basification step. Even after this clean up on the crude aqueous reaction, the partitioning of the organic and aqueous layers tended to be poor, but further centrifugation of the organic/aqueous mixture gave better partitioning. Inevitably, the final (*R*)-amine yield suffered as a result of the problems associated with the extraction with an e.e. >99%, but an isolated yield of 72%. The <sup>1</sup>H-NMR and  $\alpha_D$  matched well with the published data<sup>172</sup> for (*R*)-MTQ (amine 76).

#### 2.6.10. Deracemisation of (*rac*)-amine 209

After the successful deracemisation of MTQ (amine 76) had been achieved it was decided to investigate whether other amines could be deracemised in a similar fashion. It has been shown that numerous other amines are capable of being oxidised by this evolved MAO-N variant (2.2.2 and 2.3.7) and the screening has consistently shown that the enzyme has the high degree of enantioselectivity required for a deracemisation. Amine 209 appeared to offer a good chance of achieving the deracemisation of another chiral amine. Firstly, it is a secondary cyclic amine and therefore has the same advantage that MTQ (amine 76) possesses, the imine intermediate is more stable than an acyclic amine and should suffer less to hydrolysis. Secondly, in the screening of amine 209 it was found to be a highly active substrate (2.3.7) and although this was only measured on

the racemic substrate, it is reasonable to expect high enantioselectivity owing to the evidence of MAO-N's inherent excellent enantioselectivity. To explore the possibility of deracemising amine **209** and to determine the relative performance of amine **209** with MTQ (amine **76**) the same reaction conditions (2.6.8) was employed in the deracemisation of (*rac*)-amine **209** (3.6.6). [i.e. 4.71 g of MAO-N-Eupergit with a specific activity of 5.01  $\mu\text{mol}/\text{min}/\text{g}$  was used in the deracemisation giving a total of 23.6 Units]. The results of the deracemisation of (*rac*)-amine **209** (figure 2.6.10.1) shows the deracemisation is completed a lot more quickly than the equivalent (*rac*)-MTQ (amine **76**) deracemisation, in a matter of hours rather than days. The shape of the curve is also different to the one seen in the MTQ (amine **76**) deracemisation; essentially here it is linear rather than curved indicating no deceleration effects. This shows the better performance of MAO-N biocatalyst in the deracemisation of (*rac*)-amine **209** whereas the deracemisation of (*rac*)-MTQ (amine **76**) was decelerating towards the end of the reaction, here there is a no apparent decelerating effect.

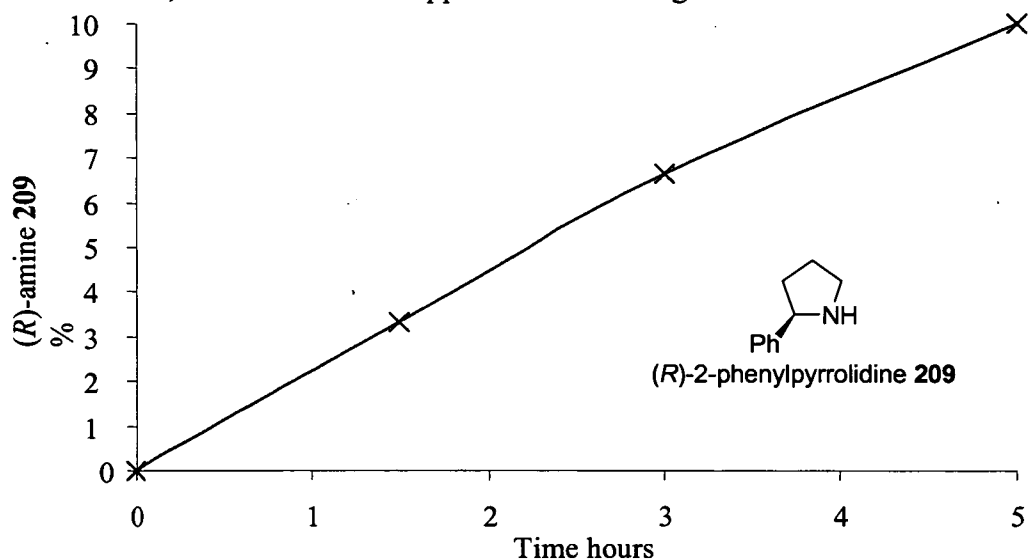


Figure 2.6.10.1. The deracemisation of (*rac*) 2-phenylpyrrolidine **209** to (*R*) 2-phenylpyrrolidine **209** under the same conditions used for the deracemisation of (*rac*)-MTQ (amine **76**).

After achieving a faster deracemisation analytically it was decided to attempt the preparative deracemisation of amine **209** at a higher substrate concentration. Slightly more MAO-N-Eupergit was used in this reaction with 4.75 g of resin used (23.8 Units) 100mM (*rac*)-amine **209** substrate was included and 250mM ammonia borane (3.6.7). This time the deracemisation was not as rapid as the 20mM substrate deracemisation with the reaction taking 48 hours to achieve a (*R*)-amine **209** e.e. >95% (figure 2.6.10.2). The same workup that had been used for the (*rac*)-MTQ (amine **76**) deracemisation was attempted, but trial amine **209** crystallisations with HCl failed and so the crystallisation was not performed on the crude oil. The colourless oil product was isolated in 83% yield and was shown to be ~90% pure by <sup>1</sup>H-NMR and the  $\alpha_D +45.2^\circ$  compared satisfactorily to  $\alpha_D +64^\circ$  for the reported value<sup>173</sup> of (*R*)-amine **209**.

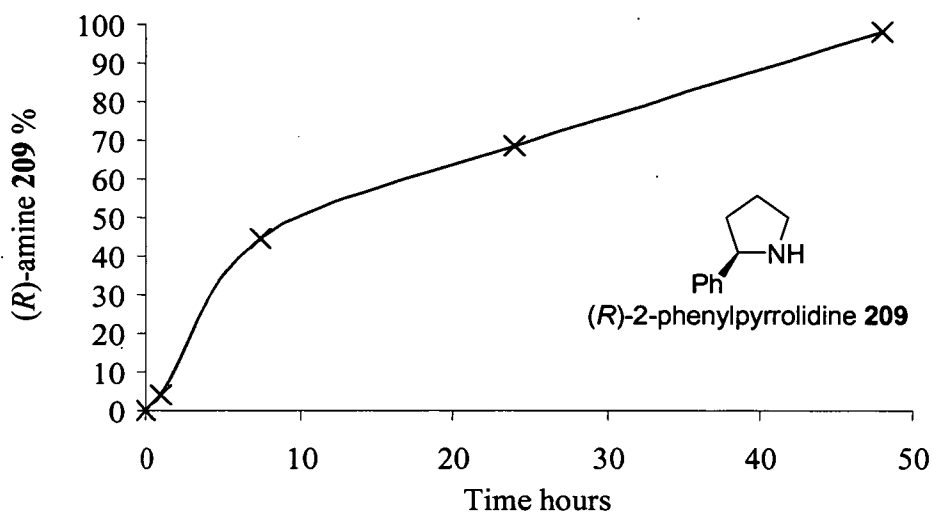


Figure 2.6.10.2. The preparative deracemisation of (*rac*)-amine **209** at 100mM with MAO-N-Eupergit.

### 2.6.11. Effect of alternative reducing agents on the deracemisation of (*rac*)-MTQ (amine **76**)

It has been shown the reduction of the MDQ (imine)-**224** is not solely limited to ammonia borane in an aqueous system (2.5.3). Several other boranes have shown

superior rates of imine reduction over ammonia borane. However, it is not known how they perform in the deracemisation reaction. To explore the possibility of being able to use none ammonia borane reducing agents in the deracemisation of (*rac*)-MTQ (amine **76**) several identical deracemisations were attempted, varying only in the choice of borane. From the quicker group of faster reducing agents reductant-11 and 14 were selected, along with ammonia borane to determine the differences in the deracemisation of MTQ (amine **76**) with each of these reducing agents. A control oxidation was also performed where no reducing agent was added. To 10mM of (*rac*)-MTQ (amine **76**) was added 2 g of 0.373  $\mu\text{mol}/\text{min}/\text{g}$  MAO-N-Eupergit (0.746 Units) and 10 equivalents of the reducing agent (3.5.4). The bar chart (figure 2.6.11.1) shows that all of the reducing agents significantly retard the rate of oxidation compared to the control reaction where no reducing agent was added. Although the reducing agents all lower the biocatalysts performance, they did not all inhibit the rate of oxidation to the same degree. Reductant-**233** (ammonia borane) showed the least inhibition in the trial deracemisation producing an e.e. of 81.4% after 96 hours; reductant-**238** had a final e.e. of 18.4% and reductant-**235** showed the highest level of MAO-N inhibition with essentially no oxidation occurring in this deracemisation.

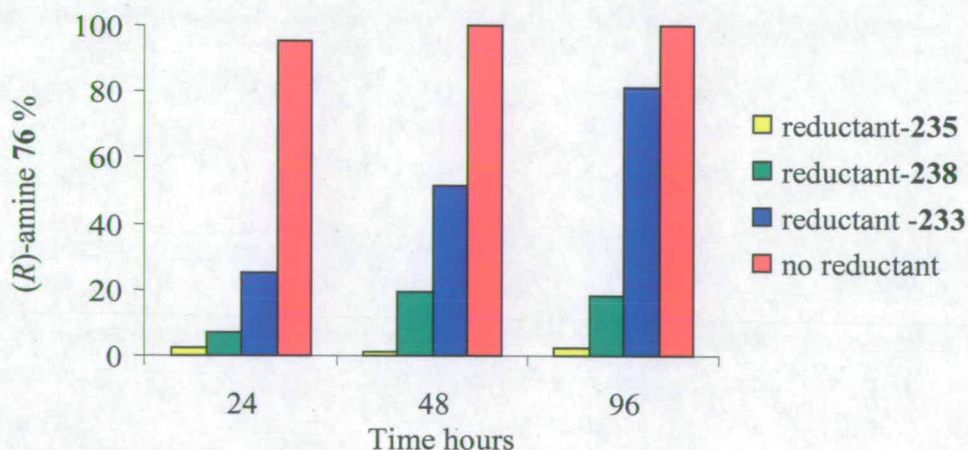


Figure 2.6.11.1. The effect of various reducing agents on the rate of (*rac*)-MTQ (amine **76**) oxidation in a deracemisation.

---

### 2.6.12. Catalytic transfer hydrogenation (CTH) in the deracemisation of amine 76

Evidence in the literature led to the concept that CTH could be used in the deracemisation process<sup>174,175,176</sup>. CTH offers the advantage of being a cheaper method than ammonia borane for imine reductions and although the cost is not significant on small scale deracemisations attempted here, on scale up cost evaluation becomes more important. To make this deracemisation process more attractive in terms of transferring the technology into a process the use of CTH needed to be examined. Typically the cost of the metal catalyst in CTH is relatively expensive and the source of formate used in CTH (e.g. ammonium formate) is cheap. [The Aldrich 2003-2004 list prices for 10g of ammonia borane is £72.50 compared to 100g of ammonium formate at £24.10]. The metal catalyst can be removed in the workup of the reaction and potentially reused saving on cost. It had been shown (correspondence with I.Archer) that 2.1mol% catalyst was sufficient to generate enough of a reducing environment to affect the amino-acid oxidase catalysed deracemisation of pipercolic acid prior to the CTH work under taken here. Before deracemisations with CTH were attempted the physical absorbance of MTQ (amine 76) and its imine substrate (224) onto the catalyst had to be investigated and it was shown that neither amine nor imine was significantly absorbed onto the catalyst (3.5.2). Two catalysts were selected for examination in their ability to reduce 10mM MDQ 224 (3.5.3). After 18 hours the imine and amine peak areas were measured and the results showed that at 15mM ammonium formate the reduction was failing. At 200mM ammonium formate both showed almost total reduction of the imine. The 5mol% Pd/alumina appear to be a better catalyst than 10% Pd/carbon because it showed partial imine reduction at 50mM ammonium formate and even better reduction at 100mM ammonium formate. The 10% Pd/carbon catalyst showed no reduction at 50mM ammonium formate and less reduction at 100mM ammonium formate than the Pd/alumina catalyst.

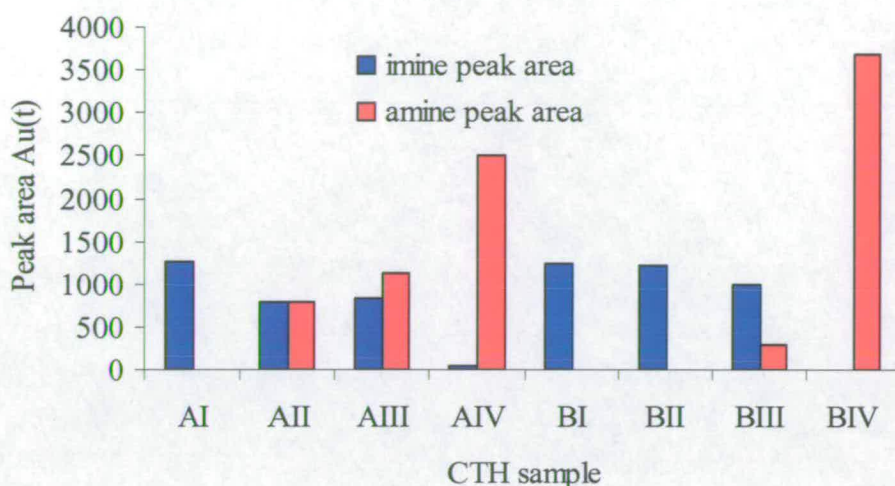


Figure 2.6.12.1. The reduction of MDQ **224** with CTH using ammonium formate and Pd catalyst. A = 2.1mol% of 5% Pd/alumina; B = 2.1mol% of 10% Pd/carbon; I = 15mM  $\text{NH}_4\text{CO}_2$ , II = 50mM  $\text{NH}_4\text{CO}_2$ , III = 100mM  $\text{NH}_4\text{CO}_2$  and IV = 200mM  $\text{NH}_4\text{CO}_2$ .

Based on these findings, the deracemisation of 10mM (*rac*)-MTQ (amine **76**) was attempted using 2.1mol% of Pd catalyst with 200mM ammonium formate and 0.642 Units of 0.366g MAO-N-Eupergit (specific activity = 1.75  $\mu\text{mol}/\text{min}/\text{g}$ ) (3.6.8). Two control oxidations were carried out with and without the presence of 200mM ammonium formate, reactions 2 and 1 respectively. Reaction 3 had 2.1mol% of 5% Pd/alumina catalyst added and reaction 4 had 2.1mol% of 10% Pd/carbon catalyst added. The rate of oxidation of (*rac*)-MTQ (amine **76**) in reaction 1 was rapid but this rate was substantially reduced by 200mM ammonium formate in reaction 2. The observed rate of reaction in reaction 2 was reduced in reaction 3 and the rate slowed even further with the Pd/carbon catalyst of reaction 4. The CE method used to follow the progress of the deracemisation, allows the monitoring of imine formation as well as determining product e.e. The imine peak area for reaction 3 after 68 hours was the same for reaction 2 suggesting the reduction was failing. The imine peak area was present in approximately 30% relative area in both reactions 2 and 3 indicating the reduction was failing for reaction 3.

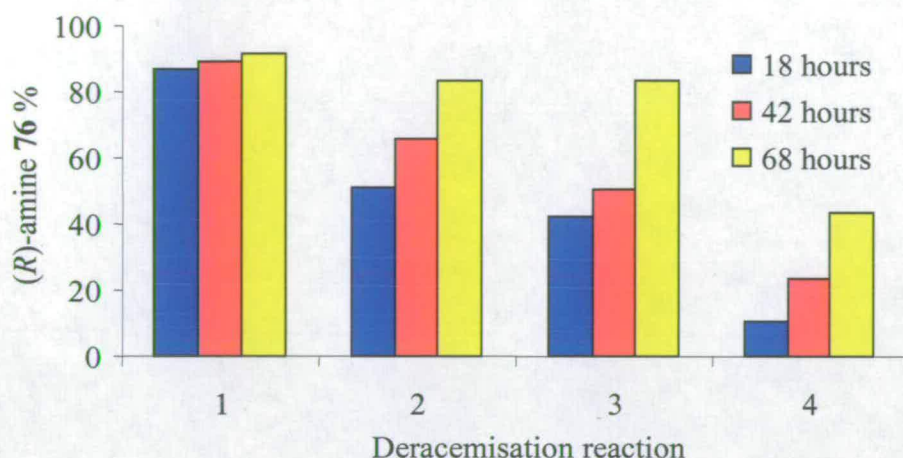


Figure 2.6.12.2. Deracemisation of (*rac*)-MTQ (amine **76**) with CTH. Reaction 1 = control oxidation (MAO-N-Eupergit only), reaction 2 = control oxidation + 200mM ammonium formate, reaction 3 = deracemisation with 2.1mol% of 5% Pd/alumina and reaction 4 = deracemisation with 2.1mol% of 10% Pd/carbon.

The imine reduction was successful with 2.1mol% catalyst, but failed to achieve complete reduction in the equivalent deracemisation reaction. Doubling the amount of palladium catalyst to 4.2mol% from 2.1mol% allowed the complete deracemisation of (*rac*)-MTQ (amine **76**) to (*R*)-MTQ (amine **76**) with the 5% Pd/alumina catalyst. This reaction was completed in 40 hours (97.6% e.e., yield not determined) using 2.92 Units of MAO-N-Eupergit (1.665g resin) with no detection by CE of any imine being present (3.6.9).

### 2.6.13. Conclusions

The MAO-N 2 variant has been used in the preparative deracemisation of (*rac*)-MTQ (amine **76**) and (*rac*)-2-phenylpyrrolidine (amine **209**) to the (*R*)-enantiomer product at 20mM and 100mM substrate concentrations respectively. MAO-N has been applied in the deracemisation reaction either in the whole cell form or as the immobilised purified

---

protein. Both forms of MAO-N gave excellent final e.e.s in the deracemisation. Whole cells giving a faster reaction, but at the expense of yield and the immobilised enzyme gave a slower reaction but with a higher isolated yield. The deracemisation of (*rac*)-MTQ (amine 76) has been shown to moderately successful with reducing agents other than ammonia borane that had previously been shown to efficiently reduce MDQ imine (2.5.2), but generally these other reducing agents retarded the deracemisation. The CTH has successfully been demonstrated in the (*rac*)-MTQ (amine 76) deracemisation, however again the presence of the reducing agent (200mM ammonium formate) significantly retarded the rate of substrate oxidation compared to the oxidative half reaction. Another approach has recently reported for the enzymatic resolution of (*rac*)-MTQ (amine 76) using *Candida rugosa* lipase<sup>69</sup>. The main disadvantage of this kinetic resolution compared with the deracemisation technique used in this report is outlined earlier (1.2.2). The benefit with the deracemisation of (*rac*)-MTQ (amine 76) to (*R*)-MTQ (amine 76) is that it has been achieved in a 100% yield here, compared to the 46% yield with the kinetic resolution method.

This work has been conducted alongside Vicente Gotor-Fernandez<sup>168</sup> and because of the relevance of this work to the study here, it is appropriate to include these findings here. These studies have compared the whole cell deracemisation of (*rac*)-MTQ (amine 76) expressing the MAO-N 1 and the MAO-N 2 variants which leads to a 52% and a 99% e.e. respectively for (*R*)-MTQ (amine 76) under identical reaction conditions. The difference in e.e. between the MAO-N variants correlates well with the difference in kinetic measurements (2.3.6). The improvement in turnover for the I246M mutation in (*S*)-MTQ (amine 76) oxidation rates is translated into an improvement seen in the whole cell deracemisation.

This study also investigated the effect of different boranes, in place of ammonia borane, in the deracemisation of (*rac*)-MTQ (amine 76). It was found that reductant-14 giving a poorer e.e. than with ammonia borane and reductant-11 strongly inhibited the amine oxidation. Although reducing the equivalence of reductant-14 from 10 equivalents used



---

in the deracemisation did allow higher e.e.s to be achieved, with 58% and 99% e.e. seen for a 1 equivalent of reductant-14 for the MAO-N 1 variant and MAO-N 2 variants respectively.

Further studies by V. Gotor-Fernandez<sup>168</sup> into the use of organic solvents to suppress the inherent hydrolysis problem in the deracemisation reaction showed that use of polar solvents led to inactivation of the enzyme. Non-polar solvents such as cyclohexane, octane and toluene allowed the deracemisation to proceed in a biphasic reaction. In the deracemisation of (*rac*)-amine **24** up to 80% cyclohexane in buffer allowed complete (*S*)-amine **24** oxidation in 24 hours. In fact, even better enantioselectivities in amine **24** oxidations were seen when cyclohexane was used in the biphasic reaction rather than with buffer alone. Addition of ammonia borane into these biphasic reactions was deleterious and led to lower e.e.s than the buffer only deracemisation. This was probably a result of concentrating the reducing agent into the aqueous phase and therefore increasing inhibition of the enzyme. Attempts to increase the reactivity of the deracemisation by raising the temperature to 40°C in the biphasic reaction and reducing the ammonia borane concentration to 5 equivalents in the reaction led to 50% e.e. being achieved. Employment of a higher boiling point non-polar organic solvent, octane in place of cyclohexane, prevented the evaporation of the organic solvent and the deracemisation of amine **24** was achieved with (*R*)-amine **24** measured to be 99% e.e. and 85% yield after 20 hours.

More recently the MAO-N 4 variant has been shown to deracemise (*rac*)- $\alpha$ -methylbenzylamine (amine **24**)<sup>177</sup>. Interestingly it was shown that by increasing the  $\alpha$ -methylbenzylamine (amine **24**) concentration in a biphasic deracemisation gave higher yields of (*R*)- $\alpha$ -methylbenzylamine (amine **24**). A deracemisation of 10mM of (*rac*)- $\alpha$ -methylbenzylamine (amine **24**) with 2.5 equivalents of ammonia borane gave >99% e.e. and 68% yield, whilst performing the reaction under the same conditions but with 100mM gave a 98% e.e and 86% yield in 24 hours<sup>177</sup>. Presumably the ability to

---

deracemise higher concentrations of (*rac*)- $\alpha$ -methylbenzylamine (amine **24**) results from the improvements generated by directed evolution (see figure 2.4.9.2)

#### 2.6.14. Future work

Many of the issues that relate to future work are concerned with bringing together the biocatalyst and the reducing agent in the deracemisation process. Particularly important are scaling up the reactions, reduction of cost and improved productivity. For instance, would it be possible to carry out the 2-phenylpyrrolidine (amine **209**) deracemisation at concentrations greater than at 100mM? Could the CTH deracemisation be achieved preparatively? Would alternative immobilisation supports be advantageous in terms of cost, reusability, stability and immobilisation efficiency?

All of the deracemisation studies carried out here involved the use of the MAO-N 2 variant. However it has been shown that the MAO-N 4 variant had a 19 fold improvement in  $k_{\text{cat}}$  for (*S*)-MTQ (amine **76**) (2.4.9.). The higher  $k_{\text{cat}}$  should translate to a much more efficient biocatalyst and enable the deracemisation of (*rac*)-MTQ (amine **76**) to be completed at higher substrate concentrations and over a shorter time as was observed for (*rac*)- $\alpha$ -methylbenzylamine (amine **24**). The deracemisation studies described in this thesis have focussed on just 2 amines out of the many that are known to be active from the screening of amines performed (2.2.2. and 2.3.7.). It will be important to investigate whether similar deracemisation protocols will allow the deracemisation of other amines that are known to shown activity in MAO-N catalysed oxidations. The problem of imine hydrolysis has been investigated<sup>168,177</sup> with the best acyclic amine deracemisation being achieved at 86% yield. It is interesting to speculate whether it will be possible to suppress the hydrolysis further.

It is known that prochiral ketones can undergo reductive amination to give the racemic amine with ammonium formate and Pd/C under aqueous reaction conditions<sup>175</sup>. The

amine product could potentially be enantioselectively oxidised by MAO-N and thus deracemised. This would give a one-pot asymmetric reductive amination of a ketone to an optically active amine. Any material lost by hydrolysis could be potentially recovered by the reductive amination, thereby achieving higher yields than the equivalent deracemisation process.

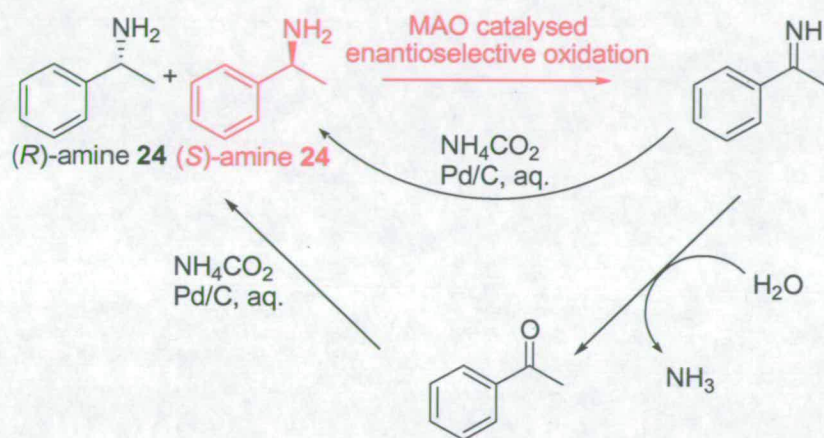


Figure 2.6.14.1. The asymmetric reductive amination from a prochiral ketone (acetophenone) to an optically active amine (*R*)-MTQ (amine 76).

### 3.1. MAO-N assay methods

#### 3.1.1. The horseradish peroxidase coupled liquid assay

The following chromogenic solution was prepared; 1M aminoantipurine (37.5 $\mu$ l), 2% (w/v) TBHBA in DMSO (500 $\mu$ l), 10mM (after dilution) of amine **124** (54 $\mu$ l), 1M potassium phosphate buffer pH 7.6 (5ml) and finally water to give a final volume of 50ml.

5 $\mu$ l of 1mg/ml HRP (Horseradish peroxidase, Sigma P-6782) was added to 10 $\mu$ l of the purified MAO-N protein sample in a U-shaped 96-well microtitre plate. To this was added 185 $\mu$ l of the chromogenic solution giving a final volume of 200 $\mu$ l. The colourimetric production formation was monitored by the 510<sub>nm</sub> absorbance with a plate reader (Molecular Devices, Versa Max tunable microplate reader) at 30°C ( $\epsilon = 29400 \text{ M}^{-1} \text{ cm}^{-1}$ )<sup>178</sup>. The activity of MAO-N towards 10mM amine **124** was calculated from rate of change of the 510<sub>nm</sub> absorbance. The specific activity can be determined (as shown below) by dividing the activity measured on the assay by the measured soluble protein concentration from the Bradford assay (3.2.6)

$$[(\text{Activity}/(\epsilon \times L)) \times 20 \times 60 \times 1 \times 10^3]/P = \text{Specific Activity } \text{Umg}^{-1}$$

Activity = rate measured on the peroxidase assay (OD/sec)

$\epsilon$  = Extinction coefficient of colourimetric product, 29,400  $\text{M}^{-1} \text{ cm}^{-1}$

L = path length (cm)

P = protein concentration based on Bradford assay (mg/ml)

U = Units ( $\mu\text{mol min}^{-1}$ )

### 3.1.2. Measurement of U-shaped well path length

When a 96-well plate was used to measure the change in  $OD_{510nm}$  there is not a fixed path length, as is the case for a single 1cm cuvette. It is dependent on the volume used in the measurement since the path is measured from top to bottom in the microtitre plate. The path length of 200 $\mu$ l volume in a U-shaped 96 well microtitre plate was measured based on the averaging of three measurements of an identical sample measured in triplicate from the reading of a 1cm path length cuvette. The 1cm fixed path gave an average path length measured to be 0.318 OD. This compared with 0.170 OD average measured in the microtitre plate in a 200 $\mu$ l volume. Therefore the path length for a 200 $\mu$ l volume in a U-shaped 96-well microtitre plate was measured to be 0.53cm.

### 3.1.3. Relative rate calculation

The unreliability of measuring consistent specific activities for the rate of amine oxidation by purified MAO-N was primarily caused by the inherent instability of the enzyme upon storage (2.1.4). To circumvent this difficulty it was decided a % relative rate activity would be undertaken.

Amines were either purchased from commercial sources (Aldrich, Lancaster, Sigma, Lancaster or Acros) or synthesised in house (V. Gotor-Fernandez, C. E. Humphrey or G. J. Roff). Chromogenic solutions were prepared with replacement of amine **124** with the desired substrate a final concentration of 10mM (3.1.1). A second chromogenic solution was prepared with part 3 replaced with (*rac*)-amine **24**. The rate of (*rac*)-amine **24** was measured and the rate of the sample amine was measured in parallel on a 96-well microtitre plate. The rate of the sample amine was then calculated by division of the rate

measured against (*rac*)-amine **24** to give the percentage relative rate. For each assay a negative control assay was performed to ensure the rate measure is a result of enzyme turnover and an artefact of the particular assay. If a response was recorded with the negative control, the amine was purified by distillation and fresh chromogenic solution prepared. The negative control assay had the addition of 10 $\mu$ l of purified MAO-N protein sample replaced with 10 $\mu$ l of water.

#### **3.1.4. CFE rate calculation**

Method as 3.1.3. except that the 10 $\mu$ l of the purified MAO-N protein sample is replaced by 10 $\mu$ l of CFE.

#### **3.1.5. Michaelis-Menten calculations**

Chromogenic solution was prepared but with amine substrate added to give a final substrate concentration of 50mM (3.1.1). The chromogenic solutions pH was measured and the pH lowered if necessary back to pH 7.8 by dropwise addition of 2M sodium hydroxide. A second preparation of chromogenic solution was used to dilute the stock 50mM amine substrate chromogenic solution to give the following chromogenic solutions with amine substrate concentrations of 50, 30, 20, 10, 8, 6, 4, 2, 1, 0.8, 0.6, 0.4, 0.2, 0.1 mM and 50, 20, 10, 5 and 1 $\mu$ M. Each chromogenic solution was assayed for MAO-N activity as described (3.1.1). These measurements were carried out on freshly prepared protein samples to ensure any loss of activity on storage of the protein was minimal.

The calculated specific activities were entered into the Enzyme kinetic module of SigmaPlot<sup>179</sup> selecting the Michaelis-Menten type calculation to generate the  $V_{\max}$  ( $\mu\text{mol}/\text{min}/\text{mg}$ ) and  $K_M$  (mM). The  $k_{\text{cat}}$  is calculated by multiplication of the by the  $V_{\max}$  and the molecular weight of MAO-N (55.6 kDa).

### 3.1.6. The solid phase assay

The DNA sample was transformed into *E. coli* BL21 (DE3) competent cells (3.3.1) but rather than spread directly onto the agar, a nitrocellulose membrane (Amersham) was overlaid the agar. The transformation was spread over the membrane. After 16 hours growth at 37°C to allow the colonies to develop to an adequate size, the membrane was peeled off the agar and the membrane frozen at -20°C until required. Prior to the assay, the membrane was thawed and allowed to warm up to ambient room temperature. The following chromogenic solution was prepared; 2 DAB tablets (Sigma, D4418), 1M potassium phosphate pH 7.6 (8ml), water (72ml), HRP 1mg/ml (24 $\mu$ l) and 10mM (after dilution) of (*rac*)-amine **76** (104 $\mu$ l).

2% (w/v) agarose in water was melted and then cooled to 50°C in a water bath. 10ml of the chromogenic solution was mixed with 10ml of the molten agarose and immediately poured over the thawed nitrocellulose membrane (2.3.3). The assay was left to develop on the bench at room temperature.

### 3.1.7. Solid phase MAO-N-Eupergit assay

Due to the problem of measuring the MAO-N activity on immobilisation a discontinuous assay was required (2.6.6). A weighed amount of MAO-N-Eupergit

---

(3.6.4) in an eppendorf tube (typically 2-5 mgs of resin), had 5 $\mu$ l of 1mg/ml HRP added, followed by 995  $\mu$ l of 10mM amine **124** chromogenic solution. The reaction was left to proceed for four minutes with occasional inverting of the tube (~20 second intervals) to allow even distribution of the colourimetric product throughout the assay. The final OD<sub>510nm</sub> was measured and the rate calculated.

The rate of the activity of the resin can be calculated by:

$$\text{Final OD}_{510\text{nm}}/4 = \text{Activity (OD}_{510\text{nm}}/\text{min)}$$

The activity (OD<sub>510nm</sub>/min) is converted to  $\mu\text{mol/ml/min}$  with:

$$[(\text{Activity}/(\epsilon \times L)) \times 1 \times 10^3] = \text{Activity } (\mu\text{mol/ml/min})$$

Division of the activity ( $\mu\text{mol/ml/min}$ ) by the mass of resin (g) gives the specific activity of the MAO-N-Eupergit towards amine **124** ( $\mu\text{mol min}^{-1} \text{g}^{-1}$ ).



## **3.2. MAO-N purification techniques**

### **3.2.1. Q-Sepharose purification**

Cell pellet (8.2g) from the MAO-N *I* variant fermentation (3.3.5.2) was thawed on ice and resuspended in 50ml of Q-Sepharose resuspension buffer (Q Sepharose resuspension buffer; 25mM Tris/HCl pH 7.8, 1mM PMSF and 1mM DTT). The sample was subjected to sonication and centrifugation (3.3.6) to give the CFE. The CFE was diluted with resuspension buffer to give a 100ml final volume. A HiLoad 26/10 50ml Q Sepharose column operated by a UPC-900 Amersham pharmacia biotech FPLC was used during the purification at 4°C. The column was pre-equilibrated with 2 column volumes of buffer A (identical to Q Sepharose resuspension buffer), 2 column volumes of buffer B (Q Sepharose resuspension buffer and 1M NaCl) and 3 column volumes of buffer B. The CFE was loaded onto the column and the column washed with 2 column volumes (100ml) of 100% buffer A to remove unbound sample, the flow rate set at 5ml/minute. The column was subsequently washed with buffer A in buffer B linear gradient (0-1M NaCl) over 20 column volumes (1 litre) at 5ml/minute with collection of 30ml fractions after the dead volume (50ml) had eluted. The column was cleaned with 4 column volumes (200ml) buffer B. All fractions were assayed (3.1.1) and MAO-N activity was found in fractions 35-37 corresponding to a NaCl concentration of 238-277mM. The active fractions were aliquoted in 1ml portions and stored at -80°C.

### **3.2.2. Nickel affinity purification**

Cell pellet (1g) from the MAO-N *I* variant fermentation (3.3.5.2) was thawed on ice and resuspended in Ni-NTA resuspension buffer (Ni-NTA resuspension buffer; 25mM Tris/HCl pH 7.8, 300mM NaCl, 1mM PMSF and 1mM  $\beta$ -mercaptoethanol) (10ml). The sample was subjected to sonication and centrifugation (3.3.6) to give the CFE. Ni-NTA

slurry (Qiagen 30210) (10ml) was applied to a sintered resin column and equilibrated with Ni-NTA resuspension buffer (30ml) at 4°C. The CFE was applied to the top of the column and passed through the column under gravity. The column was washed with wash buffer (Ni-NTA resuspension buffer and 60mM imidazole) (30ml) and the protein eluted in 1ml fractions with elution buffer (Ni-NTA resuspension buffer and 200mM imidazole) (10ml). Each of the fractions was checked for MAO-N activity (3.1.1) and the active fractions combined, divided into 1ml portions and stored at -80°C.

### **3.2.3. PD10 desalting**

Desalting of the freshly purified protein from the nickel affinity resin (3.2.2) was attempted to help improve the stability of the protein (2.1.4.). Disposable Amersham Bioscience PD-10 desalting columns were used (Amersham Biosciences). The column was equilibrated with 25ml of the chosen storage buffer (2.1.4). 2.5ml of the sample was loaded onto the top of the column and the flow through discarded. 3.5ml of the choice storage buffer was applied to the top of the column and the flow through collected.

### **3.2.4. Ammonium sulfate precipitation**

Ammonium sulfate precipitation is an alternative method to PD-10 desalting (3.2.3) to replace the storage buffer from the preparation of purified MAO-N protein from the nickel affinity purification (3.2.2). Post purification, the protein sample was placed onto ice on a stirrer plate. Aliquot addition of ammonium sulfate was added to a stirred solution of the purified MAO-N sample, ensuring complete dissolution after each addition before the next. 60% ammonium sulfate saturation (36.6g/100ml) was found to complete precipitation of the MAO-N protein. The sample was centrifuged at 4000 rpm for 20 minutes affording a bright yellow pellet. The supernatant was discarded and the MAO-N protein pellet was redissolved into 0.1M potassium phosphate buffer pH 7.0.

### 3.2.5. SDS PAGE protein gel

Analysis of the purity of protein and MAO-N expression samples was done using SDS PAGE. Precast gels were purchased (SDS Biorad 10-15% polyacrylamide gel) and New England Biolabs markers (P77085) were used as with the molecular weights of the standard proteins being 175, 83, 62, 47.5, 32.5, 25, 16.5 and 6.5 kDa. 20 $\mu$ l of the protein sample was mixed with 20 $\mu$ l of the loading buffer, boiled for 1 minute and centrifuged at maximum speed in a desktop centrifuge for 1 minute. Each sample was loaded into each lane (30 $\mu$ l) of the SDS PAGE gel and the gel was placed into the gel apparatus (Biorad) and submerged in SDS gel running buffer. The electrophoresis was carried out at 200V for appropriately 80 minutes. The gel was placed into staining solution for 1 hour minimum and then destained to develop the bands in the destaining solution.

### 3.2.6. The Bradford assay

Protein concentrations were determined using the Bradford assay<sup>180</sup>. The protein sample (20 $\mu$ l) had the Bradford reagent (980 $\mu$ l) added. The sample was left to develop for 2 minutes and then the OD<sub>595nm</sub> was measured in triplicate (200 $\mu$ l) on a 96-well microtitre plate using a plate reader. The protein concentration was obtained by comparison with a calibration curve derived from known concentrations of BSA. Bradford reagent (980 $\mu$ l) was added to a known BSA concentration sample (20 $\mu$ l) (BSA standard concentrations; 0, 2, 4, 6, 8, 10, 12, 14, 16, 18, 20  $\mu$ g/ml). The sample was left to develop for 2 minutes and then the OD<sub>595nm</sub> measured in triplicate (200 $\mu$ l) on a 96-well microtitre plate using a plate reader. A straight line of best fit was overlaid the plot of BSA concentration against OD<sub>595nm</sub>.

### 3.2.7. Estimation of error in the Bradford assay

The same purified protein sample was measured six times by the Bradford assay method described (3.2.6). The OD<sub>595nm</sub> for the six measured samples was 0.573, 0.543, 0.550, 0.593, 0.574 and 0.602. From this data set the mean = 0.5725 and the standard deviation = 0.02310. Rearranging the equation for the line of best fit of the protein concentration for the known BSA standards plotted against OD<sub>595nm</sub> allowed the concentration for the purified protein sample to be calculated. Using the mean of 0.5725 the protein concentration for the sample was determined to be 235.6µg/ml. The Michaelis-Menten rate was measured (3.1.5) for the mean protein concentration. The error in V<sub>Max</sub> resulting from the error in protein concentration measured by the Bradford assay can be determined by the 95% likelihood that an individual value falls within 2 standard deviations of the mean; mean = 0.5725 OD<sub>595nm</sub> ± (2 x 0.02310 = 0.0462). There is a 95% likelihood that the measured OD<sub>595nm</sub> of the sample is within the range 0.5263 to 0.6187 OD units and by using the upper limit and lower limits, a new V<sub>Max</sub> can be determined. The upper and lower estimation of V<sub>Max</sub> for (*rac*)-2-Phenylpyrrolidine **209** with the MAO-N 4 variant, at 95% confidence was determined (table 2.4.11.1).

### 3.2.8. Mass spectrometry characterisation of MAO-N

Mass spectrometry was performed on a MicroMass Platform II quadrupole mass spectrometer equipped with an electrospray ion source. The spectrometer cone voltage was ramped from 40 to 70 V and the source temperature set to 140°C. Protein samples were separated with a Waters HPLC 2690 with a Phenomenex C5 reverse phase column directly connected to the spectrometer. The proteins were eluted from the column with a 5-95% acetonitrile (containing 0.01% trifluoroacetic acid) gradient at a flow rate of 0.4ml/min. The total ion count in the range 500-2000 m/z was scanned at 0.1 s intervals.

The scans were accumulated and spectra combined and the molecular mass determined by the MaxEnt and Transform algorithms of the Mass Lynx software (MicroMass).

### **3.2.9. UV-visible spectrum of MAO-N**

The purified MAO-N sample was placed in a 1ml quartz cuvette and the UV-visible spectrum measured in a Perkin Elmer instrument, Lambda 900, UV/VIS/NIR spectrometer. The spectrometer was zeroed against water and then the sample placed in the holder and the UV-visible spectrum recorded from 300-750nm.

### **3.3. MAO-N transformation and fermentation methods**

#### **3.3.1. Transformation of *E. coli* BL21 (DE3)/BL21 (DE3) star chemically competent cells**

Plasmid DNA and a single shot of *E. coli* BL21 (DE3) or BL21 (DE3) star chemically competent cells (Invitrogen C6000-03 or C6030-03) were thawed on ice. 1  $\mu$ l of the plasmid DNA was added to the shot and the DNA mixed by gentle tapping of the tube. The tube was returned to ice for 30 minutes. The sample was then subjected to heat-shock for 30 seconds at 42°C and quickly placed back on ice. After a few minutes on ice 500  $\mu$ l of pre-warmed SOC media was added and the sample was left shaking at 250rpm 37°C for 1 hour. 100  $\mu$ l was spread onto a LB agar plate containing 100  $\mu$ g/ml ampicillin and the plate left to grow overnight at 37°C.

#### **3.3.2. Transformation of *E. coli* TOP10 chemically competent cells**

Plasmid DNA and a single shot of *E. coli* TOP10 chemically competent cells (Invitrogen C4040-10) were thawed on ice. Remainder of method is as described in section 3.3.1.

#### **3.3.3. Electroporation of *E. coli* XL1-blue electrocompetent cells**

Plasmid DNA and a single shot of *E. coli* XL1-blue electrocompetent cells (Stratagene 200158) were thawed on ice. 1  $\mu$ l of the plasmid DNA was added to the shot and the DNA mixed by gentle tapping of the tube. The sample was transferred to an electrode cuvette and tapped to ensure removal of trapped air bubbles. A 4.32msec electroporation was carried out at 1.7kV, 25  $\mu$ F and 200  $\Omega$ . The sample had 940  $\mu$ l of pre-warmed SOC media added and the sample was left shaking at 250rpm 37°C for 1 hour. 100  $\mu$ l was

---

spread onto a LB agar plate containing 100µg/ml ampicillin and the plate left to grow for 16 hours at 37°C.

### **3.3.4. Transformation of *E. coli* XL1-red chemically competent cells and preparation of library of variants**

Plasmid DNA and a single shot of *E. coli* XL1-red chemically competent cells (Stratagene 200129) were thawed on ice. Prior to the addition of DNA 1.7µl of β-mercaptoethanol was added to each shot (giving a final concentration of 25mM) followed by 1µl of the plasmid DNA and the DNA was mixed by gentle tapping of the tube. The tube was returned to ice for 30 minutes. The sample was subjected to heat-shock for 45 seconds at 42°C and quickly placed back on ice. The sample had 940µl of pre-warmed SOC media added and the sample was left shaking at 250rpm 37°C for 1 hour. 100µl was spread onto a LB agar plate containing 100µg/ml ampicillin and the plate left to grow overnight at 37°C to check the transformation efficiency. To the remaining 900µl, 9ml of LB containing 100µg/ml ampicillin was added and the sample was returned to grow at 250rpm 37°C overnight. 100µl of the overnight culture was added to a further 10ml of LB containing 100µg/ml ampicillin and returned to grow for a further 24 hours at 250rpm 37°C. After sub-culturing, 1ml was removed and the plasmid DNA purified (3.4.1). This generated the first library of variants and this DNA was retransformed, as before, into *E. coli* XL1-red and the process repeated giving the second generation of variants. This cycle was repeated four times to give the fourth generation of variants. The fourth generation of variants was screened by the solid phase assay technique using (*rac*)-amine **76** (3.1.6).

### **3.3.5. Fermentation of *E. coli* BL21 (DE3) expressing MAO-N**

#### **1. Small scale expression**

A single colony from a fresh transformation (3.3.1) was picked and added to 10ml of LB containing 100µg/ml ampicillin in a 50ml falcon tube. The culture was left to grow overnight at 30°C after which the cells had reached stationary phase ( $OD_{600nm} = 3.0-4.0$ ). The cells were harvested by microcentrifuge at 10,000rpm for 10 minutes. The pelleted cells had the supernatant discarded and the cells were stored at -20°C until required.

#### **2. Medium scale expression**

A single colony of a fresh transformant (3.3.1) was picked and added to 10ml of LB containing 100µg/ml ampicillin. The cells were left to grow at 30°C until  $OD_{600nm}$  was between 0.6 and 1.0. At this point the cells were subcultured by a 1000 fold dilution addition into further LB containing 100µg/ml ampicillin. In the medium scale expression, 6 x 200ml fermentations in 1 litre baffled flasks were each inoculated with 200µl of the starter culture. The fermentation was left to grow for a further 24 hours at 200rpm and 30°C in an Innova 4430 incubator shaker. After the fermentation had reached stationary phase it was harvested by centrifugation at 6000rpm for 10 minutes at 4°C in a Sorval RC5C refrigerated centrifuge. The pelleted cells had the supernatant discarded and the cells were stored at -20°C until required.

#### **3. Large scale expression**

A single colony of a fresh transformant (3.3.1) was picked and added to 100ml of LB containing 100µg/ml ampicillin. The cells were left to grow at 30°C until O.D. 600nm was between 0.6 and 1.0. At this point the cells were subcultured by addition of the entire contents into a 10 litre batch fermentor (New Brunswick Scientific, BIOFLO 4500, Fermentator/Bioreactor). The cells were grown at 200 rpm 30°C in 10 litres of LB



---

containing 100µg/ml ampicillin overnight. The cells were harvested by centrifugation at 6000rpm for 10 minutes at 4°C in a Sorval RC5C refrigerated centrifuge. The pelleted cells had the supernatant discarded and the cells were stored at -20°C until required.

### **3.3.6. Preparation of CFE**

The cell pellet was thawed on ice and resuspended in the desired buffer (10ml/g concentration of wet weight cells in buffer). The sample was sonicated at 10 micron amplitude on ice in a Soniprep 150 for 30secs with 30secs intervals. The homogenate was centrifuged for 20,000rpm at 4°C for 1 hour and the pellet discarded. The CFE was stored on ice prior to use.

### **3.3.7. Spreading of fermentation onto LB agar +/- ampicillin plates**

A stationary phase culture ( $OD_{600nm} \sim 3.5$ ) was serially diluted  $10^6$  fold in LB (10µl of sample into 990µl of LB three times). The dilution (100µl) was spread onto 2 plates, one containing LB agar with 100µg/ml ampicillin and the other with LB agar only. The plates were left to grow overnight at 37°C and the colonies counted the following morning.

### **3.3.8. Isolation of plasmid DNA from clones on LB agar plate**

To a plate containing colonies of *E. coli* 1 ml of LB was added. The LB was gently spread over all the plate until all the colonies had been resuspended (i.e. no more individual colonies were visible). The *E. coli* broth suspension was drawn off the plate by pipetting and the cells pelleted by microcentrifugation at 10,000rpm for 10 minutes. The supernatant was discarded and the plasmid DNA extracted from the *E. coli* cells as described (3.4.1).

### **3.3.9. IPTG induction during fermentation**

2 x 100ml LB containing 100µg/ml ampicillin in 1 litre baffled flasks were inoculated with 1ml of the same overnight starter culture. The cultures were left to grow at 250rpm and 30°C until their OD<sub>600nm</sub> reached 0.4. At which point one flask had 100µl of 1M IPTG added. Periodically during the fermentation 1ml aliquots were removed for evaluation of MAO-N expression. The analyses of MAO-N expression was determined by SDS PAGE (3.2.5) and by the peroxidase coupled liquid assay (3.1.1). The fermentation (20ml) had loading buffer (20ml) added and the sample was analysed by SDS PAGE (3.2.5). For the peroxidase assay the samples were frozen/thawed prior to analysis by the peroxidase coupled liquid assay (3.1.1).

### **3.4. DNA purification and manipulation**

#### **3.4.1. DNA plasmid purification**

1ml of fermentation was spun using a maximum microcentrifuge at maximum speed for 10 minutes and the supernatant was discarded. The remainder of the method was followed as described in the manufacturer's protocol (Qiagen, QIA prep Spin Miniprep kit protocol). The purified plasmid DNA was stored at -80°C.

#### **3.4.2. DNA agarose gel**

The DNA agarose gel was prepared by addition of agarose (0.4g) to TAE x 1 (50ml), the mixture was melted and the molten agarose was left to cool by stirring at room temperature. Ethidium bromide (10mg/ml) was added (2.5µl) and the molten agarose was left stirring for a further 2 minutes. The gel was poured into a small gel tray and a loading comb inserted.

To each of the DNA samples (18µl) blue juice x 10 (2µl) (New England Biolabs) was added. Each sample (15µl) was loaded into each lane and the gel was ran at full power until the bromophenol blue band had travelled just over half way through the gel. The gel was visualised by UV irradiation.

#### **3.4.3. DNA gel extraction**

The desired DNA band as visualised by UV irradiation, was cut from the rest of the gel and weighed. The DNA was recovered from the gel using the Qiagen QIAquick gel extraction kit following the manufacturer's protocol. The recovered DNA was stored at -80°C.

### 3.4.4. DNA sequencing

Plasmid DNA from *E. coli* was purified using the Miniprep kit (3.4.1). The following reaction mixture (20 $\mu$ l) was prepared in a PCR tube:

Oligonucleotide primer (3.2pmol)	1 $\mu$ l
ABI Prism BigDye Terminator v3.1 cycle sequencing ready reaction kit	4 $\mu$ l
Plasmid DNA template (250ng) and water	final volume of 20 $\mu$ l

To sequence the internal region of the MAO-N gene, three primers were used (design by T. Fleming) in separate reactions:

MAO-N complementary start site at the 169 nucleotide

5' gacttgactgtagcaggcttc 3' (21 mer 52%GC)

Molecular weight 6438.2 g/mol

MAO-N complementary start site at the 512 nucleotide

5' cgcatgacatgttctatgttctgagt 3' (32 mer 46%GC)

Molecular weight 9822.4 g/mol

MAO-N complementary start site at the 830 nucleotide

5' gtccggttaggagtggttaatgagagag 3' (30 mer 46% GC)

molecular weight 9398.1 g/mol

For the end regions of the gene, commercial oligonucleotides were used:

5'-end of the gene

5' taatacgaactcactataggg 3' (Novagen T7 promoter primer 69348-3)

3'-end of the gene

5' gctagttattgctcagcgg 3' (Novagen T7 terminator primer 69337-3)

The PCR was carried out in the following manner on the Eppendorf mastercycler personal:

1. 95°C	1 minute
2. Pause	
3. 96°C	30 seconds
4. 50°C	30 seconds
5. 60°C	4 minutes
6. Repeat steps 3-5,	30 cycles
7. 4°C	hold

Samples were transferred into a 1.5ml eppendorf tube; water added to give a final volume of 20µl and sent for sequencing at the ICMB automated sequencing service, Swann Building, King's Buildings, University of Edinburgh.

#### 3.4.5. Quikchange PCR I246 saturation library

The two mutagenic oligonucleotide primers containing the NNS site (figure 2.4.2.1) were made up to 100pmol/µl with water and the reaction prepared in a PCR tube:

Reaction buffer 10x (Stratagene 600153-82)	5µl
Plasmid DNA containing MAO-N <u>2</u> variant gene (33ng/µl)	1µl
Oligonucleotide primer – forward NNS	1µl
Oligonucleotide primer – reverse NNS	1µl
dNTP mix (Sigma D-7295)	1µl
Water	20µl

The last addition was Pfu Turbo DNA Polymerase (1 $\mu$ l) (2.5U/ $\mu$ l) (Stratagene 600250-52) into the PCR mixture. The PCR was carried out in the following manner on the Eppendorf mastercycler personal:

- |                      |           |
|----------------------|-----------|
| 1. 95°C              | 1 minute  |
| 2. 95°C              | 1 minute  |
| 3. 55°C              | 1 minute  |
| 4. 68°C              | 8 minutes |
| 5. Repeat steps 2-4, | 16 cycles |
| 6. 4°C               | hold      |

The PCR product was prepared for screening the library by nick repair and transformation into the *E. coli* expression system (3.4.7).

#### 3.4.6. Quikchange PCR 384/385 saturation library

The two oligonucleotide primers containing the NNSNNS site (2.4.6.1) were made up to 10pmol/ $\mu$ l with water and the reaction prepared in a PCR tube as follows:

Reaction buffer 10x	5 $\mu$ l
Plasmid DNA containing MAO-N <u>2</u> variant gene (31ng/ $\mu$ l)	1.6 $\mu$ l
Oligonucleotide primer – forward NNS	1.3 $\mu$ l
Oligonucleotide primer – reverse NNS	1.3 $\mu$ l
dNTP mix	0.5 $\mu$ l
Water	40.3 $\mu$ l

---

After the addition of Pfu Turbo DNA Polymerase (1 $\mu$ l) (2.5U/ $\mu$ l) to the PCR mixture; the PCR was carried out in the following manner on:

- |                      |            |
|----------------------|------------|
| 1. 95°C              | 30 seconds |
| 2. 95°C              | 30 seconds |
| 3. 55°C              | 1 minute   |
| 4. 68°C              | 9 minutes  |
| 5. Repeat steps 2-4, | 30 cycles  |
| 6. 4°C               | hold       |

The PCR product was prepared for screening the library by nick repair and transformation into the *E. coli* expression system (3.4.7).

#### **3.4.7. Nick repair and preparation of DNA for screening**

The crude PCR product had Dpn1 restriction enzyme (1 $\mu$ l) (New England Biolabs R0176S) added and the reaction was mixed by gentle pipetting and spun for 1 minute at maximum speed in a microcentrifuge. The digestion of methylated DNA was allowed to proceed at 37°C, 200rpm for 1 hour. Meanwhile *E. coli* XL1-blue chemically competent cells (Stratagene) were thawed on ice. The cells were divided into two 50 $\mu$ l samples in pre-chilled eppendorf tubes and the digested PCR product (1 $\mu$ l) was added to one tube and to the other was added the pUC18 control (1 $\mu$ l). The tube was gently tapped to mix the contents and returned to ice for 30 minutes. Both tubes were heat shocked at 42°C for 45 seconds and quickly placed back on ice. Pre-warmed LB (500 $\mu$ l) was added to each tube and the samples were placed at 200rpm, 37°C for 1 hour. 100 $\mu$ l of *E. coli* pUC18 control transformation was spread onto a LB agar plate containing 100 $\mu$ g/ml ampicillin. 100 $\mu$ l of *E. coli* saturation library transformation was spread onto five LB agar plates containing 100 $\mu$ g/ml ampicillin. All the plates were placed overnight at 37°C. The pUC18 control transformation had several thousand colonies the following morning. The saturation library tended to produce fewer colonies per plate than the

pUC18 control, but enough transformants were used to represent the library adequately (figure 2.4.1.1). The DNA was isolated (3.3.8) and the library screened by the solid phase assay incorporating the desired amine substrate (3.1.6).

#### **3.4.8. Verification of representation of the mutagenesis**

In order to verify the success of the saturation mutagenesis random clones were picked after the *E. coli* XL1-blue transformation (3.4.7). They were grown overnight in (10ml) LB containing 100µg/ml ampicillin at 200rpm, 37°C and the plasmid DNA isolated (3.4.1). The plasmid DNA was sequenced with the appropriate primer (3.4.4).



### 3.5. Reducing agent screening

#### 3.5.1. The half reaction reduction screen

10mM of imine MDQ 224 (10ml) in Q-Sepharose resuspension buffer had 10 equivalents of the sample reducing agent added. If dissolution was not possible dropwise addition of DMSO to assist solubility of the reducing agent was required. The reaction was left in a sealed tube shaking at 200rpm 37°C.

To measure the amount of imine remaining after the desired period of time, 1ml was drawn up with a syringe from the reaction and filtered (0.2µm) prior to HPLC analysis (3.7.4). The percentage of remaining imine was calculated by dividing the imine peak area measured by the peak area at the start of the experiment.

The reducing agents were either commercially purchased (Aldrich) or synthesised in the group (V. Gotor-Fernandez).

#### 3.5.2. Measurement of amine 76 and imine substrate onto palladium catalyst

Three mixtures were prepared each had 10mM of (*rac*)-amine 76 (5ml) in 0.1M potassium phosphate buffer pH 7.0. To the first mixture, 2.1mol% of 5% Pd/alumina was added, to the second 2.1mol% of 10% Pd/carbon and to the third mixture nothing was added (i.e. a control). Duplicate mixtures were prepared with replacement of (*rac*)-amine 76 with the corresponding imine. All six preparations were left for 24 hours on a blood rotator at room temperature, after which time a 1ml aliquot was removed and analysed by CE (3.7.2.2).

### 3.5.3. Catalytic transfer hydrogenation of MDQ

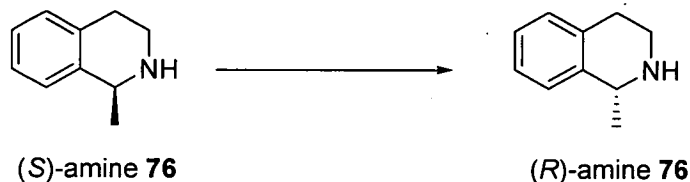
Each reaction was prepared with 10mM of MDQ **224** (5ml) in 0.1M potassium phosphate buffer pH 7.0 and the addition of ammonium formate to the required concentration (to give a final concentration of either 15, 50, 100 or 200mM). After dissolution of the ammonium formate, 2.1mol% of the palladium catalyst was added (either 5% Pd/alumina or 10% Pd/carbon) and the reactions were left on the blood rotator at room temperature overnight, after which time a 1ml aliquot was removed and analysed by CE (3.7.2.2).

### 3.5.4. Deracemisation of (*rac*)-amine **76** with various boranes

Each reaction was prepared with 10mM of (*rac*)-amine **76** (5ml) in 0.1M potassium phosphate pH 7.0 followed by the addition of reducing agent (2.6.11.1) to give a final concentration of the reductant at 100mM (except the control oxidation where no reducing agent was added). To each reaction was added MAO-N-Eupergit (2g) (3.6.4) with a specific activity 0.373 $\mu$ mol/min/g (3.1.7). The reactions were left on the blood rotator at room temperature overnight, after which time a 1ml aliquot was removed and analysed by CE (3.7.2.1).

### 3.6. Deracemisation reactions

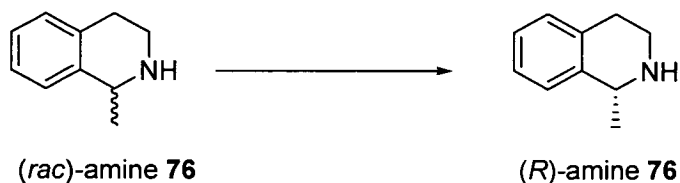
#### 3.6.1. Stereoconversion of (*S*)-amine 76 with purified MAO-N protein



A 600 $\mu$ l solution of (*S*)-amine 76 (final 20mM) and ammonia borane (final 400mM) in Ni-NTA resuspension buffer was left shaking at 200rpm 30°C. A 100 $\mu$ l aliquot was removed and the  $t = 0$  sample's e.e. was measured by chiral HPLC (3.7.1.A). To the remaining 500 $\mu$ l of the solution was added 0.430mg/ml purified MAO-N 2 protein (500 $\mu$ l) (3.2.2). The mixture was left shaking at 200 rpm 30°C for a further 90 hours and a further 100 $\mu$ l aliquot was removed and analysed by chiral HPLC (3.7.1.A).

Microcentrifugation of the reaction after 90 hours and measurement of the concentration of the supernatant to quantify the soluble protein by the Bradford assay (3.2.6) found there to be no protein remaining in solution.

#### 3.6.2. Deracemisation of (*rac*)-amine 76 to (*R*)-amine 76 with whole cells expressing MAO-N



Whole cells (0.456g) containing the expressed MAO-N 2 protein (3.3.5) were thawed on ice. The cells were resuspended in 0.1M potassium phosphate buffer pH 7.0 (10ml). To this cell suspension was added (*rac*)-amine 76 (14 $\mu$ l, final 10mM) and ammonia borane

---

(0.0309g, final 100mM). The reaction was left shaking at 200 rpm, 30°C and periodically 1ml samples were removed for analysis. The sample was spun at maximum speed on a microcentrifuge, the supernatant drawn off by pipetting and the e.e. determined by chiral HPLC (3.7.1.B).

### 3.6.3. Preparative deracemisation of (*rac*)-amine 76 to (*R*)-amine 76 with whole cells expressing MAO-N

Whole cells (10.3g) containing the expressed MAO-N 2 protein (3.3.5) was thawed on ice. The cells were resuspended in 0.1M potassium phosphate buffer pH 7.0 (100ml). (*Rac*)-amine 76 was added (0.294g, final 20mM) followed by ammonia borane (0.309g, final 100mM). The reaction was left shaking at 200rpm and 30°C. Periodically, a 1ml sample was removed and the sample spun at maximum speed on a microcentrifuge. The supernatant was drawn off by pipetting and the e.e. determined by chiral HPLC (3.7.1.B). After 18 hours the (*R*)-amine 76 e.e. had reached >95% e.e. as determined by HPLC and the reaction was worked up.

The crude reaction mixture was centrifuged at 4000rpm for 1 hour. The supernatant was decanted off and basified with 2M NaOH until pH > 10 as determined by universal indicator paper testing and the reaction mixture was filtered (0.45µm). The crude reaction was extracted (5 x 50ml) into tert-butylmethylether (TBME). The organic extractions were combined, dried over magnesium sulfate, filtered and dried to evaporation giving a clear oil. The oil was taken up in acetone and several drops of 2M HCl were added until pH < 2 as determined by universal indicator paper testing. After evaporation, a white crystalline solid was isolated in 0.258g yield (71.2% after accounting for the loss of removal of samples for HPLC analysis). The crude (*R*)-amine 76 product was shown to be pure by <sup>1</sup>H-NMR without the need for further purification. The optical rotation was measured to be  $[\alpha]_D +42^\circ$  in DCM which compared well with published data<sup>172</sup>  $[\alpha]_D +42^\circ$ .

---

$\delta$ H (250MHz, D<sub>2</sub>O) 1.55 (3H, d,  $J$  = 6.9Hz, CH<sub>3</sub>), 2.95 (2H, m, CH<sub>2</sub>), 3.32-3.47 (2H, m, CH<sub>2</sub>), 4.55 (1H, q,  $J$  = 6.9Hz CH), 7.20 (4H, m, ArH).

#### 3.6.4. Immobilisation of MAO-N onto Eupergit-C

The ammonium sulfate precipitated purified MAO-N protein (3.2.4) was redissolved in 0.1M potassium phosphate buffer (40ml). Eupergit C (Degussa) was added (3.038g) and the immobilisation left on a blood rotator at room temperature for 24 hours. The resin was filtered and washed with 0.1M potassium phosphate buffer pH 7.0 (5 x 20ml). The resin was capped with 3M glycine pH 8.5 and left on the blood rotator for a further 24 hours. The resin was washed with 0.1M potassium phosphate buffer pH 7.0 (5 x 20ml) and stored at 4°C.

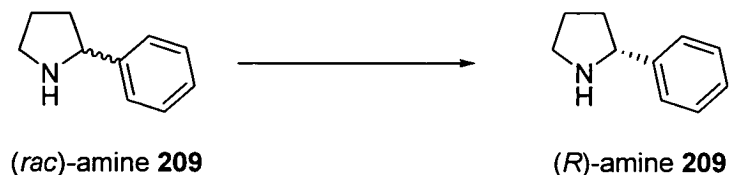
#### 3.6.5. Preparative deracemisation of (*rac*)-amine 76 to (*R*)-amine 76 with MAO-N-Eupergit

MAO-N-Eupergit (6.642g), specific activity measured to be 1.011  $\mu$ mol/min/g (3.1.7), was added to a 0.1M potassium phosphate solution (100ml) containing (*rac*)-amine 76 (0.294g, final 20mM) and ammonia borane (0.309g, final 100mM). The reaction was left shaking at 200 rpm and 30°C. Periodically, 1ml samples were removed and the e.e. determined by CE (3.7.2). After 5.5 days the (*R*)-amine 76 e.e. had reached >95% e.e. and the reaction was worked up.

The MAO-N-Eupergit resin was filtered and extensively washed with 0.1M potassium phosphate buffer pH 7.0. The washes and crude reaction mixture were combined and basified to pH>10 with 2M NaOH and the reaction extracted into TBME (5 x 50ml). The organic extractions were combined, dried over magnesium sulfate, filtered and dried to evaporation giving a clear oil. The oil was taken up in acetone and several drops of

2M HCl were added. After evaporation a white crystalline solid (*R*)-amine **76**, was isolated in 0.350g yield (99.4%) and shown to be pure by <sup>1</sup>H-NMR.

### 3.6.6. Deracemisation of (*rac*)-amine **209** to (*R*)-amine **209** with MAO-N-Eupergit



0.1M potassium phosphate buffer pH 7.0 (100ml) containing (*rac*)-2-phenylpyrrolidine (CHESS, Germany 1840) (0.294g, final 20mM) and ammonia borane (0.3087g, final 100mM) had MAO-N-Eupergit (4.71g), specific activity measured to be 5.01  $\mu\text{mol}/\text{min}/\text{g}$  (3.1.7.), added to the reaction mixture. At various time intervals 500  $\mu\text{l}$  aliquots of the reaction were removed and 500  $\mu\text{l}$  of 0.1M potassium phosphate buffer pH 7.0 was added. The e.e. was determined by CE (3.7.3).

### 3.6.7. Preparative deracemisation of (*rac*)-amine **209** to (*R*)-amine **209** with MAO-N-Eupergit

0.1M potassium phosphate buffer (50ml) containing (*rac*)-2-phenylpyrrolidine **209** (0.735g, final 100mM) and ammonia borane (0.385g, final 250mM) was adjusted to pH 7.5 with a few drops of 2M HCl. MAO-N-Eupergit (4.751g), specific activity measured to be 5.01  $\mu\text{mol}/\text{min}/\text{g}$  (3.1.7.), was added to the reaction. The mixture was left shaking at 250 rpm and 30°C. Periodically, 100  $\mu\text{l}$  samples were removed and diluted with 0.1M potassium phosphate buffer pH 7.0 (900  $\mu\text{l}$ ). The e.e. was determined by CE (3.7.3), after 48 hours the (*R*)-2-phenylpyrrolidine **209** e.e. had reached >95% e.e. and the reaction was worked up.

---

The MAO-N-Eupergit resin was filtered and extensively washed with 0.1M potassium phosphate buffer pH 7.0. The washes and crude reaction mixture were combined and basified to pH>10 with 2M NaOH and the reaction extracted into TBME (5 x 50ml). The organic extractions were combined, washed with brine, dried over magnesium sulfate, filtered and dried to evaporation giving a clear oil in 0.604g yield (83%). The crude product was shown to be pure (*R*)-amine **209** by <sup>1</sup>H-NMR without the need for further purification. The optical rotation was measured to be  $[\alpha]_D +45.2^\circ$  in DCM compared to published  $[\alpha]_D 64.0^\circ$  <sup>173</sup>.

$\delta$ H (250MHz, CDCl<sub>3</sub>) 1.82-2.45 (4H, m, CH<sub>2</sub>, CH<sub>2</sub>), 3.22 (1H, m, NH-CH<sub>2</sub>), 3.42 (1H, m, NH-CH<sub>2</sub>), 4.36 (1H, t, *J* = 7.7Hz Ar-CH), 7.42-7.67 (5H, m, ArH).

### 3.6.8. Deracemisation of (*rac*)-amine **76** to (*R*)-amine **76** using CTH and MAO-N-Eupergit

Each reaction was prepared in the same manner. To 10mM (*rac*)-amine **76** (5ml), in 0.1M potassium phosphate buffer pH 7.0, was added MAO-N-Eupergit (0.366g) (specific activity measured to be 1.75μmol/min/g (3.1.7)). This was followed by the addition of ammonium formate (0.062g, final 200mM) and 2.1mol% of the palladium catalyst (either 5% Pd/alumina catalyst or 10% Pd/carbon catalyst). The reactions were left on a blood rotator at room temperature. Samples were taken and filtered prior (0.2μm) to analysis by CE to determine e.e.

### 3.6.9. Deracemisation of (*rac*)-amine **76** to (*R*)-amine **76** using CTH with palladium catalyst and MAO-N-Eupergit

To 10mM (*rac*)-amine **76** (5ml), in 0.1M potassium phosphate buffer pH 7.0, was added MAO-N-Eupergit (1.665g) (specific activity measured to be 1.75μmol/min/g (3.1.7)). This was followed by the addition of ammonium formate (0.062g, final 200mM) and 4.2mol% of 5% palladium/alumina catalyst. The reaction was left on a blood rotator at

room temperature. After 40 hours a sample was taken and filtered prior (0.2 $\mu$ m) to analysis by CE to determine e.e.



### 3.7. Analytical methods

#### 3.7.1. Chiral HPLC of MTQ

HPLC analysis was performed on a Waters 2695 separation module with a Waters 486 tunable absorbance detector.

##### 1. HPLC method A.

The sample from the reaction (100 $\mu$ l) was extracted with hexane (2 x 150 $\mu$ l) and the combined hexane extracts were combined and injection (20 $\mu$ l) was analysed directly by HPLC. Chiralcel OD-H column 46cm, eluent hexane:ethanol 98:2 (v/v), flow rate = 0.5ml/min, column temperature = 0°C. Retention times, imine **224** = 18.7 min, (*S*)-amine **76** = 22.4 min and (*R*)-amine **76** = 26.2 min with monitoring at 195nm.

##### 2. HPLC method B

The sample from the reaction (500 $\mu$ l) was basified with a few drops of 2M NaOH and the reaction was extracted into an equal volume of TBME. The organic phase was analysed directly by injection (40 $\mu$ l) onto the HPLC. Chiralcel OD-H column 250 x 4.6mm, eluent methanol:isopropyl alcohol:hexane 8:3:89 (v/v/v), flow rate = 1ml/min, column temperature = 0°C. Retention times, imine **224** = 7.9 min, (*S*)-amine **76** = 11.4 min and (*R*)-amine **76** = 14.5 min with monitoring at 210nm.

#### 3.7.2. CE analysis of MTQ

An Agilent CE system G1601A was used to carry out these analyses. A capillary diameter of 50 $\mu$ m and length 64.5cm (effective length 56cm) using a 30kV potential and column temperature of 20°C. All buffers and samples were filtered (0.2 $\mu$ m) prior to analysis.

### 1. Chiral CE method

0.1M potassium phosphate buffer pH 3 containing 20mM HP- $\beta$ -cyclodextrin. Injection pressure of 200 mbar/sec. Migration times; (*S*)-amine **76** = 10.6 min and (*R*)-amine **76** = 11.5 min with monitoring at 195nm.

### 2. Non-chiral CE method

0.1M potassium phosphate buffer pH 3. Injection pressure of 200mbar/sec. Migration times; imine **224** = 10.8 min and (*rac*)-amine **76** = 11.5 min with monitoring at 195nm.

### 3.7.3. CE analysis of 2-phenylpyrrolidine

0.1M potassium phosphate buffer pH 3 containing 75mM HP- $\beta$ -cyclodextrin and 75mM 18-crown-6. Injection pressure of 50 mbar/sec. Migration times, (*S*)-amine **209** = 10.6 min and (*R*)-amine **209** = 11.5 min with monitoring at 195nm.

### 3.7.4. Reverse phase MDQ analysis

The sample was filtered (0.2 $\mu$ m) prior to analysis and injected (50 $\mu$ l) onto a 250 x 4.6mm Hichrom 250A (C-18) column. Water (containing 0.5% triethylamine):acetonitrile 1:1 (v/v) flow rate = 1ml/min, column temperature = ambient temperature. Retention times, imine **224** = 8.5 min and amine **76** = 18.9 min with monitoring at 254nm.

### **3.8. Buffer and reagent recipes**

#### **3.8.1. SDS loading buffer**

0.5M Tris/HCl pH 6.8 (2ml), glycerol (2ml), 10% (w/v) SDS (3.2ml),  $\beta$ -mercaptoethanol (0.8ml) and 0.05% (v/v) bromophenol blue (0.4ml).

#### **3.8.2. SDS gel running buffer 5x**

In 50ml: Tris (15.1g), glycine (94g) and 10% w/v SDS.

#### **3.8.3. SDS gel staining solution**

Methanol (450ml), acetic acid (100ml), water (450ml) and Coomassie blue G-250 (500mg).

#### **3.8.4. SDS gel destaining solution**

Methanol (450ml), acetic acid (100ml) and water (450ml).

#### **3.8.5. Bradford reagent**

Coomassie blue G-250 (100mg), ethanol (50ml), 85% phosphoric acid (100ml) and water (850ml).

#### **3.8.6. SOC media**

In 1 litre: yeast extract (5g), tryptone (20g), 5M NaCl (2ml), KCl (0.19g), 1M MgCl<sub>2</sub> (10ml), 1M MgSO<sub>4</sub> (10ml) and *D*-glucose (3.6g).

#### **3.8.7. LB medium**

In 1 litre: tryptone (10g), NaCl (10g) and yeast extract (5g).

**3.8.8. LB agar medium**

LB medium (100ml) and agar (1.5g).

**3.8.9. TAE (Tris acetate EDTA buffer) 50x**

Tris base (242g), acetic acid (57.1ml) and 0.5M EDTA pH 8.0 (100ml).

---

**References**

1. <http://www.fda.gov/cder/guidance/stereo.htm>.
2. A. M. Rouhi, *Chemical and Engineering News*, **2004** *82*, 47.
3. C. D. Reeve, R. A. Holt, S. R. Rigby and K. Hazel, *Chimica Oggi*, **2001** *19* (718), 31.
4. D. Enders and U. Reinhold, *Tetrahedron Asymmetry*, **1997** *8*, 1895.
5. J. Clayden, N. Greeves, S. Warren and P. Wothers, *Organic Chemistry*, **2001** Oxford University Press, 135 and 898.
6. D. Enders, *Asymmetric Synthesis*, J.D. Morrison, Ed. Academic: New York **1984** 275.
7. Y. Suzuki and H. Takahashi, *Chem. Pharm. Bull.*, **1983** *31*, 31 and 2895.
8. G. K. Friestad *Tetrahedron*, **2001** *57*, 5461.
9. H. Miyabe, *Org. Lett.* **1999** *1*, 569.
10. G. K. Friestad, *J. Org. Chem.*, **2004** *69*, 863.
11. A. J. J. Beckwith and C. H. Schiesser, *Tetrahedron* **1985** *41*, 3925.
12. C. Palomo, J. M. Aizpurua, I. Ganboa and M. Oiarbide, *Eur. J. Org. Chem.*, **1999** 3223.
13. A. E. Taggi, *J. Am. Chem. Soc.*, **2000** *122*, 7831.
14. G. C. Fu and B. L. Hodous, *J. Am. Chem. Soc.*, **2002** *124*, 1578.
15. T. E. Müller and M. Beller, *Chem. Rev.*, **1998** *98*, 675.
16. P.W. Roesky and T. E. Müller, *Angew. Chem., Int. Ed.*, **2003** *42*, 2708.
17. M. Kawatsura and J. F. Hartwig, *J. Am. Chem. Soc.*, **2000** *122*, 9546.
18. G. Zassinovich, G. Mestroni and S. Gladiali, *Chem. Rev.*, **1992** *92*, 1051.
19. C. Fragale, M. Gargano and M. Rossi, *J. Mol. Catal.*, **1979** *5*, 65.
20. T. Nishiguchi, H. Imai, Y. Hirose and K. Fukuzumi, *J. Catal.*, **1976** *41*, 249.
21. M. J. Palmer and M. Wills, *Tetrahedron Asymmetry*, **1999** *10*, 2045.

- 
22. N. Uematsu, A. Fujii, S. Hashiguchi, T. Ikariya and R. Noyori, *J. Am. Chem. Soc.*, **1996** *118*, 4916.
  23. A. Fujii, S. Hashiguchi, N. Uematsu, T. Ikariya and R. Noyori, *J. Am. Chem. Soc.*, **1996** *118*, 2521.
  24. E. Vedejs, P. Trapencieris and E. Suna, *J. Org. Chem.*, **1999** *64*, 6724.
  25. G. Z. Wang and J. E. Bäckvall, *Chem. Commun.*, **1992** *14*, 980.
  26. E. J. Corey, R. K. Bakshi and S. Shibata, *J. Am. Chem. Soc.*, **1987** *109*, 5551.
  27. S. Itsuno, M. Nakano, K. Miyazaki, H. Masuda, K. Ito, A. Hirao and S. Nakahama, *J. Chem. Soc. Perkin Trans. 1*, **1985** 2039.
  28. S. Itsuno, Y. Sakurai, K. Ito, A. Hirao and S. Nakahama, *Bull. Chem. Soc. Jpn.*, **1987** *60*, 395.
  29. C. Bolm and M. Felder, *Synlett.*, **1994** 655.
  30. M. A. Yurovskaya and A. V. Karchava, *Tetrahedron Asymmetry*, **1998** *9*, 3331.
  31. M. Yamakawa, H. Ito and R. Noyori, *J. Am. Chem. Soc.*, **2000** *122*, 1466.
  32. J. Holz, D. Heller, R. Stürmer and Armin Börner, *Tetrahedron Lett.*, **1999** *40*, 7059.
  33. C. A. Willoughby and S. L. Buchwald, *J. Am. Chem. Soc.*, **1994** *116*, 8952.
  34. N. J. Lawrence, M. D. Drew and S. M. Bushell, *Perkin Trans. 1* **1999** 3381.
  35. T. Ireland, F. Fontanet and G. Tchao, *Tetrahedron Lett.*, **2004** *45*, 4383.
  36. F. Alexandre, D. P. Pantaleone, P. P. Taylor, I. G. Fotheringham, D. J. Ager and N. J. Turner, *Tetrahedron Lett.*, **2002** *43*, 707.
  37. T. Tsukinoki, Y. Mitoma, S. Nagashima, T. Kawaji, I. Hashimoto and M. Tashiro, *Tetrahedron Lett.*, **1998** *39*, 8873.
  38. H. U. Blaser, H. P. Buser, H. P. Jalett, B. Pugin and F. Spindler, *Synlett*, **1999** 867.
  39. Y. Chi, Y. G. Zhou and X. Zhang, *J. Org. Chem.*, **2003** *68*, 4120.
  40. R. Kadyrov and T. H. Riermeier, *Angew. Chem. Int. Ed.*, **2003** *42*, 5472.
  41. R. Sreekumar and C. N. Pillai, *Tetrahedron: Asymmetry*, **1993** *4*, 2095.
  42. A. L. Gutman, M. Etinger, G. Nisnevich and F. Polyak, *Tetrahedron: Asymmetry* **1999** *9*, 4369.
-

- 
43. H. E. Schoemaker, D. Mink and M. G. Wubbolts, *Science* **2003** *299*, 1694.
  44. <http://www.biowise.org.uk>.
  45. L. Pasteur, *Compt. Rend. Acad. Sci.*, **1848** *26*, 535.
  46. K. Faber, *Pure Appl. Chem.*, **1997** *69*, 1613.
  47. R. J. Kazlauskas, A. N. E. Weissfloch, A. T. Rappaport and L. A. Cuccia, *J. Org. Chem.*, **1991** *56*, 2656.
  48. R. Noyori, *Adv. Synth. Catal.*, **2003** *345*, 15.
  49. N. Aoyagi and T. Izumi, *Tetrahedron Lett.*, **2002** *43*, 5529.
  50. J. Palomo, G. Fernandez-Lorente, C. Mateo, M. Fuentes, R. Fernandez-Lafuente and J. M. Guisan, *Tetrahedron: Asymmetry*, **2002** 1337.
  51. K. Faber, *Chem. Eur. J.*, **2001** *7*, 5005.
  52. O. Pàmies and J-E Bäckvall, *Chem. Rev.*, **2003** *103*, 3247.
  53. B. A. Persson, A. L. E. Larsson, M. Le Ray and J. E. Bäckvall, *J. Am. Chem. Soc.*, **1999** *121*, 1645.
  54. H. Stecher and K. Faber, *Synthesis*, **1997** 1.
  55. U. T. Strauss, U. Felfer and K. Faber, *Tetrahedron Asymmetry*, **1999** *10*, 107.
  56. S. Pedragosa-Moreau, A. Archelas and R. Furstoss, *J. Org. Chem.*, **1993** *58*, 5533.
  57. W. Kroutil, M. Mischitz and K. Faber, *J. Chem. Soc. Perkin Trans. 1*, **1997** *24*, 3629.
  58. W. Kroutil and K. Faber, *Tetrahedron: Asymmetry*, **1998** *9*, 2901.
  59. E. W. Hafner and D. Wellner *Proc. Nat. Acad. Sci.*, **1971** *68*, 987.
  60. J. W. Huh, K. Yokoigawa, N. Esaki and K. Soda, *J. Ferment. Bioeng.*, **1992** *74*, 189.
  61. J. W. Huh, K. Yokoigawa, N. Esaki and K. Soda, *Biosci. Biotech. Biochem.*, **1992** *56*, 2081.
  62. T. M. Beard and N. J. Turner, *Chem. Commun.*, **2002** 246.
  63. A. Enright, F. R. Alexandre, G. Roff, I. G. Fotheringham, M. J. Dawson and N. J. Turner, *Chem. Commun.*, **2003** 2636.

- 
64. M. Alexeeva, A. Enright, M. J. Dawson, M. Mahmoudian and N. J. Turner, *Angew. Chem., Int. Ed.*, **2002** *41*, 3177.
  65. G. Hieber and K. Ditrach, *Chimica Oggi*, **2001** *16*.
  66. F. Balkenhohl, K. Ditrach, B. Hauer and W. Ladner, *J. Prakt. Chem.*, **1997** *339*, 381.
  67. M. T. Reetz and K. Schimossek *CHIMIA* **1996** *12*, 668.
  68. J. W. Lee, J. S. Chae, C. S. Kim, J. K. Kim, D. S. Lim, M. K. Shon, Y. S. Choi and S. H. Lee **1996** Patent WO9605177.
  69. G. F. Breen, *Tetrahedron: Asymmetry*, **2004** *15*, 1427.
  70. M. Breuer K. Ditrach, T. Habicher, B. Hauer, M. Kessler, R. Stuermer and T. Zelinski, *Angew. Chem., Int. Ed.*, **2004** *43*, 788.
  71. J. Knoll, *Med. Res. Rev.*, **1992** *12*, 505.
  72. W. Birkmayer, P. Riederer, M. B. Youdim and W. Linauer, *J. Neural. Transm.*, **1975** *36*, 303.
  73. M. L. C. Hare *Biochem. J.*, **1928** *22*, 968.
  74. T. Nagatsu, *Neurotoxicology* **2004** *25*, 11.
  75. E. A. Zeller and S. Sarkar, *J. Biol. Chem.*, **1962** *237*, 2333.
  76. J. P. Johnston, *Biochem. Pharmacol.*, **1968** *17*, 1285.
  77. A. W. J. Bach, N. C. Lan, D. L. Johnson, C. W. Abell, M. E. Bembenek, S. W. Kwan, P. H. Seeburg and J. C. Shih, *Proc. Nat. Acad. Sci.*, **1988** *85*, 4934.
  78. Z. Y. Chen, G. S. Hotamisligil, J. K. Huang, L. Wen, D. Ezzeddine, N. Aydin-Muderrisoglu, J. F. Powell, R. H. Huang and X. O. Breakefield, *Nucleic Acids Research* **1991** *19*, 4537.
  79. P. Newton-Vinson, F. Hubalek, D. E. Edmondson, *Protein Expr. Purif.*, **2000** *20*, 334.
  80. C. Binda, P. Newton-Vinson, F. Hubalek, D. E. Edmondson and A. Mattevi, *J. Biol. Chem.*, **2002** *277*, 23973.
  81. C. Binda, A. Coda, R. Angelini, R. Federico, P. Ascenzi and A. Mattevi, *Struct. Fold. Design*, **1999** *7*, 265.
  82. R. A. Casero Jr. and P. M. Woster, *J. Med. Chem.*, **2001** *44*, 1.
-



- 
83. N. Léonard, C. Lambert, E. Depiereux and J. Wouters, *Neurotoxicology*, **2004** 25, 47.
  84. C. Binda, P. Newton-Vinson, F. Hubalek, D. E. Edmondson and A. Mattevi, *Nat. Struc. Biol.*, **2002** 9, 22.
  85. R. M. Geha, K. Chen, J. Wouters, F. Ooms and J. C. Shih, *J. Bio. Chem.*, **2002** 277, 17209.
  86. F. Hubálek, C. Binda, M. Li, A. Mattevi and D. E. Edmondson, *Acta Crystallogr. D.*, **2003** D59, 1874.
  87. C. Binda, L. Min, F. Hubalek, N. Restelli, D. E. Edmondson and A. Mattevi, *Proc. Nat. Acad. Sci.*, **2003** 100, 9750.
  88. C. Binda, F. Hubalek, L. Min, N. Restelli, D. E. Edmondson and A. Mattevi, *FEBS Letters*, **2004** 564, 225.
  89. C. Binda, R. Angelini, R. Federico, P. Ascenzi, A. Mattevi, *Biochemistry*, **2001** 40, 2766.
  90. P. Trickey, M. A. Wagner, M. S. Jorns and F. S. Matthews, *Struc. Fold Des.*, **1999** 7, 331.
  91. R. M. G. Hynson, S. M. Kelly, N. C. Price and R. R. Ramsay, *Biochimica et Biophysica Acta*, **2004** 1672, 60.
  92. B. Schilling and K. Lerch, *Biochim. BioPhys. Acta* **1995** 1243, 529.
  93. B. Monodovi (Ed.) *Structure and Function of Amine Oxidase* **1985** 304.
  94. S. O. Sablin, V. Yankovskaya, S. Bernard, C. N. Cronin and T. P. Singer, *Eur. J. Biochem.*, **1998** 253, 270.
  95. R. B. Silverman, J. P. Zhou, and P. E. Eaton, *J. Am. Chem. Soc.*, **1993** 115, 8841.
  96. R. B. Silverman and P. A. Zieske, *Biochemistry*, **1986** 135, 154.
  97. R. R. Ramsay, *Biochemistry* **1991** 30, 4624.
  98. R. R. Ramsay, S. C. Koerber and T. P. Singer, *Biochemistry*, **1987** 26, 3045.
  99. R. H. Suva and R. H. Abeles, *Biochemistry*, **1978** 17, 3538.
  100. M. D. Houslay and K. F. Tipton *Biochem. J.*, **1975** 145, 311.
  101. J. C. G. Woo and R. B. Silverman, *J. Am. Chem. Soc.*, **1995** 117, 1663.
-

- 
102. J. E. Cragg, R. B. Herbert, and M. M. Kgaphola, *Tetrahedron Lett.*, **1990** *31*, 6907.
  103. A. Yoshida, Y. Takenaka, H. Tamaki, I. Frébort, O. Adachi and H. Kumagai, *J. Ferm. Bioeng.* **1997** *84*, 603.
  104. J. A. Chaplin, C. L. Budde and Y. L. Khmelnitsky, *J. Mol. Cat. B: Enzymatic*, **2001** *13*, 69.
  105. J. C. G. Woo, X. Wang and R. B. Silverman, *J. Org. Chem.*, **1995** *60*, 6235.
  106. A. Zaks and A. M. Klibanov, *J. Biol. Chem.*, **1988** *17*, 8017.
  107. S. M. Janes, D. Mu, D. Wemmer, A. J. Smith, S. Kaur, D. Maltby, A. L. Burlingame and J. P. Klinman, *Science*, **1990** *248*, 981.
  108. K. Tanizawa, R. Matsuzaki, E. Shimizu, T. Yorifuji and T. Fukui, *Biochem. Biophys. Res. Commun.*, **1994** *199*, 1096.
  109. B. Schwartz, J. E. Dove and J. P. Klinman, *Biochemistry* **2000** *39*, 3699.
  110. M. Kim, T. Okajima, S. Kishishita, M. Yoshimura, A. Kawamori, K. Tanizawa and H. Yamaguchi, *Nat. Struct. Biol.*, **2002** *9*, 591.
  111. B. J. Brazeau, B. J. Johnson and C. M. Wilmot, *Archives of Biochemistry and Biophysics*, **2004** *428*, 22.
  112. C. M. Wilmot, J. Hajdu, M. J. McPherson, P. F. Knowles and S. E. V. Phillips, *Science*, **1999** 1724.
  113. S. A. Mills, Y. Goto, Q. Su, J. Plastino and J. P. Klinman, *Biochemistry*, **2002** *41*, 10577.
  114. Q. Su and J. P. Klinman, *Biochemistry*, **1998** *37*, 12513.
  115. P. S. Daugherty, *Proc. Nat. Acad. Sci.*, **2000** *97*, 2029.
  116. R. C. Cadwell and G. F. Joyce, *PCR Meth. Appl.*, **1994** *3*, 5136.
  117. C. Neylon, *Nucl. Acids Res.*, **2004** *32*, 1448.
  118. <http://www.stratagene.com/manuals/200129.pdf>.
  119. L. Styer, *Biochemistry*, (1995) 4<sup>th</sup> edition, pages 787.
  120. N. D. Sinha, J. Biernat, J. McManus, and H. Koster, *Nucl. Acids Res.* **1984**, *12*, 4539.
-

- 
121. A. Kayushin, M. Korosteleva and A. Miroshnikov, *Nucleosides and Nucleotides Nucleic Acids* **2000** *19*, 1967.
  122. M. D. Hughes, D. A. Nagel, A. F. Santos, A. J. Sutherland and A. V. Hine, *J. Mol. Biol.*, **2003** *331*, 973.
  123. R. Georgescu, G. Bandara and L. Sun, *Methods Mol. Biol.*, **2003** *231*, 75.
  124. K. Miyazaki and M. Takenouchi, *Biotechniques*, **2002** *33*, 1033 and 1036.
  125. W. P. C. Stemmer, *Proc. Nat. Acad. Sci.*, **1994** *91*, 10747.
  126. W. P. C. Stemmer, *Nature*, **1994** *370*, 389.
  127. H. Zhao, L. Giver, Z. Shao, J. A. Affholter and F. H. Arnold, *Nat. Biotechnol.*, **1998** *16*, 258.
  128. W. M. Coco, *Methods Mol. Biol.*, **2003** *231*, 111.
  129. M. Ostermeier, J. H. Shim and S. J. Benkovic, *Nat. Biotechnol.*, **1999** *17*, 1205.
  130. S. Lutz, M. Ostermeier M and S. J. Benkovic, *Nucleic Acid Res.*, **2001** *29*, 16.
  131. M. M. Meyer, J. J. Silberg, C. A. Voigt, J. B. Endelman, S. L. Mayo, Z. G. Wang and F. H. Arnold, *Protein Sci.*, **2003** *12*, 1686.
  132. K. Hiraga and F. H. Arnold, *J. Mol. Biol.*, **2003** *330*, 287.
  133. E. M. González-García, J. Grognum, D. Wahler and J. L. Reymond, *Helv. Chim. Acta*, **2003** *86*, 2458.
  134. E. Leroy, N. Bensele and J. L. Reymond, *Adv. Synth. Catal.*, **2003** *345*, 859.
  135. E. Leroy, N. Bensele and J. L. Reymond, *Bioorg. Med. Chem. Lett.*, **2003** *13*, 2105.
  136. J. P. Goddard and J. L. Reymond, *Current Opinion in Biotechnology*, **2004** *15*, 314.
  137. E. Henke and U. T. Bornscheuer, *Anal. Chem.*, **2003** *75*, 255.
  138. M. Konarzycka-Bessler and U. T. Bornscheuer, *Angew. Chem., Int. Ed.*, **2003** *42*, 1418.
  139. <http://www.kairos-scientific.com/searchable/kcat.html>.
  140. G. DeSantis, K. Wong, B. Farwell, K. Chatman, Z. Zhu, G. Tomlinson, H. Huang, X. Tan, L. Bibbs, P. Chen, K. Kretz and M. J. Burk, *J. Am. Chem. Soc.*, **2003** *38*, 11476.
-

- 
141. M. T. Reetz, A. Eipper, P. Tielmann and R. Mynott, *Adv. Synth. Catal.*, **2002** *344*, 1008.
  142. P. Tielmann, M. Boese, M. Luft, and M. T. Reetz, *Chem. Eur. J.*, **2003** *9*, 3882.
  143. S. Becker, H. Schmoldt, T. M. Adams, S. Wilhelm and H. Kolmar, *Current Opinion in Biotechnology*, **2004** *15*, 323.
  144. <http://www.gsf.de/Forschung/Institute/zs/application/principle.html>.
  145. S. W. Santoro, L. Wang, B. Herberich, D. S. King and P. G. Schultz, *Nat. Biotechnol.*, **2002** *20*, 1044.
  146. L. A. Castle, D. L. Siehl, R. Gorton, P. A. Patten, Y. H. Chen, S. Bertain, H. J. Cho, N. Duck, J. Wong, D. Liu, and M. W. Lassner, *Science*, **2004** *304*, 1151.
  147. L. A. Castle, D. L. Siehl, R. Gorton, P. A. Patten, Y. H. Chen, S. Bertain, H. J. Cho, N. Duck, J. Wong, D. Liu, and M. W. Lassner, *Science – Supporting online material*, **2004** *1*.
  148. M. T. Reetz, A. Zonta, K. Schimossek, K. E. Jaeger and K. Liebeton, *Angew. Chem., Int. Ed.*, **1997** *36*, 2830.
  149. K. Liebeton, A. Zonta, K. Schimossek, M. Nardini, D. Lang, B. W. Dijkstra, M. T. Reetz and K. E. Jaeger, *Chem. Biol.*, **2000** *7*, 709.
  150. M. T. Reetz, S. Wilensek, D. Zha and K. E. Jaeger, *Angew. Chem., Int. Ed.*, **2001** *40*, 3589.
  151. D. Zha, S. Wilensek, M. Hermes, K. E. Jaeger and M. T. Reetz, *Chem. Commun.*, **2001** 2664.
  152. M. T. Reetz, *Proc. Nat. Acad. Sci.*, **2004** *101*, 5716.
  153. M. Alexeeva, *PhD thesis, Edinburgh University*, **2003**.
  154. A. Enright, *PhD thesis, Edinburgh University*, **2001**.
  155. Novagen, pET system manual.
  156. Current Protocols in Protein Science **2001** 5.2 Selection of *Escherichia coli* Expression Systems (5.2.8 – Support protocol 2).
  157. André Matagne, A. Dubus, M. Galleni and J. M. Frère, *Nat. Prod. Rep.*, **1999** *16*, 1.
  158. <http://www.stratagene.com/manuals/200129.pdf>.
-

- 
159. [http://www.stratagene.com/faq/\\_answer/FAQS-RED.PDF](http://www.stratagene.com/faq/_answer/FAQS-RED.PDF).
  160. R. B. Lofthield, *Biochim. Biophys. Acta*, **1966** 130, 426.
  161. M. Alexeeva, R. Carr and N. J. Turner, *Org. Biomol. Chem.*, **2003** 1, 4133.
  162. C. Binda, A. Mattevi, and D. E. Edmondson, *J. Biol. Chem.* **2002** 277, 23973.
  163. C. Chen-Shih, Y. Fujimoto, G. Girdaukas and C. J. Sih, *J. Am. Chem. Soc.*, **1982** 104, 7294.
  164. A. Fersht, *Structure and mechanism in protein science*, **1999** p.341 Freeman publication.
  165. <http://web.mit.edu/esgbio/www/chem/review.html>.
  166. P. J. Winn, S. K. Ludemann, R. Gauges, V. Lounnas and R. C. Wade, *Proc. Nat. Acad. Sci.*, **2002** 99, 5361.
  167. S. E. Graham-Lorence, G. Truan, J. A. Peterson, J. R. Falck, S. Wei, C. Helvig and J. H. Capdevila, *J. Biol. Chem.*, **1997** 269, 1127.
  168. V. Gotor-Fernandez, *Project Report, Univeristy of Edinburgh*, **2004**.
  169. N. Itoh Y. Makino, and T. Dairi, *Chem. Listy*, **2003** 97, 434.
  170. H. Li, P. Williams, J. Micklefield, J. M. Gardiner and G. Stephens, *Tetrahedron* **2004** 60, 753.
  171. C. Mateo, A. Archelas, R. Fernandez-Lafuente, J. M. Guisan and R. Furstoss, *Org. Biomol. Chem.*, **2003** 1, 2739.
  172. I. M. P. Huber and D. Seebach, *Helvetica Chimica Acta*, **1987** 70, 1944.
  173. C. A. Willoughby and S. L. Buchwald, *J. Am. Chem. Soc.*, **1994** 116, 8963.
  174. E. Vedejs, P. Trapencieris and E. Suna, *J. Org. Chem.*, **1999** 64, 6724.
  175. J. González-Sabín, V. Gotor and F. Rebolledo, *Tetrahedron: Asymmetry*, **2002** 13, 1315.
  176. S. Ram and R. E. Ehrenkauf, *Synthesis*, **1988** 91.
  177. G. J. Roff, *Project Report, Univeristy of Edinburgh*, **2004**.
  178. P. Trinder and D. Webster, *Ann. Clin. Biochem.*, **1984** 21, 430.
  179. [www.spss.com](http://www.spss.com).
  180. M. Bradford, *Anal. Biochem.*, **1976** 72, 248.

181. S. E. J. Rigby, R. M. G. Hynson, R. R. Ramsay, A. W. Munro and N. S. Scrutton, *Journal of Biological Chemistry*, **2005**, *280*, 4627.

**Appendices**

**MAO wild-type sequence:**

	M	T	S	R	D	G	Y	Q	W	T	P	E
1	ATG	ACC	TCC	CGA	GAC	GGA	TAC	CAG	TGG	ACA	CCC	GAG
	T	G	L	T	Q	G	V	P	S	L	G	V
37	ACA	GGG	CTC	ACG	CAG	GGC	GTC	CCC	TCT	CTA	GGA	GTC
	I	S	P	P	T	N	I	E	D	T	D	K
73	ATC	TCC	CCG	CCC	ACT	AAT	ATC	GAA	GAC	ACG	GAC	AAA
	D	G	P	W	D	V	I	V	I	G	G	G
109	GAT	GGT	CCA	TGG	GAC	GTG	ATT	GTC	ATT	GGT	GGA	GGG
	Y	C	G	L	T	A	T	R	D	L	T	V
145	TAC	TGC	GGG	TTG	ACT	GCC	ACT	AGG	GAC	TTG	ACT	GTA
	A	G	F	K	T	L	L	L	E	A	R	D
181	GCA	GGC	TTC	AAA	ACC	CTT	CTC	CTC	GAA	GCC	CGA	GAC
	R	I	G	G	R	S	W	S	S	N	I	D
217	CGC	ATA	GGC	GGC	CGC	TCC	TGG	TCC	TCT	AAC	ATC	GAC
	G	Y	P	Y	E	M	G	G	T	W	V	H
253	GGC	TAT	CCT	TAC	GAG	ATG	GGC	GGC	ACA	TGG	GTC	CAC
	W	H	Q	S	H	V	W	R	E	I	T	R
289	TGG	CAC	CAA	TCG	CAC	GTA	TGG	CGC	GAA	ATC	ACG	CGC
	Y	K	M	H	N	A	L	S	P	S	F	N
325	TAC	AAG	ATG	CAC	AAC	GCC	CTA	TCA	CCC	TCC	TTC	AAC
	F	S	R	G	V	N	H	F	Q	L	R	T
361	TTC	TCC	CGC	GGC	GTG	AAT	CAC	TTC	CAG	CTA	CGG	ACC
	N	P	T	T	S	T	Y	M	T	H	E	A
397	AAC	CCC	ACC	ACA	TCA	ACC	TAC	ATG	ACT	CAC	GAA	GCC
	E	D	E	L	L	R	S	A	L	H	K	F
433	GAG	GAC	GAG	CTC	CTC	CGC	TCC	GCA	TTG	CAC	AAG	TTC

Appendices

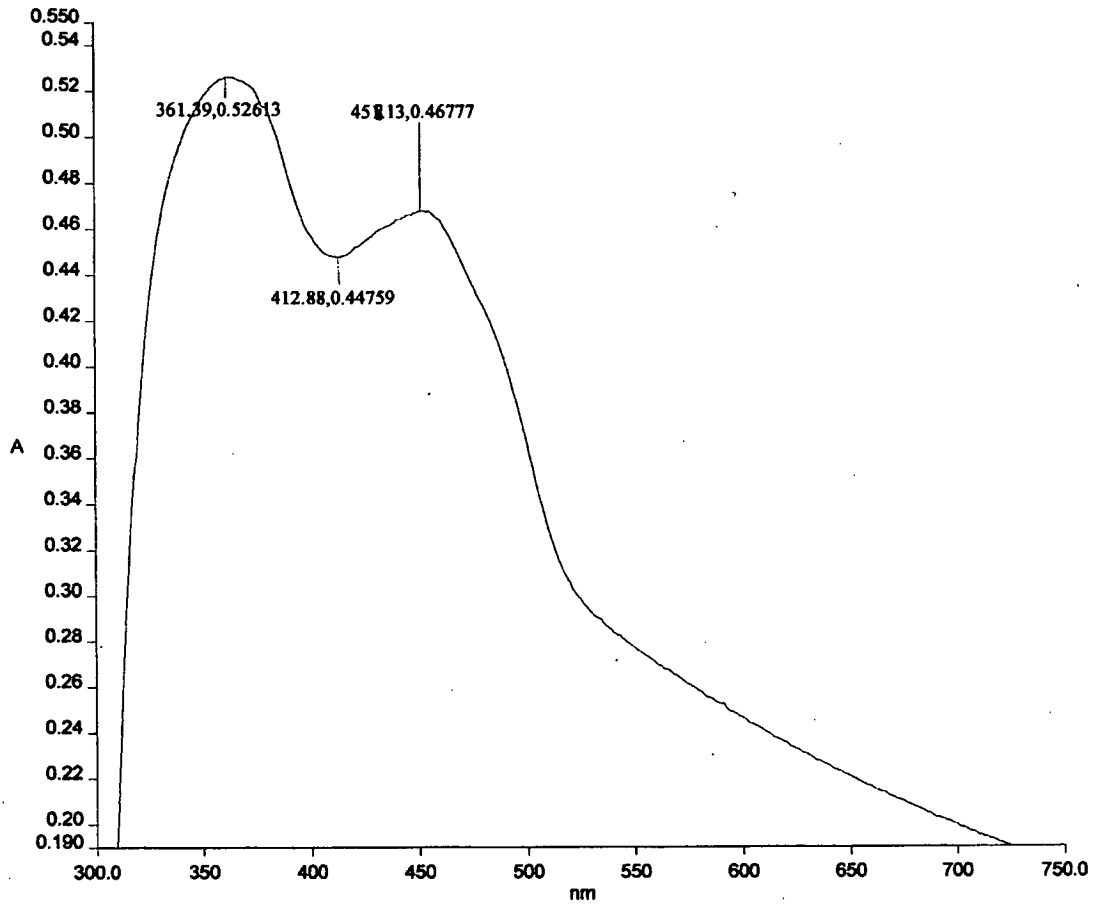
469 T N V D G T N G R T V L  
 ACC AAC GTG GAT GGC ACC AAC GGC CGT ACT GTC CTG  
  
 505 P F P H D M F Y V P E F  
 CCC TTC CCG CAT GAC ATG TTC TAT GTT CCT GAG TTC  
  
 541 R K Y D E M S Y S E R I  
 AGG AAG TAT GAT GAG ATG TCA TAC TCG GAG CGG ATT  
  
 577 D Q I R D E L S L N E R  
 GAT CAA ATC CGG GAT GAG TTG AGC CTT AAT GAA CGG  
  
 613 S S L E A F I L L C S G  
 AGT TCT CTG GAA GCG TTT ATA TTG CTT TGC TCT GGC  
  
 649 G T L E N S S F G E F L  
 GGA ACG CTG GAG AAT AGC TCA TTT GGA GAA TTC CTG  
  
 685 H W W A M S G Y T Y Q G  
 CAT TGG TGG GCG ATG AGC GGA TAT ACG TAT CAG GGA  
  
 721 C M D C L I S Y K F K D  
 TGC ATG GAC TGC TTG ATA AGT TAT AAG TTC AAG GAT  
  
 757 G Q S A F A R R F W E E  
 GGG CAG TCT GCA TTT GCG AGG AGG TTT TGG GAG GAG  
  
 793 A A G T G R L G Y V F G  
 GCG GCC GGG ACG GGG AGG TTG GGG TAT GTG TTT GGG  
  
 829 C P V R S V V N E R D A  
 TGT CCG GTT AGG AGT GTT GTT AAT GAG AGA GAT GCG  
  
 865 A R V T A R D G R E F A  
 GCG AGA GTG ACG GCG AGG GAT GGC AGG GAG TTC GCT  
  
 901 A K R L V C T I P L N V  
 GCG AAG CGG CTG GTT TGC ACT ATT CCC CTC AAT GTC  
  
 937 L S T I Q F S P A L S T  
 TTG TCC ACG ATC CAG TTC TCA CCT GCG CTG TCG ACG  
  
 973 E R I S A M Q A G H V N  
 GAG AGG ATC TCT GCT ATG CAG GCA GGT CAT GTG AAT



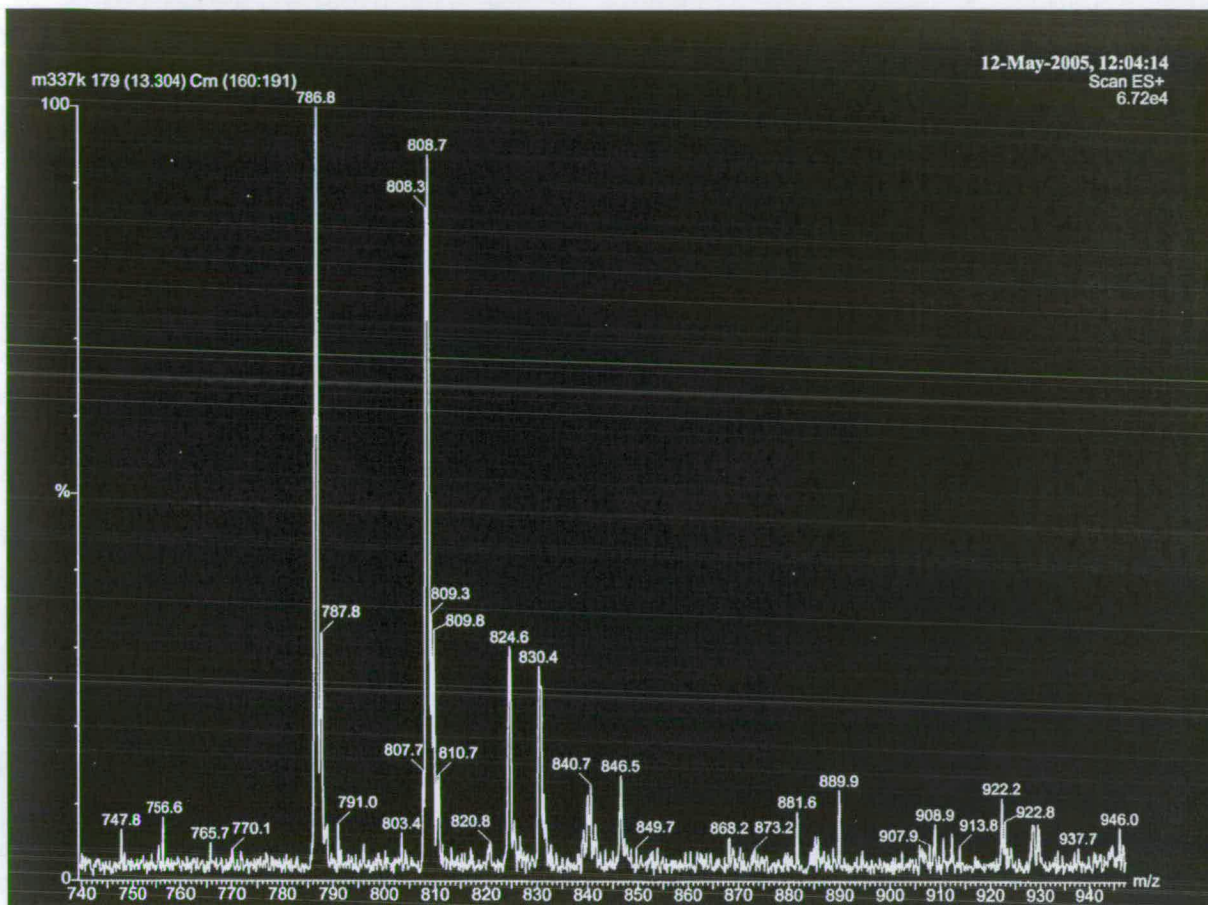
Appendices

1009	M	C	T	K	V	H	A	E	V	D	N	K
	ATG	TGC	ACG	AAG	GTG	CAT	GCC	GAA	GTG	GAC	AAT	AAG
1045	D	M	R	S	W	T	G	I	A	Y	P	F
	GAT	ATG	CGG	TCG	TGG	ACG	GGC	ATT	GCG	TAC	CCT	TTC
1081	N	K	L	C	Y	A	I	G	D	G	T	T
	AAT	AAA	CTG	TGC	TAT	GCT	ATT	GGT	GAT	GGG	ACG	ACT
1117	P	A	G	N	T	H	L	V	C	F	G	T
	CCC	GCG	GGA	AAC	ACG	CAT	CTG	GTG	TGT	TTC	GGG	ACG
1153	D	A	N	H	I	Q	P	D	E	D	V	R
	GAT	GCG	AAT	CAT	ATC	CAG	CCG	GAT	GAG	GAC	GTG	CGG
1189	E	T	L	K	A	V	G	Q	L	A	P	G
	GAG	ACG	TTG	AAG	GCG	GTT	GGG	CAG	TTA	GCG	CCT	GGG
1225	T	F	G	V	K	R	L	V	F	H	N	W
	ACA	TTT	GGA	GTG	AAG	CGG	TTG	GTG	TTT	CAC	AAT	TGG
1261	V	K	D	E	F	A	K	G	A	W	F	F
	GTG	AAG	GAT	GAG	TTT	GCG	AAG	GGC	GCG	TGG	TTC	TTC
1297	S	R	P	G	M	V	S	E	C	L	Q	G
	TCT	AGG	CCT	GGG	ATG	GTG	AGT	GAG	TGT	TTG	CAG	GGG
1333	L	R	E	K	H	R	G	V	V	F	A	N
	TTG	AGG	GAG	AAG	CAT	CGC	GGT	GTT	GTG	TTT	GCG	AAT
1369	S	D	W	A	L	G	W	R	S	F	I	D
	TCA	GAT	TGG	GCG	TTG	GGG	TGG	AGG	AGC	TTT	ATT	GAT
1405	G	A	I	E	E	G	T	R	A	A	R	V
	GGG	GCG	ATT	GAG	GAG	GGG	ACG	AGA	GCT	GCT	AGG	GTG
1441	V	L	E	E	L	G	T	K	R	E	V	K
	GTG	TTG	GAG	GAA	TTG	GGA	ACG	AAG	AGG	GAG	GTG	AAG
1477	A	R	L	*								
	GCT	CGT	TTG	TGA								

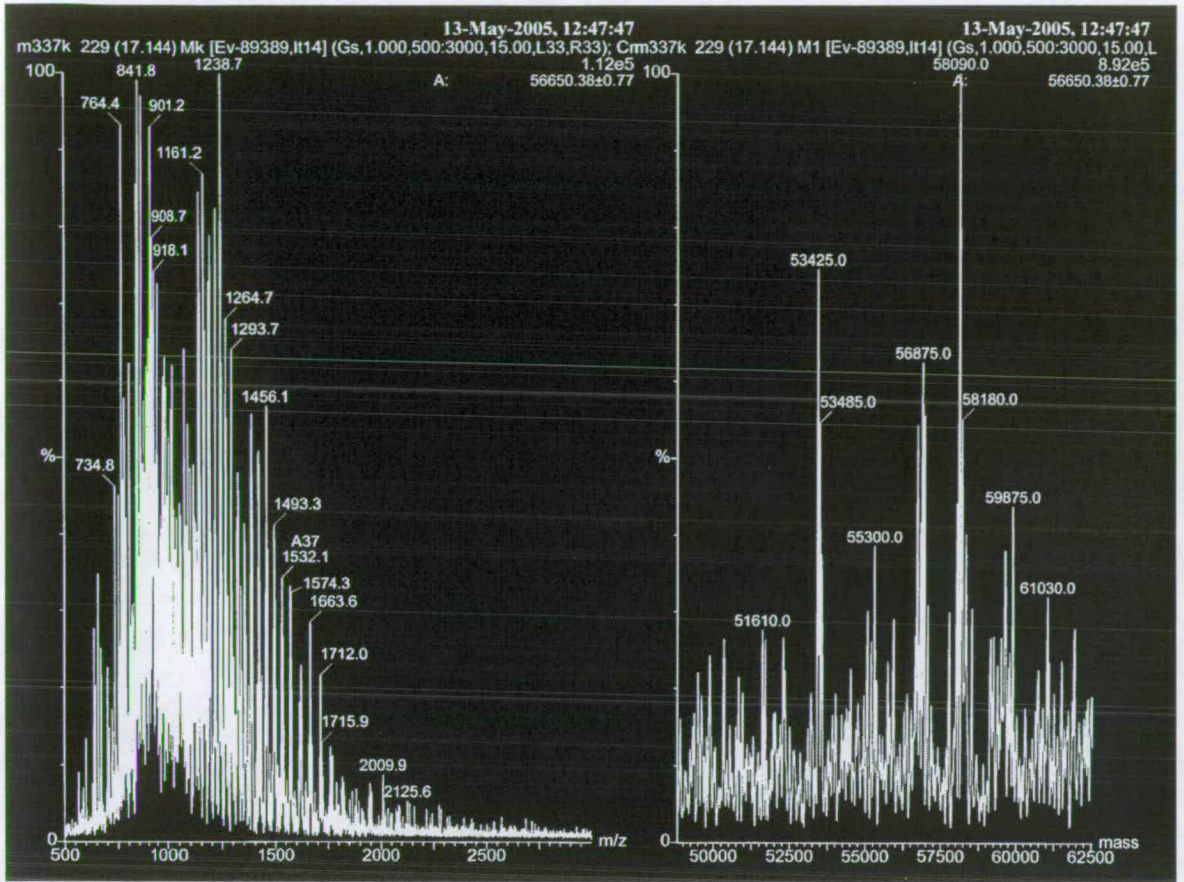
## UV-vis scan of MAO wild type:



## Electrospray mass spectrum of FAD cofactor from MAO wild type:



Electrospray mass spectrum of MAO wild type:



**The Genetic code**

	T	C	A	G
T	TTT Phe TTC Phe TTA Leu TTG Leu	TCT Ser TCC Ser TCA Ser TCG Ser	TAT Tyr TAC Tyr TAA Ter TAG Ter	TGT Cys TGC Cys TGA Ter TGG Trp
C	CTT Leu CTC Leu CTA Leu CTG Leu	CCT Pro CCC Pro CCA Pro CCG Pro	CAT His CAC His CAA Gln CAG Gln	CGT Arg CGC Arg CGA Arg CGG Arg
A	ATT Ile ATC Ile ATA Ile ATG Met	ACT Thr ACC Thr ACA Thr ACG Thr	AAT Asn AAC Asn AAA Lys AAG Lys	AGT Ser AGC Ser AGA Arg AGG Arg
G	GTT Val GTC Val GTA Val GTG Val	GCT Ala GCC Ala GCA Ala GCG Ala	GAT Asp GAC Asp GAA Glu GAG Glu	GGT Gly GGC Gly GGA Gly GGG Gly

**Symbols for amino acids**

Letter	code	Amino acid	Letter	code	Amino acid
A	Ala	Alanine	M	Met	Methionine
C	Cys	Cysteine	N	Asn	Asparagine
D	Asp	Aspartic acid	P	Pro	Proline
E	Glu	Glutamic acid	Q	Gln	Glutamine
F	Phe	Phenylalanine	R	Arg	Arginine
G	Gly	Glycine	S	Ser	Serine
H	His	Histidine	T	Thr	Threonine
I	Ile	Isoleucine	V	Val	Valine
K	Lys	Lysine	W	Trp	Tryptophan
L	Leu	Leucine	Y	Tyr	Tyrosine

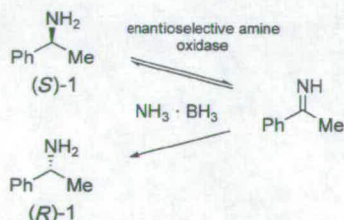
**Publications**

## Directed Evolution of an Amine Oxidase Possessing both Broad Substrate Specificity and High Enantioselectivity\*\*

Reuben Carr, Marina Alexeeva, Alexis Enright,  
Tom S. C. Eve, Michael J. Dawson, and  
Nicholas J. Turner\*

Enantiomerically pure chiral amines are of increasing value in organic synthesis, especially as resolving agents,<sup>[1]</sup> chiral auxiliaries/chiral bases,<sup>[2]</sup> and catalysts for asymmetric synthesis.<sup>[3]</sup> In addition, chiral amines often possess pronounced biological activity in their own right and hence are in demand as intermediates for agrochemicals and pharmaceuticals.<sup>[4]</sup> Current methods for the preparation of enantiomerically pure chiral amines are largely based upon the resolution of racemates, either by recrystallization of diastereomeric salts<sup>[5]</sup> or by enzyme-catalyzed kinetic resolution of racemic substrates using lipases and acylases.<sup>[6]</sup> To develop more efficient methods, attention is turning towards asymmetric approaches or their equivalent, for example, the asymmetric hydrogenation of imines<sup>[7]</sup> or the conversion of ketones into amines by using transaminases.<sup>[8]</sup> Attempts to develop dynamic kinetic resolutions, which employ enzymes in combination with transition-metal catalysts, have unfortunately been hampered by the harsh conditions required to racemize amines.<sup>[9]</sup>

Recently we reported a novel catalytic method for the preparation of optically active chiral amines by deracemization of the corresponding racemic mixture (Figure 1).<sup>[10]</sup> The deracemization approach relies upon coupling an enantioselective amine oxidase with a nonselective reducing agent to



**Figure 1.** Deracemization of  $\alpha$ -methylbenzylamine using an enantioselective amine oxidase in combination with ammonia-borane as the reducing agent.

[\*] Prof. Dr. N. J. Turner, R. Carr, M. Alexeeva, Dr. A. Enright, T. S. C. Eve  
School of Chemistry  
The University of Edinburgh  
King's Buildings, West Mains Road, Edinburgh EH9 3JJ (UK)  
Fax: (+44) 131 650 4717  
E-mail: n.j.turner@ed.ac.uk

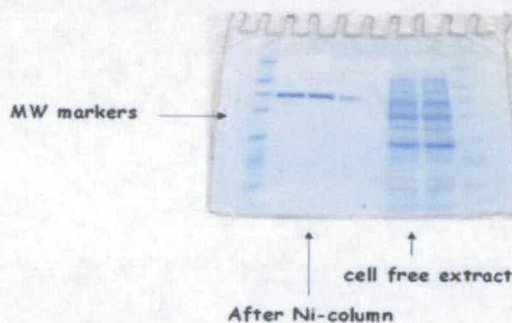
Dr. M. J. Dawson  
GlaxoSmithKline R&D  
Medicines Research Centre  
Gunnels Wood Road, Stevenage, Hertfordshire, SG1 2NY (UK)

[\*\*] We are grateful to the BBSRC and GlaxoSmithKline for funding a postdoctoral fellowship (MA) and CASE awards (RC, AE). We also thank the Wellcome Trust for financial support.

effect stereoinversion of the *S* to *R* enantiomer via the intermediate achiral imine.

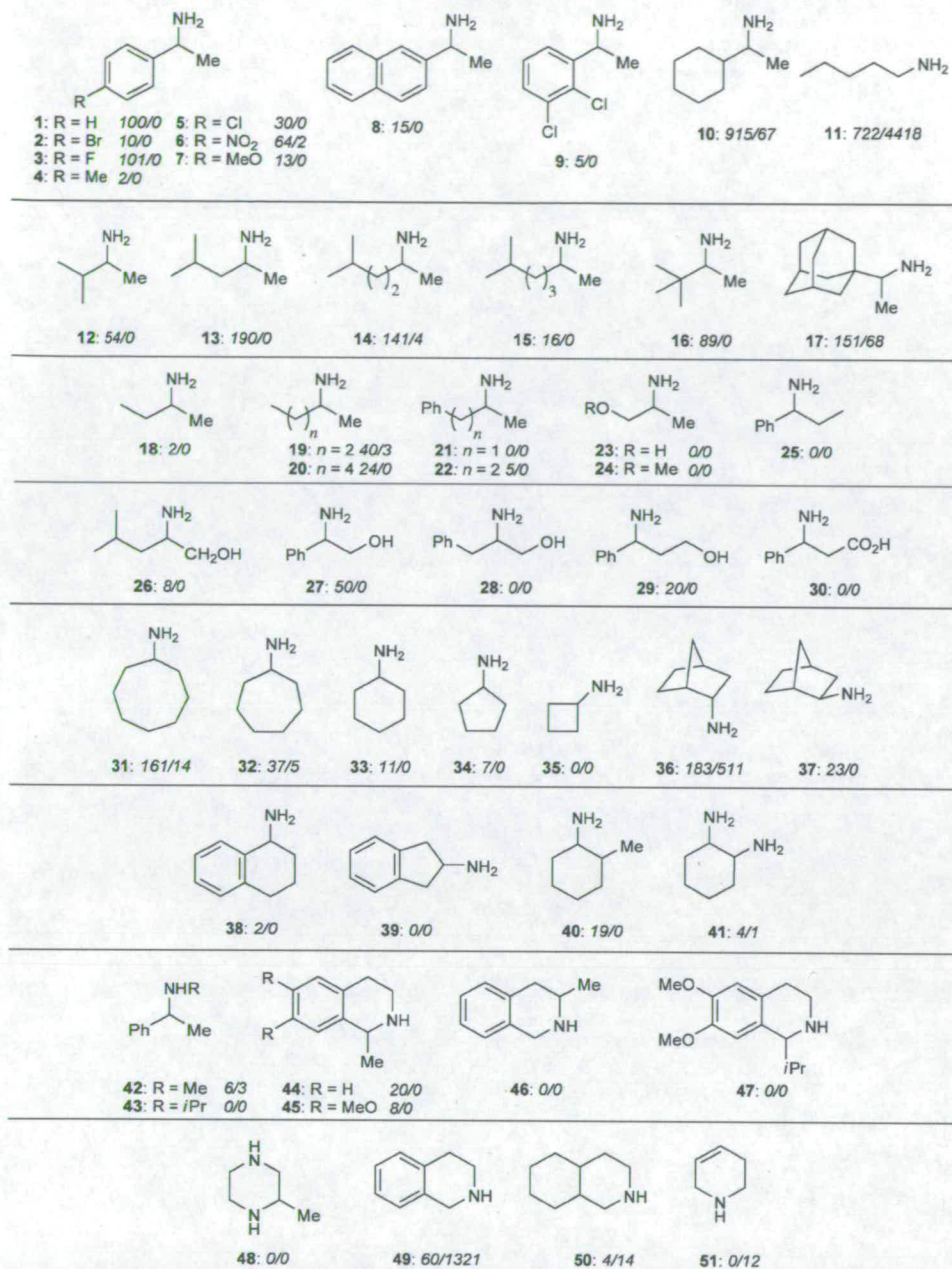
The *S* enantiomer selective amine oxidase used for the deracemization of (*R/S*)- $\alpha$ -methylbenzylamine was identified from a library of variants of the wild-type enzyme, from *Aspergillus niger*, by using a high-throughput colorimetric screen to guide selection.<sup>[10]</sup> The library of variants was generated by randomly mutating the plasmid harboring the amine oxidase gene by using the *E. coli* XL1-Red mutator strain. Using (*S*)- $\alpha$ -methylbenzylamine as the target substrate we were able to identify a variant (Asn336Ser) that possessed significantly improved catalytic activity (47 fold) and enantioselectivity (sixfold) towards this particular substrate compared to the wild type enzyme. To explore the opportunities for using this variant amine oxidase to deracemize other racemic chiral amines we decided to undertake a more detailed study of its substrate specificity. Herein we show that the Asn336Ser variant possesses broad substrate specificity and high enantioselectivity towards a wide range of chiral amines.

Prior to carrying out further studies with the Asn336Ser amine oxidase, an additional mutation was introduced into the sequence (Met348Lys) that resulted in a variant enzyme (hereafter referred to as Asn336Ser) with higher specific activity and expression levels although its substrate specificity appeared unchanged (data not shown). Incorporation of an *N*-terminal histidine tag into the amine oxidase allowed facile purification of both the wild-type and Asn336Ser variant in one step, by a nickel-affinity column, to yield protein of >90% purity as evidenced by gel electrophoresis (Figure 2, see Experimental Section). Solutions of the amine oxidases prepared in this manner were used for all the subsequent substrate specificity studies.



**Figure 2.** Polyacrylamide gel of amine oxidase enzyme after affinity purification on a nickel column.

A panel of amine substrates **1–51**, with broad structural features, was selected to characterize both the wild-type amine oxidase and Asn336Ser variant (Figure 3). Each substrate was screened individually, at 10 mM substrate concentration, against the partially purified wild-type and mutant amine oxidase in 96-well microtitre plate format using a UV/Vis plate-reader. The rate of oxidation was monitored by measuring hydrogen peroxide production by using a coupled enzyme assay.<sup>[11]</sup> For each substrate the  $k_{\text{cat}}$  and  $K_m$  values were calculated but for clarity only the relative activities are shown. These values have been calculated by



**Figure 3.** Panel of amines used in the screening experiments. Numbers in italics beneath the structures refer to relative rates of oxidation for Asn336Ser mutant/wild-type enzyme compared to  $\alpha$ -methylbenzylamine.

setting the activity of the Asn336Ser variant towards  $\alpha$ -methylbenzylamine as 100% and reporting all other rates as relative values. In addition, for a number of the chiral racemic substrates which gave positive assay results, the individual *R* and *S* enantiomers were also examined to determine the enantioselectivity of the reaction.

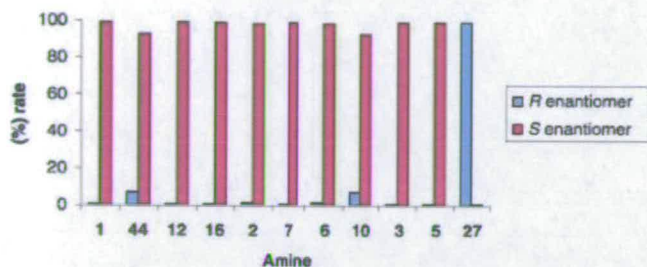
The wild-type amine oxidase was found to be inactive towards most of the amines shown in Figure 3. Of the 51 substrates examined, only nine gave relative activities of over 5%. The wild-type enzyme is most active towards simple straight-chain amines (e.g. pentylamine (11)) and generally shows poor activity towards more sterically demanding

branched amines. By comparison, however, the Asn336Ser variant amine oxidase showed a quite different substrate profile with significant activity ( $\geq 5\%$ ) towards more than half of the substrates examined (33 out of 51). Eight of the substrates tested (3, 10, 11, 13, 14, 17, 31, and 36) were more reactive than  $\alpha$ -methylbenzylamine itself with 1-cyclohexylethylamine (10) reacting approximately nine-times faster. The Asn336Ser variant amine oxidase showed high reactivity towards certain classes of chiral amines, particularly substituted phenethylamines (2, 3, 5–8) and 1-alkylethylamines (12–17, 19, 20). Secondary amines reacted more slowly (cf. 42 versus 1) although 2-methyltetrahydroisoquinoline 44 was



oxidized with a relative activity of 20% and the dimethoxy derivative **45** with a relative activity of 8%. Other substrates of interest that showed good activity were 2-phenyl-2-aminoethanol (**27**; rel. activity = 50%), *endo*-1-amino-norbornane (**36**; 183%), and 3-amino-3-phenylpropanol (**29**; 20%).

The enantioselectivity of the Asn336Ser variant towards 11 selected chiral amine substrates was then examined and the results are shown in Figure 4 and Table 1. The enantio-



**Figure 4.** Graph showing relative rate of oxidation of individual *S* and *R* enantiomers by Asn336Ser amine oxidase. The rate of each substrate has been normalized to 100%.

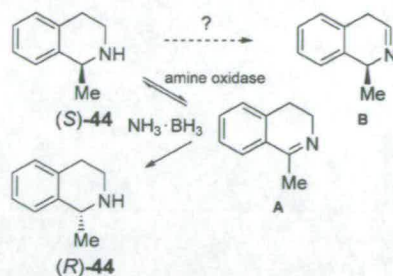
**Table 1:** Enantioselectivity of Asn336Ser mutant towards selected chiral amines.<sup>[a]</sup>

Amine	<i>E</i>	Amine	<i>E</i>
1	199	6	86
44	13	10	13
12	142	3	275
16	96	5	110
2	84	27	270
7	184		

[a] The numbers reported refer to the enantiomeric ratio (*E*) for the individual substrates.

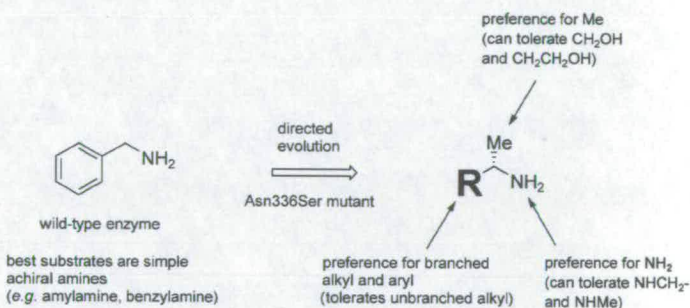
meric ratio  $E^{[12]}$  for  $\alpha$ -methylbenzylamine was very high ( $E = 199$ ) and was in general maintained with most of the other chiral amines. Such *E* values translate to *ee* values of around 97–99%. Only 1-methyltetrahydroisoquinoline (**44**) and 1-cyclohexylethylamine (**10**) gave significantly lower values (both  $E = 13$ ) although even these values would equate to an *ee* value of about 85%. Significantly, in all cases the Asn336Ser variant amine oxidase was found to be selective for the *S* enantiomer of the amine substrate (note that for **27** the *R* enantiomer is oxidized owing to the change in priority of the substituents).

For secondary amine substrates, for example, **42**, **44**, **45**, **49**, and **50** the possibility arose as to the regioselectivity of oxidation with respect to the amine functionality. Thus **44** could, in principle undergo oxidation to yield either imine **A** or **B**, or a mixture of both (Figure 5). To establish that the former pathway operated at least to some extent, we carried out the Asn336Ser amine oxidase catalyzed oxidation of (*S*)-**44** in the presence of the reducing agent ammonia-borane which we have previously shown to be effective for reduction of the intermediate imine.<sup>[10]</sup> Analysis of the chiral HPLC profile clearly showed that after 90 h significant production of (*R*)-**44** had occurred. The formation of (*R*)-**44** from (*S*)-**44** can only occur via the achiral imine **A** and not the chiral imine **B** (see Experimental Section).



**Figure 5.** Stereoinversion of (*S*)-**44** to (*R*)-**44**, via imine **A**, by using Asn336Ser amine oxidase with ammonia borane.

In summary, we have shown that a directed evolution approach, based initially upon screening a library of mutant amine oxidases for activity against one enantiomer of a specific substrate ((*S*)- $\alpha$ -methylbenzylamine), has led to the identification of an enzyme possessing much broader substrate specificity whilst retaining high enantioselectivity. The Asn336Ser variant shows highest activity towards substrates containing a primary amine group flanked by a methyl group and a bulky alkyl/aryl group (Figure 6). In all cases so far examined the variant enzyme is selective for the *S* enantiomer



**Figure 6.** Comparison of substrate specificity of wild-type and Asn336Ser mutant amine oxidase.

of the chiral amine substrate. Other groups have also reported the identification of highly enantioselective enzymes by screening against single enantiomer substrates.<sup>[13]</sup> Although the *A. niger* Asn336Ser amine oxidase is suitable at present for small-scale deracemization reactions,<sup>[10]</sup> we are continuing to evolve this enzyme to develop an enzyme that has the required characteristics (e.g. stability, activity, selectivity) to be used for large-scale applications.

The development of enzymes possessing broad substrate specificity combined with high enantioselectivity remains an important goal in biocatalysis. Previous studies have demonstrated that directed evolution can be used to alter the substrate specificity and enantioselectivity of enzymes and moreover such variant enzymes often possess broader specificity when compared with the wild-type enzyme.<sup>[14]</sup> The results described herein represent the most in-depth study to date of how the substrate specificity of an enzyme can be dramatically altered by a point-mutation. The ability to select for such enzymes, using appropriate high-throughput screens, is critical to success in this area and highlights the need for new methods to enable the detection of a wider range of enzyme activities than is currently possible.<sup>[15]</sup>

## Experimental Section

**Expression and purification of amine oxidase:** BL21 star was transformed with the wild-type/mutant amine oxidase gene and plated onto LB (70  $\mu\text{g mL}^{-1}$  ampicillin) petri dishes. A single colony was added to LB media (6  $\times$  300 ml) containing ampicillin and grown at 30°C for 24 h. The cells were spun and the cell pellet stored at -20°C. Lysis of the cells was performed in 25 mM Tris/HCl pH 7.8, 10 mM imidazole, 1 mM  $\beta$ -mercaptoethanol, 1 mM phenylmethanesulfonyl fluoride (PMSF), and 300 mM NaCl and the lysate centrifuged. The cell-free extract from a 1 g pellet was loaded onto a 1-mL Ni-*N,N*-bis(carboxymethyl) glycine (nitrilotriacetic acid (NTA)) column. Column wash (five column volumes); 25 mM Tris/HCl pH 7.8, 60 mM imidazole, 1 mM  $\beta$ -mercaptoethanol, 1 mM PMSF, and 300 mM NaCl. Protein elution (the amine oxidase elutes in  $\approx$ 2nd–7th 1 ml fractions); 25 mM Tris/HCl pH 7.8, 200 mM imidazole, 1 mM  $\beta$ -mercaptoethanol, 1 mM PMSF, and 300 mM NaCl. The protein was desalted in 25 mM Tris/HCl pH 7.8, 1 mM threo-1,4-dimercapto-2,3-butanediol (dithiothreitol (DTT)), 1 mM PMSF, and 300 mM NaCl using a Pharmacia PD10 column. Samples were stored frozen at -80°C and thawed prior to use.

**Stereoinversion of (S)-44:** A solution (600  $\mu\text{L}$ ) containing 20 mM (S)-44, 400 mM  $\text{NH}_3\cdot\text{BH}_3$ , 25 mM Tris/HCl pH 7.8, 1 mM DTT, 1 mM PMSF, and 300 mM NaCl aqueous buffer was held at 30°C with shaking for 2 h. A 100- $\mu\text{L}$  aliquot was removed and analyzed by HPLC as a  $t = 0$  sample. amine oxidase (0.215 mg) in 500  $\mu\text{L}$  of 25 mM Tris/HCl pH 7.8, containing 1 mM DTT, 1 mM PMSF and 300 mM NaCl was added to the remaining 500  $\mu\text{L}$  of the (S)-44 solution. The mixture was shaken at 30°C and after  $t = 90$  h a 100  $\mu\text{L}$  aliquot was removed and analyzed by HPLC. Some precipitation was observed over the course of the reaction.

**HPLC sample preparation:** An aliquot (100  $\mu\text{L}$ ) of the reaction mixture was extracted with hexane (2  $\times$  150  $\mu\text{L}$ ). The combined hexane extracts were analyzed directly by HPLC: Chiracel OD-H column 46 cm, eluent hexane:ethanol 98:2 (v/v), flow rate = 0.5  $\text{mL min}^{-1}$ , column temperature = 0°C; retention times, imine A = 18.7 min, (S)-44 = 22.4 min, (R)-44 = 26.2 min.

Received: June 10, 2003 [Z52100]

**Keywords:** amines · deracemization · directed evolution · enzymes

- A. H. Ell, J. S. M. Samec, N. Hermanns, J.-E. Bäckvall, *Tetrahedron Lett.* **2002**, 43, 4699.
- [10] M. Alexeeva, A. Enright, M. J. Dawson, M. Mahmoudian, N. J. Turner, *Angew. Chem.* **2002**, 114, 3309; *Angew. Chem. Int. Ed.* **2002**, 41, 3177.
- [11] M. Braun, J. M. Kim, R. D. Schmid, *Appl. Biochem. Biotechnol.* **1992**, 37, 594.
- [12] For the definition of enantiomeric ratio (*E*) see; C. S. Chen, Y. Fujimoto, G. Girdaukas, C. J. Sih, *J. Am. Chem. Soc.* **1982**, 104, 7294; C. S. Chen, S. H. Wu, G. Girdaukas, C. J. Sih, *J. Am. Chem. Soc.* **1987**, 109, 2812.
- [13] B. Lingen, J. Grötzinger, D. Kolter, M.-R. Kula, M. Pohl, *Protein Eng.* **2002**, 15, 585.
- [14] L. Sun, T. Bulter, M. Alcalde, I. P. Petrounia, F. H. Arnold, *ChemBioChem* **2002**, 3, 781; O. May, P. T. Nguye, F. H. Arnold, *Nat. Biotechnol.* **2000**, 18, 317; D. Zha, S. Wilensek, M. Hermes, K.-E. Jaeger, M. T. Reetz, *Chem. Commun.* **2001**, 2664; G. J. Williams, S. Domann, A. Nelson, A. Berry, *Proc. Natl. Acad. Sci. USA* **2003**, 100, 3143; M. Wada, C.-C. Hsu, D. Franke, M. Mitchell, A. Heine, I. Wilson, C.-H. Wong, *Bioorg. Med. Chem.* **2003**, 11, 2091.
- [15] N. J. Turner, *Trends Biotechnol.* **2003**, 21, in press.

- [1] J. W. Nieuwenhuijzen, R. F. P. Grimbergen, C. Koopman, R. M. Kellogg, T. R. Vries, K. Pouwer, E. van Echten, B. Kaptein, L. A. Hulshof, Q. B. Broxterman, *Angew. Chem.* **2002**, 114, 4457; *Angew. Chem. Int. Ed.* **2002**, 41, 4281.
- [2] K. W. Henderson, W. J. Kerr, J. H. Moir, *Chem. Commun.* **2000**, 479.
- [3] M. F. A. Adamo, V. K. Aggarwal, M. A. Sage, *J. Am. Chem. Soc.* **2000**, 122, 8317.
- [4] M. Berger, B. Albrecht, A. Berces, P. Etmayer, W. Neruda, M. Woisetschläger, *J. Med. Chem.* **2001**, 44, 3031.
- [5] T. R. Vries, H. Wynberg, E. van Echten, J. Koek, W. ten Hoeve, R. M. Kellogg, Q. B. Broxterman, A. Minnaard, B. Kaptein, S. van der Sluis, L. A. Hulshof, J. Kooista, *Angew. Chem.* **1998**, 110, 2491; *Angew. Chem. Int. Ed.* **1998**, 37, 2349.
- [6] F. Messina, M. Botta, F. Corelli, M. P. Schneider, F. Fazio, *J. Org. Chem.* **1999**, 64, 3767; M. I. Youshko, F. van Rantwijk, R. A. Sheldon, *Tetrahedron: Asymmetry* **2001**, 12, 3267; A. Luna, I. Alfonso, V. Gotor, *Org. Lett.* **2002**, 4, 3627.
- [7] S. Kainz, A. Brinkmann, W. Leitner, A. Pfaltz, *J. Am. Chem. Soc.* **1999**, 121, 6421.
- [8] J.-S. Shin, B.-G. Kim, *Biosci. Biotechnol. Biochem.* **2001**, 65, 1782.
- [9] M. T. Reetz, K. Schimossek, *Chimia* **1996**, 50, 668; Y. K. Choi, M. J. Kim, Y. Ahn, M.-J. Kim, *Org. Lett.* **2001**, 3, 4099; O. Pamies,

## Directed evolution of enzymes: new biocatalysts for asymmetric synthesis

Marina Alexeeva, Reuben Carr and Nicholas J. Turner\*

School of Chemistry, University of Edinburgh, King's Buildings, West Mains Road, Edinburgh, UK EH9 3JJ. E-mail: n.j.turner@ed.ac.uk

Received 10th September 2003, Accepted 2nd October 2003

First published as an Advance Article on the web 21st October 2003

Directed evolution has been employed to generate new enzymes for the deracemisation of chiral amines.

### Introduction

The use of combinatorial methods for lead discovery and optimisation has become a powerful and now firmly established technique within the pharmaceutical industry. More recently, analogous approaches of parallel synthesis and screening have been applied to the discovery and development of new catalysts for asymmetric synthesis.<sup>1</sup> The underlying principles are simple and very appealing, namely coupling systematic variations in catalyst structure, ligand composition, reaction conditions *etc.*, with effective methods for high-throughput screening for a range of properties (*e.g.* turnover number, enantioselectivity) resulting in catalysts that are fine tuned and optimised for specific applications.<sup>2</sup> Not surprisingly, similar concepts of combinatorial optimisation have recently gained popularity in the discovery and development of biocatalysts. However, here the situation is somewhat different given the relative complexity of enzymes. A typical enzyme is composed of between 250–

1000 amino acids and hence the notion of systematically varying even a small number of amino acids in an enzyme sequence, to explore the effect on activity or selectivity, is unrealistic since the number of possible permutations rapidly exceeds the capabilities of high-throughput screens, let alone conventional analytical HPLC or GC-MS methods. Even if only one amino acid in any part of the sequence is replaced by any other of the 19 other amino acids the number of permutations<sup>3</sup> is in the region of *ca.* 10<sup>4</sup> whereas for combinatorial mutagenesis, where in two or more residues are simultaneously randomised, the library sizes can become truly vast (no. of permutations = 20<sup>*n*</sup> where *n* is the number of amino acids that are simultaneously varied). Furthermore, it is generally not obvious which amino acids, or combinations thereof, are important for controlling specific characteristics (*e.g.* enantioselectivity, catalytic activity, stability). Although the increased availability of X-ray structures can help to guide identification of important residues, in practice it is mainly active-site residues that are targeted on the

Marina Alexeeva, graduated from the Moscow State Pirogov Medical Institute in 1980 with a degree in Biochemistry. Following a period as a Research Assistant in the Institute of Molecular Genetics at the Russian Academy of Sciences, she joined Edinburgh University in 1992 as a Technical Officer, a position she held for 7 years until beginning her PhD in 1999 with Nick Turner. Her thesis research involved the directed evolution of amine oxidases for deracemisation reactions. At the beginning of 2003 she joined Ingenza as a Senior Scientist.

Reuben Carr, graduated with a first class honours degree in Chemistry and Biochemistry from the University of Southampton in 2000. He moved to Edinburgh in 2001 to begin his PhD under the supervision of Nick Turner as a CASE student in collaboration with GlaxoSmithKline. His research involves the deracemisation of chiral amines using enzymes in combination with chemical reducing agents.

Nicholas Turner, obtained his D. Phil. in 1985 under the supervision of Professor Sir Jack Baldwin, followed by postdoctoral studies as a Royal Society Junior Research Fellow with Professor George Whitesides at Harvard University, USA. In 1987 he joined the Chemistry Department at Exeter University as a Lecturer before moving to Edinburgh University in 1995 as a Reader. In 1998 he was promoted to a Personal Chair in Biological Chemistry. Recently, along with his colleagues Ian Fotheringham, Robert Speight and Sunil Srivastava, he founded Ingenza, a new company based within the School of Chemistry at Edinburgh, that is developing novel bioprocesses for the pharmaceutical and fine chemical industry.



Marina Alexeeva



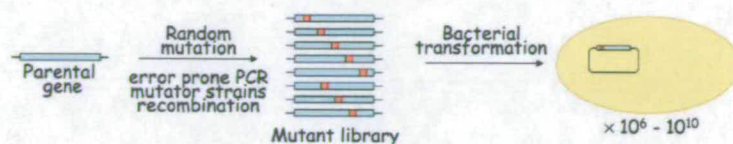
Reuben Carr



Nicholas Turner

## Directed evolution of enzymes

### Generation of variant gene libraries



### Library evaluation

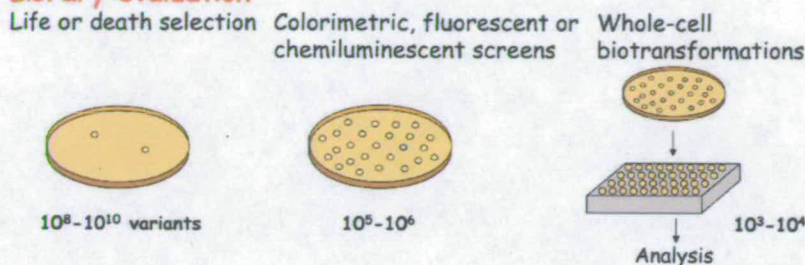


Fig. 1 Strategies for the directed evolution of enzymes involving (a) generation of libraries of variant genes and (b) high-throughput screening of the libraries using different analytical methods.

basis that they make important non-bonding interactions with the substrate.<sup>4</sup>

The past 5–10 years has witnessed the emergence of ‘directed evolution’ strategies in order to change the properties of enzymes in a targeted manner.<sup>5</sup> Directed evolution of enzymes combines two distinct events, namely (i) random mutagenesis of the parent gene to provide a library of variant enzymes and (ii) methods for screening the individual members of the library for specific characteristics (e.g. reactivity towards a specific substrate, resistance to product inhibition, thermal/organic solvent stability) (Fig. 1). The power of this approach is that it requires no prior knowledge of the structure (or in some cases sequence) of the enzyme since the variants are selected simply on their ability to carry out a specific transformation, without regard to prior assumptions as to which particular amino acids might be important. The real challenge in this area is to devise high-throughput screens that are able to handle sufficiently large libraries (ca.  $10^5$ – $10^9$ ) such that significant improvements over the activity of the wild-type enzyme can be achieved. Such levels of throughput (i.e.  $>10^5$  samples per day) have been achieved using *in vivo* ‘life or death’ selection and *in vitro* detection (e.g. colorimetric/fluorescence detection, capillary array electrophoresis) but new methods are required to expand the range of enzyme activities that can be detected.<sup>6</sup>

The aim of this article is to provide an insight into the field of ‘directed evolution’ and to consider how this technology can best be employed to develop new enzyme-catalysed reactions and processes for the future. To assist in this objective, the authors have provided a personal case study from their own laboratory in which many of the current themes surrounding directed evolution have been encountered.

### Deracemisation reactions: the development of a platform technology

Inspired by the early work of Hafner *et al.*,<sup>7</sup> and Soda *et al.*,<sup>8</sup> we set out to develop general and practical methods for the cyclic deracemisation of chiral compounds *via* an oxidation–reduction sequence (Fig. 2). In this catalytic cycle the combination of an enantioselective oxidase, together with a non-selective chemical reducing agent, results in the conversion of a racemic mixture to a single enantiomer. Provided that the oxidase enzyme is highly enantioselective, only 7 cycles are required to achieve an ee of  $>99\%$ .<sup>9</sup> We have successfully applied this method to the deracemisation of a variety of

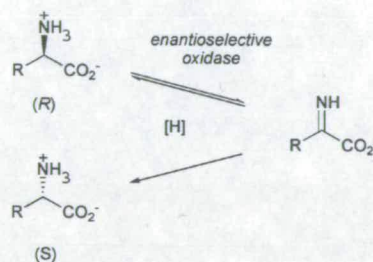
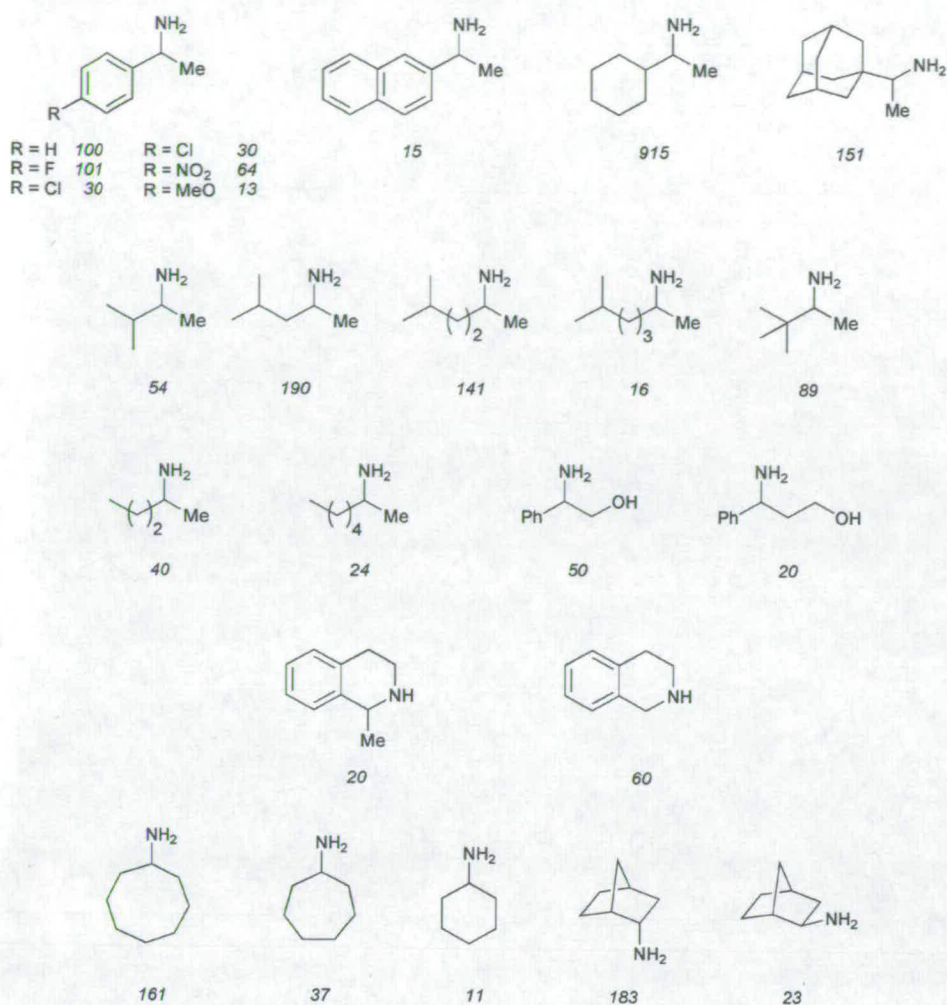


Fig. 2 Deracemisation of  $\alpha$ -amino acids using an enantioselective amino acid oxidase in combination with a non-selective chemical reducing agent.

$\alpha$ -amino acids in high yield (70–85%) and ee ( $>98\%$ ) using both D- and L-amino acid oxidases together with a variety of reducing agents (NaCNBH<sub>3</sub>; NaBH<sub>4</sub>; amine–boranes; Pd/C–ammonium formate).<sup>10,11</sup> Because the reaction is in essence a stereoinversion process, we have also shown that it can be used to interconvert diastereomeric amino acids bearing more than one stereogenic centre.<sup>12</sup> Encouraged by this success with  $\alpha$ -amino acids, we sought to broaden the range of substrates amenable to deracemisation and considered amines in view of their increasing value as chiral intermediates for pharmaceutical drugs and also ligands for asymmetric catalysis.<sup>13</sup> The key issue at the outset was the availability of enantioselective amine oxidases that could be applied to deracemisation reactions. Unfortunately, we could not find any convincing literature precedent for the presence of enantioselective Type II amine oxidases in microbial sources (some Type I enzymes were known to be enantioselective but these amine oxidases generate an enzyme-bound imine and hence were unsuitable for use in deracemisation reactions). Thus we decided to undertake a directed evolution approach to evolve enzymes that had the characteristics required for our deracemisation reactions.

### Directed evolution of an amine oxidase

The starting point for any successful directed evolution project is a reliable and robust high-throughput screen. *In vitro* screens, based upon the production of a coloured or fluorescent product, have the advantage that they can be used to screen colonies directly on an agar plate thus enabling  $10^5$ – $10^6$  clones to be assayed in a short period of time. We developed a colorimetric screen, based upon capture of the hydrogen peroxide generated



**Fig. 3** Range of amines that are substrates for the Asn336Ser variant of the amine oxidase from *Aspergillus niger*. The numbers in italics below the structures indicate the activity relative to  $\alpha$ -methylbenzylamine.

by the oxidase enzyme, and demonstrated that it could be used to detect colonies expressing amino acid or amine oxidases. The next decision concerned the starting gene to be used for generation of the library of variants. It was known that the monoamine oxidase (MAO-N) from *Aspergillus niger* catalysed the oxidation of simple alkyl amines including benzylamine although no data was reported for any chiral amines.<sup>14</sup> A plasmid harbouring the MAO-N gene was obtained, subcloned into *Escherichia coli*, and used to express the wild-type enzyme which was found to have very low, but detectable activity towards  $\alpha$ -methylbenzylamine, the amine chosen for our model studies. Interestingly there was also evidence that the wild-type enzyme was enantioselective although the intrinsic rates were very low. Next the MAO-N gene was randomly mutated, using the *E. coli* XL1-Red mutator strain,<sup>15</sup> and the library of variants (*ca.* 150 000) screened against (*S*)- $\alpha$ -methylbenzylamine as a substrate using the agar-plate colorimetric assay. The frequency of mutation was adjusted such that individual clones possessed *ca.* 1–2 nucleotide mutations per gene. Approximately 30 clones were selected at this stage, on the basis of their activity in the screen, and amongst these one clone in particular was found to have very high (*S*)-selectivity. Small scale growth of this clone and partial purification of the amine oxidase revealed that this variant possessed approximately 47 fold greater activity, and 6 fold greater enantioselectivity towards  $\alpha$ -methylbenzylamine compared with the wild-type enzyme, a substantial improvement from a single round of directed evolution. This variant was sufficiently catalytically active to be used

in combination with ammonia–borane to deracemise  $\alpha$ -methylbenzylamine yielding the (*R*)-enantiomer in 77% yield and 93% ee.<sup>16</sup>

Sequencing of this variant revealed that it possessed a single mutation (Asn336Ser). The variant amine oxidase was subsequently purified to homogeneity, by Ni affinity chromatography, and examined for its reactivity towards a panel of *ca.* 50 different chiral amines. Interestingly, more than 60% of these structurally different amines were found to be substrates, some with greater activity than  $\alpha$ -methylbenzylamine itself (Fig. 3). For those substrates where the individual enantiomers were available we determined the enantioselectivity and found that in all cases the enzyme was highly (*S*)-selective ( $E > 10$ ). By contrast, the wild-type enzyme was active towards only *ca.* 15% of the substrates, confirming that the Asn336Ser variant possessed a substantially different substrate specificity.<sup>17</sup> Analysis of the relationship between structure and reactivity led us to propose a simple model to summarise the effect of directed evolution of the wild-type amine oxidase (Fig. 4). Overall, this first round of directed evolution had resulted in the identification of a variant with substantially improved catalytic activity and enantioselectivity together with significantly broadened substrate specificity.

#### Further rounds of 'real time' directed evolution

An attractive aspect of directed evolution is that variants selected from the first round of evolution can form the starting

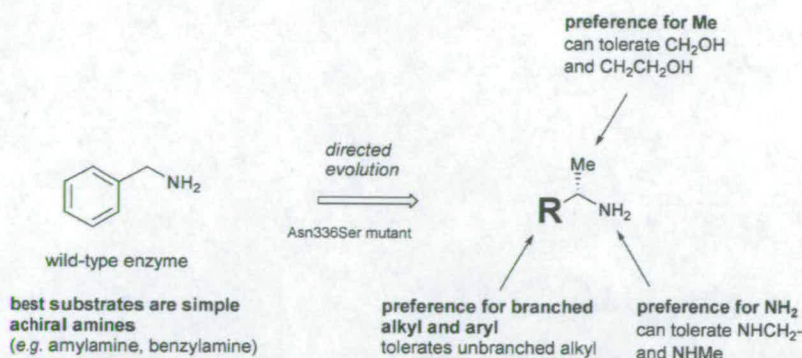


Fig. 4 Schematic illustration of the change in substrate of specificity of the Asn336Ser mutant relative to the wild-type enzyme.

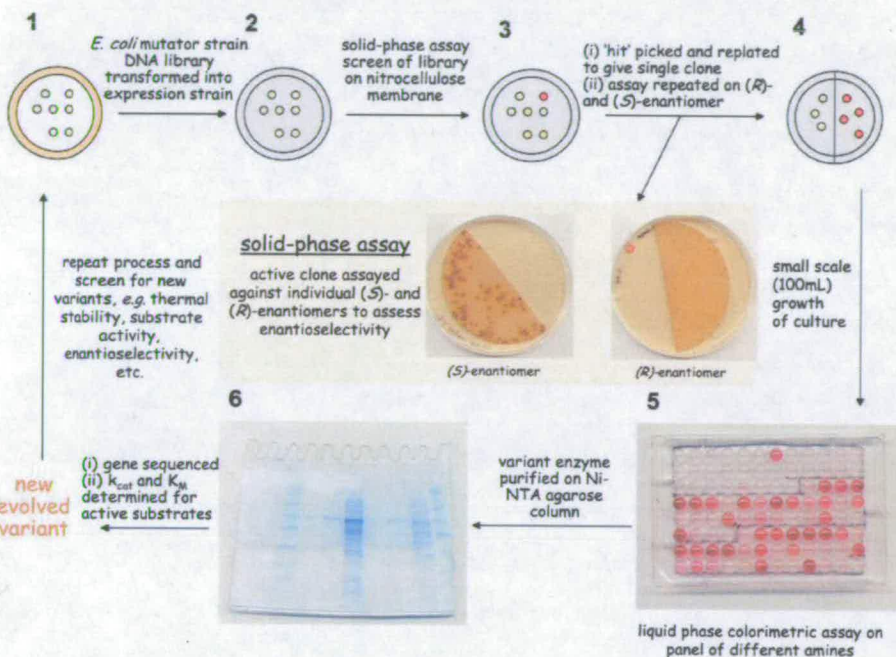


Fig. 5 Strategy for iterative evolution of enzymes in 'real time' by employing hierarchical screening protocols; *Step 1*: Library of variants generated from parent gene using *E. coli*, XL1-Red mutator strain. *Step 2*: DNA library transformed into *E. coli*, expression strain and colonies streaked and grown on nitrocellulose membrane on agar plate. *Step 3*: Membrane lifted, colonies partially lysed (freeze-thaw) and then screened for activity using colorimetric assay containing specific amine substrate. *Step 4*: 'Hits' picked and replated to give single colonies. Active colonies checked for enantioselectivity towards individual (*R*)- and (*S*)-enantiomers of amine substrate. *Step 5*: Variants that are both highly active and enantioselective grown on small scale (100 ml) and screened against range of chiral amines (ca., 32) in 96-well microtitre plate using liquid-phase colorimetric assay. This step allows differentiation between 'expression mutants' and 'specificity mutants'. *Step 6*: Individual variants purified using Ni-affinity column and subjected to full kinetic characterisation ( $k_{\text{cat}}$  and  $K_M$ ). Gene sequenced to identify positions of mutations. *Step 7*: Steps 1–6 repeated varying target amine substrate or introducing additional selection criteria (e.g., thermostability, high substrate concentration).

point for further rounds of mutagenesis/selection in the anticipation that additional mutations might lead to further changes in an additive manner. These further cycles can be carried out rapidly (3–4 weeks), in a highly automated fashion, in order to fine tune the enzyme towards substrates of specific interest. Fig. 5 illustrates the approach we have recently developed involving initial passage through the mutator strain, to generate new libraries (ca. 10 000–300 000 clones) which are then screened for specific characteristics including substrate specificity, thermal stability, enantioselectivity etc. Libraries can also be generated at this stage using error-prone PCR or combinatorial mutagenesis in which several amino acids are simultaneously randomised. Any identified 'hits', which typically arise with a frequency of ca. 1 in 10 000 using the mutator strain, are rapidly checked against a panel of substrates (ca. 32 structurally different compounds) in order to roughly define the substrate range and enantioselectivity. At this stage we are also able to identify 'expression mutants' i.e. those variants in which the protein expression levels have been enhanced without any change in specific activity or substrate specificity. Variants of

particular interest are subsequently purified to homogeneity, via Ni-chelation chromatography, and then fully characterised against specific chiral amines of interest including determination of  $k_{\text{cat}}$  and  $K_M$  values. Further rounds of evolution can then be carried out until an enzyme possessing suitable characteristics is obtained. In this way we have been able to evolve new types of amine and amino acid oxidases, i.e. enzymes that possess greater activity towards secondary, rather than primary, amines or variants that are able to oxidise sterically demanding substrates. The goal is to rapidly generate a family of (*S*)- and (*R*)-selective amine and amino acid oxidases that possess complementary substrate specificities allow us to deracemise a wide range of chiral amines and amino acids respectively.

#### Future directions

Directed evolution represents a powerful strategy for altering the properties of an enzyme in a rapid and targeted manner. However, the challenge now for applying this technology to biocatalysis is to identify the best strategy for evolving enzymes

such that they ultimately possess all of the characteristics required for ultimate use in a large scale bioprocess.<sup>18</sup> The ideal biocatalyst should possess most, if not all of the following properties; high  $k_{\text{cat}}$ ,  $K_M$  in the millimolar range, high enantioselectivity ( $E > 50$ ), broad substrate specificity, high tolerance towards organic solvents and stability at elevated temperatures. Each of these characteristics can probably be screened for by adjusting the assay conditions and in principle it may be possible to select for more than one property in a single step.<sup>19</sup> For example in our experience, based upon the directed evolution of amine and amino acid oxidases, variants selected primarily for their activity in the solid-phase assay against a single enantiomer substrate, often turn out to be also highly enantioselective. Since high catalytic activity is a fundamental prerequisite for any biocatalyst, this observation is guiding our thinking in terms of the way forward for the directed evolution of enzymes. Perhaps the most exciting aspect of this area is that directed evolution can now be carried out in 'real time', at a rate that is commensurate with the expectations of those wishing to develop and optimise enzymes for applications in the commercial synthesis of fine chemicals and chiral intermediates.<sup>20</sup> Undoubtedly, as we learn more about the best strategies for evolving an enzyme in a particular direction, this process of optimisation will become faster, more automated, and hence increasingly attractive to synthetic organic chemists.

## References

- 1 For recent reviews see: J. P. Stambuli and J. F. Hartwig, *Curr. Opin. Chem. Biol.*, 2003, **7**, 7-420; J. F. Traverse and M. L. Snapper, *Drug Discovery Today*, 2002, **7**, 1002.
- 2 D. B. Berkowitz, M. Bose and S. Choi, *Angew. Chem., Int. Ed.*, 2002, **41**, 1603; M. Müller, T. W. Mathers and A. P. Davis, *Angew. Chem., Int. Ed.*, 2001, **40**, 3813.
- 3 The number of permutations ( $N$ ) of an enzyme, containing  $X$  amino acids, in which a single amino acid is replaced by any one of the remaining 19 amino acids is given by the equation:  $N = 19X! / [(X - 1)!]$ .
- 4 G. P. Horsman, A. M. F. Liu, E. Henke, U. T. Bornscheuer and R. J. Kazlauskas, *Chem. Eur. J.*, 2003, **9**, 1933.
- 5 For recent reviews see: *Directed Molecular Evolution of Proteins*, eds. S. Brakmann and K. Johnsson, Wiley VCH, Weinheim, 2002; E. T. Farinas, T. Bulter and F. H. Arnold, *Curr. Opin. Biotech.*, 2001, **12**, 545; J. D. Sutherland, *Curr. Opin. Chem. Biol.*, 2000, **4**, 263.
- 6 M. T. Reetz, *Angew. Chem., Int. Ed.*, 2002, **41**, 1335.
- 7 E. W. Hafner and D. Wellner, *Proc. Nat. Acad. Sci.*, 1971, **68**, 987.
- 8 J. W. Huh, K. Yokoigawa, N. Esaki and K. Soda, *J. Ferment. Bioeng.*, 1992, **74**, 189; J. W. Huh, K. Yokoigawa, N. Esaki and K. Soda, *Biosci. Biotech. Biochem.*, 1992, **56**, 2081.
- 9 K. Faber, *Chem. Eur. J.*, 2001, **7**, 5005.
- 10 T. Beard and N. J. Turner, *Chem. Commun.*, 2002, 246.
- 11 F.-R. Alexandre, D. P. Pantaleone, P. P. Taylor, I. G. Fotheringham, D. J. Ager and N. J. Turner, *Tetrahedron Lett.*, 2002, **43**, 707.
- 12 A. Enright, F.-R. Alexandre, G. Roff, I. G. Fotheringham, M. J. Dawson and N. J. Turner, *Chem. Commun.*, 2003, 2636.
- 13 M. Berger, B. Albrecht, A. Berces, P. Ettmayer, W. Neruda and M. Woisetschläger, *J. Med. Chem.*, 2001, **44**, 3031; S. France, D. J. Guerin, S. J. Miller and T. Lectka, *Chem. Rev.*, 2003, **103**, 2985.
- 14 S. O. Sablin, V. Yankovskaya, S. Bernard, C. N. Cronin and T. P. Singer, *Eur. J. Biochem.*, 1998, **253**, 270.
- 15 A. Greener, M. Callahan and B. Jerpseth, *Mol. Biotechnol.*, 1997, **7**, 189.
- 16 M. Alexeeva, A. Enright, M. J. Dawson, M. Mahmoudian and N. J. Turner, *Angew. Chem., Int. Ed.*, 2002, **41**, 3317.
- 17 R. Carr, M. Alexeeva, A. Enright, T. S. C. Eve, M. J. Dawson and N. J. Turner, *Angew. Chem., Int. Ed.*, 2003, **42**, 4807.
- 18 N. J. Turner, *TIBTECH*, 2003, **21**, 474.
- 19 D. R. Yazbeck, J. Tao, C. A. Martinez, B. J. Kline and S. Hu, *Adv. Synth. Catal.*, 2003, **345**, 524.
- 20 G. Huisman and D. Gray, *Curr. Opin. Biotech.*, 2002, **13**, 352; R. N. Patel, *Curr. Opin. Biotech.*, 2001, **12**, 587.

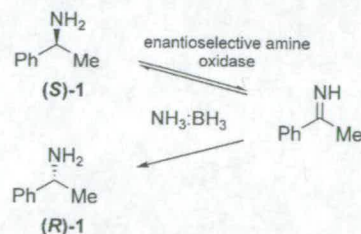
# Directed Evolution of an Amine Oxidase for the Preparative Deracemisation of Cyclic Secondary Amines

Reuben Carr,<sup>[a]</sup> Marina Alexeeva,<sup>[a]</sup> Michael J. Dawson,<sup>[b]</sup> Vicente Gotor-Fernández,<sup>[a]</sup> Cara E. Humphrey,<sup>[a]</sup> and Nicholas J. Turner<sup>\*,[a]</sup>

Enantiomerically pure primary and secondary amines are widely used as chiral auxiliaries and resolving agents and are also valuable intermediates for the synthesis of pharmaceuticals and agrochemicals.<sup>[1]</sup> Although enantiomerically pure amines are traditionally prepared by classical resolution of the corresponding racemate, alternative approaches have been developed based upon i) asymmetric reduction of imines,<sup>[2]</sup> ii) hydroamination of alkenes<sup>[3]</sup> and iii) lipase-catalysed kinetic resolution of racemic amines.<sup>[4]</sup> However, secondary amines, many of which have pronounced biological activity,<sup>[5]</sup> are poor substrates for lipases compared to the corresponding primary amines, with only a few documented examples in the literature.<sup>[6]</sup> Hence the use of lipase resolution does not offer a general route to this class of chiral molecule. Moreover, to date it has generally not been possible to achieve the *in situ* racemisation of amines to effect a dynamic kinetic resolution process due to the relatively harsh conditions required to racemise amines.<sup>[7]</sup>

Against this backdrop, we sought to extend our chemo-enzymatic deracemisation method to encompass chiral secondary amines. Based upon our earlier work with  $\alpha$ -amino acids,<sup>[8]</sup> we recently reported the deracemisation of  $\alpha$ -methylbenzyl amine ( $\alpha$ -MBA, **1**) in a one-pot procedure by the combined use of an enantioselective amine oxidase and ammonia borane as the reducing agent (Scheme 1).<sup>[9]</sup>

In order to identify an enzyme with appropriate activity and enantioselectivity towards  $\alpha$ -methylbenzylamine, the amine oxidase from *Aspergillus niger* (MAO-N) was subjected to directed evolution,<sup>[10]</sup> with (S)-**1** as the probe substrate, by random mutagenesis and selection employing a high-throughput agar-plate-based colorimetric screen. This approach led to the identification of an important amino acid substitution (Asn336Ser) that resulted in a variant enzyme possessing significantly enhanced activity (ca. 50-fold) and greater enantioselectivity towards **1** than the wild-type enzyme.<sup>[9]</sup> Subsequently, we



Scheme 1. Deracemisation of  $\alpha$ -methylbenzylamine (**1**) with an amine oxidase in combination with ammonia borane.

showed that this variant was also characterised by broad substrate specificity, being able to oxidize a wide range of chiral primary amines with high enantioselectivity.<sup>[11]</sup> However, although this variant showed some activity towards chiral secondary amines (relative activity of 1-methyltetrahydroisoquinoline (MTQ, **2**)  $\approx$  15% of  $\alpha$ -MBA), the rates of oxidation were too low to permit efficient preparative deracemisation reactions. Our goal therefore was to evolve a "secondary amine oxidase" for preparative-scale deracemisation reactions to complement the existing "primary amine oxidase".

The MAO-N gene used as the starting point for further directed evolution contained four amino acid substitutions compared to the wild-type. In addition to the Asn336Ser mutation, which is important for catalytic activity/enantioselectivity, mutations were Arg259Lys and Arg260Lys (improved expression) and Met348Lys (improved activity). This gene was subjected to random mutagenesis, by using the *E. coli* XL1-Red mutator strain (mutation frequency ca. 1–2 base changes per gene), followed by transformation and screening of the library (ca. 20000 clones) against (R/S)-**2** as the substrate, as previously described.<sup>[9]</sup> A number of clones (ca. 10) showed greater activity than the parent, with one in particular appearing to be significantly more active. Purification of this variant amine oxidase showed that it possessed a  $k_{cat}$  value about 5.5-fold higher than the parent towards (S)-**2** (Table 1) and also a higher  $K_M$  value (0.31 vs. 0.06 mM). The new variant displayed very high (S)-selectivity ( $E > 100$ ; calculated from ratio of  $k_{cat}/K_M$  for (S) vs. (R) enantiomer) towards MTQ and, upon sequencing, was found to possess an additional point mutation (Ile246Met) compared to the parent.

Interestingly, this new variant was found to have  $k_{cat}$  values towards  $\alpha$ -MBA and amylamine (**3**) comparable to those of the parent. However, the new variant showed evidence for en-

[a] R. Carr, Dr. M. Alexeeva, Dr. V. Gotor-Fernández, Dr. C. E. Humphrey, Prof. N. J. Turner  
School of Chemistry, The University of Edinburgh  
King's Buildings, West Mains Road, Edinburgh EH9 3JJ (UK)  
Fax: (+44) 131-650-4717  
E-mail: n.j.turner@ed.ac.uk

[b] Dr. M. J. Dawson  
Novacta Biosystems Ltd, UH Innovation Centre  
University of Hertfordshire, College Lane  
Hatfield, Herts AL10 9AB (UK)

Supporting information for this article is available on the WWW under <http://www.chembiochem.org> or from the author.

Table 1. Kinetic parameters of Asn336Ser and Asn336Ser/Ile246Met variants towards selected amines.

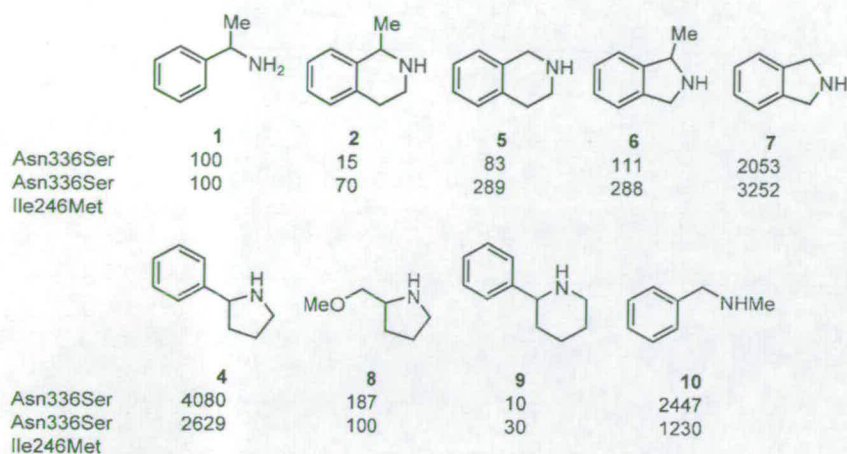
Amine	Asn336Ser			Asn336Ser/Ile246Met		
	$k_{cat}$ [min <sup>-1</sup> ]	$K_M$ [mM]	$k_{cat}/K_M$ [min <sup>-1</sup> mM <sup>-1</sup> ]	$k_{cat}$ [min <sup>-1</sup> ]	$K_M$ [mM]	$k_{cat}/K_M$ [min <sup>-1</sup> mM <sup>-1</sup> ]
(S)- <b>2</b>	1.10	0.06	18.33	6.00	0.31	19.35
(R)- <b>2</b>	0.06	0.70	0.09	0.08	3.58	0.02
(R/S)- <b>1</b>	6.01	1.11	5.41	7.00	2.88	2.43
(R/S)- <b>4</b>	150.07	0.38	394.92	128.20	0.72	178.06
amylamine ( <b>3</b> )	72.10	0.54	133.52	72.49	2.46	29.47



hanced activity towards chiral secondary amines (i.e., **2**, **5**, **6**, **7** and **9**) as shown in Scheme 2, with 2-phenylpyrrolidine (**4**) showing the highest  $k_{\text{cat}}$  (Table 1). Although in some cases the activity was reduced (**8** and **10**), in general, the initial aim of

ammonia borane was chosen for all subsequent preparative-scale reactions.

Initial small-scale deracemisation reactions of (*R/S*)-MTQ were carried out at 10 mM substrate concentration with 10 equiv of ammonia borane and washed whole cells (*E. coli*) expressing the Asn336Ser/Ile246Met variant amine oxidase. Complete deracemisation ( $ee = 99\%$ ) was achieved within 8 h. At 20 mM MTQ, on a preparative scale, the reaction was complete after 48 h and yielded (*R*)-MTQ in 71% isolated yield ( $ee = 99\%$ ). To complement the whole-cell approach, we also developed an immobilised form of the amine oxidase. The soluble fraction from the cell-free extract was subjected to purification by Ni-affinity chromatography to give the amine oxidase in >80% purity. Treatment with Eupergit C resulted in immobilisation onto



Scheme 2. Relative activities of various amines towards Asn336Ser and Asn336Ser/Ile246Met variants.

using a model secondary amine substrate (**2**) to select for a variant enzyme with improved activity towards a wider range of chiral secondary amines had been realised.

To further probe the importance of Ile246 as a key residue in controlling substrate specificity, we screened a second library in which position 246 was fully randomized. By using the Quik-change kit (Stratagene), a library of 220 colonies was screened, with (*R/S*)-**2** as substrate, to ensure a 99% probability of all possible 32 NNS codons being represented ( $p = 1 - e^{-NV}$  where  $p = \%$  probability,  $N =$  sample size required,  $V =$  total number of combinations). Eight colonies showed distinctly greater activity than the rest and, when picked and sequenced, to our surprise all contained methionine at position 246 (statistically expected 6.9 clones). Thus although the use of the mutator strain places constraints on the range of amino acids that can be introduced at specific sites, in the present example the optimal amino acid was indeed found by this approach.

Prior to assessing the suitability of the Asn336Ser/Ile246Met variant for preparative-scale deracemisation reactions of secondary amines, we screened a variety of reducing agents for their ability to reduce 1-methyl-3,4-dihydroisoquinoline (MDQ) to MTQ. (Figure 1). Amine boranes were generally found to be highly reactive under aqueous conditions with the following order of activity: 4-dimethylaminopyridine borane (DMAP borane) > 2-(methylamino)pyridine borane > ammonia borane. Catalytic transfer hydrogenation (Pd/C ammonium formate) was also found to be effective. By using ammonia borane, it was found that as little as 1.0 equivalent (0.5 equiv for DMAP borane), relative to the substrate, could be used for complete reduction of MDQ to MTQ. For ease of use,

the resin. By using the immobilised amine oxidase with 20 mM MTQ, the deracemisation process was found to be slower (ca. 96 h) than with the whole-cell approach, but the isolated yield was considerably higher (yield = 95%;  $ee = 99\%$ ). Finally to demonstrate the generality of the approach and explore the effect of working at higher substrate concentration, we examined the preparative deracemisation of (*R/S*)-2-phenylpyrrolidine, analogues of which are potent ligands for the nicotinic acetylcholine receptor.<sup>[12]</sup> With the immobilized enzyme, a substrate concentration of 100 mM (14.7 gL<sup>-1</sup>) and ammonia borane (2.5 equiv), the deracemisation was complete within 48 h and, after work-up, yielded (*R*)-2-phenylpyrrolidine in 80% yield and 98%  $ee$ .

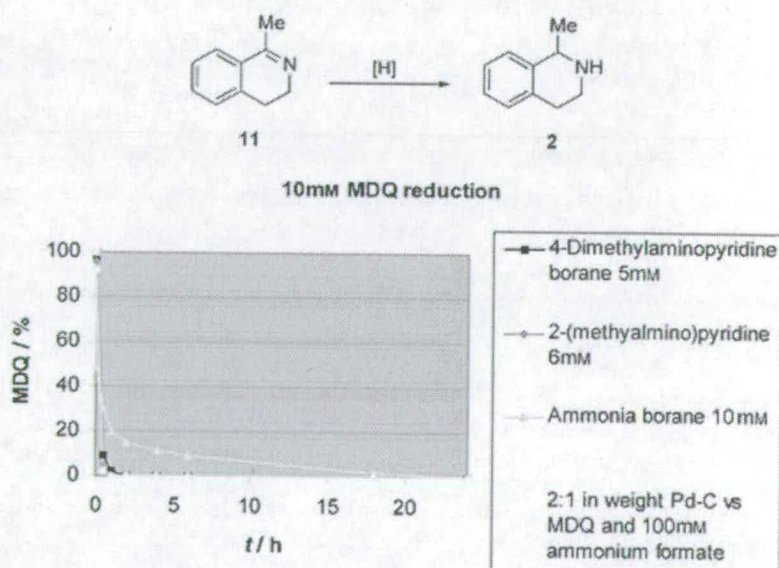
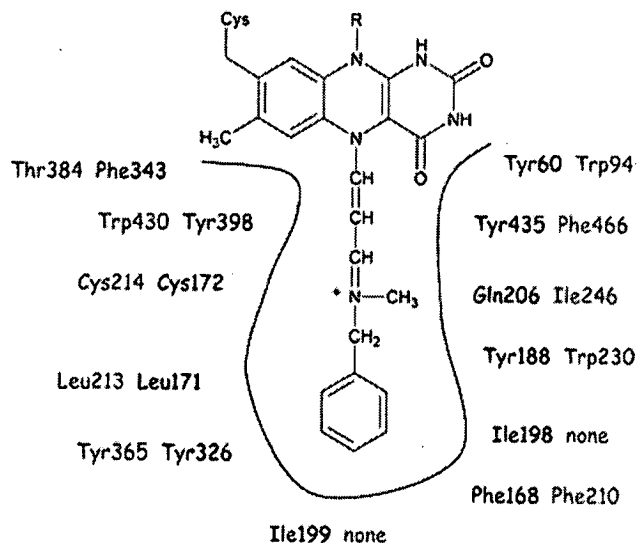


Figure 1. Reduction of MDQ **11** to MTQ **2** by using various reducing agents.

In order to gain insights into the possible significance of the mutation at Ile246, we generated an homology model of the active site. Although there is no X-ray structure available for monoamine oxidase N (MAO-N) from *A. niger*, the related enzyme monoamine oxidase B (MAO-B) from human liver has been crystallized, and the structure has been solved to a resolution of 2.5 Å.<sup>[13]</sup> Figure 2 shows a picture of the suicide inhibi-



**Figure 2.** Model of the active site of MAO-B showing the residues that make contact with the inhibitor. The corresponding residues of MAO-N are shown alongside.

tor pargyline covalently bound at the active site of MAO-B, together with the key amino acid residues that line the active site (black). We carried out a WU-Blast2 sequence alignment (EMBL-EBI) between MAO-N and MAO-B which revealed 24% sequence identity and 43% sequence similarity between the two proteins. The corresponding residues from MAO-N are shown in grey, and it is interesting to note that i) the active sites of both enzymes contain a high proportion of aromatic residues and ii) there is considerable homology, and often identity, between the two enzymes (e.g. Tyr60/Trp94, Tyr435/Phe466, Tyr188/Trp230, Phe168/Phe210, Tyr365/Tyr326, Leu171/Leu213, Cys172/Cys214, Tyr398/Trp430). Ile246 (MAO-N) maps onto Gln206 (MAO-B), the latter appearing to make intimate contact with the substrate. It is also perhaps significant that these two amino acids are quite different in nature and steric demand, and might therefore represent important residues in the respective proteins for controlling substrate specificity.

In summary we have developed a practical procedure for deracemisation of cyclic secondary amines by a further round of directed evolution of the monoamine oxidase from *A. niger*.

By using a representative secondary amine as the substrate for screening the library, we were able to identify a variant enzyme that possessed general activity towards a range of structurally related, but different, secondary amines. Furthermore the key mutation Ile246Met appears to be important in terms of controlling substrate specificity, and therefore constitutes a "hot spot" that can be explored for altering specificity towards other amine substrates of interest.

## Acknowledgements

We are grateful to the BBSRC and GlaxoSmithKline for funding a CASE award (R.C.) and to the EU for a Marie-Curie Fellowship (V.G.-F.). We also thank the Wellcome Trust for financial support.

**Keywords:** amine oxidase • amines • biocatalysis • deracemisation • directed evolution • enantioselectivity

- [1] For a recent review see: M. Breuer, K. Dittrich, T. Habicher, B. Hauer, M. Keßler, R. Stürmer, T. Zelinski, *Angew. Chem.* **2004**, *116*, 806; *Angew. Chem. Int. Ed.* **2004**, *43*, 788.
- [2] A. A. Boezio, J. Pytkowicz, A. Côté, A. B. Charette, *J. Am. Chem. Soc.* **2003**, *125*, 14260; G. D. Williams, R. A. Pike, C. E. Wade, M. Wills, *Org. Lett.* **2003**, *5*, 4227.
- [3] C. A. Kiener, C. Shu, C. Incarvito, J. F. Hartwig, *J. Am. Chem. Soc.* **2003**, *125*, 14272.
- [4] F. Balkenhohl, K. Dittrich, B. Hauer, W. Ladner, *J. Prakt. Chem. Chem. Ztg.* **1997**, *339*, 381; F. van Rantwijk, R. A. Sheldon, *Tetrahedron* **2004**, *60*, 501.
- [5] T. S. Kaufman, *Tetrahedron: Asymmetry* **2004**, *15*, 1203.
- [6] See G. F. Breen, *Tetrahedron: Asymmetry* **2004**, *15*, 1427, and references therein.
- [7] M. T. Reetz, K. Schimossek, *Chimia* **1996**, *50*, 668; Y. K. Choi, M. J. Kim, Y. Ahn, M.-J. Kim, *Org. Lett.* **2001**, *3*, 4099; O. Pamies, A. H. Eil, J. S. M. Samec, N. Hermanns, J.-E. Bäckvall, *Tetrahedron Lett.* **2002**, *43*, 4699.
- [8] F.-R. Alexandre, D. P. Pantaleone, P. P. Taylor, I. G. Fotheringham, D. J. Ager, N. J. Turner, *Tetrahedron Lett.* **2002**, *43*, 707; T. Beard, N. J. Turner, *Chem. Commun.* **2002**, 246; A. Enright, F.-R. Alexandre, G. Roff, I. G. Fotheringham, M. J. Dawson, N. J. Turner, *Chem. Commun.* **2003**, 2636; G. J. Roff, R. C. Lloyd, N. J. Turner, *J. Am. Chem. Soc.* **2004**, *126*, 4098.
- [9] M. Alexeeva, A. Enright, M. J. Dawson, M. Mahmoudian, N. J. Turner, *Angew. Chem.* **2002**, *114*, 3309; *Angew. Chem. Int. Ed.* **2002**, *41*, 3177.
- [10] M. T. Reetz, *Proc. Natl. Acad. Sci. USA* **2004**, *101*, 5716; F. H. Arnold, *Nature* **2001**, *409*, 253; S. Brakmann, K. Johnsson, *Directed Molecular Evolution of Proteins*, Wiley-VCH, Weinheim, **2002**.
- [11] R. Carr, M. Alexeeva, A. Enright, T. S. C. Eve, M. J. Dawson, N. J. Turner, *Angew. Chem.* **2003**, *115*, 4955; *Angew. Chem. Int. Ed.* **2003**, *42*, 4807.
- [12] R. L. Elliott, K. B. Ryther, D. J. Anderson, J. L. Raszkievicz, J. Campbell, J. P. Sullivan, D. S. Garvey, *Bioorg. Med. Chem. Lett.* **1995**, *5*, 991; R. A. Glennon, *Prog. Med. Chem.* **2004**, *42*, 55.
- [13] C. Binda, P. Newton-Vinson, F. Hubálek, D. E. Edmonson, A. Mattevi, *Nat. Struct. Biol.* **2002**, *9*, 22.

Received: September 14, 2004

Published online on ■ ■ ■, 2005